

Photoredox Catalysis Using Copper Complexes

Dissertation

Zur Erlangung des Doktorgrades der Naturwissenschaften

Dr. rer. nat.

der Fakultät für Chemie und Pharmazie

der Universität Regensburg



vorgelegt von

Christian Lankes

aus Cham

Regensburg 2017

Die Arbeit wurde angeleitet von: Prof. Dr. Oliver Reiser

Promotionsgesuch eingereicht am: 08.12.2017

Promotionskolloquium am: 31.01.2018

Prüfungsausschuss:

Vorsitz:	Prof. Dr. Jörg Heilmann
1. Gutachter:	Prof. Dr. Oliver Reiser
2. Gutachter:	Prof. Dr. Robert Wolf
3. Prüfer:	Prof. Dr. Bernhard Dick

Der experimentelle Teil der vorliegenden Arbeit wurde in der Zeit von Oktober 2013 bis Mai 2017 unter der Leitung von Herrn Prof. Dr. Oliver Reiser am Institut für Organische Chemie der Universität Regensburg angefertigt.

Herrn Prof. Dr. Oliver Reiser möchte ich besonders für die Aufnahme in seinen Arbeitskreis, die Überlassung des interessanten Themas, die anregenden Diskussionen und seine stete Unterstützung während der Durchführung dieser Arbeit danken.

Meiner Familie

“Darkness cannot drive out darkness; only light can do that.”

Martin Luther King Jr.

Table of Contents

List of Abbreviations

A. Introduction	1
1. Copper Catalysts in Photoredox Catalysis	1
3. Copper(III) Species in Organic Chemistry	10
2. Outline of this Study	20
B. Synthesis, Characterization and Application of New Diimine-Based Copper Complexes	22
1. Introduction	22
2. Synthesis of Modified Phenanthroline Ligands and Complexation with Copper	24
2.1 Synthesis of $[\text{Cu}(\text{dapacetal})_2]^+$	24
2.2 Synthesis of $[\text{Cu}(\text{phenazino-dap})_2]^+$	28
2.3 Synthesis of $[\text{Cu}(\text{dap})\text{Cl}_2]$	31
3. Characterization of New Complexes	33
3.1 X-ray Structures	33
3.2 Spectroscopic Investigation	35
3.3 Cyclovoltammetric Measurements	38
3.4 Summary and Assessment of Photophysical and Electrochemical Properties	40
4. Comparison of Phenanthroline Complexes in Photoreactions	42
4.1 Copper(I) Phenanthroline Complexes	42
4.2 Copper(II) Phenanthroline Complex	49
5. 1,4-Diaza-1,3-butadienes: An Alternative to Phenanthrolines?	52
5.1 Photophysical and Electrochemical Properties of $[\text{Cu}(\text{DABMes})_2]\text{BF}_4$	53
5.2 Investigation of Photocatalytic Activity of $[\text{Cu}(\text{DABMes})_2]\text{BF}_4$	55
6. Conclusion and Outlook	58
C. Atom Transfer Radical Addition Reactions – Investigation of New Reagents	61
1. Introduction	61
2. Investigation of Different Reagents	62
2.1 Ruppert-Prakash Reagent	62

2.2 Trifluoromethanesulfonic Acid	64
2.3 Phenyl Triflates.....	66
2.4 Trichloromethanesulfonyl Chloride	69
3. Conclusion and Outlook.....	75
D. Elucidating the Reaction Pathways of Visible-Light-Mediated Chloramination of Alkenes.....	77
1. Introduction	77
2. Screening of Substrate Scope.....	79
3. Reactions with <i>N</i> -Centered Radicals.....	87
4. Investigation of UV-Absorption Spectra and Quantum Yield Measurements	91
5. Reaction Mechanism	94
6. Conclusion.....	96
E. Summary / Zusammenfassung	97
1. Summary	97
2. Zusammenfassung	99
F. Experimental Part.....	101
1. General Comments.....	101
2. Synthesis of Known Compounds and Reagents.....	104
3. Chapter B: Synthesis, Characterization and Application of New Diimine-Based Copper Complexes	105
3.1 Compound Characterization	105
3.2 Luminescence Properties of [Cu(dapacetal) ₂] ⁺ and [Cu(phenazino-dap) ₂] ⁺	115
3.3 NMR Spectra.....	117
3.4 X-ray	128
4. Chapter C: Atom Transfer Radical Addition Reactions – Investigation of New Reagents	131
4.1 Compound Characterization	131
4.2 NMR Spectra.....	137
4.3 Cyclic Voltammograms.....	146
4.4 X-ray	147

5. Chapter D: Elucidating the Reaction Pathways of Visible-Light-Mediated Chloramination of Alkenes	148
5.1 Synthesis of <i>N</i> -Chlorosulfonamides	148
5.2 General Procedure for Chloramination of Olefins	150
5.3 Compound Characterization	151
5.4 Absorption Spectra	164
5.5 Quantum Yield Determination.....	165
5.6 NMR and IR Spectra	168
5.7 X-ray	197
G. References	198
Curriculum Vitae.....	208
Acknowledgement.....	210
Declaration.....	212

List of Abbreviations

A	acceptor	DEPT	distortionless enhancement
Å	Ångström		by polarization transfer
Ac	acetyl	DMF	<i>N,N</i> -dimethylformamide
AIBN	azobisisobutyronitrile	dmp	2,9-dimethyl-
APCI	atmospheric pressure chemical ionization		1,10-phenanthroline
Ar	aryl	DMSO	dimethyl sulfoxide
ATRA	atom transfer radical addition	dnp	2,9-dinaphthyl-
			1,10-phenanthroline
binc	bis (2-isocyanophenyl) phenylphosphonate	dpp	2,9-diphenyl-
			1,10-phenanthroline
Boc	<i>tert</i> -butyloxycarbonyl	dr	diastereomeric ratio
bpy	2,2'-bipyridine	dtbbpy	4,4'-di- <i>tert</i> -butyl-2,2'- bipyridine
Bu	butyl	E _{1/2}	standard reduction potential
Cat	catalyst	EI	electron ionization
CI	chemical ionization	EPR	electron paramagnetic resonance
COSY	correlation spectroscopy		
CT	charge-transfer	equiv	equivalents
CV	cyclic voltammetry	ESI	electrospray ionization
Cy	cyclohexyl	Et	ethyl
D	donor	<i>et al.</i>	and others (co-authors)
DAB	1,4-diaza-1,3-butadiene	Et ₂ O	diethyl ether
DABMes	(1 <i>E</i> ,2 <i>E</i>)- <i>N</i> ¹ , <i>N</i> ² -dimesityl ethane-1,2-diimine	EtOAc	ethyl acetate
		<i>fac</i>	facial
dap	2,9-bis(<i>para</i> -anisyl)-1,10- phenanthroline	Fc	ferrocene
		FTIR	Fourier-transform infrared spectroscopy
dapacetal	6,9-bis(4-methoxyphenyl)- 2,2-dimethyl-[1,3]dioxolo [4,5- <i>f</i>][1,10]phenanthroline	glyme	1,2-dimethoxyethane
		<i>h</i>	Planck's constant
dba	dibenzylideneacetone	HRMS	high resolution mass spectrometry
DCE	1,2-dichloroethane		
DCM	dichloromethane	HSQC	heteronuclear single- quantum correlation
deg	degree		

List of Abbreviations

IR	infrared spectroscopy	PMMA	poly(methyl methacrylate)
ISC	intersystem crossing	POP	bis(2-(diphenylphosphino)phenyl)ether
J	coupling constant (spectroscopy)	ppm	parts per million
L	ligand, liter	ppy	2-phenylpyridine
LED	light emitting diode	Q	quencher
LRMS	low resolution mass spectrometry	R	arbitrary residue
M	molar (mol L^{-1}); ground state molecule	ref	reference
m	meta	R_f	retention factor
max	maximum	RI-NMR	rapid-injection nuclear magnetic resonance spectroscopy
Me	methyl	rt	room temperature
MeCN	acetonitrile	rxn	reaction
Mes	mesitylene	SCE	saturated calomel electrode
min	minimum; minute	SET	single electron transfer
MLCT	metal-to-ligand charge- transfer	SM	starting material
mp	melting point	$t\text{Bu}$	<i>tert</i> -butyl
MS	mass spectrometry	Tf	trifluoromethanesulfonyl
n.r.	no reaction	THF	tetrahydrofuran
$n\text{BuLi}$	<i>n</i> -butyllithium	TLC	thin layer chromatography
NMR	nuclear magnetic resonance	TMS	trimethylsilyl
NOESY	nuclear Overhauser effect spectroscopy	tosyl	4-toluenesulfonyl
nosyl	<i>N</i> -chloro- <i>N</i> -methyl- 4-nitrobenzenesulfonamide	Ts	tosyl = 4-toluenesulfonyl
Nu	nucleophile	UV	ultraviolet
<i>o</i>	ortho	Vis	visible light
<i>p</i>	para	Φ	quantum yield
P_{abs}	absorbed radiant power	Φ_{PL}	photoluminescence quantum yield
PCat	photoredox catalyst	δ	chemical shift (ppm)
Ph	phenyl	ε	molar extinction coefficient
phenazino-	3,6-bis(4-methoxyphenyl)	λ	wavelength
dap	dipyrido[3,2- <i>a</i> :2',3'- <i>c</i>] phenazine	λ_{Abs}	wavelength of absorption
		λ_{max}	wavelength at maximum
		ν	frequency
		τ	lifetime

A. Introduction

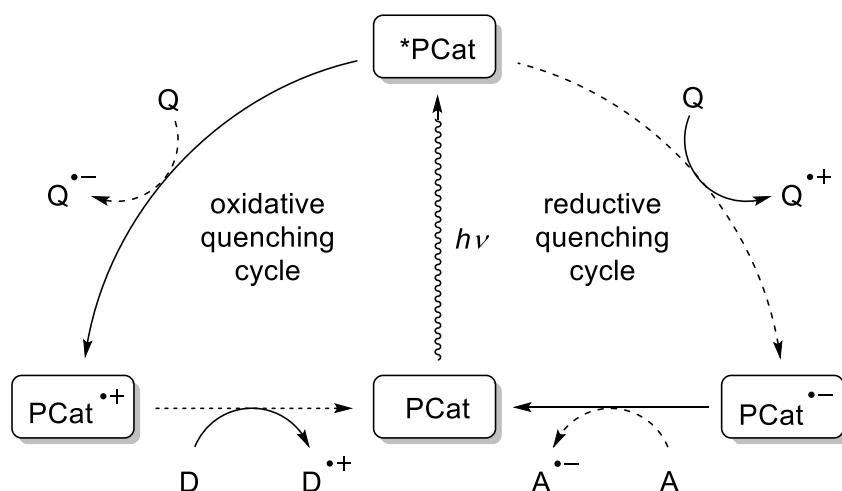
1. Copper Catalysts in Photoredox Catalysis

Due to the climate change^[1] and because of a still growing global population of currently more than 7.5 billion^[2] people, modern society is forced to make economical use of available natural resources. Hence, now more than ever, there is an increasing need for sustainable “green” sources and processes for chemical products as well as clean, safe and inexhaustible energy sources.^[3] Over a century ago, Giacomo Ciamician outlined in his pioneering article titled “The photochemistry of the future” in 1912 the potential of sunlight as an abundant, safe, inexpensive and sustainable energy source usable for chemical transformations.^[4] During the past decade, remarkable progress towards the efficient conversion of solar energy into electrical energy^[5] and chemical fuels^[6] has been achieved. By contrast, the use of visible light for the synthesis of structurally challenging organic compounds is less developed even though in nature, biological photosynthesis is omnipresent.^[7,8] One reason for this discrepancy is that only a few molecules absorb visible light and most molecules usually require irradiation with short-wave and high-energy ultraviolet (UV) light for direct excitation. However, UV-light is unfavorable as it is not abundant in the solar radiation spectrum that penetrates the atmosphere and most molecular bonds are instable against this energy-rich radiation often causing considerable unproductive decomposition.^[8] In order to use the abundant and mild visible light for efficient chemical transformations, suitable photosensitizers and photocatalysts¹ have been developed.^[10] After absorbing photons, these compounds form excited species which are able to transfer energy or electrons to an organic substrate.^[7,12]

As the present thesis focuses on photoredox catalysis, in which single electron transfer (SET) is the crucial pathway, these processes are explained in more detail hereafter. In principle, the excited state of the photoredox catalyst is both more strongly reducing and more strongly oxidizing than the corresponding ground state which makes the photoredox catalyst either a regenerable electron donor or acceptor in the catalytic cycle (Scheme 1).^[7,10,13] Hence, photoredox catalysis is convenient for both oxidation and reduction processes which can be described in simplified form by two different catalytic cycles, the oxidative and the reductive quenching cycle. Both cycles start with the absorbance of a photon by the photoredox catalyst (PCat) leading to a short-lived excited singlet state via a metal-to-ligand charge-transfer (MLCT). By means of subsequent intersystem crossing (ISC),

¹ IUPAC definition: “Catalyst able to produce, upon absorption of light, chemical transformations of the reaction partners. The excited state of the photocatalyst repeatedly interacts with the reaction partners forming reaction intermediates and regenerates itself after each cycle of such interactions.”^[9]

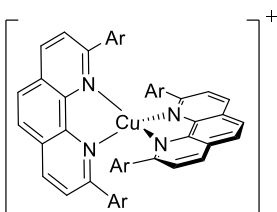
a more stable triplet state ($^*\text{PCat}$) with a longer lifetime forms, which can undergo SET. In the reductive quenching cycle, the excited photocatalyst $^*\text{PCat}$ accepts an electron from a quencher (Q) resulting in $\text{PCat}^{\bullet-}$. For this pathway a non-productive quencher, often termed as a “sacrificial electron donor”, such as tertiary amines or ascorbate is usually necessary.^[14,15] By transferring an electron from strongly reducing $\text{PCat}^{\bullet-}$ to an acceptor molecule, the catalytic cycle closes. Regarding the oxidative quenching cycle, the excited photocatalyst $^*\text{PCat}$ reduces a quencher Q such as viologens, aryldiazonium salts or haloalkanes, resulting in $\text{PCat}^{\bullet+}$ which subsequently serves as an electron acceptor.^[10,14]



Scheme 1. General scheme for photoredox catalysis via reductive or oxidative quenching (A = acceptor, D = donor, PCat = photoredox catalyst, Q = quencher; solid arrows: oxidation steps, dashed arrows: reduction steps, curled arrow: excitation by light irradiation).

Due to their ease of access, stability, long excited state lifetimes and excellent photoredox properties, the most commonly used visible light photoredox catalysts in organic synthesis are ruthenium- or iridium-based metal complexes or organic dyes such as Eosin Y.^[16] Over the last decade $[\text{Cu}(\text{dap})_2]^+$ (**C1**) has emerged as an efficient photocatalyst with valuable reducing properties.^{[17][18]} In contrast to ruthenium or iridium, copper is beneficial as it is more abundant, less expensive and more environmentally friendly. In order to provide an overview of the photophysical behavior of such complexes, some prominent representatives, which were also employed in this thesis, are illustrated in Table 1.

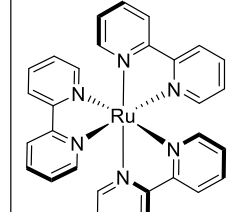
Table 1. Selected photophysical properties of established metal-based photoredox catalysts used in this thesis.^{a)}



Ar = p-OMe-Ph

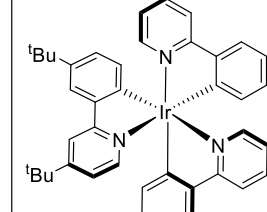
[Cu(dap)₂]⁺

C1



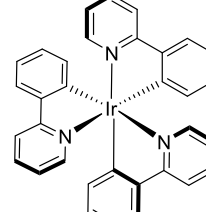
[Ru(bpy)₃]²⁺

C2



[Ir(ppy)₂(dtbbpy)]⁺

C3



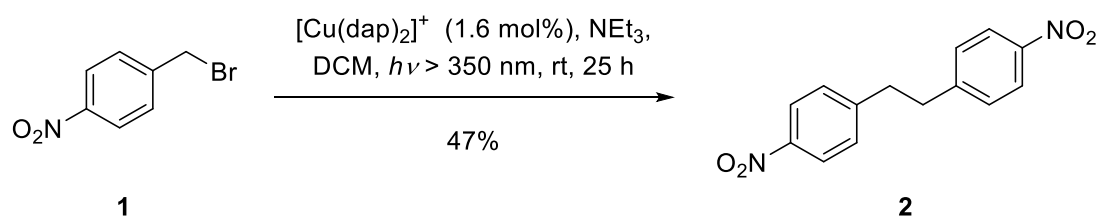
fac-Ir(ppy)₃

C4

Photocatalyst	$E_{1/2}$ (M ⁺ /M [*])	$E_{1/2}$ (M [*] /M ⁻)	$E_{1/2}$ (M ⁺ /M)	$E_{1/2}$ (M/M ⁻)	Excited State Lifetime τ / ns	Ref
[Cu(dap) ₂] ⁺	-1.43	-	+0.62	-	130 ^{b)}	[19,20]
[Ru(bpy) ₃] ²⁺	-0.81	+0.77	+1.29	-1.33	1100	[21]
[Ir(ppy) ₂ (dtbbpy)] ⁺	-0.96	+0.66	+1.21	-1.51	557	[22,23]
<i>fac</i> -Ir(ppy) ₃	-1.73	+0.31	+0.77	-2.19	1900	[10]

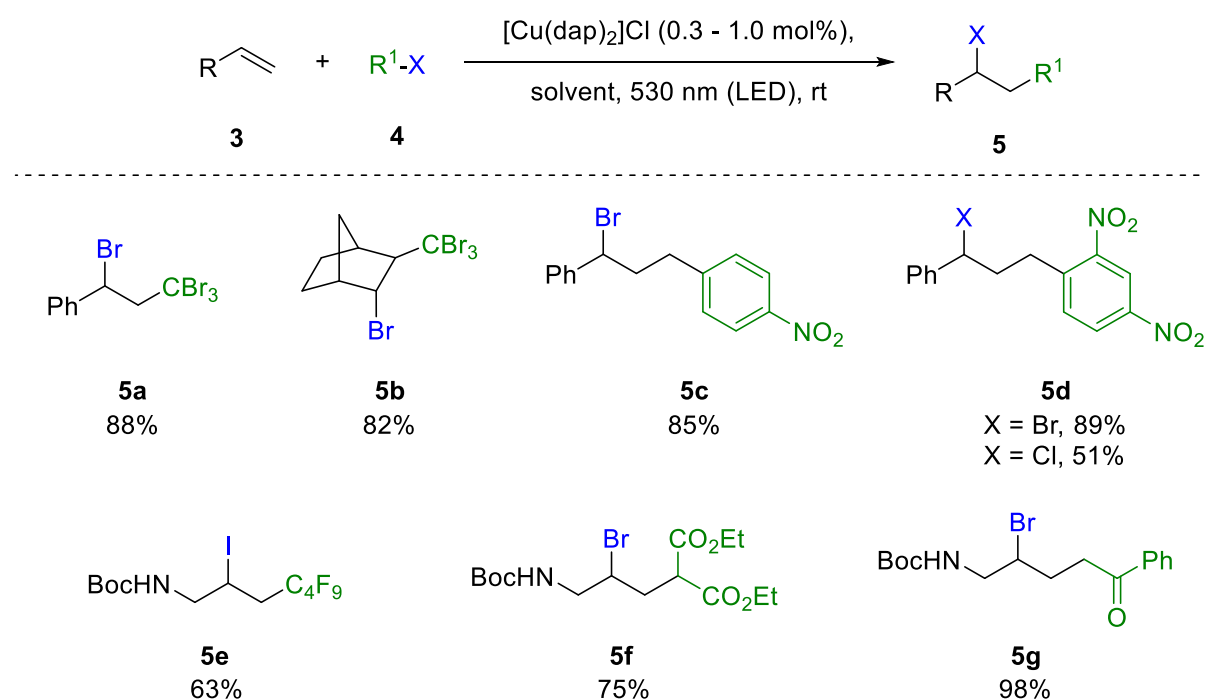
a) Data obtained in acetonitrile at room temperature. Potentials are given in V versus the saturated calomel electrode (SCE). b) Sauvage *et al.*^[19] reported a lifetime of 270 ns, however, experimental details for this measurement are not available. Reiser *et al.*^[20] reported a lifetime of 130 ns in MeCN and a lifetime of 540 ns in PMMA.

Besides the economic benefits, copper complexes have developed into an important class of photocatalysts alongside established ruthenium- or iridium-based catalysts. More and more examples show that copper-phenanthroline complexes are of special interest, as they are prone to structural redistribution and ligand exchange which enables access to new reactions by running through alternative reaction pathways (*vide infra*). In particular [Cu(dap)₂]⁺ (**C1**) has been applied as an efficient photocatalyst in various reactions. The synthesis of 2,9-bis(*para*-anisyl)-1,10-phenanthroline (dap) and its formation of stable bischelate complexes with copper(I) was first mentioned by J.-P. Sauvage and C. O. Dietrich-Buchecker in 1983.^[24] Just four years later, Sauvage *et al.* reported the usage of [Cu(dap)₂]⁺ (**C1**) for photoredox reactions, exemplified by the photoassisted transformation of 4-nitrobenzyl bromide (**1**) into the bibenzyl coupling product **2** in the presence of triethylamine (Scheme 2).^[19]

**Scheme 2.** First example of photoredox catalysis with [Cu(dap)₂]⁺ (**C1**).^[19]

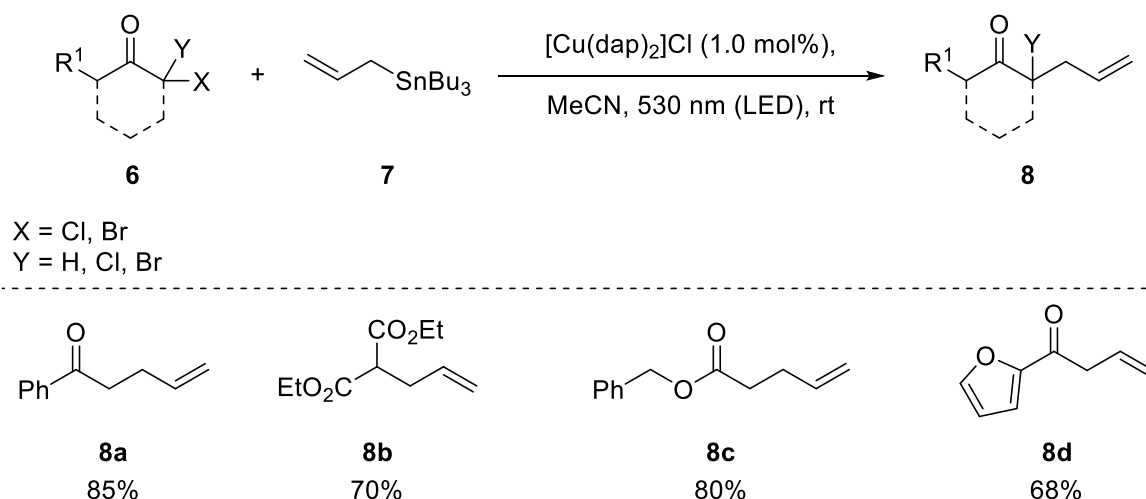
Following the oxidative quenching cycle, the authors assume that triethylamine acts as a reductant of copper(II) species being formed after SET to substrate **1**. When oxygen was present during the reaction, oxidation to 4-nitrobenzaldehyde was observed in 95% yield.

In 2012, the group around O. Reiser started to explore the catalytic scope of $[\text{Cu}(\text{dap})_2]^+$ (**C1**) for modern photoredox catalysis.^[20,25–29] Using green light for photoexcitation, for example, visible-light-mediated atom transfer radical addition (ATRA) reactions of various activated organohalides **4** such as CBr_4 , nitro-substituted benzyl halides or α -haloketones with alkenes **3** were developed (Scheme 3).^[25,26] A sacrificial electron donor is not necessary within this protocol, as the reaction runs through the oxidative quenching cycle, with the organohalide substrates acting as the oxidative quencher. This particularly atom economic^[30] strategy via the oxidative quenching cycle has recently been reported by Stephenson *et al.* using ruthenium(II)- or iridium(III)-based photoredox catalysts.^[31,32] ATRA reactions, also known as Kharasch addition reactions, are in general an atom economic method for alkene or alkyne difunctionalization, making them a versatile tool for organic synthesis.^[33–37] In redox neutral ATRA process, atom transfer reagents, usually haloalkanes, formally undergo σ bond cleavage followed by addition across a π bond of an alkene or alkyne under formation of two new σ bonds with all atoms of the starting materials being incorporated in the final product.^[10] By means of photoredox catalysis, problems commonly encountered with this transformation such as the requirement of radical initiators or harsh conditions as well as limited functional group tolerance can be overcome.^[31,36]



Scheme 3. Visible-light-mediated ATRA reactions between alkenes **3** and organohalides **4** catalyzed by $[\text{Cu}(\text{dap})_2]\text{Cl}$ (**C1-Cl**).^[25,26]

In another process, copper phenanthroline complex **C1-Cl** was utilized for the visible-light-mediated allylation of α -haloketones **6** (Scheme 4).^[25] Remarkably, until then, this reaction had not been reported to be possible using visible light. Thus, $[\text{Cu}(\text{dap})_2]\text{Cl}$ (**C1-Cl**) is beneficial for this transformation because radical initiators such as AIBN or BET_3 as well as high power UV irradiation are not required any longer. However, using ecologically more benign allyltrimethylsilane instead of allyltributyltin (**7**) was less efficient and only one example, coupling with tetrabromomethane, was reported.



Scheme 4. Visible-light-mediated allylation of α -haloketones **6** with allyltributyltin (**7**) catalyzed by $[\text{Cu}(\text{dap})_2]\text{Cl}$ (**C1-Cl**).^[25]

Since then the synthetic application of copper(I) phenanthroline complexes in photoredox catalysis as an environmentally benign alternative to established photoredox catalysts such as $[\text{Ru}(\text{bpy})_3]^{2+}$ (**C2**) or *fac*- $\text{Ir}(\text{ppy})_3$ (**C4**) has been demonstrated by several groups by means of various further reactions such as photocyclizations^[38], azidations^[39,40], aminodifluoromethylations^[41] or α -amino C-H bond functionalizations^[42]. Beyond that, promising heteroleptic alternatives of copper(I) phenanthroline complexes have also emerged and have been evaluated as visible light photocatalysts, demonstrating that such complexes have special features (Figure 1).^[20,27,43,44,45,46] These complexes can be easily formed and their steric and electronic properties can be extensively tuned by changing the chelating ligands which allows adaptation for a given photochemical process. Thus it was possible to significantly increase the short lifetime of copper(I) phenanthroline complexes, which is usually one of their major drawbacks. By changing from homoleptic $[\text{Cu}(\text{dap})_2]^+$ (**C1**) to heteroleptic $[\text{Cu}(\text{dpp})(\text{binc})]^+$ (**C6**), for instance, the lifetime of the excited state was increased from 560 nanoseconds to 17 microseconds in poly(methyl methacrylate).^[20]

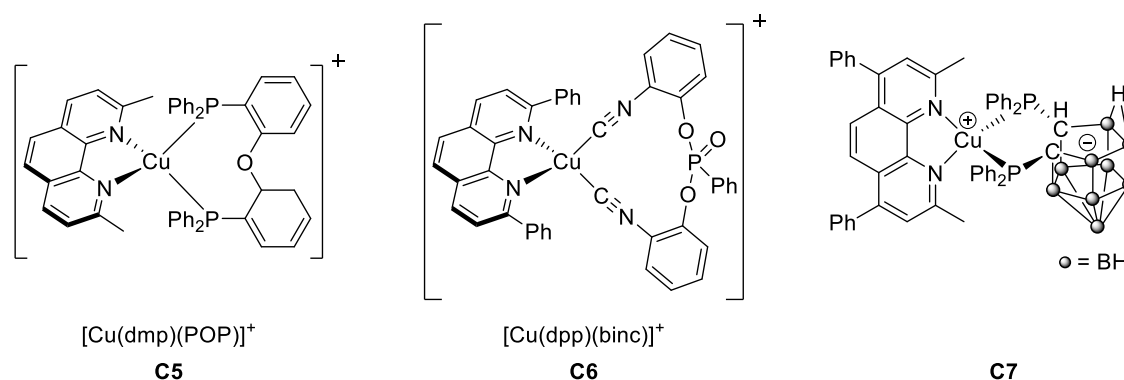
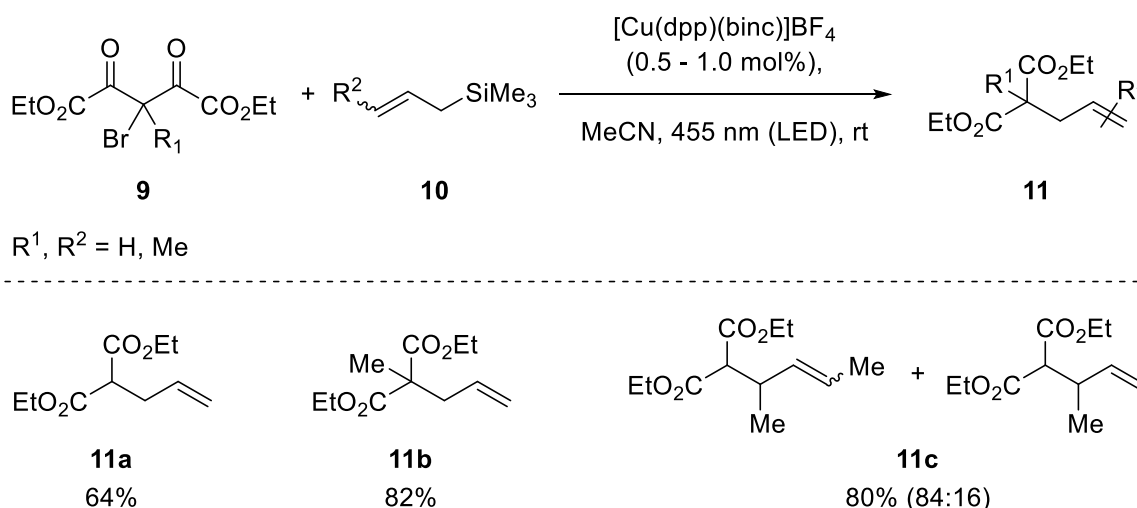


Figure 1. Examples of heteroleptic copper(I) phenanthroline complexes used as visible light photoredox catalysts.^[20,43,46]

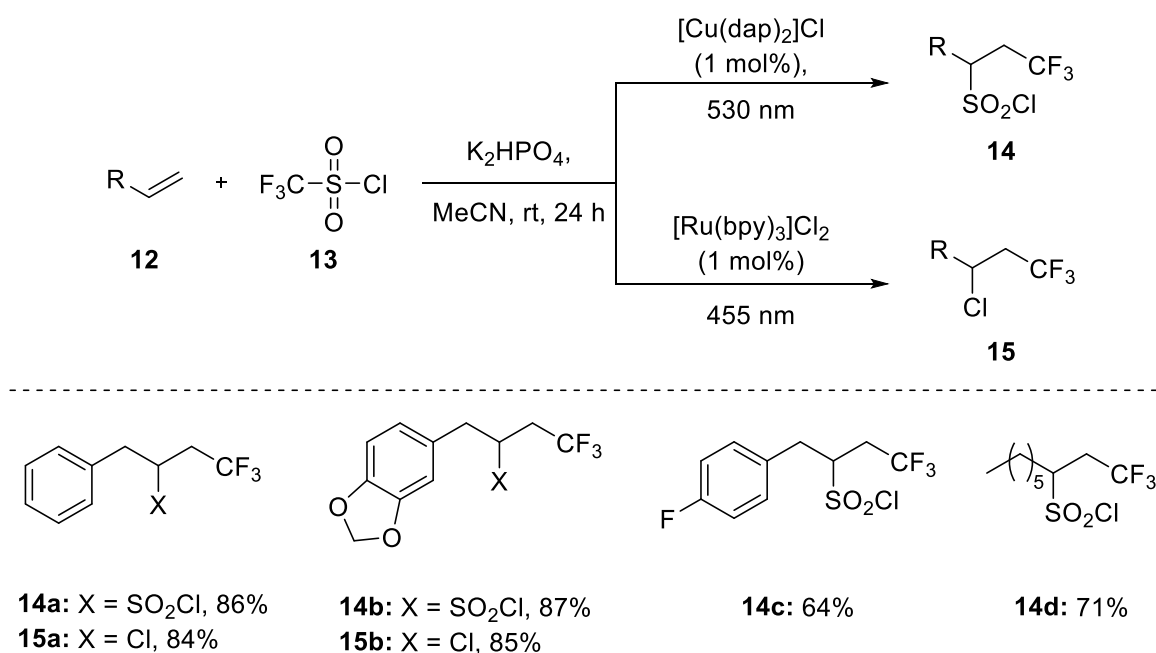
Heteroleptic copper complex **C6**, for example, proved to be beneficial for visible-light-mediated allylations. While homoleptic complex **C1-CI** was only efficient in couplings with allyltributyltin (**7**) (cf. Scheme 4)^[25], complex **C6-BF₄** also showed good activity for the transformation of allyltrimethylsilanes **10** (Scheme 5).^[47,20]



Scheme 5. Visible-light-mediated allylation of organohalides **9** with allyltrimethylsilanes **10** catalyzed by $[\text{Cu}(\text{dpp})(\text{binc})]\text{BF}_4$ (**C6-BF₄**).^[20]

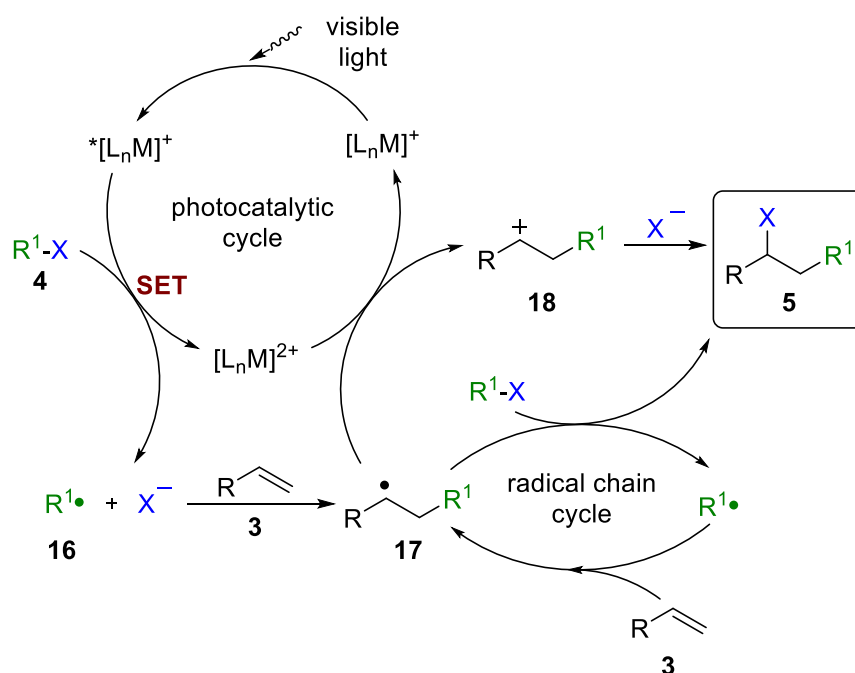
Recently, the group around O. Reiser has developed the photoredox catalyzed trifluoromethylchlorosulfonylation of alkenes (Scheme 6), demonstrating that copper-based photocatalysts are not only alternatives to ruthenium- or iridium-based photocatalysts for electron transfer to substrates but have special features providing unique opportunities.^[27] Using triflyl chloride (**13**) and typical photoredox catalysts such as $[\text{Ru}(\text{bpy})_3]\text{Cl}_2$, $[\text{Ir}(\text{ppy})_2(\text{dtbbpy})]\text{PF}_6$ or Eosin Y, a known trifluoromethylchlorination^[48] under loss of sulfur dioxide was observed and chlorinated products **15** were formed as the main products.^[27] In contrast, $[\text{Cu}(\text{dap})_2]\text{Cl}$ (**C1-CI**) proved to be extraordinary, as sulfur dioxide was retained in

the course of the reaction and trifluoromethylchlorosulfonylation products **14** were obtained, given the absence of strong donor atoms in the substrate.^[27]



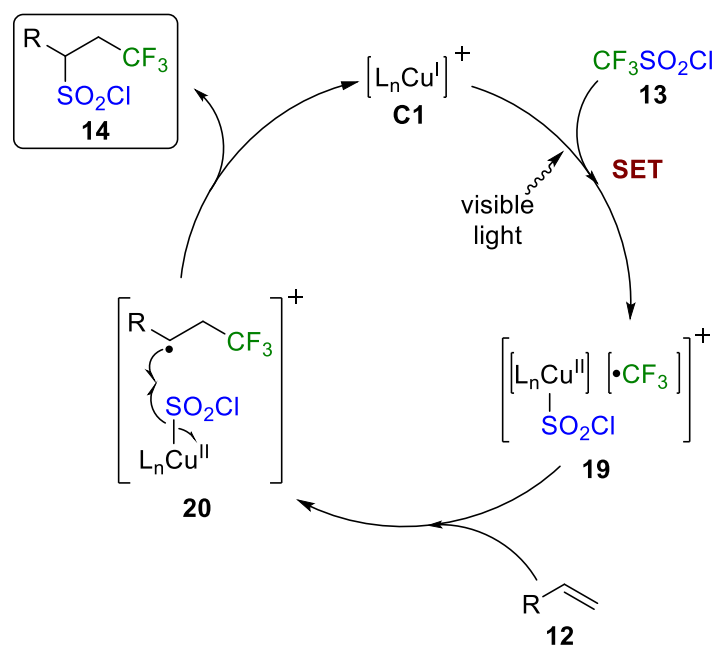
Scheme 6. Examples of visible-light-mediated trifluoromethylchlorosulfonylation (**14**) and trifluoromethylchlorination (**15**) of alkenes **12**.^[27]

Regarding this photocatalyzed reaction, it is remarkable that different photoredox catalysts furnish different products under otherwise unchanged reaction conditions. These results raise new questions concerning the reaction mechanism. For visible light mediated ATRA reactions two different commonly assumed mechanistic pathways are established (Scheme 7), both being initiated by a single electron transfer (SET) from photoexcited catalyst to an organohalide **4**.^[10,25,26,31,32,49] After fission of **4** under release of X⁻, the resulting radical **16** adds to an alkene **3** to form the carbon-centered radical **17**. In the photocatalytic cycle, the radical intermediate **17** is oxidized to a carbocation **18** with concurrent regeneration of the photocatalyst by back electron transfer. The recombination of cation **18** and the halide to the ATRA product **5** concludes the transformation. Alternatively, radical intermediate **17** can engage in a radical chain cycle with the organohalide **4**.



Scheme 7. General mechanism for photoredox catalyzed ATRA reactions illustrated on basis of the example of alkenes **3** and an oxidative photocatalytic quenching cycle.

The formation of chlorinated products **15**, for example using $[\text{Ru}(\text{bpy})_3]^{2+}$ via loss of sulfur dioxide, can be explained by such an established outer-sphere mechanism.^[27] After initial SET from photocatalyst to triflyl chloride (**13**), the resulting radical intermediate $(\text{CF}_3\text{SO}_2\text{Cl})^{\bullet-}$ is unstable under the reaction conditions and decomposes under loss of SO_2 to the $\text{CF}_3\text{-}$ radical and halide Cl^- . Subsequently, the general mechanism for photoredox catalyzed ATRA reactions is followed. However, this mechanism does not explain the formation of trifluoromethylchlorosulfonylation products **14** using copper catalysts, because SO_2 is retained in the product. With a quantum yield of 12% and the formation of different products depending on the catalyst employed, a free radical chain mechanism was ruled out.^[27] Therefore, an inner-sphere mechanism was proposed, in which SO_2Cl^- is coordinated directly to copper and stabilized (Scheme 8).^[27] Mainly due to the fact that the reaction is not stereospecific, initial single electron transfer from the photoexcited copper(I) catalyst **C1** to triflyl chloride (**13**) was assumed, resulting in the formation of copper(II) species **19**. After trifluoromethyl radical is added to the alkene, SO_2Cl is transferred to the resulting carbon-centered radical intermediate leading to sulfur dioxide containing product **14** and regeneration of the catalyst. The involvement of a substrate-coordinating copper intermediate is plausible as for example steric hindrance of substrate or catalyst disfavored the chlorosulfonylation reaction leading to increased amounts of chlorination product **15**.^[27,45]



Scheme 8. Proposed inner-sphere mechanism for $[Cu(dap)_2]Cl$ (**C1-CI**) catalyzed trifluoromethylchlorosulfonylation according to O. Reiser *et al.*^[27]

As a variation in this mechanistic proposal, the formation of a copper(III) intermediate can also be envisioned, which was already speculated for UV-mediated photocatalyzed ATRA reactions with CuCl by M. Mitani and co-workers^[50]. Over recent decades there has been considerable research into copper(III) species in organic catalysis, with proof and elucidation of organometallic copper(III) compounds as well as an increasing number of reports about reactions running assumedly via high-valent copper intermediates. The significance of copper(III) species for organic chemistry will be outlined in the next chapter.

3. Copper(III) Species in Organic Chemistry

Due to the limited stability of copper(III) complexes, their isolation and characterization has been elusive. The late transition element copper occurs in the oxidation states of 0, +1, +2, +3 and +4, whereby copper(0) and copper(IV) species are extremely rare.^[51,52] The most common oxidation states of copper are +1 and +2.^[51,53] Concerning the scarcer oxidation state +3, the copper(III) atom with d^8 electron configuration is dominated by coordination number four, mostly in a square-planar arrangement with different degrees of distortion, but several examples of pentacoordinated complexes are also reported.^[53–59] In contrast to these prevalent diamagnetic complexes, copper(III) complexes with an octahedral geometry show paramagnetic properties.^[53,54,59,60]

Until 2000, only a few examples of well-defined high-valent copper complexes had been reported. In the early years, Margerum and co-workers established the strategy of using anionic tetradentate ligands to force square-planar geometry (cf. compound **21**), which has been widely applied (Figure 2).^[53,54,61–65] Based on the same concept, porphyrins and corrole ligands have also been employed to stabilize copper(III).^[66]

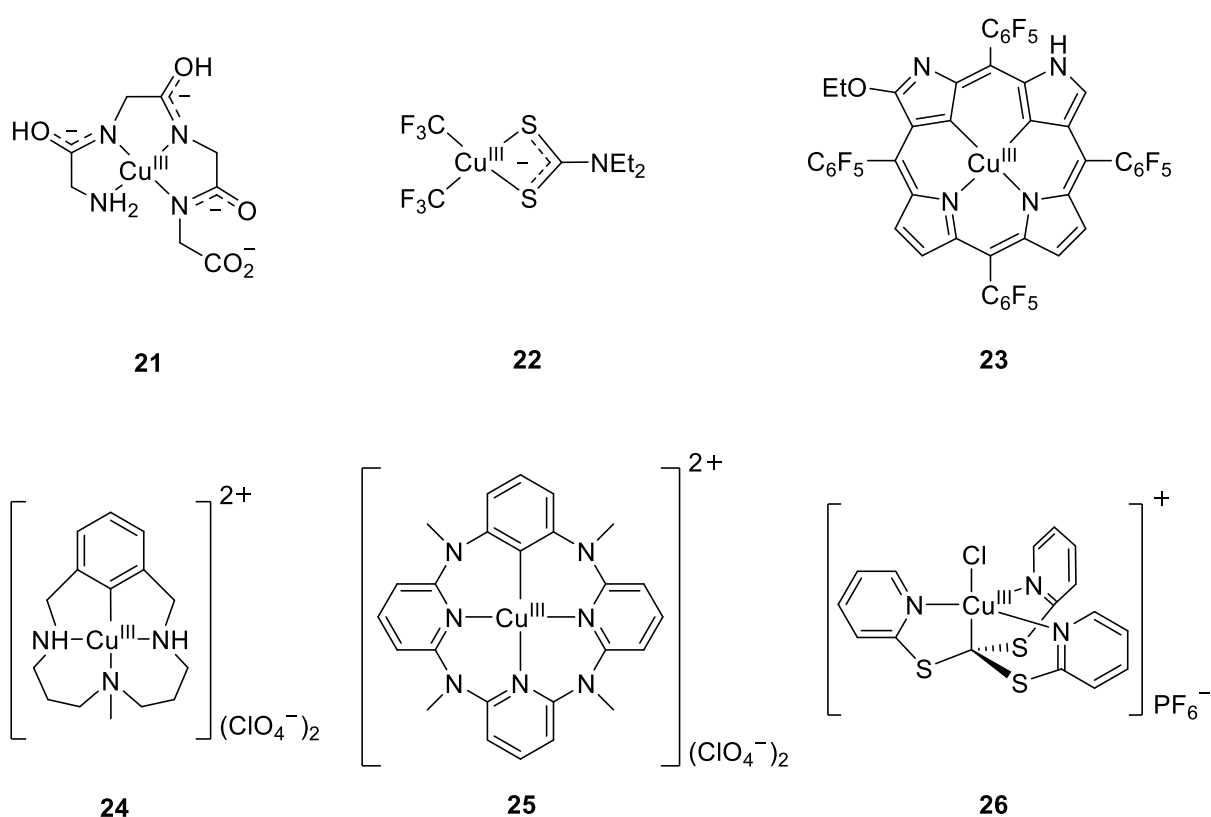


Figure 2. Selection of early examples of stable non-organometallic (**21**) and organometallic (**22** to **26**) copper(III) complexes.^[54,61–65]

In order to stabilize organometallic copper(III) complexes, that is complexes containing a carbon-copper bond, trifluoro- or perfluoroalkyl anionic ligands were initially used. In 1989, Burton and co-workers disclosed with the crystal structure of $[\text{Cu}^{\text{III}}(\text{CF}_3)_2(\text{SC}(\text{S})\text{NEt}_2)]$ (**22**) the first characterized organometallic copper(III) complex.^[62,67] Alternatively, carbaporphyrinoid systems such as the doubly *N*-confused porphyrin^[63] **23** are suitable ligands for stable high-valent organometallic copper complexes.^[53,66]

By using electron-donating triazamacrocyclic ligands, X. Ribas *et al.* were able to isolate the first monoaryl copper(III) complex **24**.^[64] In contrast to previous isolable copper(III) complexes, which do not have the characteristic reactivity attributed to copper(III) in catalysis^[68], this compound is reactive to bond formation such as $\text{C}_{\text{aryl}}\text{-nitrogen}$ ^[69], $\text{C}_{\text{aryl}}\text{-halide}$ ^[56] or even $\text{C}_{\text{aryl}}\text{-C}_{\text{sp}}$ ^[70] coupling.^[68] Investigations of this complex as well as of the bond forming reactions revealed that copper(III) can be actually catalytically relevant in copper-catalyzed cross-coupling reactions. With the disclosure of complex **25** by M.-X. Wang and co-workers in 2009^[65], the spectrum of aryl-copper complexes was extended with azacalix[1]arene[3]pyridine ligands.^[71] By means of this compound class it was possible to show the involvement of copper(III) intermediates in further transformations such as a catalytic halogenation and acyloxylation of aryl triflates or a C-H bond azidation.^[72] Thus, detailed studies on well-defined complexes showed that reductive elimination from aryl-copper(III) complexes occurs easily under mild reaction conditions (*vide infra*). With trigonal-bipyramidal, diamagnetic, tris(2-pyridylthio)methylcopper(III) (**26**), an example of less frequent pentacoordinated well-defined copper(III) complex was also reported.^[54] Remarkably, it was shown that it was possible to convert this complex into a paramagnetic octahedral copper(III) complex upon addition of chloride.

Over the past two decades, there have been notable developments in the observation and investigation of catalytically relevant copper(III) species in carbon-carbon and carbon-heteroatom bond formation reactions. High-valent copper compounds are often too short-lived for detection with standard spectroscopic techniques but computational studies often implicate copper(III) intermediates in the key bond-forming steps.^[68] With the introduction of rapid-injection NMR spectroscopy (RI-NMR), the direct detection of unstable organometallic copper(III) species (Figure 3) became possible in 2007 facilitating the mechanistic investigation of organocuprate reactions such as the conjugate addition reactions or ligand exchange reactions.^{[53,68,73], [74–77]}

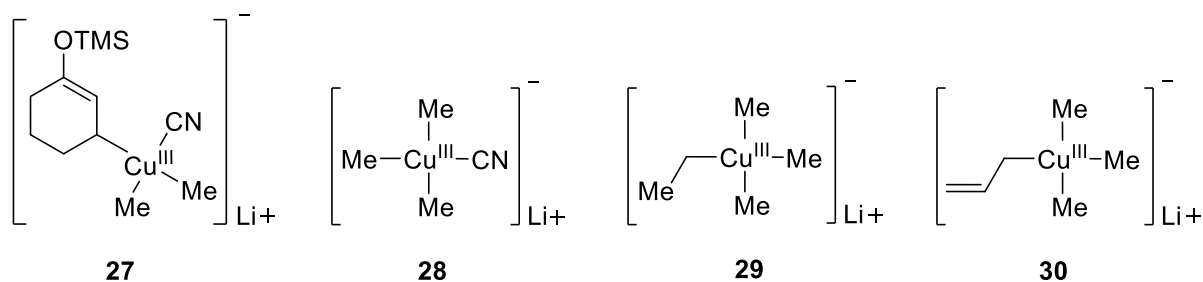


Figure 3. Copper(III) intermediates of organocuprate reactions detected by rapid-injection NMR spectroscopy at low temperatures.^[74–77]

In addition, the relevance of copper(III) oxidation state in copper-oxygen intermediates, especially in biological redox processes such as dioxygen activation, has been under discussion for some time. Since no spectroscopic or structural evidence exists in real biologic systems, over recent years well-defined synthetic copper-oxygen complexes have been prepared to obtain deeper mechanistic insights. In this context, examples of copper(III) complexes including multinuclear copper cores were reported (Figure 4), which underlines the existence of copper(III) species in biological systems.^[78,79,80]

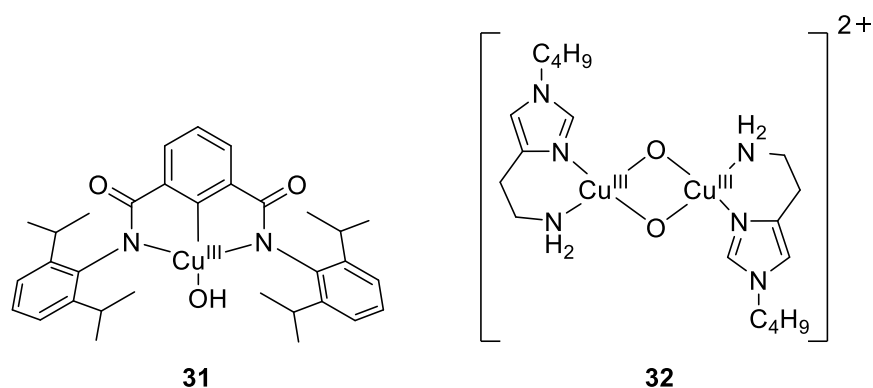
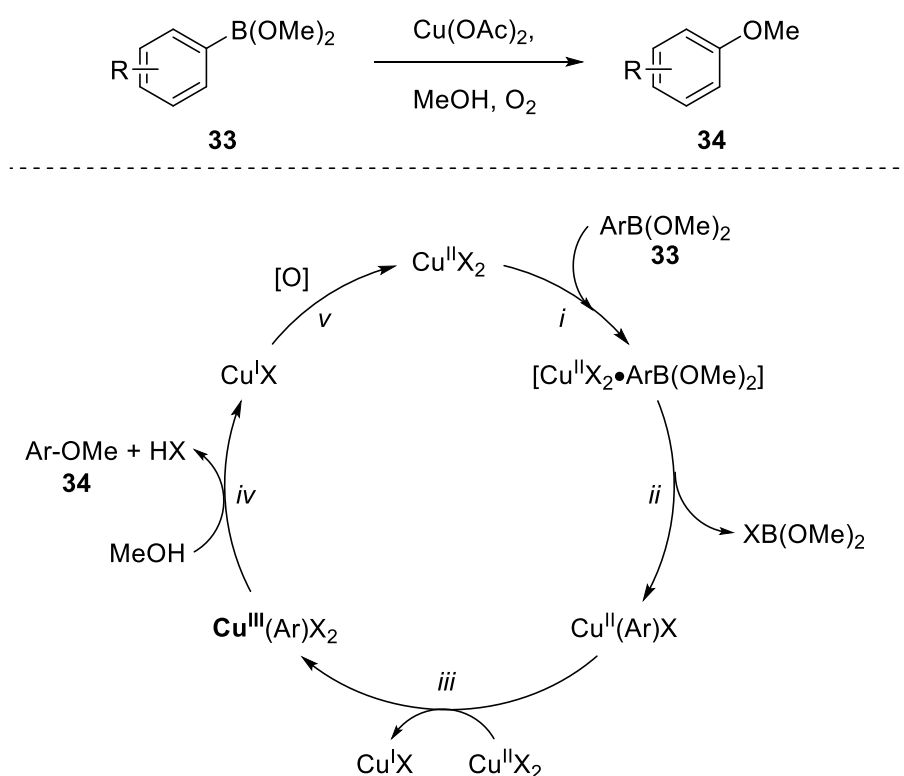


Figure 4. Selected examples of recently disclosed copper(III)-oxygen complexes.^[78,79]

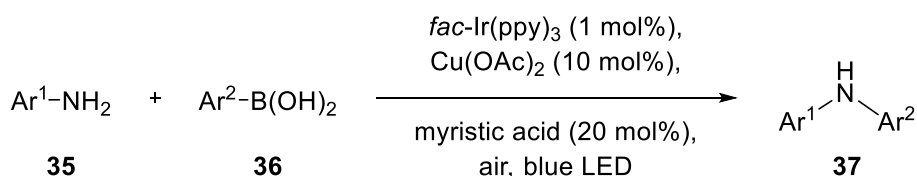
With the help of well-studied complexes, the relevance of copper(III) species in many copper mediated organic reactions has been substantiated. The most important underlying reaction mechanisms will be subsequently discussed with reference to selected examples. In principle, the reaction mechanisms via high-valent copper species are assumed to proceed via a one- or a two-electron processes or a combination thereof.^[53,68,81–84] Thus, usually an active copper(I) species is formed by transmetalation or disproportionation which subsequently catalyzes product formation by oxidative addition and reductive elimination. Beyond that, SET even under involvement of radical intermediates is another possible pathway.

The Chan-Lam-Evans coupling reaction is a versatile method for oxidative coupling of aryl boronic acids with diverse nitrogen or oxygen based nucleophiles.^[85] Based on mechanistic studies by S. S. Stahl and co-workers, a mechanism via a one- and two-electron process involving a copper(III) species has been proposed (Scheme 9).^[84,86,87] After transmetalation of the aryl group from an aryl boronic ester **33** to copper(II), an aryl-copper(II) complex is formed (steps *i* and *ii*). A subsequent disproportionation reaction with another equivalent of $\text{Cu}^{\text{II}}\text{X}_2$ affords $\text{Cu}^{\text{I}}\text{X}$ and a copper(III) complex (step *iii*). Upon reaction of the copper(III) species with a nucleophile, reductive elimination takes place under release of product **34** (step *iv*). Finally, copper(II) is regenerated by aerobic oxidation (step *v*).



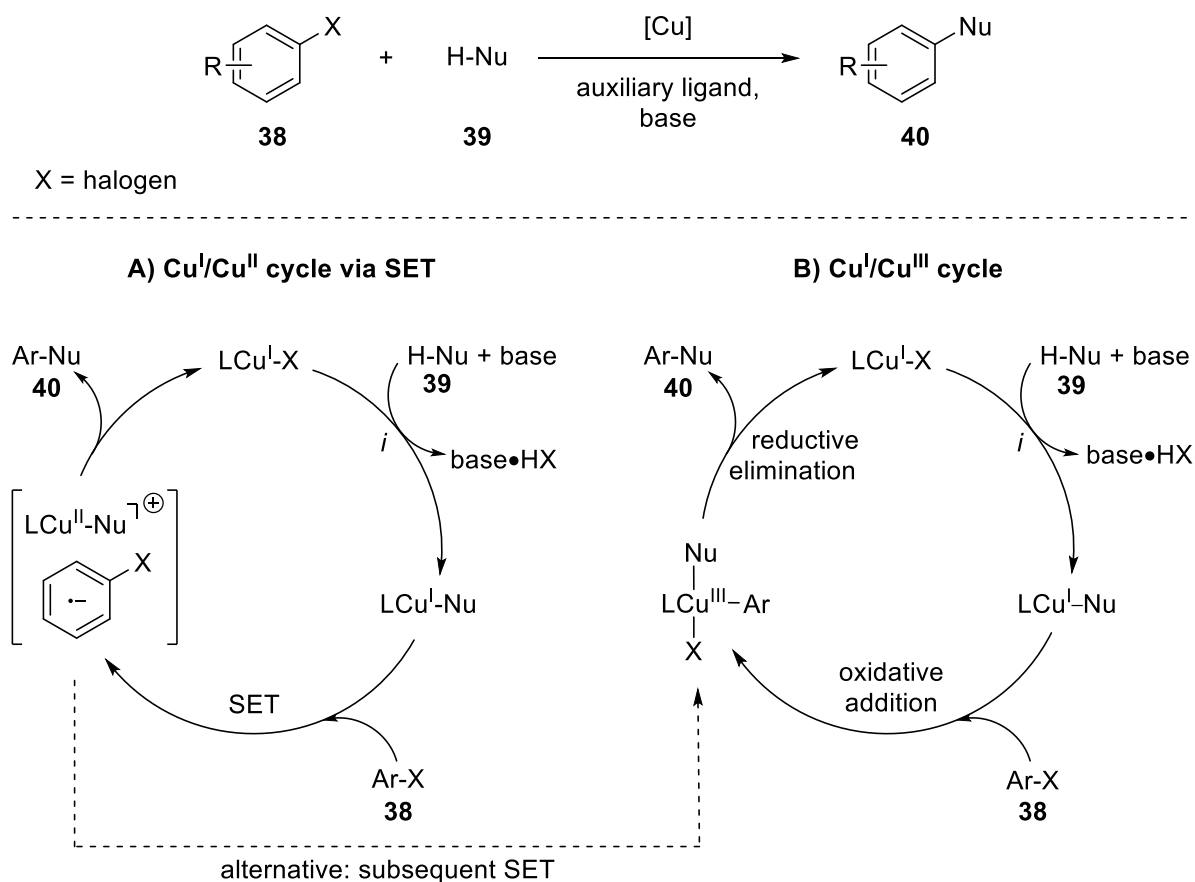
Scheme 9. Mechanistic proposal for Chan-Lam-Evans reactions between aryl boronic acids **33** and methanol as nucleophile.^[84,86]

This concept was recently used by S. Kobayashi *et al.* for a visible-light-mediated Chan-Lam procedure for the coupling of aryl boronic acids with anilines (Scheme 10).^[88] Since combining copper and photoredox catalysis expanded the substrate scope to electron-deficient aryl boronic acids **36**, the role of the photocatalyst *fac*- $\text{Ir}(\text{ppy})_3$ (**C4**) was proposed to be related to efficient turnover of the copper catalyst and to photoredox-mediated generation of a copper(III) complex.



Scheme 10. Visible-light-mediated Chan-Lam coupling according to S. Kobayashi *et al.*^[88]

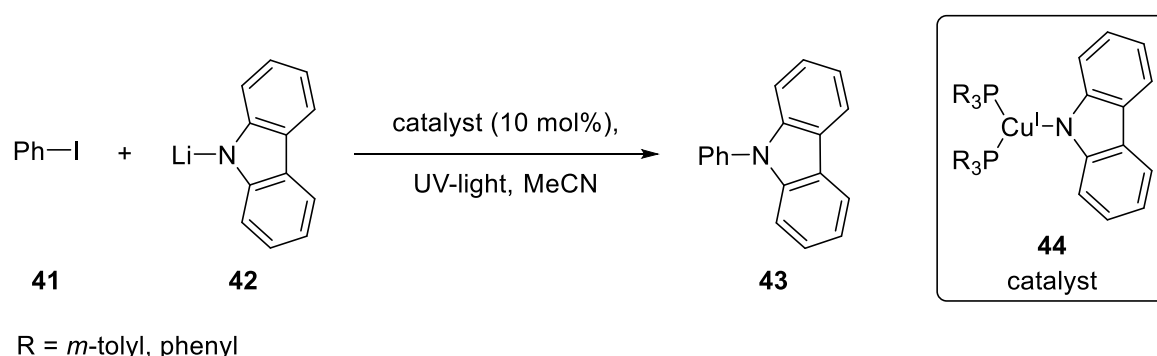
Ullmann coupling reactions of aryl halides, first disclosed in 1901, has evolved during the last century.^[89] Nowadays, besides the classical formation of biaryls, many examples of catalytic Ullmann-type coupling reactions between aryl halides **38** and a wide range of heteroatom nucleophiles **39** such as amides, amines, alcohols or thiols are available.^[90,91] The diversity of catalytic systems and conditions as well as of the ligands and substrates makes it difficult to propose one single mechanism for all Ullmann-type coupling reactions.^[53] The two main mechanistic proposals either run via radical intermediates, formed by SET, or via the more widely invoked two-electron redox process, as outlined in simplified form in Scheme 11.^[53,81,91,92]



Scheme 11. Simplified main mechanistic proposals for Ullman-type coupling reactions.

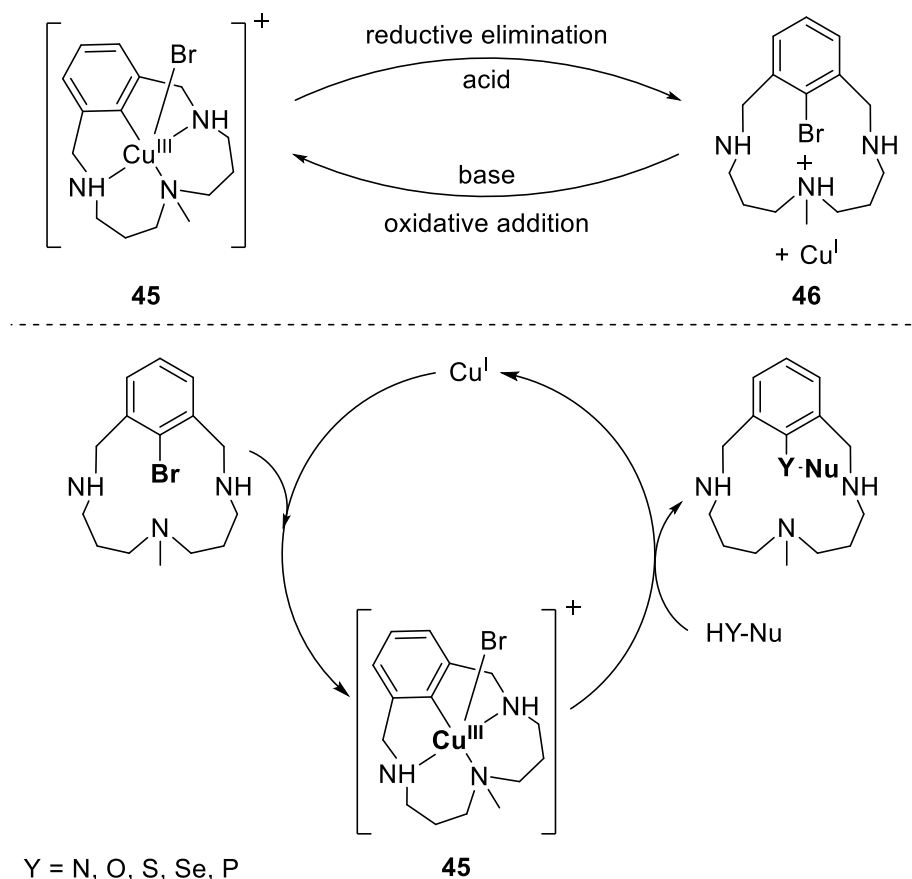
In mechanism **A**, SET from copper(I) nucleophile species to the aryl halide **38** furnishes a radical pair of an aryl halide and a copper(II) species. This radical pair can be either directly converted into product **40** accompanied by the reduction of copper(II) or could alternatively form a copper(III) intermediate after a subsequent SET step. Regarding mechanism **B**, after base mediated formation of a copper(I) nucleophile species (step *i*), oxidative addition of aryl halide **38** results in a copper(III) species. It should be noted that the coordination of the nucleophile may alternatively occur after the oxidative addition. Reductive elimination furnishes the product **40** under concurrent regeneration of the catalyst.

The photoinduced Ullmann-type C-N coupling reported by Peters, Fu and co-workers (Scheme 12) is an important example which supports the SET mechanism **A**.^[53,91,93] In this reaction system, SET to aryl halide **41**, initiated by excitation of a copper(I)-carbazolide complex **44** under irradiation with high-energy ultraviolet light, is proposed. The existence of a copper-containing radical and a radical pathway were in particular confirmed by EPR spectroscopy and a radical clock test with deuterated 2-(allyloxy)iodobenzene.



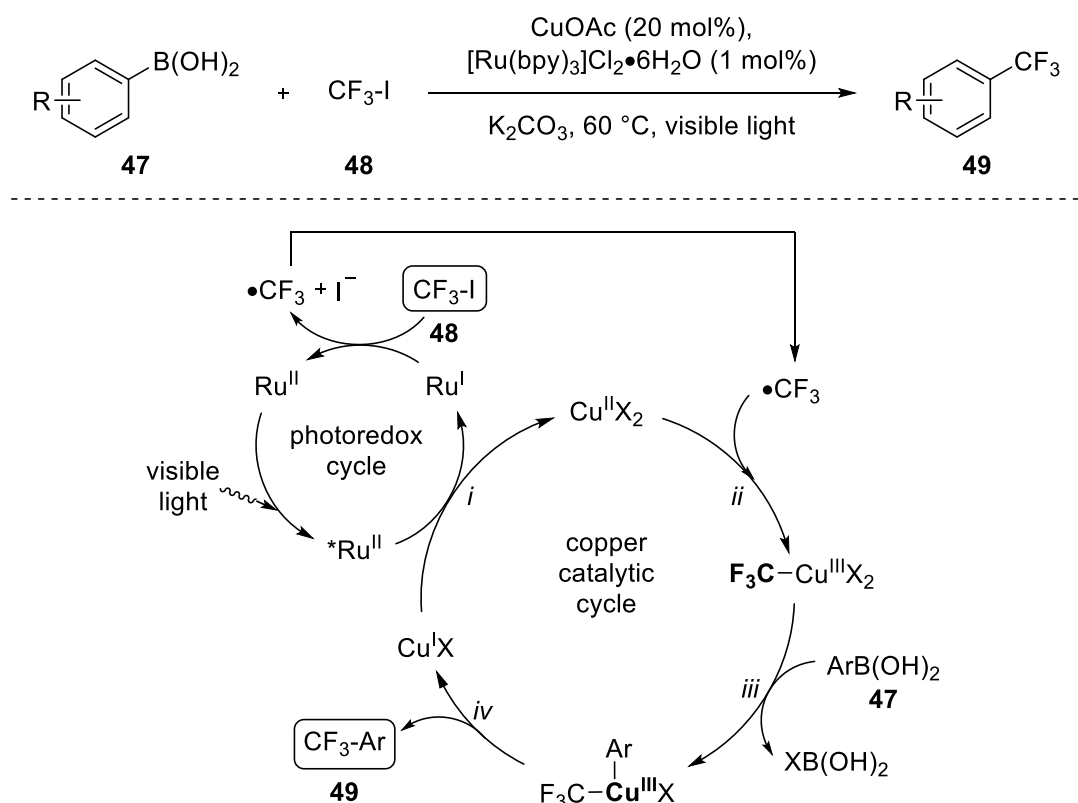
Scheme 12. Photoinduced Ullmann-type C-N coupling catalyzed by copper-carbazolide complex **44** according to Peters, Fu and co-workers.^[93]

The relevance of the two-electron redox process via Cu(III) intermediates was particularly supported by the studies of Stahl, Ribas and co-workers on the basis of well-defined macrocyclic copper(III) complexes.^[53,56,69,91] The first direct observation of Cu^I/Cu^{III} steps relevant to Ullmann-type coupling reactions, for instance, was made on a square-pyramidal pentacoordinated copper(III) complex^[56] **45**, which showed under acidic conditions reductive elimination (Scheme 13).^[53,91] This process was reversible by the addition of a base, which demonstrates on the other hand the oxidative addition of an aryl halide **46** to copper(I). The relevance of this copper(III) halide species **45** under catalytic conditions was demonstrated on the basis of coupling reactions with various nucleophiles.^[56,94]



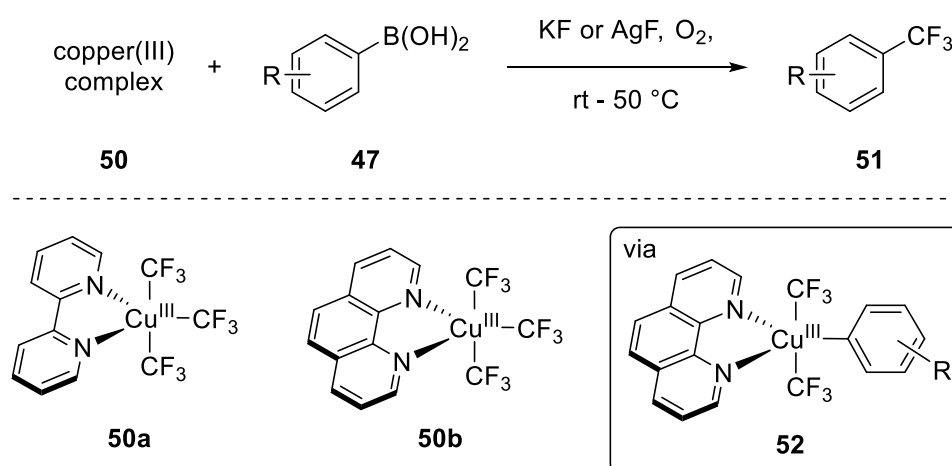
Scheme 13. Direct observation of copper(III) halide species **45** in cross-coupling reactions relevant to Ullmann-type coupling reactions.

In 2012, M. S. Sanford and co-workers disclosed a copper-catalyzed cross-coupling of boronic acids **47** and perfluoroalkyl iodides, merged with a ruthenium catalyzed photocatalytic cycle (Scheme 14).^[95] The proposed mechanism is initiated by photoexcited ruthenium catalyst, which oxidizes the copper(I) species by SET (step *i*). The Ru^{I} complex thereby obtained subsequently generates in the photoredox cycle the trifluoromethyl radical by reduction of CF_3I (**48**). This radical is trapped by the formed copper(II) species resulting in a copper(III) complex (step *ii*). After transmetalation (*iii*) with a boronic acid **47**, reductive elimination (*iv*) furnishes the trifluoromethylated product **49** under regeneration of copper(I).



Scheme 14. Trifluoromethylation of boronic acids **47** according to M. S. Sanford *et al.*^[95]

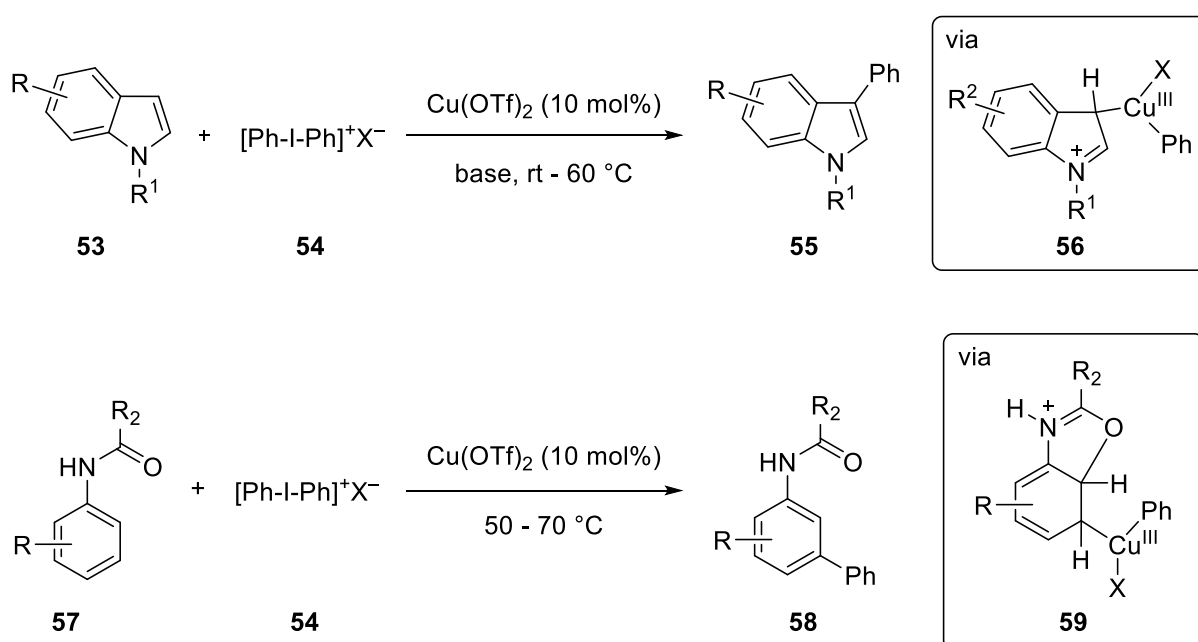
The involvement of a trifluoromethyl-copper(III) species in trifluoromethylation of arylboronic acids **47** was substantiated a few years later by the studies of S.-L. Zhang *et al.* (Scheme 15).^[58] The operational simple synthesis and characterization of stable copper(III) complex **50a** had recently been developed by V. V. Grushin and co-workers.^[57]



Scheme 15. Trifluoromethylation of arylboronic acids **47** using well-defined copper(III) complexes **50**.^[57,58]

Using a stoichiometric amount of well-defined trifluoromethyl-copper(III) complexes **50**, both showing unusual pentacoordinated trigonal bipyramidal geometry, the trifluoromethylation of preferentially *para*-substituted electron-rich arylboronic acids was possible under oxidative conditions.^[58] Based on experimental observations, the authors suggested a reaction mechanism which runs via reductive elimination of key intermediate **52**, formed by transmetallation with boronic acid **47** in the presence of a fluoride salt.

Due to deeper understanding, over recent years more and more reports about direct C-H functionalization with organocopper complexes and subsequent C-C bond forming as well as C-heteroatom cross-coupling reactions have been published in which copper(III) intermediates are proposed.^[82,83,96] For example, M. J. Gaunt and co-workers reported a mild process for the arylation of indoles^[97] **53** and *meta*-selective arylation of anilides^[98] **57** under copper(II)-catalysis using iodonium salts **54** as an oxidant (Scheme 16). After the formation of copper(I) – formed *in situ* under the reaction conditions – the mechanism is proposed to proceed via an aryl-copper(III) species (**56**, **59**) which is obtained by oxidation with iodonium salt **54**. Rearomatization and reductive elimination furnish the corresponding product under regeneration of copper(I).



R¹ = H, CH₃; X = BF₄, OTf

Scheme 16. Arylation reactions under oxidative conditions reported by M. J. Gaunt and co-workers.^[97,98]

As demonstrated above, organometallic copper(III) species are extensively assumed, and nowadays even proven in several instances, to be present in various important organic

coupling reactions. The involvement of such species in visible-light-mediated reactions has also been shown, which reinforces the assumption that copper(III) intermediates can play an important role in photoredox processes with copper-based photocatalysts. In the standard photoredox cycle of copper(I) complex $[\text{Cu}(\text{dap})_2]^+$ (**C1**), for example, copper(II) complex is formed via oxidative quenching which could be transformed to a transient copper(III) species by addition of a radical. On the other hand, it is also possible that oxidative addition takes place at copper(I) complex, again leading to a copper(III) species.

2. Outline of this Study

Since its discovery in 1983 ^[24], $[\text{Cu}(\text{dap})_2]^+$ (**C1**) has emerged as a promising photo redox catalyst, especially in ATRA reactions. With a redox potential of -1.43 V^2 , in the oxidative quenching cycle, $[\text{Cu}(\text{dap})_2]^+$ (**C1**) is an efficient reductant comparable to iridium- or ruthenium-based photocatalysts.^[10,19] However, it has not been possible to transform substrates with stronger reduction potentials such as benzyl bromide (-1.85 V^2)^[99] with this catalyst (Figure 5).

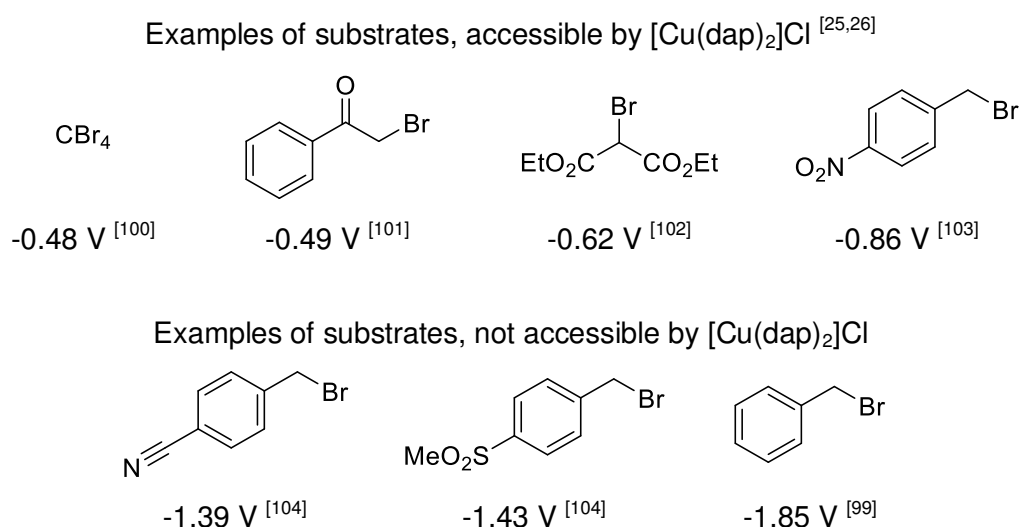


Figure 5. Reduction potentials of various substrates which are attractive for photoredox catalyzed processes. Data reported vs. SCE in MeCN.

In order to extend the scope of copper photoredox catalysts and make such substrates accessible, the first objective of this thesis was to develop a more strongly reducing catalyst. For this purpose, modifications in the core structure of dap ligand were tested and an alternative new diaza-butadiene ligand was investigated for photoredox applications.

With reference to the trifluoromethylchlorosulfonylation of alkenes developed by O. Reiser *et al.* (Scheme 6), completely new products were accessible using copper-based photoredox catalysts, which points to special features of copper providing unique opportunities. As the unusual product formation under copper catalysis cannot be explained by established outer-sphere mechanisms of photoredox catalyzed ATRA reactions, an inner-sphere mechanism was proposed, but the involvement of copper(III) intermediates can also be considered. For a deeper understanding of a potential new reaction mechanism and in order to obtain access to other new transformations, a focus was placed on a search for further reagents which

² vs. saturated calomel electrode (SCE) in MeCN

might show similar reactivity to successful triflyl chloride (**13**). In addition, with regard to potential copper(III) intermediates in photoredox catalysis, the synthesis and investigation of a new copper(II) complex was targeted. On the basis of the example of the visible-light-mediated chloramination reaction, the exclusive reactivity of copper in photoredox catalysis was elucidated by comparison with the non-catalyzed photoreaction and an iridium catalyst driven photoreaction.

B. Synthesis, Characterization and Application of New Diimine-Based Copper Complexes

1. Introduction

As outlined in the introductory chapter A, efficient protocols for using $[\text{Cu}(\text{dap})_2]^+$ (**C1**, Figure 6) as a photoredox catalyst in an oxidative quenching cycle have been developed during the last decade. However, with an excited state reduction potential of -1.43 V vs. SCE in MeCN, the substrate scope of **C1** is limited compared to more strongly reducing catalysts.^[10,19] In order to make electron-poor substrates with higher reduction potentials, such as benzyl bromide (-1.85 V vs. SCE in MeCN)^[99], accessible by copper-based photoredox catalysis, the first objective was to increase the catalyst's reduction potential.

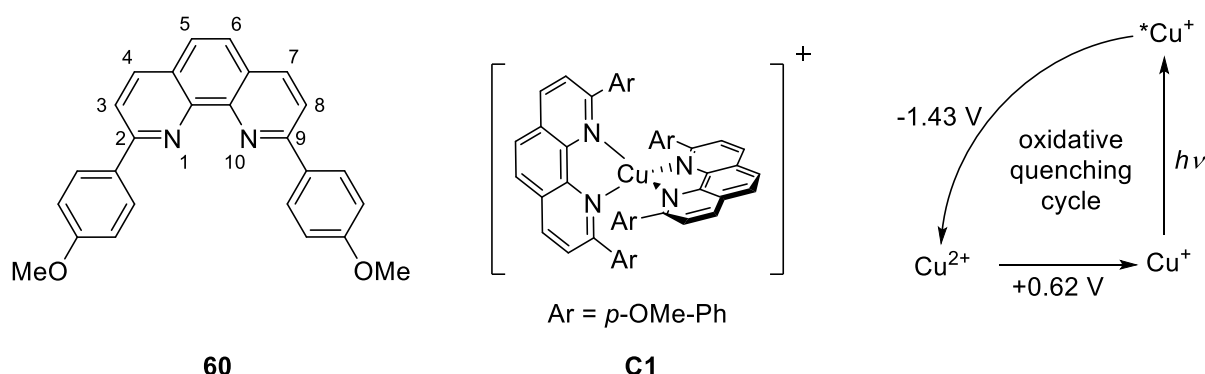
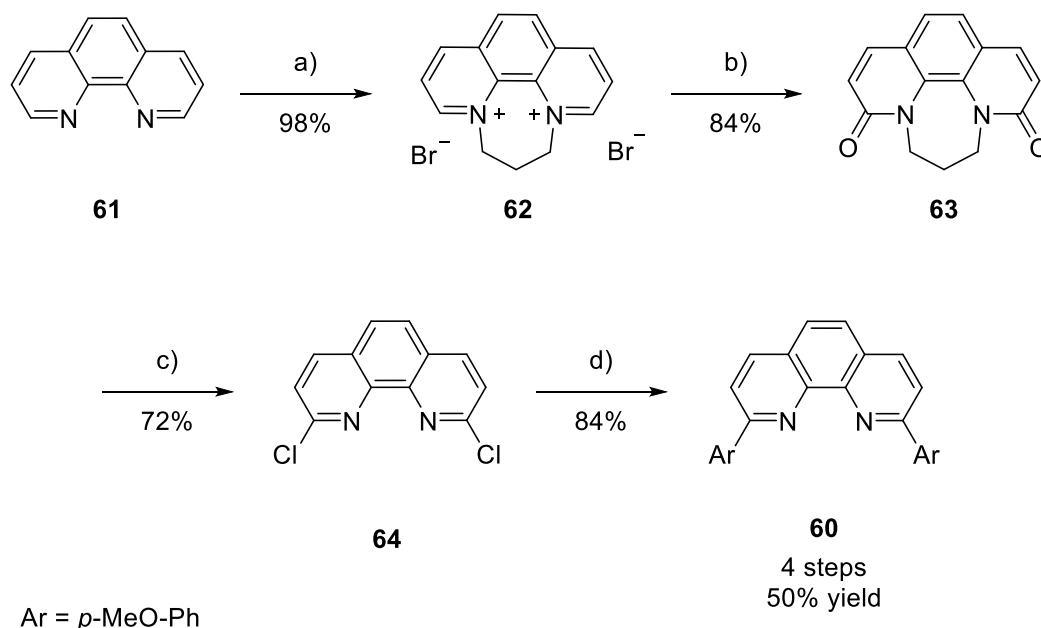


Figure 6. Dap (**60**) (2,9-bis(*para*-anisyl)-1,10-phenanthroline) and $[\text{Cu}(\text{dap})_2]^+$ (**C1**) with the corresponding redox potentials^[19] (reported vs. SCE in MeCN).

In general, photoredox catalysts have to show some special properties. In order to obtain access to mild reaction conditions, which means that harsh and energy-rich UV-light is avoided, the catalyst has to absorb in the visible range of the electromagnetic spectrum to form the excited state. In addition, the excited state lifetime has to be long enough for chemical reactions. Lastly, the redox potentials must be strong enough to transform substrates. The well-investigated system of $[\text{Cu}(\text{dap})_2]^+$ (**C1**) fulfills basically all of these properties. However, a more negative reduction potential of the excited state is necessary to make electron-poor substrates accessible as well. The photophysical properties and redox potentials of a photocatalyst can be rendered by modifications of the ligand.^[10,105,106] Using an efficient route^[25,107], it has already been possible to synthesize the dap ligand (**60**) in only four steps in a good yield of 50% as disclosed by T. Rawner in 2016^[47] (Scheme 17). As this ligand was easily accessible, the first approach aimed at extending the scope of copper-dap catalysts by modifications of dap (**60**).



a) 1,3-dibromopropane (5.0 equiv), nitrobenzene, 125 °C, 5 h. b) KO^tBu (4.2 equiv), ^tBuOH, 40 °C, 21 h. c) PCl₅ (2.0 equiv), POCl₃, 150 °C, 21 h. d) (4-methoxyphenyl)boronic acid (2.2 equiv), [Pd₂(dba)₃] (1.2 mol%), PPh₃ (5.0 mol%), K₂CO₃ (2.2 equiv), glyme/H₂O (10/1 v/v), 100 °C, 48 h.

Scheme 17. Known synthesis of dap (**60**).^[47]

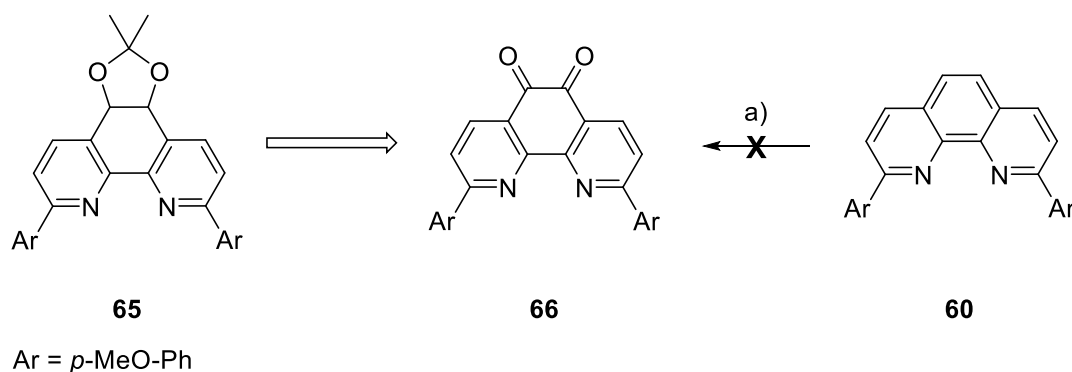
Copper(I) diimine complexes often suffer from short excited state lifetimes, because of a reorganization of the excited state from a tetrahedral to a square-planar geometry.^[105,108] Substitution with bulky substituents, for instance, in 2,9-position of the phenanthroline system hampers such a structural change and consequently the non-radiative relaxation to the ground state.^[108] For this reason, the presence of a bulky *para*-anisyl-group in 2,9-position is necessary for the catalytic properties of the system. T. Rawner screened in his PhD thesis different symmetric methoxy substitution patterns on the aryl group in 2,9-position and tested the resulting catalytic performance of the new complexes in ATRA reactions.^[47] As the established phenanthroline system with *para*-anisyl-groups proved to be the most efficient one, modifications in the 5,6-position are of special interest as the promising dap core structure can be retained. Thus, it is possible to compare the effects of the substituents regarding reduction potentials, the lifetime of the excited state as well as the catalytic activity of the new complexes.

Besides 2,9-phenanthrolines, 1,4-disubstituted 1,4-diaza-1,3-butadienes (DABs) are another easily accessible class of nitrogen chelates. As such ligands can form stable complexes with copper(I) which show promising photophysical properties, their fundamental application for photoredox catalysis was explored as well.^[109] Furthermore, with copper(II) complex [Cu(dap)Cl₂] (**C10**), the role of the oxidation state of copper in the ground state for photoredox catalysis was investigated.

2. Synthesis of Modified Phenanthroline Ligands and Complexation with Copper

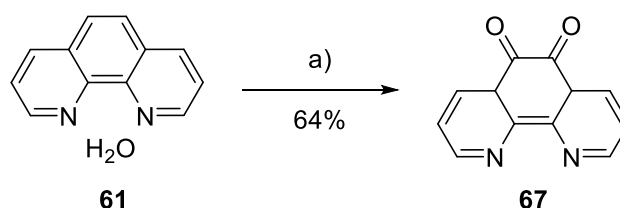
2.1 Synthesis of $[\text{Cu}(\text{dapacetal})_2]^+$

The electronic structure of ligands has a strong influence on the redox potentials of a complex. In principle, electron-donating substituents on the ligands can render complexes more strongly reducing.^[13] In order to increase the reduction potential of $[\text{Cu}(\text{dap})_2]\text{Cl}$ (**C1-Cl**), it was first planned to insert electron-pushing groups into the existing ligand system with the synthetic strategy focusing on easily accessible ether moieties. Regarding the later potential application as a catalyst, an acetal protecting group is beneficial because it makes the ligand less reactive to possible side reactions during catalysis. As 2-nitropropane had already been used as a protecting group for 5,6-dions of phenanthrolines by J.-P. Sauvage *et al.*^[107], dapacetal (dapacetal = 6,9-bis(4-methoxyphenyl)-2,2-dimethyl-[1,3]dioxolo[4,5-*f*][1,10]phenanthroline, **65**) was chosen as the target compound (Scheme 18). Due to the fact that the synthesis of the dap ligand was already reported in an efficient route (Scheme 17), in a first attempt the direct insertion of oxygen in 5,6-position of dap ligand (**60**) was carried out.



a) Dap (**60**) (1.0 equiv), $\text{H}_2\text{SO}_4/\text{HNO}_3$ (2/1 v/v), KBr (1.5 equiv), 110 °C, 3 h, complex reaction mixture.

Scheme 18. First strategy towards the target compound **65** via direct oxidation of dap ligand (**60**).

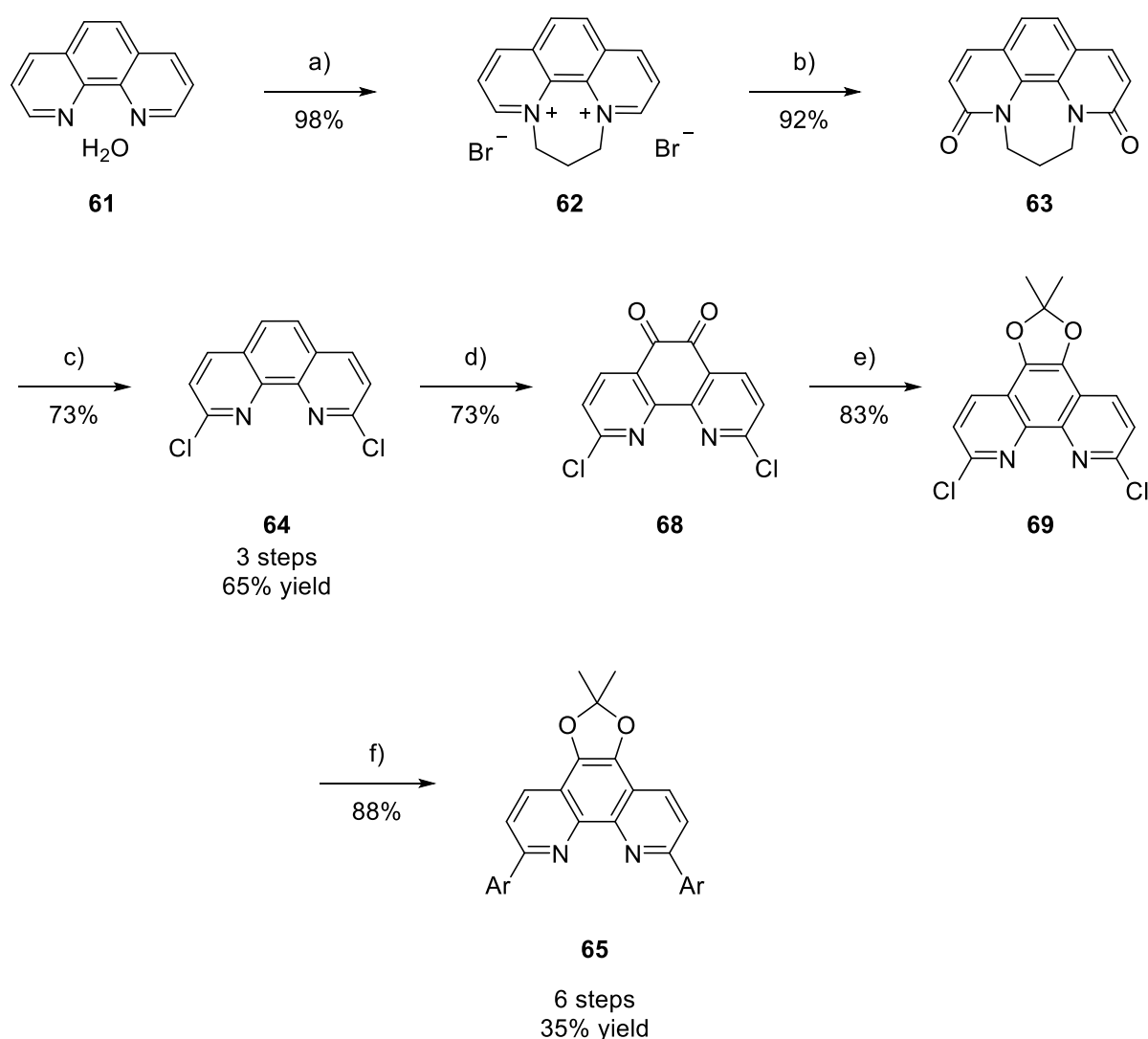


a) 1,10-phenanthroline monohydrate (**61**) (1.0 equiv), $\text{H}_2\text{SO}_4/\text{HNO}_3$ (2/1 v/v), KBr (1.5 equiv), 110 °C, 3 h.

Scheme 19. Oxidation of 1,10-phenanthroline (**61**).

The direct oxidation of 1,10-phenanthroline with $\text{H}_2\text{SO}_4/\text{HNO}_3$ and KBr had already been reported in literature^[107,110] and could be reproduced in a 64% yield (Scheme 19). However, this procedure failed for the oxidation of dap (**60**) and only a complex reaction mixture was obtained.

In order to obtain dapacetal (**65**), an alternative route had to be followed (Scheme 20). The synthetic route for compound **65** runs via 2,9-dichloro-1,10-phenanthroline (**64**), the key intermediate in the literature known dap synthesis^[47] (cf. Scheme 17).



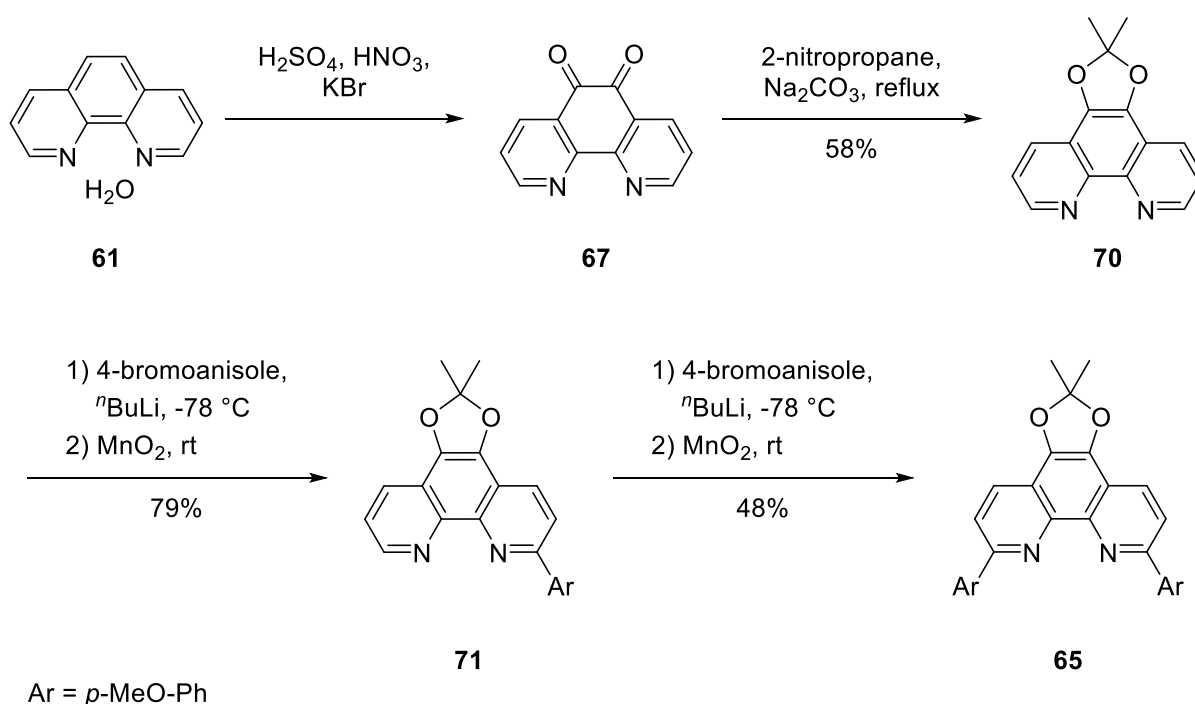
Ar = *p*-MeO-Ph

a) 1,3-dibromopropane (5.0 equiv), nitrobenzene, 130 °C, 6 h. b) KO^tBu (4.2 equiv), air, $^t\text{BuOH}$, 40 °C, 24 h. c) PCl_5 (2.0 equiv), POCl_3 , 145 °C, 15 h. d) $\text{H}_2\text{SO}_4/\text{HNO}_3$ (2/1 v/v), KBr (10.0 equiv), 0 – 80 °C, 3 h. e) 2-nitropropane (10.0 equiv), Na_2CO_3 (8.0 equiv), $\text{MeCN}/\text{H}_2\text{O}$ (1/1 v/v), 55 °C, 15 h. f) (4-methoxyphenyl)boronic acid (2.2 equiv), $[\text{Pd}_2(\text{dba})_3]$ (1 mol%), PPh_3 (4 mol%), K_2CO_3 (2.2 equiv), glyme/ H_2O (10/1 v/v), 100 °C, 63 h.

Scheme 20. Synthesis of dapacetal (**65**).

Intermediate **64** was formed in 3 steps in 65% yield. After the protection of 1,10-phenanthroline monohydrate (**61**) with 1,3-dibromopropane, the oxidation to the 3,9-dione **63** with potassium *tert*-butoxide and oxygen followed. In the end, the reaction with PCl_5 and POCl_3 furnished the key intermediate **64** which was oxidized to the 5,6-dione **68**. Since **68** is prone to degradation to a fluorenone derivative under basic conditions^[111], it has to be acetal protected before the Suzuki-Miyaura cross coupling^[47,112]. Finally, starting with 1,10-phenanthroline monohydrate (**61**), the modified phenanthroline ligand dapacetal (**65**) was accessible in 6 steps in 35% overall yield.

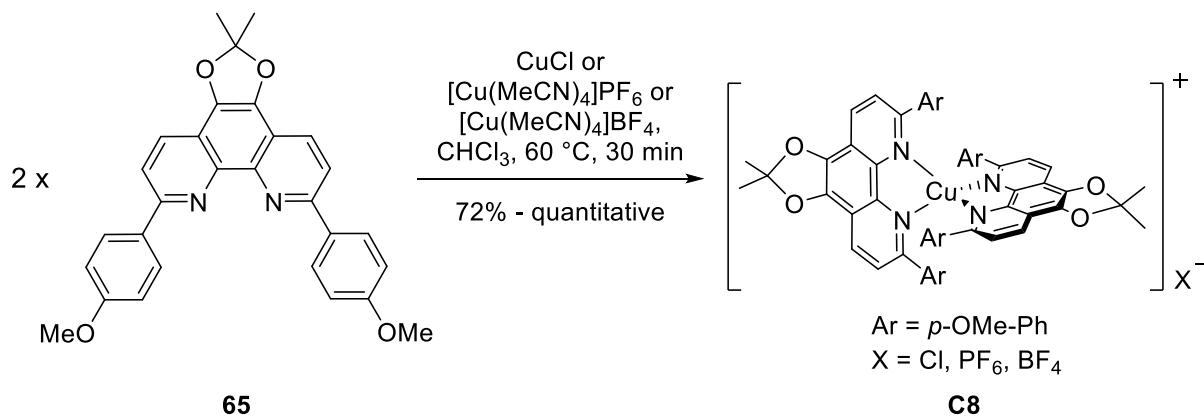
It should be noted that the work in this thesis had already been in progress before S. Rau *et al.* published the synthesis of dapacetal (**65**) via a different route (Scheme 21).^[113] Starting from 1,10-phenanthroline (**61**) and using organolithium reagents for the C-C coupling reactions in 2,9-position followed by oxidation with manganese oxide, this group achieved the synthesis in 4 steps with approximately 12%³ overall yield. Although the sequence is longer, the route demonstrated in this present thesis leads, with 35%, to much higher yields.



Scheme 21. Synthesis of dapacetal (**65**) according to S. Rau *et al.*^[113] No yield was reported for the oxidation of 1,10-phenanthroline (**61**).

³ S. Rau *et al.* reported no yield for the oxidation of 1,10-phenanthroline.^[113] Therefore the overall yield was estimated under the assumption that the oxidation of 1,10-phenanthroline furnished 55% of 1,10-phenanthroline-5,6-dione as reported by J.-P. Sauvage *et al.*^[107]

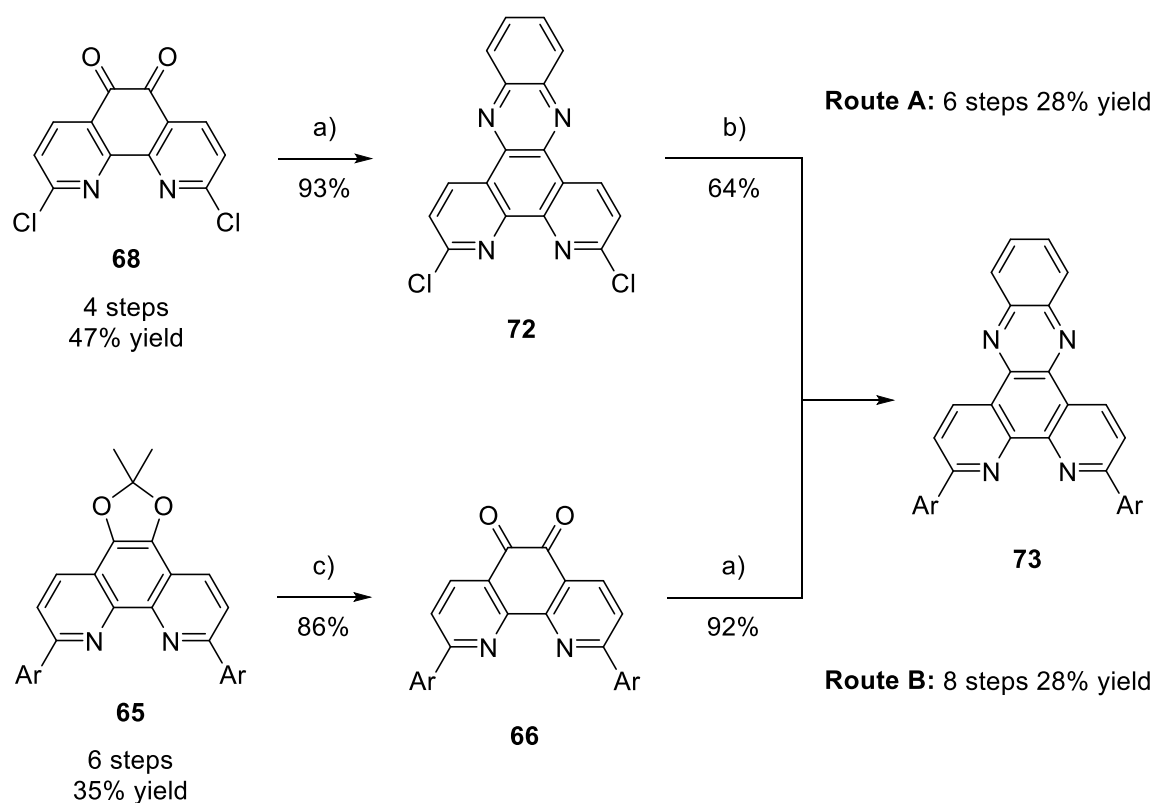
The copper complex $[\text{Cu}(\text{dapacetal})_2]^+$ (**C8**) was synthesized by mixing ligand **65** with a copper(I) salt (Scheme 22). Suitable crystals for X-ray structure analysis were obtained by vapor diffusion of diethyl ether into a dichloromethane solution.



Scheme 22. Synthesis of $[\text{Cu}(\text{dapacetal})_2]^+$ (**C8**).

2.2 Synthesis of [Cu(phenazino-dap)₂]⁺

Electrochemical and photophysical investigations revealed that [Cu(dapacetal)₂]⁺ (**C8**) has a slightly weaker excited state reduction potential than [Cu(dap)₂]⁺ (**C1**), which was not expected (*vide infra*). Due to these results, the question arose as to whether it would be possible to influence the electrons on the nitrogen atoms of the phenanthroline core by variations on the 5,6-position. In order to check this concept, the opposite direction was targeted and electron-withdrawing groups were to be inserted. In addition to this, the aim was now to improve the catalytic performance by expansion of the ligands π -system. The phenazine part is known to have an electron-withdrawing effect to the bipyridine system of the ligand.^[11] This can lead to an efficient charge separation in the excited state which might be beneficial for photochemical reactions.^[11] In 1992, Yamada *et al.* reported the condensation of 2,9-dichloro-1,10-phenanthroline-5,6-dione (**68**) with 1,2-diaminobenzene to 3,6-dichlorodipyrido[3,2-*a*:2',3'-*c*]phenazine (**72**) in 69% yield.^[11] This reaction was used to obtain the target structure phenazino-dap (phenazino-dap = 3,6-bis(4-methoxyphenyl)dipyrido[3,2-*a*:2',3'-*c*]phenazine, **73**) in a short sequence (Scheme 23).

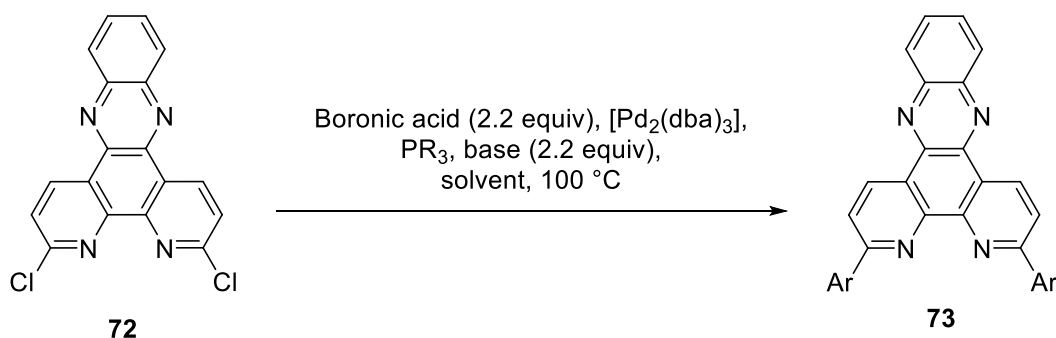


a) 1,2-Diaminobenzene, anhydrous EtOH, 95 °C, 1 – 3.5 h. b) (4-methoxyphenyl)boronic acid (2.2 equiv), [Pd₂(dba)₃] (1 mol%), PPh₃ (4 mol%), K₂CO₃ (2.2 equiv), toluene/H₂O (10/1 v/v), 100 °C, 63 h. c) Trifluoroacetic acid/H₂O (2/1 v/v), O₂ (1 bar), 50 °C, 15 h.

Scheme 23. Optimization of the synthesis of phenazino-dap (**73**).

The first strategy was to condense the 5,6-dione intermediate **68** of the dapacetal synthesis (cf. Scheme 20) before Suzuki-Miyaura cross coupling^[47,112,114] with (4-methoxyphenyl)boronic acid (Scheme 23, route A). The condensation of compound **68** with 1,2-diaminobenzene worked with 93% in excellent yield. In order to obtain satisfactory amounts of the product for further tests, the subsequent Suzuki-Miyaura cross coupling was optimized by short screening. Table 2 depicts the different reaction conditions which were tested. However, the Suzuki coupling turned out to be problematic for bigger reaction scales because solvent-consuming column chromatography is necessary for purification. This purification step requires a considerable amount of solvent given that both the product **73** and the starting material **72** are not soluble in most organic solvents, or only to a very limited extent.

Table 2. Screening of Suzuki-Miyaura cross coupling conditions.^a



Entry	Solvent	c(SM) / mol/L	Base	Phosphine	Time	Yield / %
1 ^{b)}	1,4-dioxane/H ₂ O 2/1	0.04	K ₃ PO ₄	PCy ₃	24 h	23
2	glyme/H ₂ O 10/1	0.05	K ₂ CO ₃	PPh ₃	63 h	44
3	toluene/H ₂ O 10/1	0.05	K ₂ CO ₃	PPh ₃	63 h	64

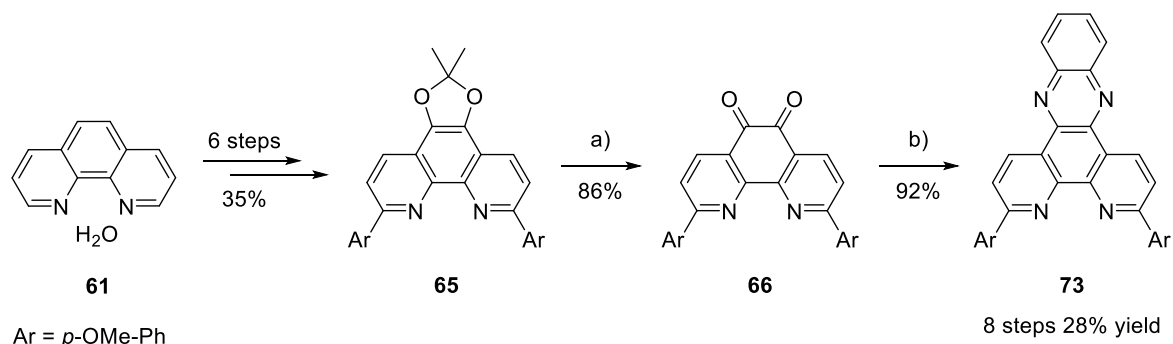
a) Reaction conditions: (4-methoxyphenyl)boronic acid (2.2 equiv), [Pd₂(dba)₃] (1 mol%), PR₃ (4 mol%), base (2.2 equiv), solvent, 100 °C. b) Conditions taken from Herron *et al.*^[114]; 2 mol% of [Pd₂(dba)₃] were used; the mono coupled product was formed as a byproduct.

Due to the limits of the reaction scale for route A, an alternative route B was tested (Scheme 23). This route starts with dapacetal (**65**) where the aryl moieties in 5,6-position are already coupled. After the deprotection to the 5,6-dione **66**, the condensation with 1,2-diaminobenzene results in product **73**. The deprotection of the acetal protected intermediate **65** was tested in two different ways. Deprotection to the diol using HCl in a mixture of chloroform and methanol⁴ at room temperature and 24 h reaction time was not possible. This shows the stability of the ligand against acidic conditions. In contrast to this, by means of

⁴ concentrated HCl/CHCl₃/MeOH = 1/4/5 (v/v/v)

diluted trifluoroacetic acid and oxygen^[107,113], the 5,6-dione **66** was obtained in 86% yield (step c). The purification problem does not occur with this route, because the hardly soluble phenazine derivative **73** is formed in the very last step and can be easily purified by washing. Consequently, route B takes two more steps, but provides the product in the same yield as route A with the advantage that the protocol can be used for bigger scales.

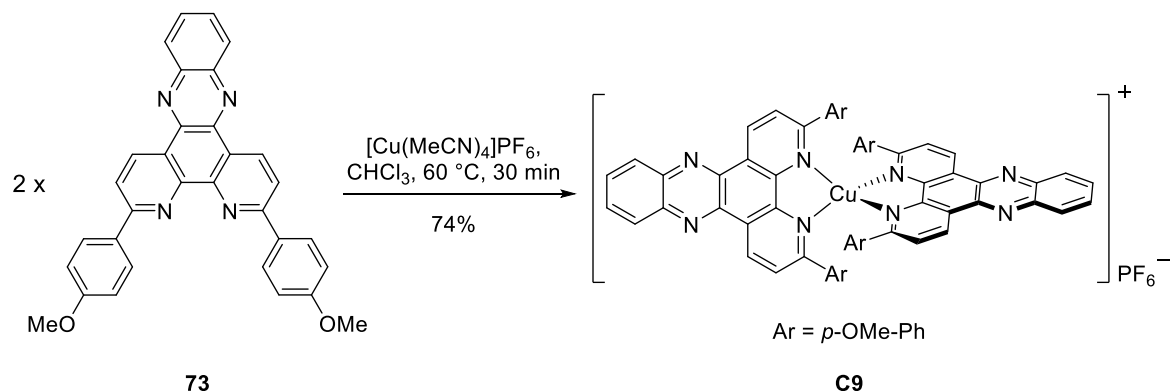
In summary, the optimized synthesis of phenazino-dap (**73**) (cf. route B) starts with dapacetal (**65**) which is synthesized from 1,10-phenanthroline hydrate (**61**) and which already bears the aryl moieties in 2,9-position (Scheme 24). After deprotection with trifluoroacetic acid and oxygen to the 5,6-dione **66**, the condensation with 1,2-diaminobenzene results in product **73** in a total of eight steps and 28% overall yield.



a) Trifluoroacetic acid/H₂O (2/1 v/v), O₂ (1 bar), 50 °C, 15 h. b) 1,2-Diaminobenzene (2.9 equiv), anhydrous EtOH, 95 °C, 3.5 h.

Scheme 24. Synthesis of phenazino-dap (**73**).

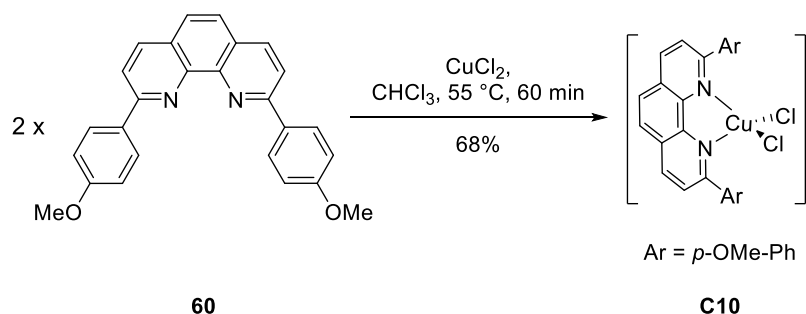
The formation and crystallization of the homoleptic copper(I) complex [Cu(phenazino-dap)₂]⁺PF₆⁻ (**C9-PF₆**) was possible by mixing ligand **73** with the corresponding copper(I) salt (Scheme 25). Suitable crystals for X-ray structure analysis were obtained by vapor diffusion of diethyl ether into a dichloromethane solution.



Scheme 25. Synthesis of [Cu(phenazino-dap)₂]⁺PF₆⁻ (**C9-PF₆**).

2.3 Synthesis of [Cu(dap)Cl₂]

In order to open the field of copper(II) complexes for photoredox catalysis, the first aim was to synthesize and isolate [Cu(dap)₂]Cl₂ which is the oxidized form of [Cu(dap)₂]Cl (**C1**). Since in both compounds copper is coordinated to the same ligands these complexes would be particularly beneficial for comparative studies. For the synthesis of [Cu(dap)₂]Cl₂, the standard protocol for the formation of copper phenanthroline complexes (*vide supra*) was applied and two equivalents of dap ligand were mixed with one equivalent of CuCl₂. However, it was only possible to isolate crystals of copper(II) complex [Cu(dap)Cl₂] (**C10**) (Scheme 26). Suitable crystals for X-ray structure analysis were obtained by liquid diffusion of diethyl ether into a dichloromethane solution. As reported by J.-P. Sauvage *et al.*, the divalent copper complex with dap ligand [Cu(dap)₂]²⁺ is accessible in solution in the presence of weak coordinating perchlorate or tetrafluoroborate anions, but when isolated it is quite unstable under ambient conditions and decomposition under loss of ligand occurs.^[115] Due to the synthetic results and the reported stability problems, the synthesis of [Cu(dap)₂]²⁺ was abandoned and investigation of the new complex **C10**, which is also a copper(II) analog of the established [Cu(dap)₂]Cl (**C1**), was pursued.



Scheme 26. Synthesis of [Cu(dap)Cl₂] (**C10**).

B. Wu, X.-J. Yang and co-workers reported in 2009 the synthesis and characterization of similar phenanthroline-based divalent copper complexes, such as [Cu(dpp)X₂] (**C11**) or [Cu(dnp)X₂] (**C12**) (dpp = 2,9-diphenyl-1,10-phenanthroline; dnp = 2,9-dinaphthyl-1,10-phenanthroline) (Figure 7).^[116] For synthesis, one equivalent of ligand and one equivalent of a copper(II) salt CuX₂ was mixed in tetrahydrofuran or dichloromethane at room temperature.^[116,117] As a special feature of such compounds, depending on solvent, steric hindrance of the ligand and on the type of the counterion, ligand (L) redistribution accompanied by reduction of copper can occur, resulting in the formation of copper(I) complexes [Cu(L)₂]⁺ (CuX₂)⁻ (**C13**).^[116,117] Regarding the conditions, this conversion is easier in acetone than in dichloromethane and the chloride ligands, as well as bulky groups in 2,9-position of the phenanthroline, hamper ligand redistribution. For example, it was possible to

convert $[\text{Cu}(\text{dpp})\text{Br}_2]$ (**C11-Br₂**), which has the smaller ligand, into the corresponding copper(I) complex $[\text{Cu}(\text{dpp})_2](\text{CuBr}_2)$ at room temperature. In contrast to this, the dibromido complex $[\text{Cu}(\text{dnp})\text{Br}_2]$ (**C12-Br₂**) with bulkier ligand could only be partially converted into $[\text{Cu}(\text{dnp})_2](\text{CuBr}_2)$ under heating whereas $[\text{Cu}(\text{dnp})\text{Cl}_2]$ (**C12-Cl₂**) showed no detectable change under the same conditions. The authors gave no rationale for the mechanism of this redistribution but the copper(I) complexes $[\text{Cu}(\text{L})_2]^+(\text{CuX}_2)^-$ (**C13**) are also accessible by mixing the corresponding copper(I) salt CuX with ligand in a 1:1 ratio.^[116,117]

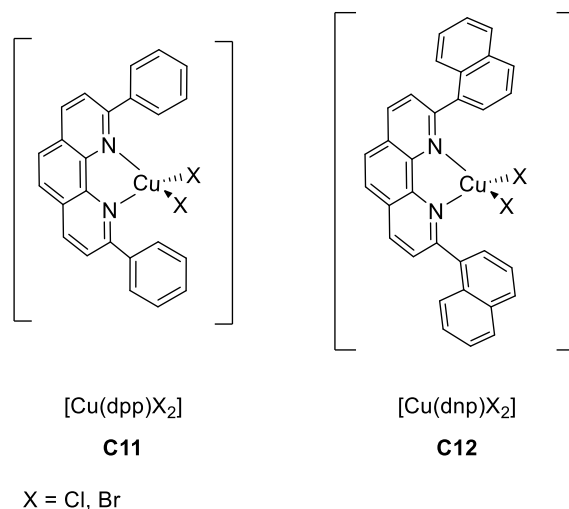


Figure 7. $[\text{Cu}(\text{dpp})\text{X}_2]$ (**C11**) and $[\text{Cu}(\text{dnp})\text{X}_2]$ (**C12**) according to B. Wu, X.-J. Yang *et al.*^[116]

The new complex $[\text{Cu}(\text{dap})\text{Cl}_2]$ (**C10**) is at least stable up to 55°C in chloroform because it was synthesized under these conditions. As outlined above, the chloride auxiliary ligand and the sterically demanding dap ligand seem to sufficiently stabilize the copper(II) complex, however, potential ligand redistribution should always be kept in mind when discussing physical properties or reaction mechanisms. With complex **C10** as a copper(II) analog to established $[\text{Cu}(\text{dap})_2]\text{Cl}$ (**C1-Cl**), it was attractive to test its potential utility for photoredox reactions.

3. Characterization of New Complexes

3.1 X-ray Structures

The structures of the bench-stable complexes were investigated by X-ray analysis. Figure 8 depicts the measured X-ray structures of the new homoleptic complexes **C8** and **C9** which both show the supposed flattened pseudo-tetrahedral coordination of the copper(I) center by the phenanthroline nitrogen atoms.

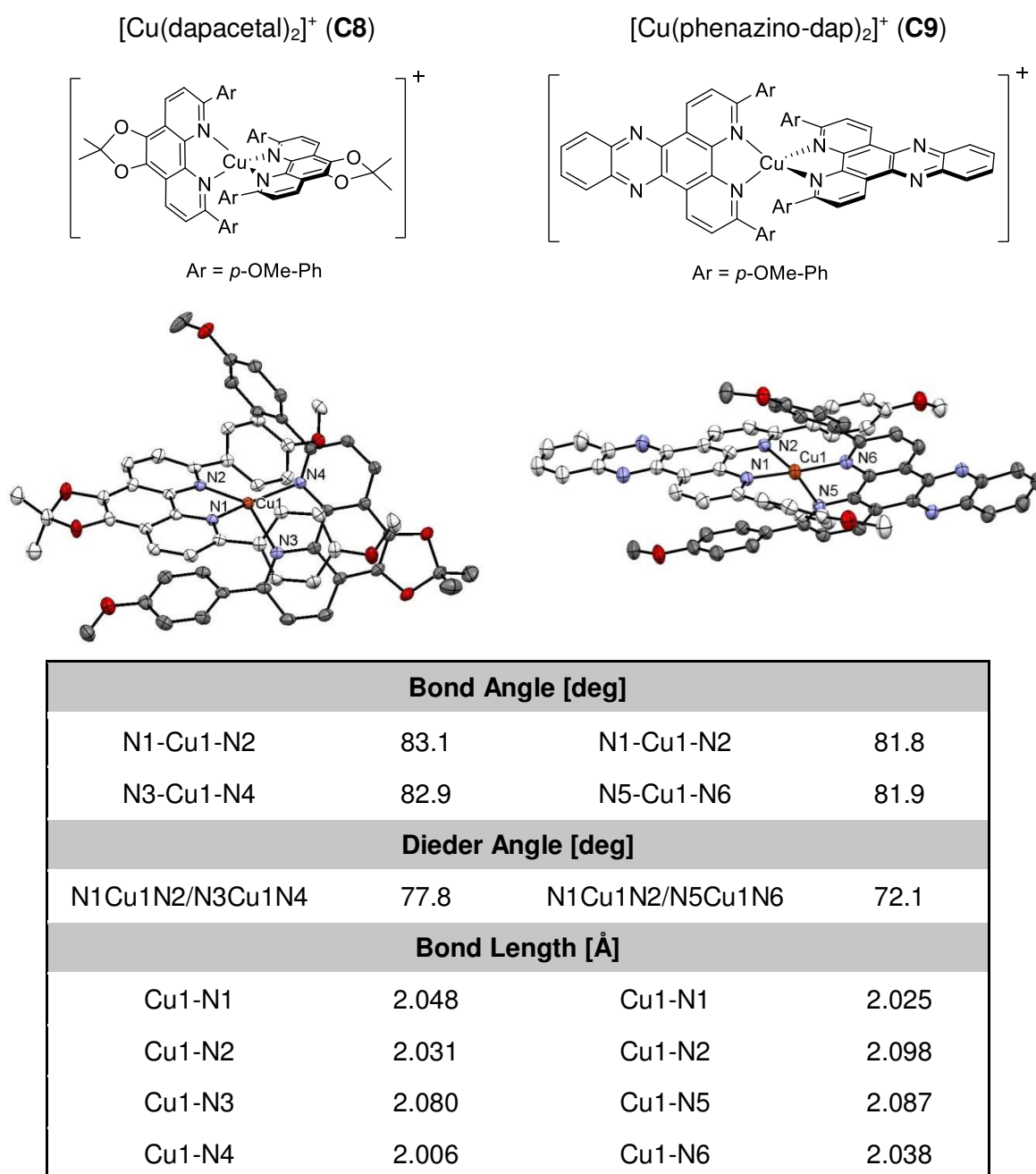
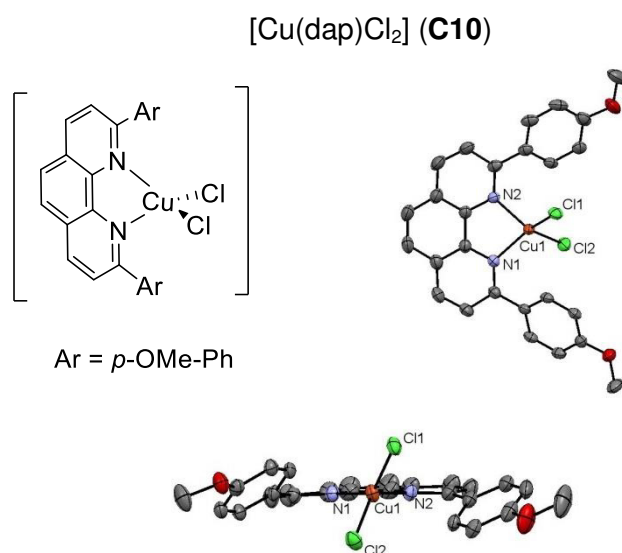


Figure 8. X-ray structures and selected data of $[\text{Cu}(\text{dapacetal})_2]^+$ (**C8**) (left) and $[\text{Cu}(\text{phenazino-dap})_2]^+$ (**C9**) (right).

The dihedral angles between the mean planes of the ligands are, with values of 72.1° and 77.8° , in agreement with reports of comparable copper phenanthroline complexes^[47,118]. The ligands bite angles in the range of 82° to 83° are in consistence as well. The distances between nitrogen and copper are in a quite narrow field (short bond 2.006 \AA to 2.048 \AA , long bond 2.080 \AA to 2.098 \AA).

Figure 9 depicts the measured X-ray structure of the heteroleptic copper(II) complex **C10**. The copper(II) center is four-coordinated by one bidentate dap ligand and two chloride ions in a pseudo-tetrahedral geometry with a pronounced flattening distortion. This unusual coordination geometry, the bite angle, as well as the bond length are in agreement with comparable phenanthroline complexes.^[116,119] The dihedral angle between N1Cu1N2/Cl1Cu1Cl2 is with 66.1° in the region of the analogous compound **C11-Cl₂** with the dpp ligand (65.7°).^[116]



Bond Angle [deg]	
N1-Cu1-N2	83.9
Cl1-Cu1-Cl2	106.7
Dieder Angle [deg]	
N1Cu1N2/Cl1Cu1Cl2	66.1
Bond Length [Å]	
Cu1-N1	2.023
Cu1-N2	2.015
Cu1-Cl1	2.226
Cu1-Cl2	2.223

Figure 9. X-ray structure and selected data of $[\text{Cu}(\text{dap})\text{Cl}_2]$ (**C10**).

3.2 Spectroscopic Investigation

The absorption and emission spectra of $[\text{Cu}(\text{dapacetal})_2]^+$ (**C8**) and $[\text{Cu}(\text{phenazino-dap})_2]^+$ (**C9**) are depicted in Figure 10. The emission spectra were measured in a PMMA (poly(methyl methacrylate)) matrix, as the luminescence quantum yields in solution are too low at ambient temperature. Nevertheless, both complexes show in PMMA weak emission with photoluminescence quantum yields Φ_{PL} of 1% with a broad unstructured emission spectrum centered at around 700 nm.

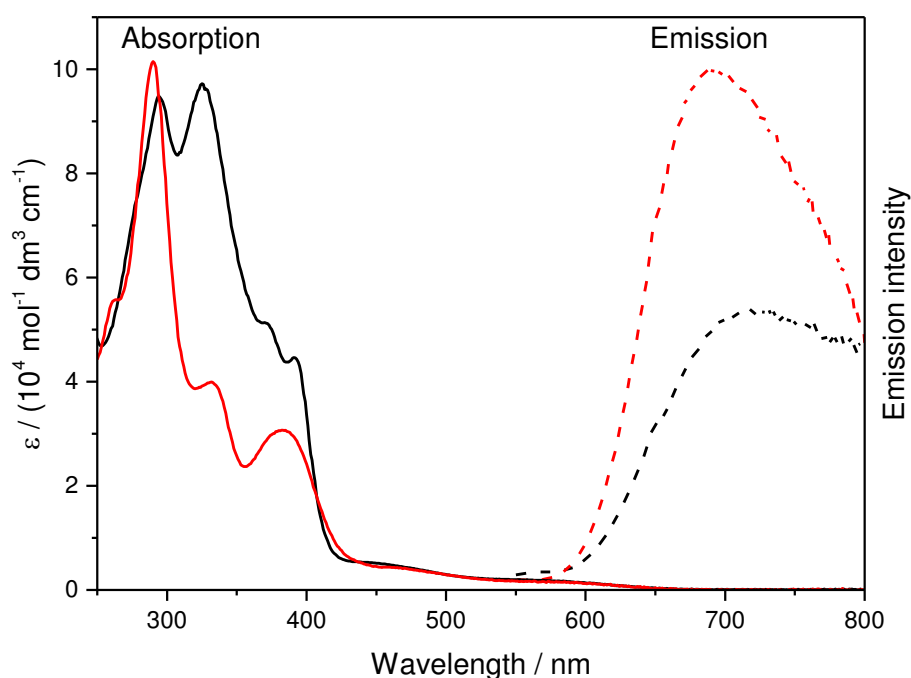


Figure 10. Absorption (solid lines) and luminescence (dashed lines) spectra of $[\text{Cu}(\text{dapacetal})_2]\text{BF}_4$ (**C8-BF₄**, red) and $[\text{Cu}(\text{phenazino-dap})_2]\text{PF}_6$ (**C9-PF₆**, black) at ambient temperature. Excitation wavelength for luminescence spectra: 300 nm for complex **C8-BF₄**, 330 nm for complex **C9-PF₆**. Absorption spectra were recorded in DCM and emission was measured in PMMA.

Both complexes showed additional weak emission in the range of 380 to 580 nm, which could be assigned to the emission spectra of free ligands (see experimental part, Figures 25 and 26). In the case of $[\text{Cu}(\text{phenazino-dap})_2]^+$ (**C9**), this emission was relatively intensive and it was still present after thorough purification and recrystallization of the complex. As the phenazino-dap ligand (**73**) shows, in contrast to the complex, a high quantum yield Φ_{PL} of 16% in a nitrogen atmosphere, traces of the ligand can lead to this emission band. Although the complex is stable under ambient conditions and ligand dissociation has not been observed during other investigations, a tiny amount must dissociate during the preparation of the PMMA matrix. Regarding copper(II) complex **C10**, it was not possible to determine the emission spectrum as this complex shows extremely poor emission ($\Phi_{\text{PL}} = 0\%$ both in an air

and a nitrogen atmosphere). The wavelengths as well as the corresponding extinction coefficients are summarized in Table 3. The average excited state lifetime τ was obtained by a biexponential fit of the emission decay function (see experimental part, Figures 23 and 24).

Table 3. Photophysical properties of copper complexes.

Complex	Emission λ_{max} / nm	Excited State Lifetime τ / ns	Absorption λ_{Abs} / nm	Extinction Coefficient ϵ / ($\text{mol}^{-1} \cdot \text{dm}^3 \cdot \text{cm}^{-1}$)
[Cu(dap) ₂]Cl (C1-Cl)	-	540 (ref ^[20])	284 331 455 530	5.9×10^4 5.1×10^4 2.0×10^3 1.4×10^3
[Cu(dapacetal) ₂]BF ₄ (C8-BF₄)	691 ^{a)}	517	262 290 332 382 455 530	5.6×10^4 1.0×10^5 4.0×10^4 3.1×10^4 4.4×10^3 2.0×10^3
[Cu(phenazino-dap) ₂]PF ₆ (C9-PF₆)	722 ^{b)}	252	294 325 372 391 455 530	9.5×10^4 9.7×10^4 5.1×10^4 4.5×10^4 5.0×10^3 2.2×10^3
[Cu(dap)Cl ₂] (C10)	-	-	300 351 455 530	2.6×10^4 2.9×10^4 7.3×10^2 4.7×10^2

Absorption data were recorded in DCM; emission data and excited state lifetime were measured in PMMA. a) Excitation wavelength: 300 nm. b) Excitation wavelength: 330 nm.

The UV-Vis absorption spectra (Figure 11) display for all four complexes below 355 nm intense absorptions (e.g. ϵ [Cu(dapacetal)₂]BF₄ (**C8-BF₄**), 290 nm = $1.0 \times 10^5 \text{ mol}^{-1} \cdot \text{dm}^3 \cdot \text{cm}^{-1}$) which are assigned to $\pi\pi^*$ transitions of the ligands^[20,105]. A weaker broad absorption occurs at wavelengths longer than 400 nm for all four complexes (e.g. ϵ [Cu(dapacetal)₂]BF₄ (**C8-BF₄**), 455 nm) = $4.4 \times 10^3 \text{ mol}^{-1} \cdot \text{dm}^3 \cdot \text{cm}^{-1}$). This absorption can be attributed to metal-to-ligand charge-transfer (MLCT) transitions^[20,105]. In this thesis, photoredox catalyzed reactions are usually performed using LEDs with blue (455 nm) or green (530 nm) light. Both new copper(I) complexes **C8-BF₄** and **C9-PF₆** show higher extinction at these wavelengths than

the established $[\text{Cu}(\text{dap})_2]\text{Cl}$ (**C1-Cl**) and can therefore theoretically take up more light energy, which is basically beneficial for photocatalysis. Copper(II) complex **C10** bears only one phenanthroline ligand and, in contrast to copper(I) complex **C1-Cl**, exhibits a lower absorbance at these wavelengths, which is in theory still high enough for photocatalysis. This behavior is not surprising as there is only one ligand available for MLCT instead of two. After all, blue (455 nm) as well as green (530 nm) LEDs can be used for adequate excitation in the visible range of all these complexes.

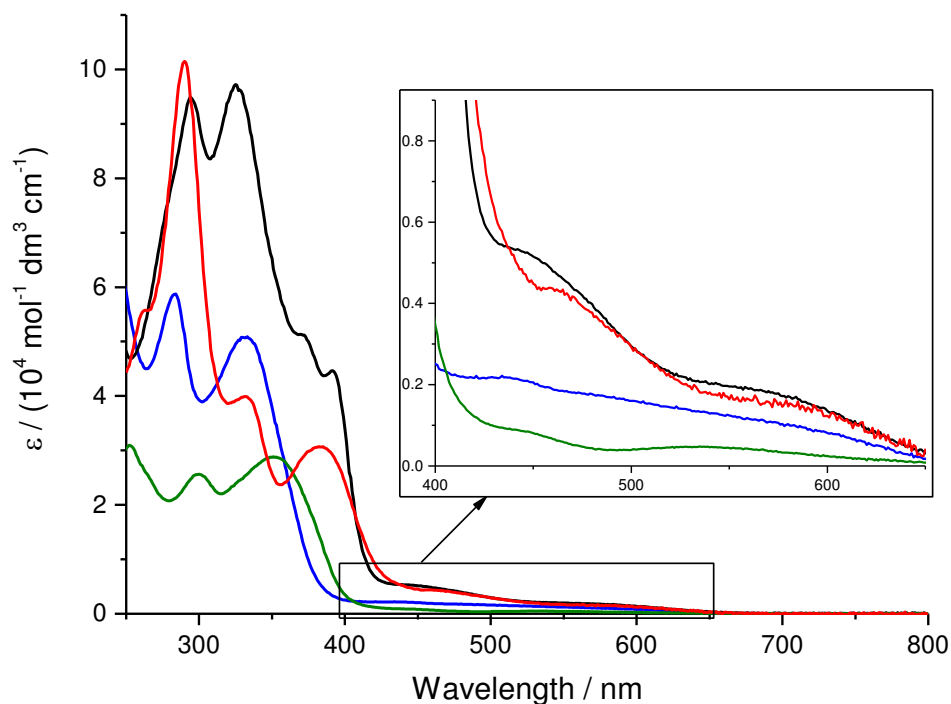


Figure 11. Comparison of UV-Vis absorption spectra of $[\text{Cu}(\text{dap})_2]\text{Cl}$ (**C1-Cl**, blue), $[\text{Cu}(\text{dapacetal})_2]\text{BF}_4$ (**C8-BF₄**, red), $[\text{Cu}(\text{phenazino-dap})_2]\text{PF}_6$ (**C9-PF₆**, black), and $[\text{Cu}(\text{dap})\text{Cl}_2]$ (**C10**, green) recorded in DCM.

3.3 Cyclovoltammetric Measurements

The new complexes were investigated by cyclovoltammetric measurements vs. ferrocene (Fc) as an internal standard and the potentials were converted to the SCE scale for better comparability. Both new copper(I) complexes show a metal-based reversible redox behavior for the $\text{Cu}^{2+}/\text{Cu}^+$ couple (Figure 12, wave A). The half-wave potential for $\text{Cu}^{2+}/\text{Cu}^+$ of $[\text{Cu}(\text{dapacetal})_2]^+$ (**C8**) is, with 0.64 V vs. SCE, within the range of $[\text{Cu}(\text{dap})_2]^+$ (0.62 V vs. SCE)^[19]. This was not expected, as the possible electron-donating effect of the oxygen atoms in 5,6-position of the dap ligand was expected to decrease this potential. In comparison to this, $[\text{Cu}(\text{phenazino-dap})_2]^+$ (**C9**) shows, with 0.81 V vs. SCE, a much higher potential, which confirms the strong electron-withdrawing influence of the phenazine group.

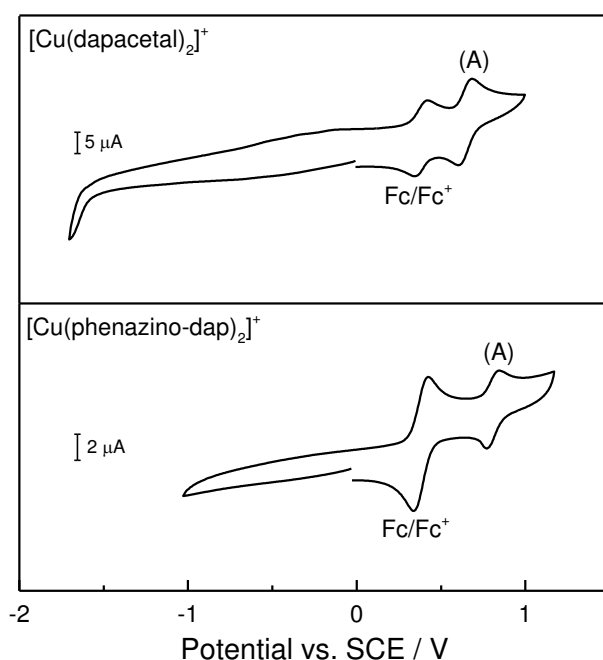


Figure 12. Cyclic voltammograms of $[\text{Cu}(\text{dapacetal})_2]\text{BF}_4$ (**C8-BF₄**) in MeCN and of $[\text{Cu}(\text{phenazino-dap})_2]\text{PF}_6$ (**C9-PF₆**) in DCM⁵ using tetrabutylammonium tetrafluoroborate as supporting electrolyte and ferrocene as internal standard at a scan rate of 50 $\text{mV}\cdot\text{s}^{-1}$.

In contrast to $[\text{Cu}(\text{L})_2]^+$ complexes (cf. for example **C1**^[47], **C8** or **C9**), which show only one reversible wave at the positive potential area, the copper(II) complex $[\text{Cu}(\text{dap})\text{Cl}_2]$ (**C10**) shows a more challenging cyclic voltammogram with irreversible processes (Figure 13). As a simple oxidation of copper(II) to a copper(III) species should result in one reversible redox wave, such an oxidation cannot be assumed for this system. However, it is known that besides redox reactions on the metal center, manifold ligand exchange and ligand redistribution processes can occur with such copper complexes.^[116,120] For example, chloride

⁵ Due to solubility reasons, $[\text{Cu}(\text{phenazino-dap})_2]\text{PF}_6$ (**C9-PF₆**) was measured in DCM.

can dissociate and lead to additional oxidation peaks by adsorbance on the electrode surface. Moreover, analog to literature report^[116], it has to be assumed that a copper(I) couple ($[\text{Cu}(\text{dap})_2](\text{CuCl}_2)$ (**C13-dapCl**) is formed by the applied potential (*vide supra*). Consequently, the observed redox waves can be most likely attributed to $\text{Cu}^{2+}/\text{Cu}^+$ transitions of different species formed in course of the measurement.^[116] Nevertheless, an unambiguous assignment of the present species with exact oxidation states cannot be made here only on the basis of simple cyclic voltammetry. Since the elucidation of such processes requires a far more in-depth physical investigation which is beyond the scope of this thesis and since it was more important to firstly see if $[\text{Cu}(\text{dap})\text{Cl}_2]$ (**C10**) exhibits any photoredox activity at all, the complex was tested without knowing the exact redox potentials.

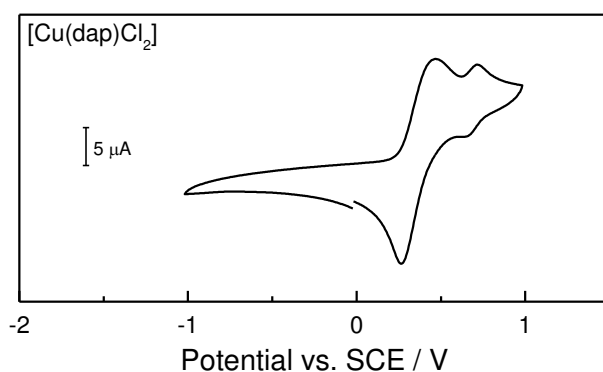


Figure 13. Cyclic voltammogram of $[\text{Cu}(\text{dap})\text{Cl}_2]$ (**C10**) in DCM using tetrabutylammonium tetrafluoroborate as supporting electrolyte at a scan rate of $50 \text{ mV}\cdot\text{s}^{-1}$. Since, in this case, ferrocene would overlap the signals, the potentials were referenced against ferrocene by using an independent measurement.

3.4 Summary and Assessment of Photophysical and Electrochemical Properties

As a yardstick for the “strength” of a photocatalyst, the excited state potentials play a crucial role in photoredox catalysis. The excited state reduction potential $E_{1/2}^*(M^+/M^*)$ of a photocatalyst can be approximated from the ground state electrochemical potential $E(M^+/M)$ and the zero spectroscopic energy of the excited state $E_{0-0}(M/M^*)$, where M is the ground state molecule and M^* is the lowest excited state molecule (equation (1)).^[121] The ground state electrochemical potential $E_{1/2}(M^+/M)$ is obtained by cyclic voltammetry and $E_{0-0}(M/M^*)$ can be estimated from the onset of the emission band.

$$E_{1/2}^*(M^+/M^*) = E_{1/2}(M^+/M) - E_{0-0}(M/M^*) \quad (1)$$

Basing on the cyclovoltammetric and spectroscopic measurements, the reduction potentials of the copper complexes were calculated using equation (1). The physical properties of copper(I) complexes are summarized and illustrated in Table 4.

Table 4. Summary of physical properties of copper(I) complexes.

Catalyst	[Cu(dapacetal) ₂] ₂ BF ₄ C8-BF₄	[Cu(dap) ₂] ₂ Cl C1-Cl	[Cu(phenazino-dap) ₂] ₂ PF ₆ C9-PF₆
Redox Potentials		 (ref ^[19])	
Excited State			
Lifetime τ	517 ns	540 ns (ref ^[20])	252 ns
Emission			
λ_{max}	691 nm	690 nm (ref ^[47])	722 nm

Redox potentials are reported vs. SCE: potentials of [Cu(dapacetal)₂]₂BF₄ (**C8-BF₄**) and [Cu(dap)₂]₂Cl (**C1-Cl**) were recorded in MeCN whereas that of [Cu(phenazino-dap)₂]₂PF₆ (**C9-PF₆**) were recorded in DCM due to solubility problems. Lifetime and emission behavior were studied in PMMA.

Regarding the redox power of the complexes, [Cu(dapacetal)₂]₂⁺ (**C8**) shows redox behavior which is surprisingly similar to that of [Cu(dap)₂]₂⁺ (**C1**). A possible electron-donating effect of the oxygen atoms in 5,6-position is assumed to increase the reduction potential of the excited state. However, this potential is, with -1.38 V, unexpectedly somewhat weaker than

that of **C1**. In contrast to the initial assumption, this is a strong indication that the acetal substitution in 5,6-position of the dap ligand has no electron-donating effect on the metal center. In contrast to this, the reduction potential of the excited state of $[\text{Cu}(\text{phenazino-dap})_2]^+$ (**C9**) is, with -1.20 V, much weaker than the potential of $[\text{Cu}(\text{dap})_2]^+$ (**C1**), which conforms the assumption of a strong electron-withdrawing influence of the phenazine group. Even though the reductive power of $[\text{Cu}(\text{phenazino-dap})_2]^+$ (**C9**) is reduced, it is theoretically still high enough to allow the reduction of interesting substrates, such as 4-nitrobenzyl bromide ($E_{1/2} = -0.86 \text{ V vs. SCE}$)^[103]. As far as the lifetime is concerned, all three complexes are located in the nanosecond timescale. Due to the fact that $[\text{Cu}(\text{dap})_2]^+$ (**C1**) is already known to be a potent photoredox catalyst (*vide supra*), the lifetime of each complex should be long enough to perform reasonable photoredox catalysis. The molar extinction coefficients of both $[\text{Cu}(\text{dapacetal})_2]^+$ (**C8**) and $[\text{Cu}(\text{phenazino-dap})_2]^+$ (**C9**) are at 455 nm and 530 nm higher than that of $[\text{Cu}(\text{dap})_2]^+$ (**C1**). Therefore, it is assumed that these new complexes are similarly accessible for photoredox catalysis by excitation with blue or green light. Even though the photophysics reveal some unexpected results for $[\text{Cu}(\text{dapacetal})_2]^+$ (**C8**) and $[\text{Cu}(\text{phenazino-dap})_2]^+$ (**C9**) with a low reduction potential, from a theoretical point of view both complexes should be applicable for photoredox catalysis. Since the copper(II) complex $[\text{Cu}(\text{dap})\text{Cl}_2]$ (**C10**) shows a challenging cyclic voltammogram with irreversible processes, and it was not possible to determine the emission spectrum due to extremely poor emission behavior, the excited state redox potentials of this complex cannot be calculated using equation (1). Nevertheless, **C10** shows sufficiently high absorbance for excitation in the spectral range of blue and green light which makes the complex interesting for photoredox catalysis. The photocatalytic potential of the new copper complexes, which was tested by means of different reactions, is illustrated in the next chapter.

4. Comparison of Phenanthroline Complexes in Photoreactions

4.1 Copper(I) Phenanthroline Complexes

In order to assess the photocatalytic potential of the new copper(I) complexes $[\text{Cu}(\text{dapacetal})_2]^+$ (**C8**) and $[\text{Cu}(\text{phenazino-dap})_2]^+$ (**C9**), their performance was tested on selected systems and compared to the established photoredox catalyst $[\text{Cu}(\text{dap})_2]^+$ (**C1**). As a first model system, the visible-light-mediated ATRA reaction between styrene (**74**) and 4-nitrobenzyl bromide (**75**) ($E_{1/2} = -0.86 \text{ V}^{\text{6}}$)^[103] was chosen, which was developed by O. Reiser and co-workers.^[26] This reaction ran excellently with $[\text{Cu}(\text{dap})_2]^+$ (**C1**) in a 99% yield in 24 h (Table 5, entry 1). Control experiments with CuCl, without catalyst or without light irradiation showed that this reaction needs both photocatalyst and light irradiation (entries 6 to 8). The ligand itself showed a slight photocatalytic activity with 15% yield (entry 9). When $[\text{Cu}(\text{dapacetal})_2]\text{BF}_4$ (**C8-BF₄**) (entry 4) was used, only 59% of the product was obtained, even after a prolonged reaction time of six days. Even though complex **C8-BF₄** showed similar redox behavior and a higher absorbance at 530 nm than $[\text{Cu}(\text{dap})_2]\text{Cl}$ (**C1-Cl**), this reaction proceeded far more slowly.

Table 5. ATRA reaction using 4-nitrobenzyl bromide (**75**).^a

Entry	Conditions	Yield ^b / %
1	$[\text{Cu}(\text{dap})_2]\text{Cl}$	99
2	$[\text{Cu}(\text{dap})_2]\text{BF}_4$	90
3	$[\text{Cu}(\text{dap})_2]\text{PF}_6$	100
4	$[\text{Cu}(\text{dapacetal})_2]\text{BF}_4$	59 ^c
5	$[\text{Cu}(\text{phenazino-dap})_2]\text{PF}_6$	n.r.
6	no catalyst, just light	n.r. (ref ^[26])
7	$[\text{Cu}(\text{dap})_2]\text{Cl}$, no light	n.r. (ref ^[26])
8	CuCl (1 mol%)	n.r.
9	dap (2 mol%)	15

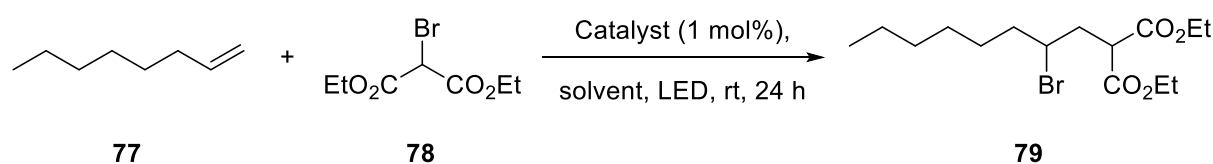
a) Reaction conditions: Styrene (**74**) (5.0 equiv, 2.5 mmol), 4-nitrobenzyl bromide (**75**) (1.0 equiv), anhydrous MeCN (1.0 mL), catalyst (0.005 mmol, 1.0 mol%), rt, 530 nm (LED-stick), 24 h. b) Determined by ¹H-NMR using 1,2-dichloroethane as internal standard. c) Isolated yield after 6 d reaction time.

⁶ vs. SCE in MeCN

Organohalide 4-cyanobenzyl bromide ($E_{1/2} = -1.39 \text{ V}^7$)^[104], which cannot be converted by the more strongly reducing catalyst $[\text{Cu}(\text{dap})_2]^+$ (**C1**), was used as a reagent in order to control the calculated reduction potential of $[\text{Cu}(\text{dapacetal})_2]^+$ (**C8**) ($E_{1/2}(\text{Cu}^{2+}/^*\text{Cu}^+) = -1.38 \text{ V}^7$). No reaction occurred, as expected. As the reduction potential of $[\text{Cu}(\text{phenazino-dap})_2]\text{PF}_6$ (**C9-PF₆**) is with a value of -1.20 V^7 theoretically still high enough to realize the reduction of 4-nitrobenzyl bromide (**75**) ($E_{1/2} = -0.86 \text{ V}^7$)^[103], this complex was tested as well (Table 5, entry 5). Interestingly, no reaction was observed in contrast to the other two complexes **C1** and **C8-BF₄**. As shown by the example of $[\text{Cu}(\text{dap})_2]^+$ (**C1**) (entries 2 and 3), the effect of the counter ion is negligible in this reaction and cannot therefore be the reason for the strange behavior of $[\text{Cu}(\text{dapacetal})_2]\text{BF}_4$ (**C8-BF₄**) and $[\text{Cu}(\text{phenazino-dap})_2]\text{PF}_6$ (**C9-PF₆**).

In a further test, diethyl bromomalonate (**78**) was used as ATRA reagent (Table 6). As this reagent is more easily reducible ($E_{1/2} = -0.62 \text{ V}^7$)^[102] than 4-nitrobenzyl bromide (**75**), it should be readily accessible with $[\text{Cu}(\text{phenazino-dap})_2]^+$ (**C9**) ($E_{1/2} = -1.20 \text{ V}^7$). In order to also have a representative for aliphatic alkenes, 1-octene (**77**) was used as reaction partner. When using standard conditions, namely acetonitrile as a solvent and green light irradiation, catalyst $[\text{Cu}(\text{dap})_2]^+$ (**C1**) furnished a reasonable yield of 51% (Table 6, entry 1). Control experiments with CuCl, without catalyst or without light irradiation showed that this reaction needs both photocatalyst and light irradiation (entries 13 to 16). Using standard conditions, catalyst $[\text{Cu}(\text{dapacetal})_2]^+$ (**C8**) again showed slower conversion and furnished only 13% of product (entry 6). However, **C8** was just as efficient as $[\text{Cu}(\text{dap})_2]^+$ (**C1**) when irradiated with blue light (entries 2 and 7). This might be explained by the higher absorbance of $[\text{Cu}(\text{dapacetal})_2]^+$ (**C8**), which is at 455 nm approximately double the value of $[\text{Cu}(\text{dap})_2]^+$ (**C1**) (cf. Table 3 and Figure 11). Interestingly, dap ligand (**60**) itself showed quite strong photocatalytic activity in this system with a 59% yield (entry 17). Nevertheless, this was much lower than with $[\text{Cu}(\text{dap})_2]^+$ (**C1**) which furnished a 91% yield under these conditions (entry 2). $[\text{Cu}(\text{phenazino-dap})_2]\text{PF}_6$ (**C9-PF₆**) did not lead to any success at all (entries 8 to 12). Since **C9-PF₆** is scarcely soluble in acetonitrile, reactions in diluted mixtures were carried out (entries 9 to 12). The use of more energy-rich blue light as well as the use of dichloromethane, where the complex is more soluble, did not show any turnover (entries 10 to 12). These results would not be expected with regard to either the reduction potential or the lifetime of the excited state of $[\text{Cu}(\text{phenazino-dap})_2]\text{PF}_6$ (**C9-PF₆**) (*vide supra*).

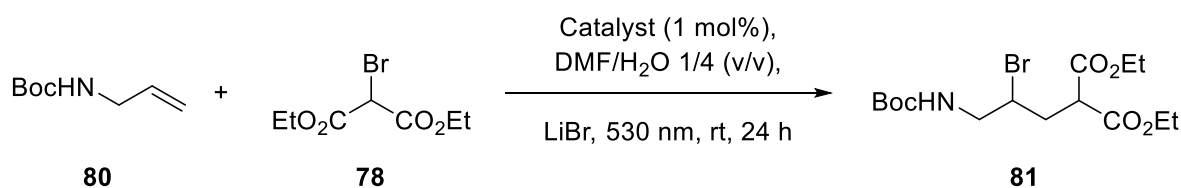
⁷ vs. SCE in MeCN

Table 6. ATRA reaction between 1-octene (**77**) and diethyl bromomalonate (**78**).^a

Entry	Catalyst	Solvent	λ / nm	c(alkene) / mol/L	Yield ^b / %
1	[Cu(dap) ₂]Cl	MeCN	530	1.0	51
2	[Cu(dap) ₂]Cl	MeCN	455	1.0	91 ^c
3	[Cu(dap) ₂]Cl	DCM	530	0.17	25
4	[Cu(dap) ₂]BF ₄	MeCN	530	1.0	40
5	[Cu(dap) ₂]PF ₆	MeCN	530	1.0	50
6	[Cu(dapacetal) ₂]BF ₄	MeCN	530	1.0	13
7	[Cu(dapacetal) ₂]BF ₄	MeCN	455	1.0	89
8	[Cu(phenazino-dap) ₂]PF ₆	MeCN	530	1.0	n.r.
9	[Cu(phenazino-dap) ₂]PF ₆	MeCN	530	0.17	n.r.
10	[Cu(phenazino-dap) ₂]PF ₆	MeCN	455	0.17	n.r.
11	[Cu(phenazino-dap) ₂]PF ₆	DCM	530	0.17	n.r.
12	[Cu(phenazino-dap) ₂]PF ₆	DCM	455	0.17	n.r.
13	no catalyst	MeCN	455	1.0	n.r.
14	no catalyst	DCM	455	1.0	n.r.
15	[Cu(dap) ₂]Cl	MeCN	no	1.0	n.r.
16	CuCl	DCM	455	1.0	n.r.
17	dap (2 mol%)	MeCN	455	1.0	59

a) Reaction conditions: 1-octene (**77**) (1.0 equiv), diethyl bromomalonate (**78**) (2.0 equiv), anhydrous solvent, catalyst (1.0 mol%), rt, irradiation via LED-stick for 24 h. b) Determined by ¹H-NMR using 1,4-dicyanobenzene as internal standard. c) 89% isolated yield.

In a next step, *N*-Boc allylamine (**80**) was tested as an alkene. This photoredox catalyzed ATRA reaction between **80** and diethyl bromomalonate (**78**) was developed by Stephenson *et al.* who reported 99% yield using Ir[(dF(CF₃)-ppy)₂(dtbbpy)]PF₆ as a photocatalyst.^[31] Using copper catalysts, the reaction furnished lower yields, with [Cu(dapacetal)₂]⁺ (**C8**) catalyzing slightly worse than [Cu(dap)₂]⁺ (**C1**) (Table 7, entries 1 and 2). The control experiments without light irradiation or with a copper(I) source as a potential catalyst showed no reaction (entries 4 and 5), which proves the necessity of both light and catalyst for this reaction.

Table 7. ATRA reaction using *N*-Boc allylamine (**80**).^a

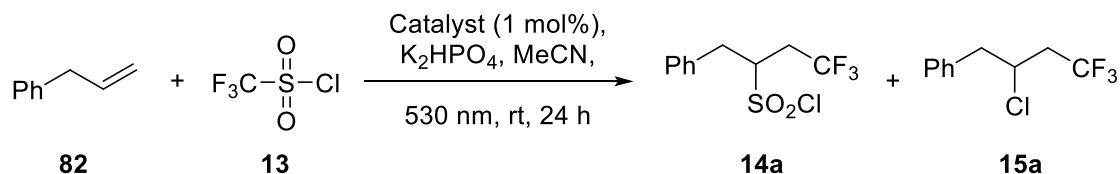
Entry	LED	Catalyst	Yield / %
1	530 nm	[Cu(dap) ₂]Cl	77 ^b
2	530 nm	[Cu(dapacetal) ₂]BF ₄	69
3	530 nm	[Cu(phenazino-dap) ₂]PF ₆	n.r.
4	-	[Cu(dapacetal) ₂]BF ₄	n.r.
5	530 nm	[Cu(MeCN) ₄]BF ₄	n.r.

a) Reaction conditions: *N*-Boc allylamine (**80**) (1.0 equiv, 0.5 mmol), diethyl bromomalonate (**78**) (2.0 equiv), LiBr (2.0 equiv), catalyst (0.005 mmol; 1 mol%), solvent DMF/H₂O 1/4 (v/v) (1.0 mL), rt, 530 nm (LED-stick), 24 h. b) Stephenson *et al.* reported 99% yield using Ir[(dF(CF₃)-ppy)₂(dtbbpy)]PF₆ (1 mol%) as a catalyst; irradiation with blue light for 24 h.^[31]

The photoredox catalyzed trifluoromethylchlorosulfonylation of alkenes developed by Reiser *et al.*^[27] (cf. chapter A, Scheme 6) is extraordinary. When using triflyl chloride (**13**) and [Cu(dap)₂]Cl (**C1-Cl**), chlorosulfonylated products **14** were obtained as the preferred products (Table 8, entry 1). In contrast, with other established photoredox catalysts such as [Ru(bpy)₃]Cl₂, trifluoromethylchlorination under loss of sulfur dioxide was observed resulting in chlorinated products **15** as the main products (entry 2). Control experiments proved that both light and photoredox catalyst are necessary for this reaction (entries 3 to 5). Since the unusual product formation under copper catalysis cannot be explained by established outer-sphere mechanism of photoredox catalyzed ATRA reactions, a new inner-sphere mechanism was proposed in which copper stabilizes SO₂Cl by coordination (cf. chapter A, Scheme 8).^[27] The new complexes were tested by the example of allylbenzene (**82**) and compared with the published results of [Cu(dap)₂]Cl (**C1-Cl**). [Cu(dapacetal)₂]BF₄ (**C8-BF₄**) furnished 42% of chlorosulfonylated product **14a** as the main product (Table 8, entry 6) but both the selectivity (83/17) and the yield dropped in comparison with [Cu(dap)₂]Cl (**C1-Cl**) (entry 1). Interestingly [Cu(phenazino-dap)₂]PF₆ (**C9-PF₆**) showed with a 37% yield a productive reaction, too. However, it was with a ratio of 70/30 less selective for **14a** with a comparable poor yield as [Cu(dapacetal)₂]BF₄ (**C8-BF₄**) (entry 7). The fact that [Cu(phenazino-dap)₂]PF₆ (**C9-PF₆**) showed no reactivity in all other tested ATRA reactions (*vide supra*) is a further indication that the trifluoromethylchlorosulfonylation proceeds via a different mechanism. Even though there is no apparent reason from the photophysical behavior investigated so far, this complex does not catalyze reactions in which the traditional outer-sphere mechanism is assumed to be predominant. Regarding their performance, the complexes [Cu(dapacetal)₂]BF₄ (**C8-BF₄**)

and [Cu(phenazino-dap)₂]₂PF₆ (**C9-PF₆**) synthesized herein are not of value for the trifluoromethylchlorosulfonylation reaction.

Table 8. Trifluoromethylchlorosulfonylation reaction of allylbenzene (**82**).

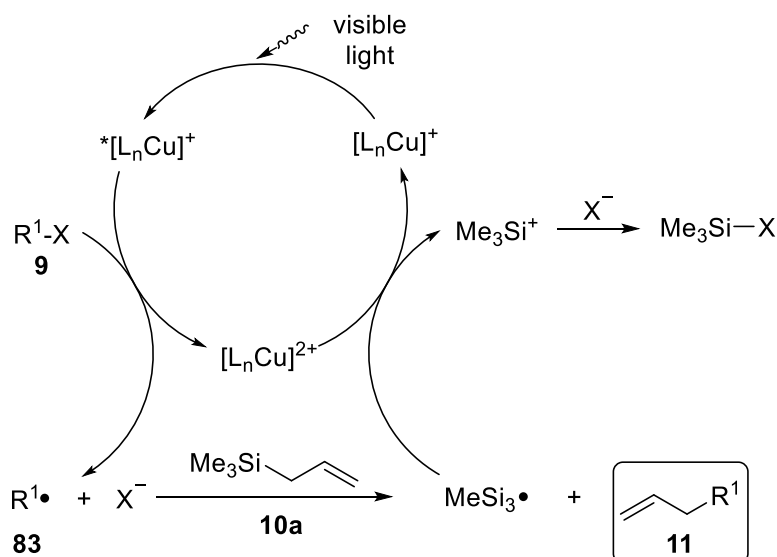
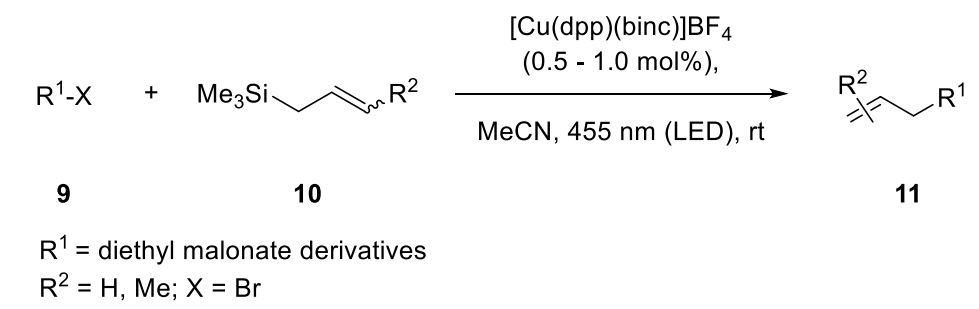


Entry	Conditions	14a/15a	Yield (14a) / %
1	[Cu(dap) ₂] ₂ Cl	95/5	86
2	[Ru(bpy) ₃] ₂ Cl ₂	4/96	84% of 15a
3	[Cu(dap) ₂] ₂ Cl, no light	99/1	10
4	no catalyst, 530 nm	-	n.r.
5	[Cu(MeCN) ₄] ₂ PF ₆	15/85	7% of 15a
6	[Cu(dapacetal) ₂] ₂ BF ₄	83/17	42 ^a
7	[Cu(phenazino-dap) ₂] ₂ PF ₆	70/30	37 ^a

 values taken from ref.^[27]

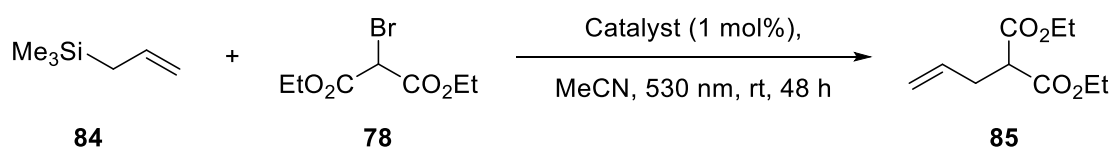
Reaction conditions: Allylbenzene (**82**) (1.0 equiv, 1.0 mmol), triflyl chloride (**13**) (2.0 equiv), K₂HPO₄ (2.0 equiv), catalyst (0.01 mmol; 1 mol%), anhydrous MeCN (3.0 mL), rt, 530 nm (LED-stick), 24 h. a) The yield was determined using 1,4-dicyanobenzene as internal standard.

The allylation of organohalides **9** using allyltrimethylsilane derivatives **10** under photoredox catalysis as developed by Reiser and co-workers, is an ecologically more favorable alternative to the allylation with allyl tributyltin reagents.^[20,25,47] The reaction mechanism was proposed to run via an oxidative quenching cycle with the copper photoredox catalyst acting as an electron shuttle (Scheme 27).^[20] After irradiation, the photoexcited copper(I) catalyst reduces organohalides **9** by SET to the corresponding alkyl radical **83** under formation of a copper(II) species. Radical **83** adds to alkene **10a** under release of trimethylsilyl radical and product formation. Oxidation of the trimethylsilyl radical to the corresponding cation by back electron transfer to copper(II) closes the catalytic cycle.



Scheme 27. Proposed mechanism for copper-based photoredox catalyzed allylation of organohalides **9** with allyltrimethylsilanes **10**.^[20]

Since the scope of this valuable reaction is still limited with regard to both more challenging allyltrimethylsilane derivatives **10** and the variation of organohalides **9**, research for better photocatalysts is ongoing. For this reason, the new copper complexes were also tested on this reaction. As a model system the well-investigated reaction between allyltrimethylsilane (**84**) and diethyl bromomalonate (**78**) was used (Table 9), which needs both light^[20] and photocatalyst^[20]. When $[\text{Cu}(\text{dapacetal})_2]\text{BF}_4$ (**C8-BF₄**) was used as a catalyst, only half the yield was obtained compared to when $[\text{Cu}(\text{dap})_2]\text{Cl}$ (**C1-Cl**) was used (entries 1 and 2). With $[\text{Cu}(\text{phenazino-dap})_2]\text{PF}_6$ (**C9-PF₆**) no reaction took place. Again, both new copper(I) complexes were inferior to $[\text{Cu}(\text{dap})_2]^+$ (**C1**).

Table 9. Allylation of diethyl bromomalonate (**78**) with allyltrimethylsilane (**84**).^a

Entry	Catalyst	Yield / %
1	[Cu(dap) ₂]Cl	40
2	[Cu(dapacetal) ₂]BF ₄	20
3	[Cu(phenazino-dap)] ₂ PF ₆	n.r.

a) Reaction conditions: Allyltrimethylsilane (**84**) (3.0 equiv, 1.5 mmol), diethyl bromomalonate (**78**) (1.0 equiv, 0.5 mmol), catalyst (0.005 mmol, 1.0 mol%), anhydrous MeCN (1.0 mL), rt, 530 nm (LED-stick), 48 h. The yield was determined using 1,4-dicyanobenzene as internal standard.

4.2 Copper(II) Phenanthroline Complex

With the new complex $[\text{Cu}(\text{dap})\text{Cl}_2]$ (**C10**), a copper(II) analog to established copper(I) photoredox catalyst $[\text{Cu}(\text{dap})_2]\text{Cl}$ (**C1-CI**) was readily available. In order to investigate whether it is possible to use a copper(II) complex to perform known copper(I) driven photoredox catalyzed reactions, **C10** was tested for the reactions presented in the previous chapter. Using $[\text{Cu}(\text{dap})\text{Cl}_2]$ (**C10**) instead of $[\text{Cu}(\text{dap})_2]\text{Cl}$ (**C1-CI**) is more favorable, as less dap ligand is needed for the catalyst synthesis. In Table 10 the results of $[\text{Cu}(\text{dap})\text{Cl}_2]$ (**C10**) for different photoredox catalyzed reactions are summarized and compared with the results with $[\text{Cu}(\text{dap})_2]\text{Cl}$ (**C1-CI**). As demonstrated in the previous chapter, all listed reactions are definitely photocatalyzed as the control experiments without light or catalyst were negative. The visible-light-mediated ATRA reaction between styrene (**74**) and 4-nitrobenzyl bromide (**75**) (Table 10, entries 1 to 3), for example, clarifies that the copper(II) complex **C10** acts with a 76% yield indeed as a photocatalyst, as the control experiments with dap ligand gave only 15% product yield (cf. Table 5, entry 9). In addition, the reaction did not work with a simple copper(I) salt such as CuCl (cf. Table 5, entry 8) or with the copper(II) salt CuCl_2 (Table 10, entry 3).

In comparison to $[\text{Cu}(\text{dap})_2]\text{Cl}$ (**C1-CI**), copper(II) complex **C10** gave with 83% yield for the ATRA reaction between triflyl chloride (**13**) and allylbenzene (**82**) comparable yields in still good selectivity of 91/9 for product **14a** (Table 10, entries 10 and 11). Regarding the reactions with diethyl bromomalonate (**78**), however, the performance depends on the alkene substrate used. With 1-octene (**77**) (Table 10, entries 4 and 5), the copper(I) catalyst **C1-CI** gave with 91% much better results whereas **C10** furnished with 37% only poor product yields which are in the order of the background reaction with the dap ligand (cf. Table 6). However, when the allylic alkenes *N*-Boc allylamine (**80**) or allyltrimethylsilane (**84**) are used, the $[\text{Cu}(\text{dap})\text{Cl}_2]$ (**C10**) outperforms with yields of 86% and 68% the $[\text{Cu}(\text{dap})_2]\text{Cl}$ (**C1-CI**) (77% and 40% yield) (Table 10, entries 6 to 9).

Table 10. Comparison of [Cu(dap)Cl₂] (**C10**) and [Cu(dap)₂]Cl (**C1-Cl**).

Entry	Catalyst	Yield ^f / %
1	[Cu(dap) ₂]Cl	99
2	[Cu(dap)Cl ₂]	76
3	CuCl ₂ (1 mol%)	n.r.
4	[Cu(dap) ₂]Cl	91
5	[Cu(dap)Cl ₂]	37
6	[Cu(dap) ₂]Cl	77
7	[Cu(dap)Cl ₂]	86
8	[Cu(dap) ₂]Cl	40
9	[Cu(dap)Cl ₂]	68
		Yield (14a) 14a/15a
10	[Cu(dap) ₂]Cl	86 (ref ^[27]) 95/05
11	[Cu(dap)Cl ₂]	83 91/9

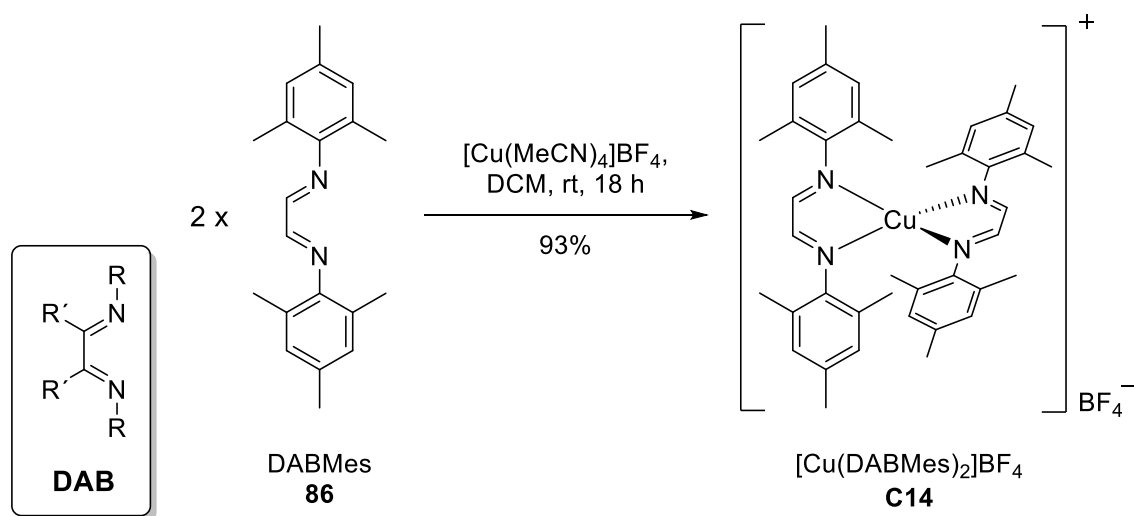
Reaction conditions: Alkene, halide, anhydrous solvent, catalyst (1 mol%), rt, irradiation via LED-stick (indicated wavelength) for the indicated time. a) styrene (5.0 equiv, 2.5 mmol), 4-nitrobenzyl bromide (1.0 equiv), MeCN (1.0 mL). b) 1-Octene (1.0 equiv, 0.5 mmol), diethyl bromomalonate (2.0 equiv), MeCN (0.5 mL). c) *N*-Boc allylamine (1.0 equiv, 0.5 mmol), diethyl bromomalonate (2.0 equiv), LiBr (2.0 equiv) was added, DMF/H₂O 1/4 (v/v) (1.0 mL). d) Allyltrimethylsilane (3.0 equiv, 1.5 mmol), diethyl bromomalonate (1.0 equiv), MeCN (1.0 mL). e) Allylbenzene (1.0 equiv, 1.0 mmol), triflyl chloride (2.0 equiv), K₂HPO₄ (2.0 equiv) was added, MeCN (3.0 mL). f) Determined by ¹H-NMR using 1,2-dichloroethane or 1,4-dicyanobenzene as internal standard.

These results raise some questions regarding the reaction mechanism with $[\text{Cu}(\text{dap})\text{Cl}_2]$ (**C10**), considering that both complexes were used under the same conditions in the respective reaction. It should be noted that the extinction coefficients of the copper(II) complex **C10** at the wavelengths of 455 nm and 530 nm which were used are just about one third of those of copper(I) complex **C1-CI** (cf. Table 3 and Figure 11). Consequently less light energy can be taken up, which could be used for a productive reaction. In this regard, the examples with *N*-Boc allylamine (**80**) or allyltrimethylsilane (**84**) (Table 10, entries 6 to 9) in which $[\text{Cu}(\text{dap})\text{Cl}_2]$ (**C10**) outperforms $[\text{Cu}(\text{dap})_2]\text{Cl}$ (**C1-CI**) are of particular interest. On the basis of the better performance of copper(II) catalyst **C10**, it can be excluded that the potential copper(I) species $[\text{Cu}(\text{dap})_2](\text{CuCl}_2)$ (**C13-dapCI**), which might be formed *in situ* from **C10** (*vide supra*)^[116], is the active species. Since **C13-dapCI** corresponds, apart from counterions, to **C1-CI** and would be available in lower concentrations in the reaction mixture, the higher yields with **C10** cannot be explained. The initial formation of a copper(I) species such as $[\text{Cu}(\text{dap})\text{Cl}_2]^-$ by simple reduction of $[\text{Cu}(\text{dap})\text{Cl}_2]$ (**C10**) and a subsequent copper(I)/copper(II) cycle is also implausible because typical electron donors such as triethylamine are missing in the investigated reactions. In contrast, the involvement of a copper(III) species is conceivable, which might form, for example, by single electron transfer from photoexcited **C10** to alkyl halide. In particular, the coordination of substrates directly to the sterically less hindered copper center with just one dap ligand and subsequent reductive elimination might play a key role.

5. 1,4-Diaza-1,3-butadienes: An Alternative to Phenanthrolines?

Copper(I) complexes with aromatic diamine ligands, for example, phenanthrolines or bipyridines, are well investigated (*vide supra*). In contrast, examples of well-defined copper(I) complexes with 1,4-disubstituted 1,4-diaza-1,3-butadiene (DAB) ligands are scarce^[109,122,123], mainly owing to the ligands' flexible backbone and different possible coordination modes.^[109,124,125] However, DAB ligands are of special interest as they show similar σ -donor properties to and better π -acceptor properties than other important bidentate nitrogen chelates such as 2,2'-bipyridines.^[124,126] In addition, such ligands can be easily synthesized by condensation reactions of glyoxals, α -ketoaldehydes or α,β -diketones with primary amines.^[124,127] In 2016, S. Díez-González and co-workers reported the synthesis and characterization of new homo- and heteroleptic copper(I) complexes with four different DAB ligands.^[109] Thereby, the homoleptic cationic complexes proved to be "stable towards oxygen and moisture and could be stored/handled without the need of any particular precautions."^{[109], p. 4650} When bulky ligand DABMes (**86**) with mesitylene substituents was used, only the homoleptic bischelatate complex $[\text{Cu}(\text{DABMes})_2]\text{BF}_4$ (**C14**) was observed and no neutral heteroleptic complex with only one diamine ligand could be formed. Due to the fact that $[\text{Cu}(\text{DABMes})_2]\text{BF}_4$ (**C14**), which had been first reported by M. A. Halcrow *et al.*^[122], showed the most resistant structure, this complex was chosen for initial photocatalytic investigations in this thesis.

The synthesis was performed following the procedure of S. Díez-González and co-workers^[109], starting with *N,N'*-bis(mesityl)-1,4-diaza-1,3-butadiene (DABMes, **86**) to obtain complex **C14** in one step (Scheme 28). In doing so, the procedure for complexation is similar to the protocol of the phenanthroline complexes.



Scheme 28. Synthesis of $[\text{Cu}(\text{DABMes})_2]\text{BF}_4$ (**C14**) using the conditions of S. Díez-González *et al.*^[109]

5.1 Photophysical and Electrochemical Properties of [Cu(DABMes)₂]BF₄

Bench-stable complex [Cu(DABMes)₂]BF₄ (**C14**) efficiently absorbs light in the visible range with broad bands at 394 nm ($\varepsilon = 1.5 \times 10^4 \cdot \text{mol}^{-1} \cdot \text{dm}^3 \cdot \text{cm}^{-1}$) and 730 nm ($\varepsilon = 3.5 \times 10^3 \cdot \text{mol}^{-1} \cdot \text{dm}^3 \cdot \text{cm}^{-1}$) (Figure 14). In agreement with related complexes^[109], these bands were attributed to MLCT as the free ligand absorbs at 365 nm ($\varepsilon = 4.6 \times 10^3 \cdot \text{mol}^{-1} \cdot \text{dm}^3 \cdot \text{cm}^{-1}$).

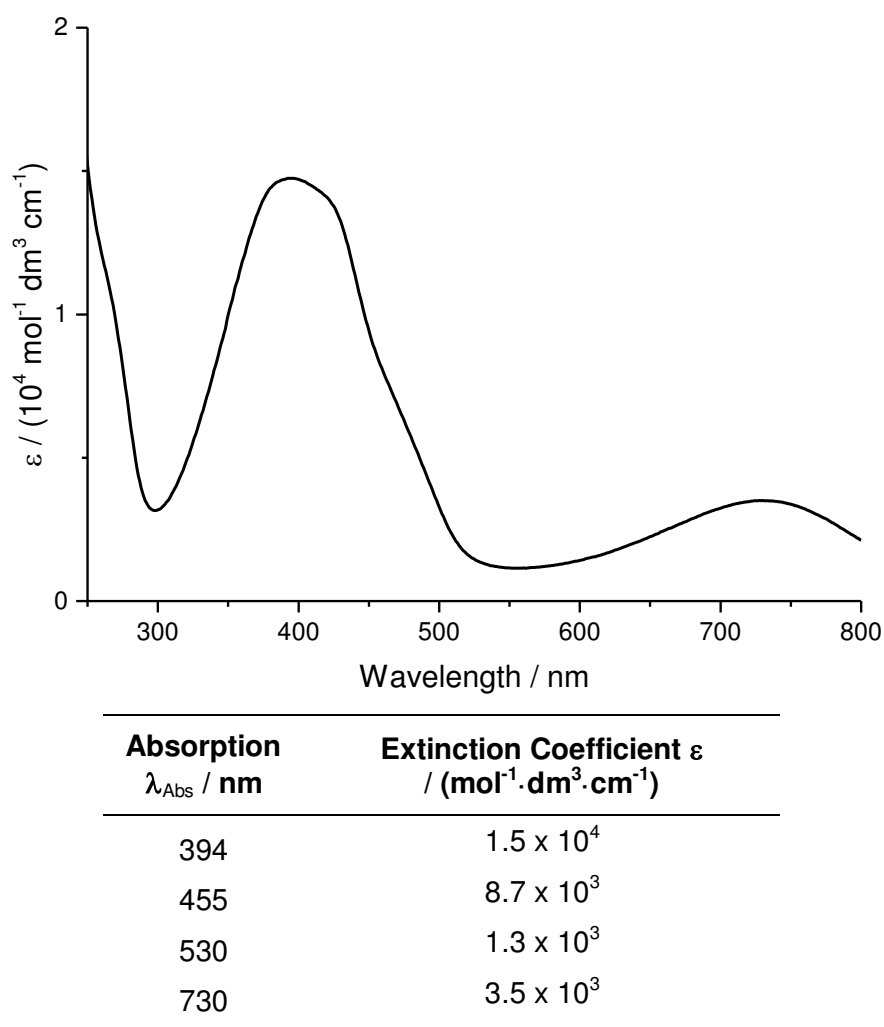


Figure 14. Absorption spectrum of [Cu(DABMes)₂]BF₄ (**C14**) in DCM.

Regarding the electrochemical properties, complex **C14** shows metal-based reversible redox behavior for the Cu²⁺/Cu⁺ couple (Wave A) with a half-wave potential of +0.86 V vs. SCE (Figure 15). A second potential (B) which occurs at -0.9 to -1.2 V corresponds to the reduction of the ligand.^[127,128]

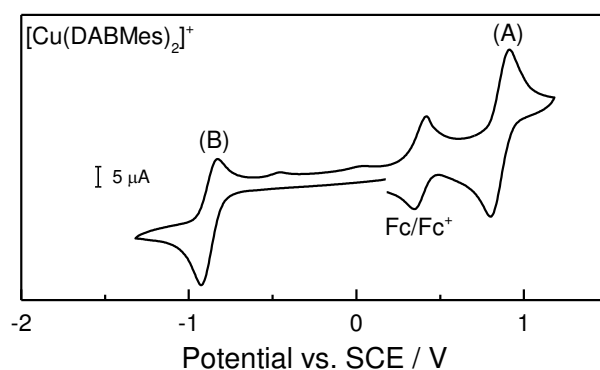


Figure 15. Cyclic voltammogram of $[\text{Cu}(\text{DABMes})_2]\text{BF}_4$ (**C14**) in DCM using tetrabutylammonium tetrafluoroborate as supporting electrolyte and ferrocene as internal standard at a scan rate of $50 \text{ mV}\cdot\text{s}^{-1}$.

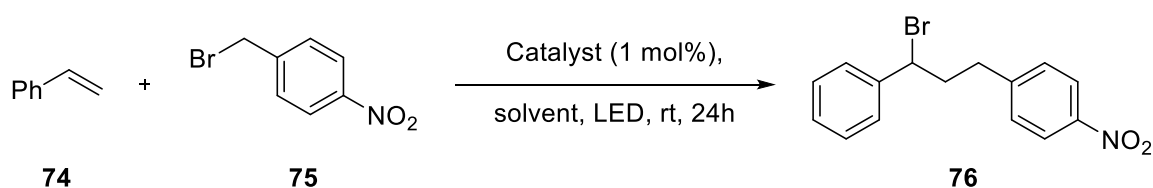
Due to the extremely poor emission behavior of this complex ($\Phi_{\text{PL}} = 0\%$ both in an air and a nitrogen atmosphere) it was not possible to determine the emission spectrum. Thus, the redox potential of the excited state could not be calculated in the context of this thesis.

5.2 Investigation of Photocatalytic Activity of [Cu(DABMes)₂]BF₄

Regarding the use of solvents, UV-Vis spectroscopic investigation revealed instability of the complex towards the coordinating ligands acetonitrile and dimethylformamide resulting in loss of ligand. Consequently, such coordinating solvents are not applicable for this system. Since this otherwise stable complex shows promising absorbance behavior, the performance was tested in selected ATRA reactions, which were already presented in the previous chapters, and compared to established [Cu(dap)₂]⁺ (**C1**). Since [Cu(DABMes)₂]BF₄ (**C14**) is not stable in acetonitrile, all reactions were run in dichloromethane instead.

The reaction between styrene (**74**) and 4-nitrobenzyl bromide (**75**) was not possible with [Cu(DABMes)₂]BF₄ (**C14**) in dichloromethane and the use of high-energy blue light did not lead to success either (Table 11, entries 1 and 2). Usually this transformation is performed in acetonitrile in reasonable yields (entry 3). In order to exclude a possible solvent effect, the reaction was repeated with [Cu(dap)₂]BF₄ (**C1-BF₄**) in dichloromethane (entry 4). However, the reactions still ran with 63% albeit in lower yield.

Table 11. ATRA reaction using 4-nitrobenzyl bromide (**75**).



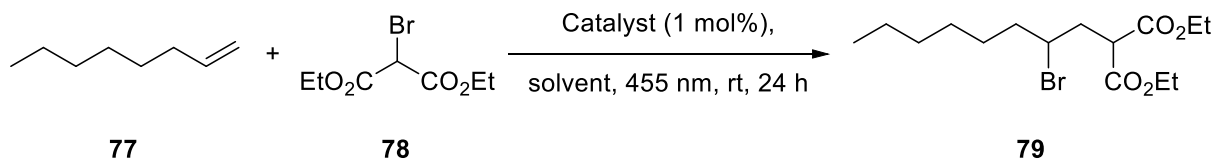
Entry	Catalyst	Solvent	λ / nm	Yield ^b / %
1	[Cu(DABMes) ₂]BF ₄	DCM	530	n.r.
2	[Cu(DABMes) ₂]BF ₄	DCM	455	n.r.
3	[Cu(dap) ₂]BF ₄	MeCN	530	90
4	[Cu(dap) ₂]BF ₄	DCM	530	63

Reaction conditions: Styrene (**74**) (5.0 equiv, 2.5 mmol), 4-nitrobenzyl bromide (**75**) (1.0 equiv), anhydrous MeCN (1.0 mL), catalyst (0.005 mmol, 1.0 mol%), rt, irradiation via LED-stick, 24 h. b) Determined by ¹H-NMR using 1,2-dichloroethane as internal standard.

In contrast to the above reaction, [Cu(DABMes)₂]BF₄ (**C14**) was with a 46% yield successful in the transformation of more easily reducible diethyl bromomalonate (**78**) (Table 12, entry 1). Considering the control experiments with ligand DABMes (**86**) or without light, which resulted in neglectable or no yields (entries 2 and 3), it is evident that [Cu(DABMes)₂]BF₄ (**C14**) here acts as a photocatalyst. However, in comparison to established [Cu(dap)₂]Cl (**C1-Cl**), which furnishes in dichloromethane a 75% yield (entry 4), the performance of the new catalyst **C14**

is worse. If acetonitrile, the best solvent in case of $[\text{Cu}(\text{dap})_2]\text{Cl}$ (**C1-CI**) (entry 5), could be used, the yield could certainly be increased.

Table 12. ATRA reaction between 1-octene (**77**) and diethyl bromomalonate (**78**).



Entry	Catalyst	Solvent	λ / nm	Yield ^b / %
1	$[\text{Cu}(\text{DABMes})_2]\text{BF}_4$	DCM	455	46
2	DABMes (2 mol%)	DCM	455	4
3	$[\text{Cu}(\text{DABMes})_2]\text{BF}_4$	DCM	no	n.r.
4	$[\text{Cu}(\text{dap})_2]\text{Cl}$	DCM	455	75
5	$[\text{Cu}(\text{dap})_2]\text{Cl}$	MeCN	455	91

Reaction conditions: 1-octene (**77**) (1.0 equiv, 0.5 mmol), diethyl bromomalonate (**78**) (2.0 equiv), anhydrous solvent (0.5 mL), catalyst (0.005 mmol, 1.0 mol%), rt, 455 nm (LED-stick), 24 h. b) Determined by $^1\text{H-NMR}$ using 1,4-dicyanobenzene as internal standard.

Finally, the trifluoromethylchlorosulfonylation of allylbenzene (**82**) was tested (Table 13). In comparison to $[\text{Cu}(\text{dap})_2]\text{Cl}$ (**C1-CI**), $[\text{Cu}(\text{DABMes})_2]\text{BF}_4$ (**C14**) catalyzed the reaction with 15% in only poor yields and a poor selectivity of 53/47 for the chlorosulfonylated product **14a**.

Table 13. Trifluoromethylchlorosulfonylation reaction of allylbenzene (**82**).



Entry	Catalyst	Solvent	14a/15a	Yield (14a) / %
1	$[\text{Cu}(\text{DABMes})_2]\text{BF}_4$	DCM	53/47	15
2	$[\text{Cu}(\text{dap})_2]\text{Cl}$	DCM	93/7	73 (ref ^[27])

Reaction conditions: Allylbenzene (**82**) (1.0 equiv, 1.0 mmol), triflyl chloride (**13**) (2.0 equiv), K_2HPO_4 (2.0 equiv), catalyst (0.01 mmol; 1 mol%), anhydrous DCM (3.0 mL), rt, 530 nm (LED-stick), 24 h. The yield was determined using 1,4-dicyanobenzene as internal standard.

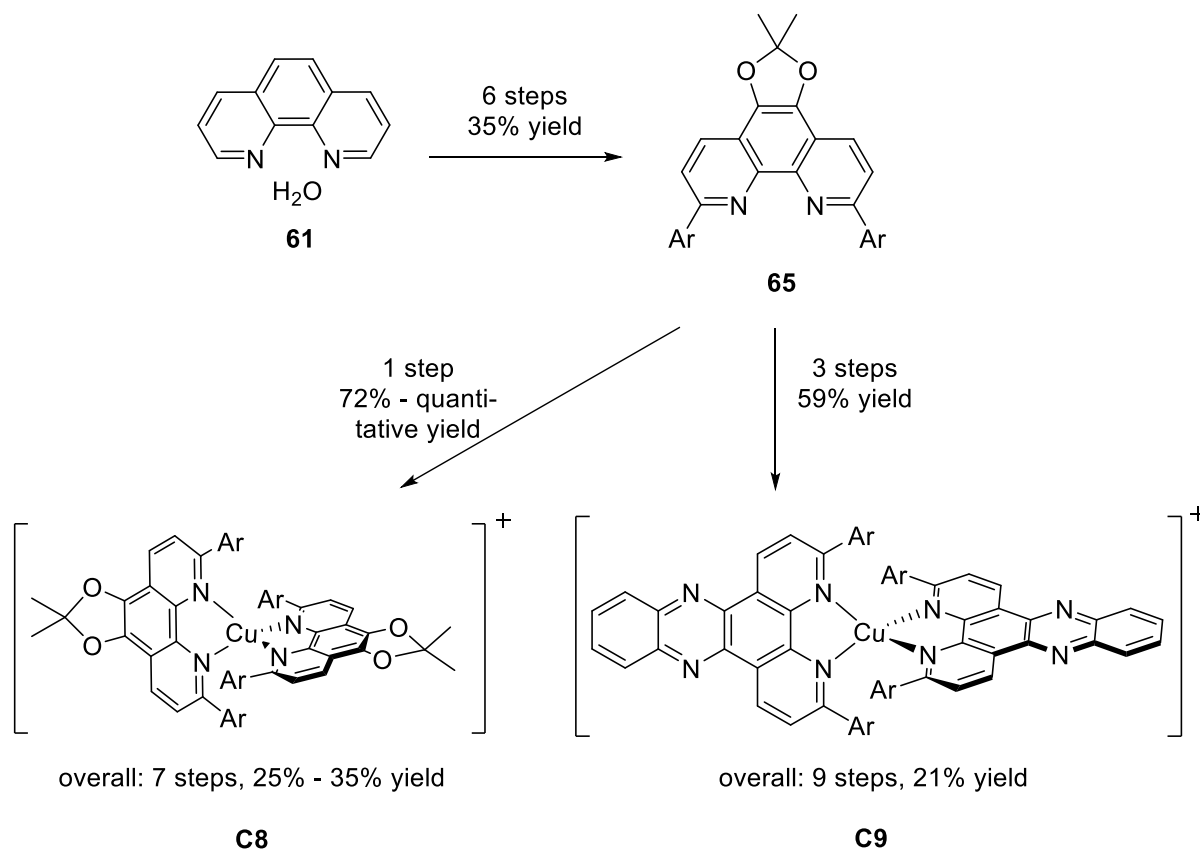
Although the trifluoromethylation was hardly catalyzed by $[\text{Cu}(\text{DABMes})_2]\text{BF}_4$ (**C14**), the example of the ATRA reaction between 1-octene (**77**) and diethyl bromomalonate (**78**) (c.f. Table 12) shows that this complex definitely exhibits photocatalytic activity. As referred to above, the redox potential of the excited state of $[\text{Cu}(\text{DABMes})_2]\text{BF}_4$ (**C14**) could not be

determined owing to extremely poor emission behavior. Nevertheless, it could be estimated in this case from the reduction potentials of applied substrates. In contrast to diethyl bromomalonate (**78**) ($E_{1/2} = -0.62 \text{ V}^8$)^[102] which was transformed with $[\text{Cu}(\text{DABMes})_2]\text{BF}_4$ (**C14**), no reaction was observed when using 4-nitrobenzyl bromide (**75**) ($E_{1/2} = -0.86 \text{ V}^8$)^[103]. Consequently, the excited state reduction potential of **C14** is likely to be too weak for 4-nitrobenzyl bromide. This would indicate a reduction potential of $[\text{Cu}(\text{DABMes})_2]\text{BF}_4$ (**C14**) between -0.62 and -0.86 V vs. SCE. However, in order to exactly determine the redox potentials of this system, more sophisticated physical investigations would be necessary.

⁸ vs. SCE in MeCN

6. Conclusion and Outlook

Two new homoleptic copper(I) phenanthroline complexes $[\text{Cu}(\text{dapacetal})_2]^+$ (**C8**) and $[\text{Cu}(\text{phenazino-dap})_2]^+$ (**C9**) were accessible starting from 1,10-phenanthroline hydrate in reasonable yields via the common intermediate dapacetal (**65**) (Scheme 29).



Scheme 29. Synthesis of $[\text{Cu}(\text{dapacetal})_2]^+$ (**C8**) and $[\text{Cu}(\text{phenazino-dap})_2]^+$ (**C9**).

Characterization and investigation of electrochemical and photophysical properties revealed redox behavior for $[\text{Cu}(\text{dapacetal})_2]^+$ (**C8**) which is very similar to that of the established $[\text{Cu}(\text{dap})_2]^+$ (**C1**). This result was surprising, as the insertion of potentially electron-donating oxygen atoms in the 5,6-position of the phenanthroline core structure was expected to increase the electron density of the complex, which should lead to more powerful reducing properties in the excited state. Due to these unexpected results, it was questionable as to whether it is possible to influence the electrons on the nitrogen atoms of the phenanthroline core by variations on the 5,6-position. In order to check this concept, the opposite path was followed by inserting electron-withdrawing groups. For this purpose, the phenazine group was chosen, as this part is already known for its electron-withdrawing effect to the bipyridine system of the ligand.^[11] Indeed, the reduction potential of the excited state of complex

[Cu(phenazino-dap)₂]PF₆ (**C9-PF₆**) is, with -1.20 V, weaker than that of [Cu(dap)₂]Cl (**C1-Cl**), which confirms the assumption of a strong electron-withdrawing influence of the phenazine group. Even though the reductive power of [Cu(phenazino-dap)₂]PF₆ (**C9-PF₆**) is reduced, it is theoretically sufficiently high enough to allow the reduction of interesting substrates.

Although the physical properties were less promising, both copper(I) complexes were tested as photoredox catalysts. Using [Cu(dapacetal)₂]⁺ (**C8**) in photoredox reactions revealed that it was inferior to [Cu(dap)₂]⁺ (**C1**) in different ATRA and allylation reactions as it showed slower conversion and furnished lower yields. Only the allylation of diethyl bromomalonate with *N*-Boc allylamine resulted in almost the same yields. Finally, the insertion of electron-donating ether functionalities in 5,6-position of the dap core structure did not lead to a better performance of the resulting homoleptic copper(I) catalyst (**C8**). As far as [Cu(phenazino-dap)₂]⁺ (**C9**) is concerned, experiments showed that it is inactive for ATRA reactions which run via a commonly assumed outer-sphere mechanism. The fact that [Cu(phenazino-dap)₂]⁺ (**C9**), on the other hand, works for the trifluoromethylchlorosulfonylation reaction, is a further indication of the existence of an alternative reaction pathway for this reaction, which is assumed to run via an inner-sphere mechanism.^[27] From the photophysical behavior investigated so far, there is no explanation for the predominant inactivity of **C9**. An explanation might be provided by the reduced lifetime of the excited state, which is still in the range of a few hundred nanoseconds, but might be too short for most of the tested reactions. Nonetheless, it was not possible to improve the catalyst performance by modifications in 5,6-position of the phenanthroline core structure. In contrast to this failed strategy, a more promising approach for developing more efficient copper(I)-based photoredox catalysts is the formation of heteroleptic complexes. The benefit of such complexes was already exemplified by Reiser's group in 2015 with the example of strong reducing [Cu(dpp)(binc)]⁺ (**C6**) (*E*_{1/2} (Cu²⁺/*Cu⁺) = -1.88 V vs. SCE in acetonitrile), which showed good activity for the allylation of organohalides with allyltrimethylsilanes.^[20] Appropriate to this concept would be, for example, the formation of so-called push-pull complexes with one phenazino-dap ligand as a strong electron-pulling ligand.

With [Cu(dap)Cl₂] (**C10**), a new copper(II) phenanthroline complex was readily synthesized and its structure was confirmed by X-ray analysis. Although it was not possible to determine the redox potentials of this complex unambiguously, this compound was tested as a photoredox catalyst. In a comparison of the catalytic performance of [Cu(dap)Cl₂] (**C10**) and established [Cu(dap)₂]Cl (**C1-Cl**) catalyst, copper(II) complex [Cu(dap)Cl₂] (**C10**) proved to be an efficient photocatalyst and showed reactivity in all investigated reactions. In the transformations of diethyl bromomalonate (**78**) with the allylic alkenes *N*-Boc allylamine or

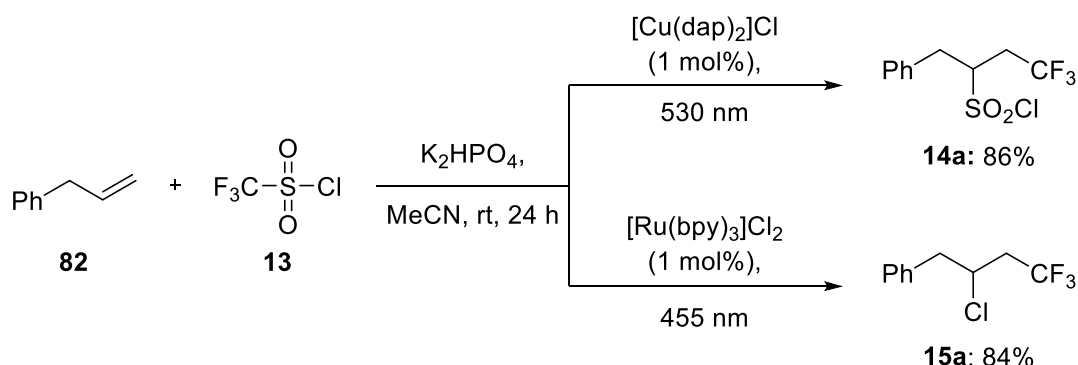
allyltrimethylsilane, **C10** surprisingly outperformed copper(I) catalyst **C1-Cl** and furnished higher product yields. Since the formation of a copper(I) species starting from $[\text{Cu}(\text{dap})\text{Cl}_2]$ (**C10**) is unlikely, and the resulting complexes could not explain the better performance, the formation of an intermediary copper(III) species as a key intermediate needs to be taken into consideration. Nevertheless, at this stage, there can only be speculation about the underlying reaction mechanism. The definitive elucidation of the mechanism requires further investigation, which is currently ongoing.

A new alternative to phenanthroline ligands for copper photoredox catalysts could be 1,4-diaza-1,3-butadienes (DAB). Since the known and bench-stable complex $[\text{Cu}(\text{DABMes})_2]\text{BF}_4$ (**C14**) showed promising photophysical properties, its photocatalytic activity was tested in visible-light-mediated ATRA reactions. Indeed, this complex proved to be a photocatalyst albeit it was inferior to established $[\text{Cu}(\text{dap})_2]^+$ (**C1**). The determination of the real scope of this complex would require the screening of more reactions, but it should be noted that the instability towards strong coordinating solvents limits this system as for example the appropriate solvent cannot always be applied. As DAB ligands can be easily synthesized, screening of different substitution patterns regarding the catalytic performance of the formed complexes and their stability against solvents would be reasonable. Since $[\text{Cu}(\text{DABMes})_2]\text{BF}_4$ (**C14**) is only one test example there is potential for improvement by systematic variation of the ligand substitution.

C. Atom Transfer Radical Addition Reactions – Investigation of New Reagents

1. Introduction

As previously reported in the introductory chapter A, the trifluoromethylchlorosulfonylation reaction (Scheme 30) showed that the kind of products formed in photoredox reactions can significantly depend on the employed catalyst.^[27] Here, trifluoromethanesulfonyl chloride (**13**), also known as triflyl chloride, was observed to be a special reagent because sulfur dioxide can be emitted in the course of the reaction. When $[\text{Cu}(\text{dap})_2]\text{Cl}$ (**C1**) is used, SO_2 is retained and chlorosulfonylated products **14** form as the main products. Hence, the question arose as to whether it is also possible to target different products with other reagents by using different photocatalysts, especially the established $[\text{Cu}(\text{dap})_2]\text{Cl}$ (**C1**). For this reason, in this chapter the investigation of new ATRA reagents is described which are quite similar in structure to the successful triflyl chloride and exhibit a comparable redox potential making them reducible by $[\text{Cu}(\text{dap})_2]\text{Cl}$ (**C1**) in the oxidative quenching cycle. After the reduction of the molecule, it should be able to dissociate into a stable radical such as the CF_3 radical and an anion.



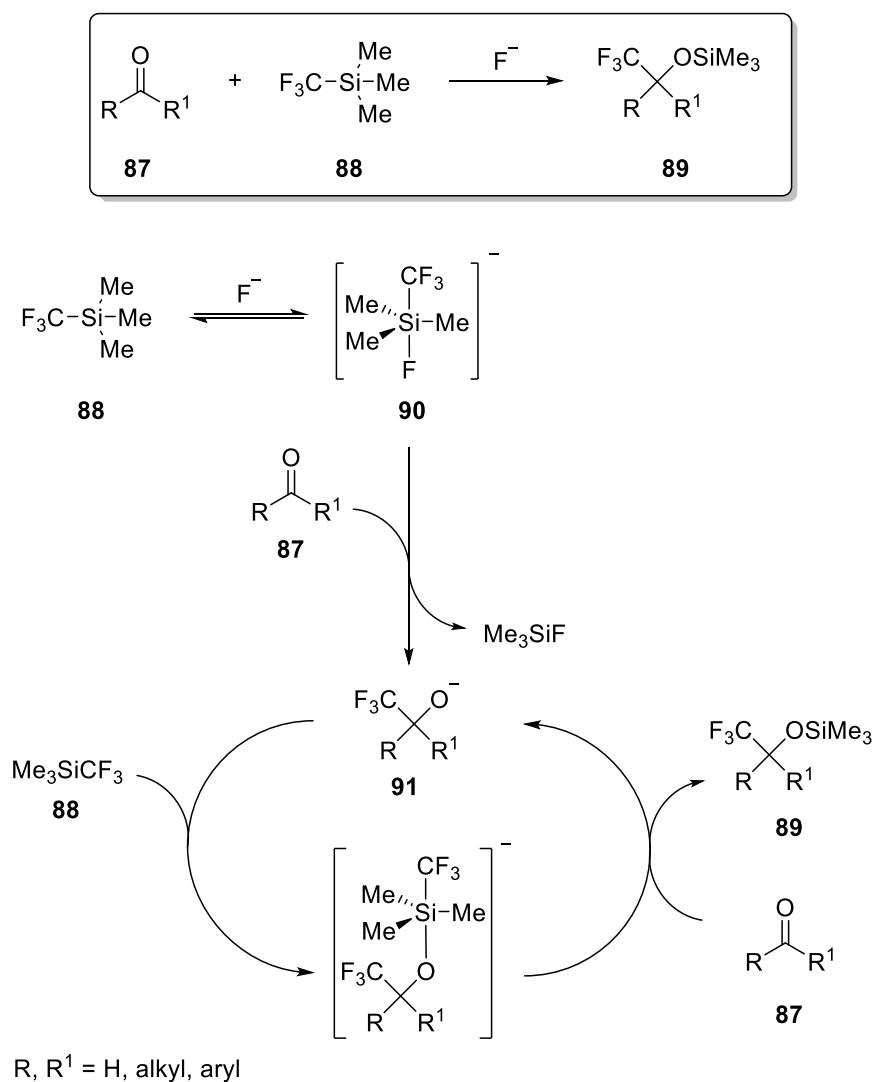
Scheme 30. Visible-light-mediated trifluoromethylchlorosulfonylation (**14a**) and trifluoromethylchlorination (**15a**) of allylbenzene (**82**).^[27]

Good ATRA reagents in this context should fulfill certain requirements. First of all, they should be known and readily available compounds which are already characterized and reported in the literature. In order to ensure easier access in a laboratory environment and to be able to control the stoichiometry precisely, the reagent should be liquid or solid and bench-stable under ambient conditions. For economic reasons, inexpensive compounds are preferable.

2. Investigation of Different Reagents

2.1 Ruppert-Prakash Reagent

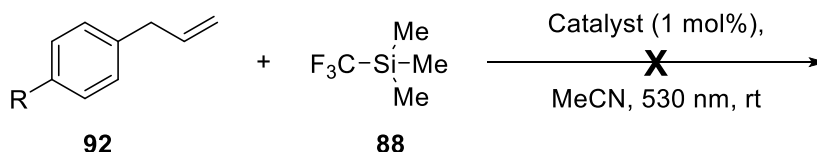
Trimethyl(trifluoromethyl)silane (TMSCF₃, **88**), also called Ruppert-Prakash reagent, fulfills the aforementioned requirements. Since its first successful preparation by Ruppert *et al.*^[129] in 1984 and the initial report on its trifluoromethylating properties by Prakash *et al.*^[130] in 1989, TMSCF₃ (**88**) has become a well-known nucleophilic reagent for trifluoromethylation^[131,132]. By using a catalytic or stoichiometric amount of a nucleophilic initiator such as tetrabutylammonium fluoride, trifluoromethyl anion “CF₃⁻” can be transferred to a suitable electrophile (Scheme 31).^[131,132] For reactions of aldehydes or ketones, for example, fluoride acts as an initiator only in the first part which runs via an unstable pentacoordinated silicon species **90**. The subsequent autocatalytic cycle is powered by the resulting alkoxide **91**.



Scheme 31. Trifluoromethylation of aldehydes or ketones using Ruppert-Prakash reagent (**88**).

As confirmed by X-ray diffraction, the Si-CF₃ bond of TMSCF₃ (**88**) is longer and weaker than the Si-CH₃ bonds.^[133] Thus, a conceivable cleavage of the Si-CF₃ bond by SET is theoretically preferred compared to a Si-CH₃ bond. With a reduction potential of the excited state of -1.43 V vs. SCE in acetonitrile^[19], [Cu(dap)₂]Cl (**C1-Cl**) should be strong enough to reduce TMSCF₃ (**88**) showing a peak potential of -0.91 V vs. SCE in acetonitrile. Table 14 illustrates test reactions which were performed in order to determine whether **88** is a suitable reagent for photocatalyzed ATRA reactions.

Table 14. ATRA test reactions with TMSCF₃ (**88**).^a



Entry	R	Catalyst, Additive	Time	Yield
1	H	[Cu(dap) ₂]Cl	4 d	n.r.
2	H	CuCl	4 d	n.r.
3	OMe	[Cu(dap) ₂]Cl	4 d	n.r.
4 ^b	H	[Cu(dap) ₂]Cl, K ₂ HPO ₄	20 h	n.r.
5 ^c	H	[Cu(dap) ₂]Cl	2 h	n.r.
6 ^{b, d}	H	<i>fac</i> -Ir(ppy) ₃ , K ₂ HPO ₄	20 h	n.r.
7 ^d	H	[Ir(ppy) ₂ (dtbbpy)]PF ₆	4 d	n.r.

a) Reaction conditions: Alkene (1.0 equiv, 0.5 mmol), trimethyl(trifluoromethyl)silane (**88**) (2.0 equiv), catalyst (5.0 μmol, 1.0 mol%), anhydrous MeCN (1.0 mL), rt, 530 nm (LED, distance 1 cm). b) 0.25 mmol scale, 1.5 mL solvent, K₂HPO₄ (2.0 equiv) was used as an additive. c) Anhydrous DCM was used as a solvent. d) 455 nm (LED, distance 1 cm).

The screening showed that reagent **88** is not reactive under the applied photoredox conditions. Even after four days, no conversion occurred and the control experiment with CuCl was also negative (entry 2). In order to exclude a possible product loss in the work up, less volatile 4-allylanisole was tested but no conversion was observed (entry 3). Both the use of the same conditions as for the trifluoromethylchlorosulfonylation reaction, where K₂HPO₄ is added as a base, and the use of dichloromethane as a solvent, did not lead to success either (entries 4 and 5). Given that even the established and strongly reducing iridium-based photoredox catalysts showed no transformation of TMSCF₃ (**88**) (entries 6 and 7), the investigation of this reagent was abandoned.

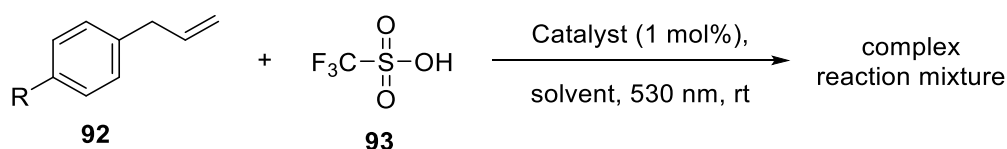
2.2 Trifluoromethanesulfonic Acid

Due to the fact that Ruppert-Prakash reagent (**88**) proved to be unreactive in photoredox catalyzed ATRA reactions, compounds more similar to triflyl chloride (**13**) were screened. First of all, variation on the side of the chloride residue was tested (Figure 16). To begin with a readily available, inexpensive and simple compound, trifluoromethanesulfonic acid (**93**) was initially investigated (Table 15).



Figure 16. Triflyl chloride (**13**) and triflic acid (**93**).

Table 15. ATRA test reactions with triflic acid (**93**).^a

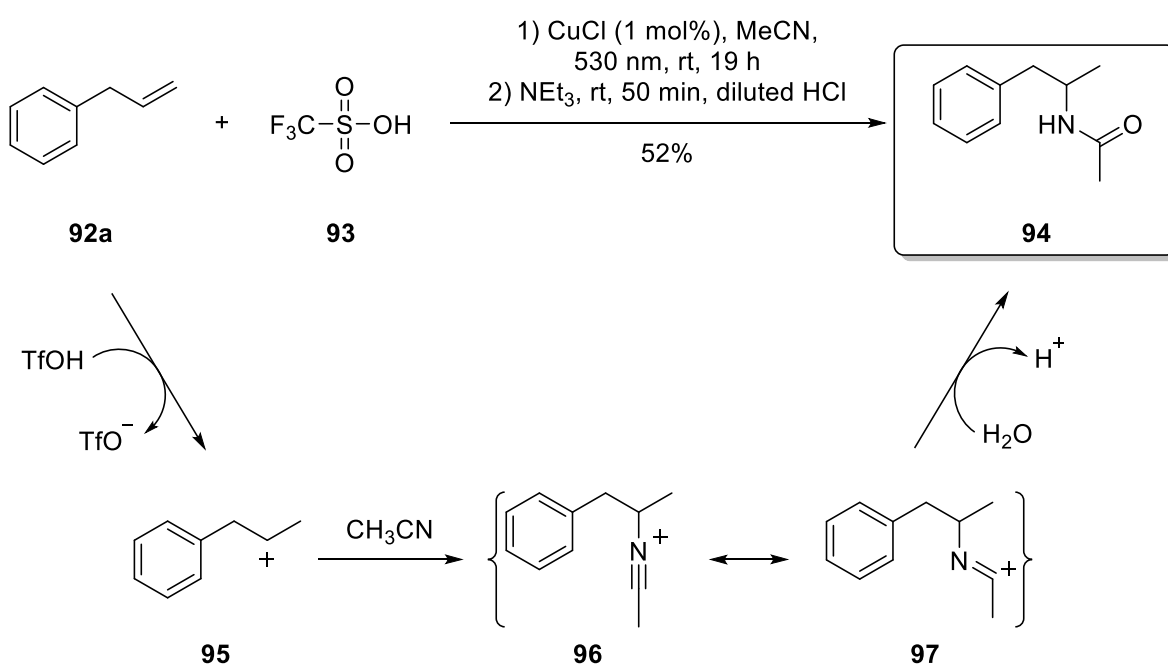


Entry	R	Catalyst	Solvent	Time	Yield
1	OMe	[Cu(dap) ₂]Cl	MeCN	3.5 h	complex
2 ^b	OMe	[Cu(dap) ₂]Cl	MeCN	2 h	complex
3	H	[Cu(dap) ₂]Cl	MeCN	19 h	29% of 94
4	H	[Cu(dap) ₂]Cl	DCM	19 h	complex
5 ^c	H	CuCl	MeCN	19 h	52% of 94

a) Reaction conditions: Alkene (1.0 equiv, 0.5 mmol), triflic acid (**93**) (2.0 equiv), catalyst (5.0 μmol, 1.0 mol%), anhydrous solvent (1.0 mL), rt, 530 nm (LED, distance 1 cm). b) Diluted reaction mixture: 1.5 mL of solvent was used; 530 nm (LED-Stick). c) 1.0 mmol scale; isolated yield after treatment with triethylamine at rt for 50 min.

All experiments resulted in complex reaction mixtures. Electrophilic addition could not explain the formation of possible side products, because the corresponding base of triflic acid, the trifluoromethanesulfonate anion, has a low degree of nucleophilicity and is known as an excellent leaving group.^[134,135] Thus, it seemed to be unlikely that an electrophilic addition to the alkene had taken place. However, it was possible to isolate the main product in two cases (entries 3 and 5). The mass analysis showed a molecule peak at 178.12 g/mol [MH⁺] which was not compatible with any reasonable ATRA or trifluoromethylation product. Since the crude ¹H-NMRs of entries 3 and 5 showed a very similar pattern it was concluded that [Cu(dap)₂]Cl (**C1-C1**) is not necessary for the reaction. Furthermore, the crude ¹H-NMR of

entry 4 showed a completely different pattern. This observation led to the conclusion that there might be a reaction with the solvent or at least that the solvent is decisive. With these results obtained, it was possible to assign the main product in the cases of entries 3 and 5 as *N*-(1-phenylpropan-2-yl)acetamide^[136] (**94**) (Scheme 32). The product is formed by a Ritter reaction, where the starting material is protonated using a strong acid.^[137] Here, triflic acid (**93**) with *pK_a* values of -12 in water and 0.7 in acetonitrile^[138], respectively, acts as an acid to form the carbocation **95**. After nucleophilic attack of acetonitrile and aqueous work up, amide **94** forms. Consequently, triflic acid is too reactive, leading to unwanted reactions, and therefore not applicable to photoredox catalyzed ATRA reactions under the investigated conditions.



Scheme 32. Ritter reaction taking place during ATRA test reaction.

2.3 Phenyl Triflates

As triflic acid (**93**) proved to be too reactive for ATRA reactions, most probably due to its strong acidity, the next approach was to block this property by substituting the acidic proton. For this purpose, in general, a methyl group or other alkyl groups could be used as easily accessible substituents. With regard to the targeted reaction system, however, an alkyl substitution cannot be expected to be reasonable, as the resulting esters **98** are known to be excellent alkylation reagents.^[135] This problem can be circumvented by using aryl substituents (**99**) instead of alkyl groups. The simplest compound would consequently be phenyl trifluoromethanesulfonate (**100**), the phenyl ester of triflic acid.

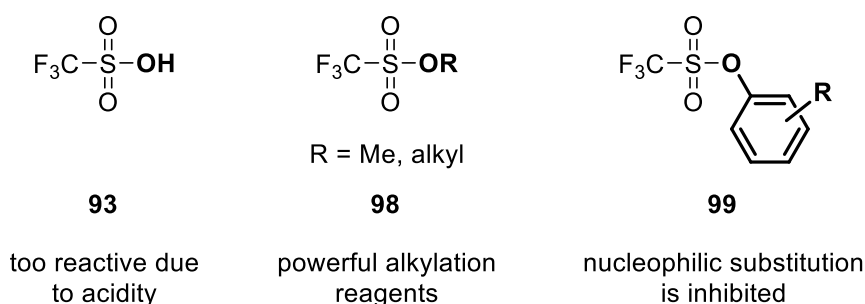
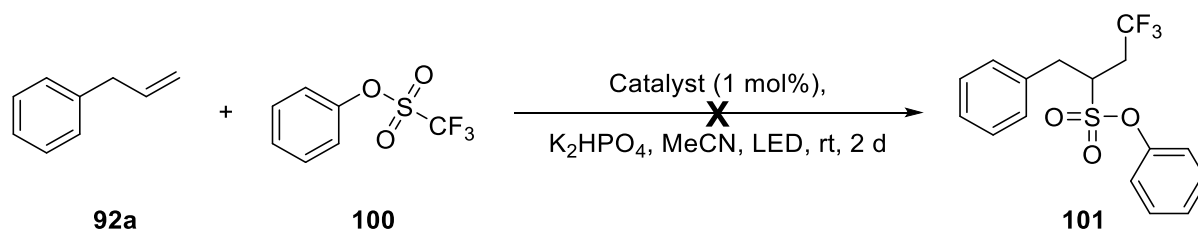


Figure 17. Properties of triflic acid (**93**) and its esters.

This known compound is, in contrast to alkyl esters, thermally more stable and does not react with nucleophiles such as water, alcohols or tertiary amines.^[135] Regarding the reduction potential, phenyl trifluoromethanesulfonate (**100**) shows a quite high reduction potential of -2.71 V vs. SCE in acetonitrile⁹. Therefore, this compound should not be accessible with established photoredox catalysts. Control experiments with [Cu(dap)₂]Cl (**C1-CI**) and more strongly reducing *fac*-Ir(ppy)₃ (**C4**) confirmed this assumption, as no reaction was detectable in the oxidative quenching cycle (Table 16).

⁹ A. Jutand *et al.* reported a reduction potential of -2.63 V vs. SCE in DMF at a gold electrode.^[139]

Table 16. Testing phenyl trifluoromethanesulfonate (**100**) as an ATRA reagent.

Entry	Catalyst	λ / nm	Yield / %
1	[Cu(dap) ₂]Cl	530	n.r.
2	<i>fac</i> -Ir(ppy) ₃	455	n.r.

Reaction conditions: Allylbenzene (1.0 equiv, 0.5 mmol), phenyl trifluoromethanesulfonate (**100**) (2.0 equiv), catalyst (5.0 μ mol, 1.0 mol%), K₂HPO₄ (2.0 equiv), anhydrous MeCN (1.5 mL), rt, irradiation via LED-stick, 2 d.

In order to make phenyl triflate accessible to visible-light-mediated photoredox catalyzed ATRA reactions, a much lower reduction potential is necessary. One strategy that can be used for lowering this potential is the substitution with electron-withdrawing groups at the phenyl ring. For this reason 2,4-dinitrophenyl trifluoromethanesulfonate (**103**) was synthesized in one step from the corresponding phenol and triflic anhydride in 30% yield following a procedure of S. J. Zhou and Z. Huang.^[140] The cyclic voltammetric measurements revealed a quite complex spectrum with four irreversible redox waves (A to D) in the negative potential area (Figure 18). The first reduction potential (wave A) shows, with a peak potential of -0.68 V vs. SCE in acetonitrile, a quite low reduction potential which is theoretically accessible by [Cu(dap)₂]Cl (**C1-Cl**) ($E_{1/2}$ (Cu²⁺/*Cu⁺) = -1.43 V vs. SCE in MeCN)^[19].

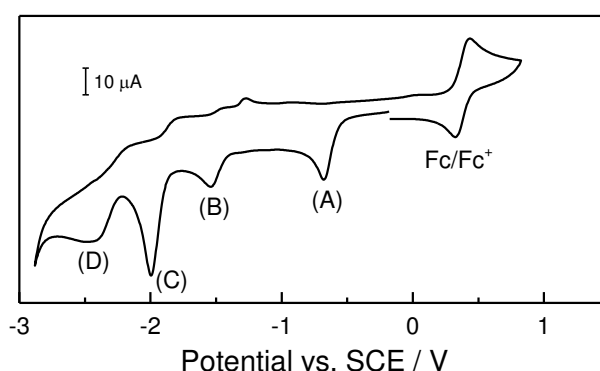


Figure 18. Cyclic voltammogram of 2,4-dinitrophenyl trifluoromethanesulfonate (**103**) in MeCN using tetrabutylammonium tetrafluoroborate as supporting electrolyte and ferrocene as internal standard at a scan rate of 50 mV*s⁻¹.

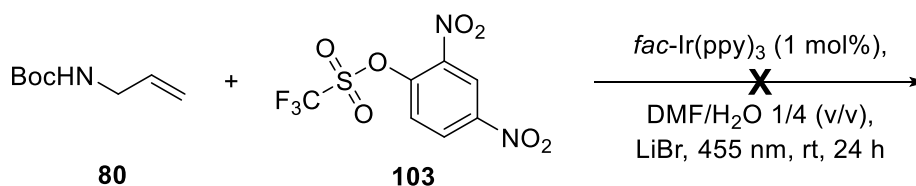
Table 17. Testing 2,4-dinitrophenyl trifluoromethanesulfonate (**103**) as an ATRA reagent.

R-CH=CH_2 (102) + $\text{F}_3\text{C-SO}_2\text{-O-C}_6\text{H}_3(\text{NO}_2)_2$ (103) $\xrightarrow[\text{solvent, LED, rt, 2 d}]{\text{Catalyst (1 mol\%)}}$ **X**

Entry	Alkene	Catalyst	Solvent	λ / nm	Yield
1		[Cu(dap) ₂]Cl	MeCN	530	n.r.
2		<i>fac</i> -Ir(ppy) ₃	MeCN	455	n.r.
3		<i>fac</i> -Ir(ppy) ₃	MeCN	455	n.r.
4		<i>fac</i> -Ir(ppy) ₃	DCM	455	n.r.

Reaction conditions: Alkene (1.0 equiv, 0.25 mmol), 2,4-dinitrophenyl trifluoromethanesulfonate (**103**) (2.0 equiv), catalyst (2.5 μmol , 1.0 mol%), K₂HPO₄ (2.0 equiv), anhydrous MeCN (0.75 mL), rt, irradiation via LED-stick, 2 d.

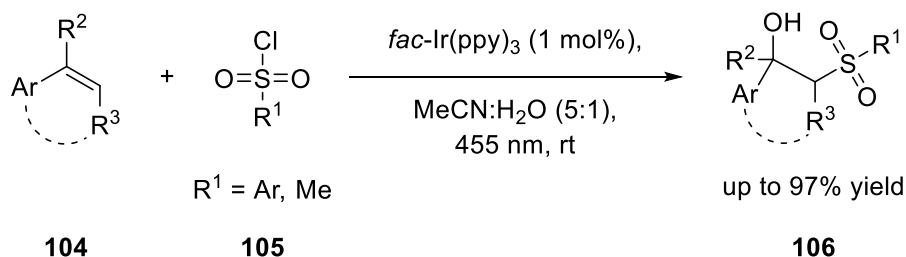
The application of 2,4-dinitrophenyl trifluoromethanesulfonate (**103**) as an ATRA reagent was firstly tested on the basis of the reaction with allylbenzene (Table 17, entry 1). As the catalyst [Cu(dap)₂]Cl (**C1-C1**) did not facilitate any reaction, more strongly reducing *fac*-Ir(ppy)₃ (**C4**) ($E_{1/2}(\text{Ir}^{4+}/\text{Ir}^{3+}) = -1.73$ V vs. SCE in MeCN)^[10] was tested (entries 2 to 4), without any success. No reaction took place with styrene or when using dichloromethane as a solvent. Due to the fact that the reduction potential of 2,4-dinitrophenyl trifluoromethanesulfonate (**103**) must be accessible by these catalysts, a further system was tested. However, also *N*-Boc allylamine showed no reaction (Scheme 33).

**Scheme 33.** Test reaction between *N*-Boc allylamine (**80**) and 2,4-dinitrophenyl trifluoromethanesulfonate (**103**).

Based on the cyclovoltammetric results, 2,4-dinitrophenyl trifluoromethanesulfonate (**103**) should be an easily reducible compound. However, this compound showed no reactivity in established reactions using theoretically suitable photoredox catalysts.

2.4 Trichloromethanesulfonyl Chloride

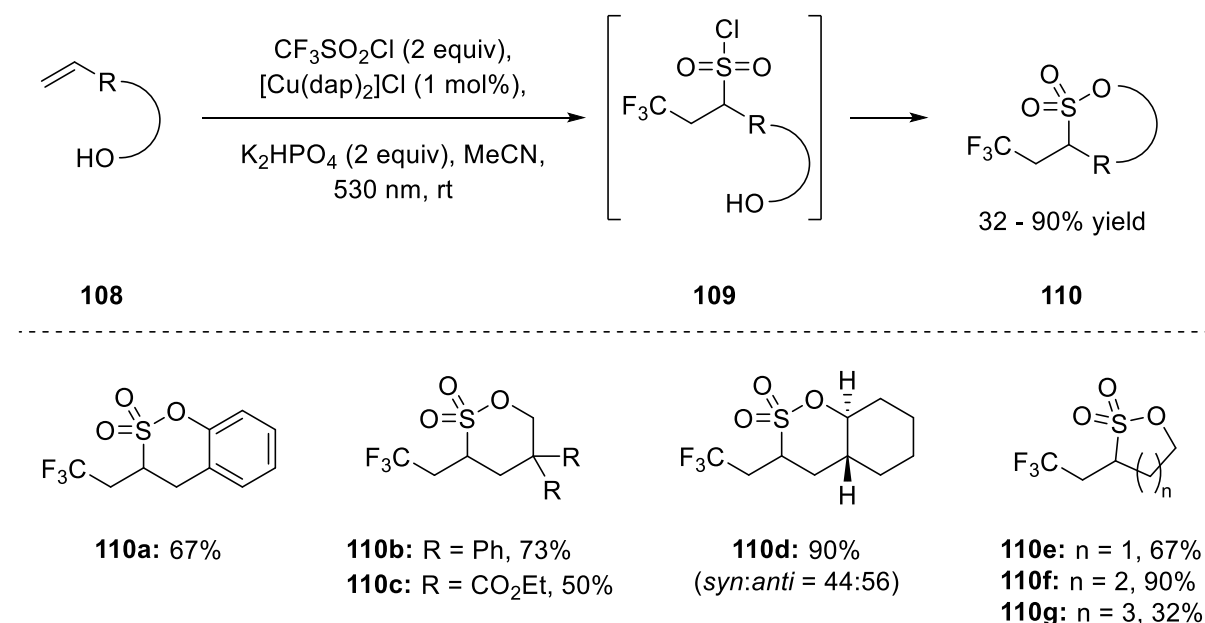
Due to the fact that the modification on the chloride side did not lead to success, the modification of the trifluoromethane group was investigated. The activation of sulfonyl chlorides via photoredox catalysis is already well known, especially for fluoroalkyl- or aryl-substituted derivatives.^[141] For instance, the application of variously substituted sulfonyl chlorides **105** for the photocatalytic synthesis of β -hydroxysulfones **106** was developed during the work on this thesis by O. Reiser and co-workers (Scheme 34).^[29] For this reaction, which is initiated by an oxidative quenching cycle, *fac*-Ir(ppy)₃ (**C4**) proved to be a more efficient photoredox catalyst than [Ru(bpy)₃]Cl₂ (**C2**) or [Cu(dap)₂]Cl (**C1-Cl**). Regarding the substitution of the sulfonyl chloride **105**, a number of different aryl groups and the methyl group were tested. As substituents for the aryl group, both electron-donating and electron-withdrawing groups were tolerated.



Scheme 34. Photocatalytic synthesis of β -hydroxysulfones **106** according to O. Reiser *et al.*^[29]

Furthermore, W. R. Dolbier and co-workers used fluoroalkylsulfonyl chlorides such as CF₃SO₂Cl, C₄F₉SO₂Cl, CF₂HSO₂Cl, CH₂FSO₂Cl or CF₃CH₂SO₂Cl under photoredox catalysis for the transformation of fluoroalkyl groups to alkenes.^[41,142] Unlike the trifluoromethylchlorosulfonylation reaction or the photocatalytic synthesis of β -hydroxysulfones developed by O. Reiser and co-workers^[27,29] (*vide supra*), these reactions are associated with a loss of SO₂.

In contrast to this, trichloromethanesulfonyl chloride (**111**), which is very similar in structure to triflyl chloride (**13**), is less investigated. During the work on this thesis, O. Reiser *et al.* reported the internal cyclization of alcohol substituted sulfonyl chlorides to sultones **110**^[28,47], the cyclic esters of hydroxyl sulfonic acids (Scheme 35). Using [Cu(dap)₂]Cl (**C10-Cl**) as a photoredox catalyst and green light, a variety of differently substituted alkenols **108** were reacted with fluoroalkylsulfonyl chlorides such as triflyl chloride (**13**) in the presence of a base.



Scheme 35. Photoredox catalyzed synthesis of sultones **110** according to O. Reiser *et al.*^[28]

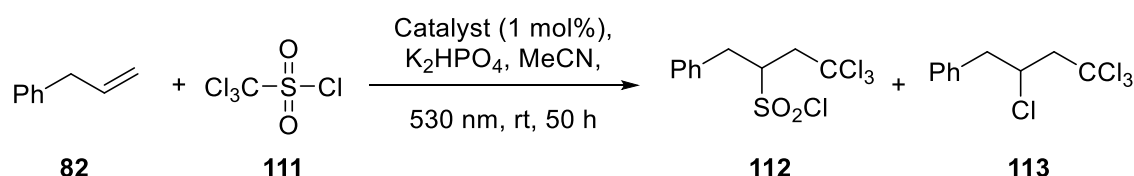
In this way, sultones **110** can be formed by an intramolecular cyclization of the intermediary formed sulfonyl chlorides **109** in a one-step synthesis. For this reaction, trichloromethanesulfonyl chloride (**111**) was tested as well, but only on two different alkenes (pent-4-en-1-ol and 2,2-diphenylpent-4-en-1-ol). In both cases, a complex reaction mixture formed and the desired cyclized product was not observed. Given that the reaction might have failed due to the subsequent cyclization reaction, this reagent was investigated further in this thesis nonetheless.

Cyclic voltammetry revealed for trichloromethanesulfonyl chloride (**111**) a reduction potential of -0.61 V^{10} , which is more negative than that of triflyl chloride (**13**) ($E_{1/2} = -0.18 \text{ V}^{10}$)^[143] but still easily accessible by established photoredox catalysts such as [Cu(dap)₂]Cl (**C1-Cl**) ($E_{1/2}(\text{Cu}^{2+}/\text{Cu}^+) = -1.43 \text{ V}^{10}$)^[19]. In order to check the reactivity of **111**, preliminary test reactions were carried out under the same conditions as the trifluoromethylchlorosulfonylation reaction (Table 18). The reaction was stopped after 50 hours and allylbenzene (**82**) was still detectable in crude ¹H-NMR spectra in all cases. The chlorosulfonylated product **112** was formed in a 5% yield under irradiation with light when using [Cu(dap)₂]Cl (**C1-Cl**) (entry 1). However, the reaction appeared to be very slow and the selectivity was improvable. Without irradiation, both products were detected only in traces by crude ¹H-NMR analysis and mass analysis (entry 2), which indicates that light irradiation is indispensable for the reaction. Traces might have formed by ambient light during sample preparation and sample taking. Without catalyst, the chlorinated product **113** was formed in

¹⁰ vs. SCE in MeCN

22% yield by mere irradiation with green light, whereas the chlorosulfonylated product **112** was not observed (entry 3). Furthermore, mass analysis revealed traces of hexachloroethane, which provides a hint of a possible radical mechanism. Consequently, the chlorosulfonylation reaction is a photoredox catalyzed reaction which needs both light and a catalyst. However, the chlorination product **113** presumably forms in a radical mechanism because it occurs with mere light irradiation.

Table 18. Preliminary ATRA test reactions with trichloromethanesulfonyl chloride (**111**).



Entry	λ / nm	Catalyst	Yield (112) / %	Yield (113) / %
1 ^a	530	[Cu(dap) ₂]Cl	5	7
2	-	[Cu(dap) ₂]Cl	traces	traces
3 ^b	530	-	-	22

Reaction conditions: Allylbenzene (**82**) (1.0 equiv, 0.5 mmol), trichloromethanesulfonyl chloride (**111**) (2.0 equiv), catalyst (5.0 μ mol, 1.0 mol%), K₂HPO₄ (2.0 equiv), anhydrous MeCN (1.5 mL), rt, irradiation via LED-stick, 50 h. a) 2% of elimination product were isolated. b) Traces of hexachloroethane were found by EI-MS analysis.

To improve the reaction yield, different reaction conditions were screened (Table 19). As for trifluoromethylchlorosulfonylation reaction with triflyl chloride (**13**)^[27], the use of K₂HPO₄ as a base is helpful for this reaction (entries 1 and 2). By screening different solvents, dichloromethane was observed to be the best choice because it furnished the highest yield of chlorosulfonylated product **112** and in contrast to tetrahydrofuran it resulted in less chlorinated product **113** (entries 3 to 7). An excess of 4.0 equivalents of halide **111** gave the best results (entries 7 to 10). When irradiating with blue light (455 nm), the yield dropped and the product ratio of **112/113** was lowered (entry 11). However, irradiation with blue light alone, without using any catalyst only furnished the chlorinated product **113** (entry 12). It was not possible to improve the conversion or yield by diluting the reaction mixture or by using prolonged reaction times (entries 13 and 14). The use of [Ir(ppy)₂(dtbbpy)]PF₆ (entry 15) or [Ru(bpy)₃]Cl₂ • 6H₂O (entry 16) furnished mainly product **113** which resulted in an inversed product ratio. This trend is in accordance with the results for triflyl chloride (**13**) (cf. Table 8). Reducing the amount of catalyst to 0.5 mol% resulted in lower yields (entry 17). Using a copper(I) salt only furnished the chlorinated product **113** which is already formed by mere light irradiation. Consequently, the formation of the chlorosulfonylated product **112** is a

PhCH=CH2 (**82**, 1.0 equiv) + ClC(S(=O)(=O)Cl)Cl (**111**, 4.0 equiv)

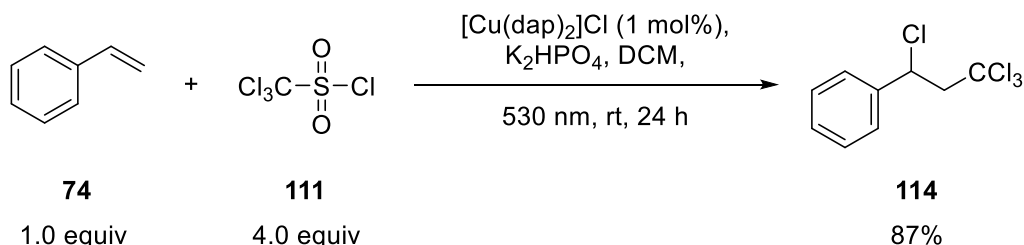
Reagents: $[\text{Cu}(\text{dap})_2]\text{Cl}$ (1 mol%), K_2HPO_4 , solvent, 530 nm, rt, 24 h

Products: PhCH2CH(SO2Cl)CH2CCl3 (**112**) + PhCH2CH(Cl)CH2CCl3 (**113**)

Entry	Solvent	Modified Conditions	112/113	Yield (112) / %	Yield (113) / %	Conversion (Alkene) / %
1	MeCN		-	32	traces	88
2	MeCN	no K ₂ HPO ₄	-	20	-	48
3	DMF		-	-	-	44
4 ^b	CHCl ₃		82/18	29	traces	44
5	THF		72/28	56	22	89
6	DMSO		-	traces	traces	87
7 ^c	DCM		89/11	64	8	80
8 ^b	DCM	0.5 equiv of halide	-	11	traces	11
9 ^b	DCM	1.0 equiv of halide	-	9	traces	9
10	DCM	2.0 equiv of halide	83/17	10	2	18
11	DCM	455 nm	79/21	30	8	49
12	DCM	455 nm, no catalyst	-	-	87	96
13	DCM	1.5 mL solvent	-	16	-	74
14	DCM	48 h		66	-	79
15 ^b	DCM	455 nm, 1 mol% [Ir(ppy) ₂ (dtbbpy)]PF ₆	23/77	18	60	100
16 ^{b, d}	DCM	455 nm, 1 mol% [Ru(bpy) ₃]Cl ₂ • 6H ₂ O	4/96	4	96	100
17	DCM	0.5 mol% [Cu(dap) ₂]Cl		61	-	66
18	DCM	1 mol% CuCl	-	-	55	56

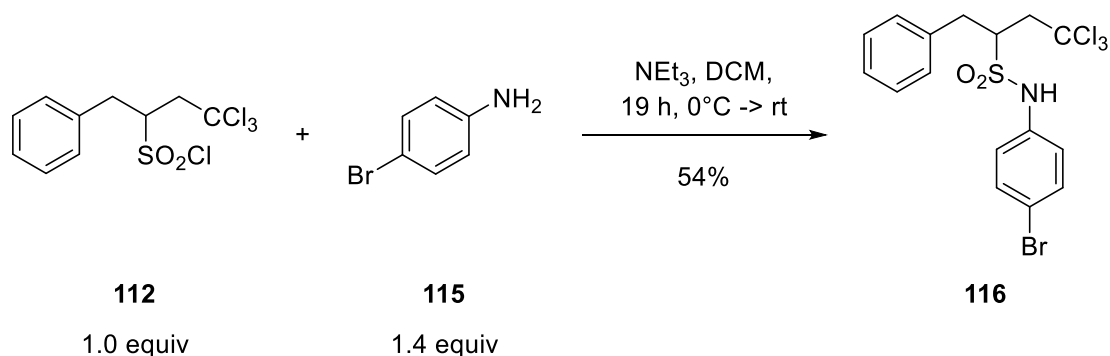
72

When using styrene as a substrate, only the chlorination product **114** was observed and isolated in a 87% yield (Scheme 36). This observation concurs with the results of triflyl chloride (**13**) where in the case of styrenes as starting material a loss of SO₂ and net addition of trifluoromethyl and chloride takes also place.^[27] In contrast to the fluorine analog, however, the trichloromethyl substituted styrene **114** is stable and elimination of HCl was not observed.



Scheme 36. Formation of the chlorination product **114** with styrene.

In the next step, consecutive reactions of the trichloromethylated sulfonyl chloride **112** were tested. Sulfonyl chlorides are known to readily react with anilines under formation of sulfonamides, an important substance class in medicinal chemistry.^[27,144] In addition to that, such derivatives readily crystallize, which opens the possibility of indirectly proving the structure of sulfonyl chloride **112** by X-ray analysis. For this reason, sulfonamide **116** was successfully synthesized in 54% yield following a procedure of O. Reiser *et al.*^[27] (Scheme 37). Since suitable crystals were now obtained by liquid diffusion of diethyl ether into a dichloromethane solution, the structure was confirmed by X-ray analysis.

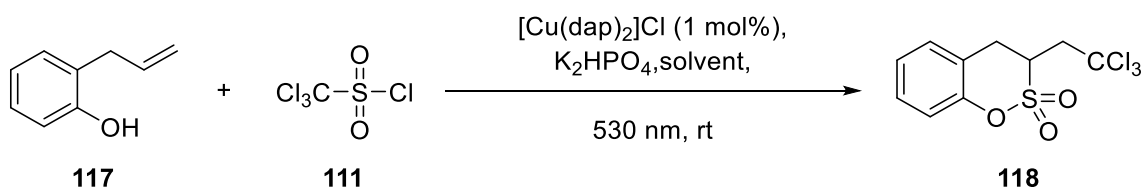


Scheme 37. Formation of sulfonamide **116**.

Another interesting reaction is the internal cyclization of alcohol substituted sulfonyl chlorides to sultones **110** (cf. Scheme 35). Since their discovery by H. Erdmann in 1888^[145], sultones have been of special interest as they are important intermediates in organic synthesis, motives in biologically active compounds or find application in material science and medicinal chemistry.^[146] In order to test a potential internal cyclization reaction with

trichloromethanesulfonyl chloride (**111**), 2-allylphenol (**117**) was reacted under the improved reaction conditions (Table 20, entry 1). In a one-pot synthesis, via a nucleophilic substitution after the ATRA reaction, sultone **118** formed and was isolated in 32% yield. Using the standard conditions of the trifluoromethylchlorosulfonylation reaction was less successful (entry 2).

Table 20. Reaction of 2-allylphenol (**117**).^a



Entry	Solvent	CCl ₃ SO ₂ Cl	Reaction Time	Yield
1	DCM	4.0 equiv	3 d	32%
2 ^b	MeCN	2.0 equiv	5 d	11%

a) Reaction conditions: 2-allylphenol (**117**) (1.0 equiv, 0.50 mmol), trichloromethanesulfonyl chloride (**111**), [Cu(dap)₂]Cl (5.0 μmol, 1 mol%), K₂HPO₄ (2.0 equiv), anhydrous solvent (0.5 mL), rt, 530 nm (LED-stick). b) 1.0 mmol scale.

Consequently, the formation of sultones is possible with trichloromethanesulfonyl chloride (**111**) in reasonable yields. However, the reaction with **111** is less efficient than with triflyl chloride (**13**), which was reported to give 67% of product using acetonitrile as a solvent and only 2.0 equiv of halide **13** after 17 h (cf. ref ^[28]).

3. Conclusion and Outlook

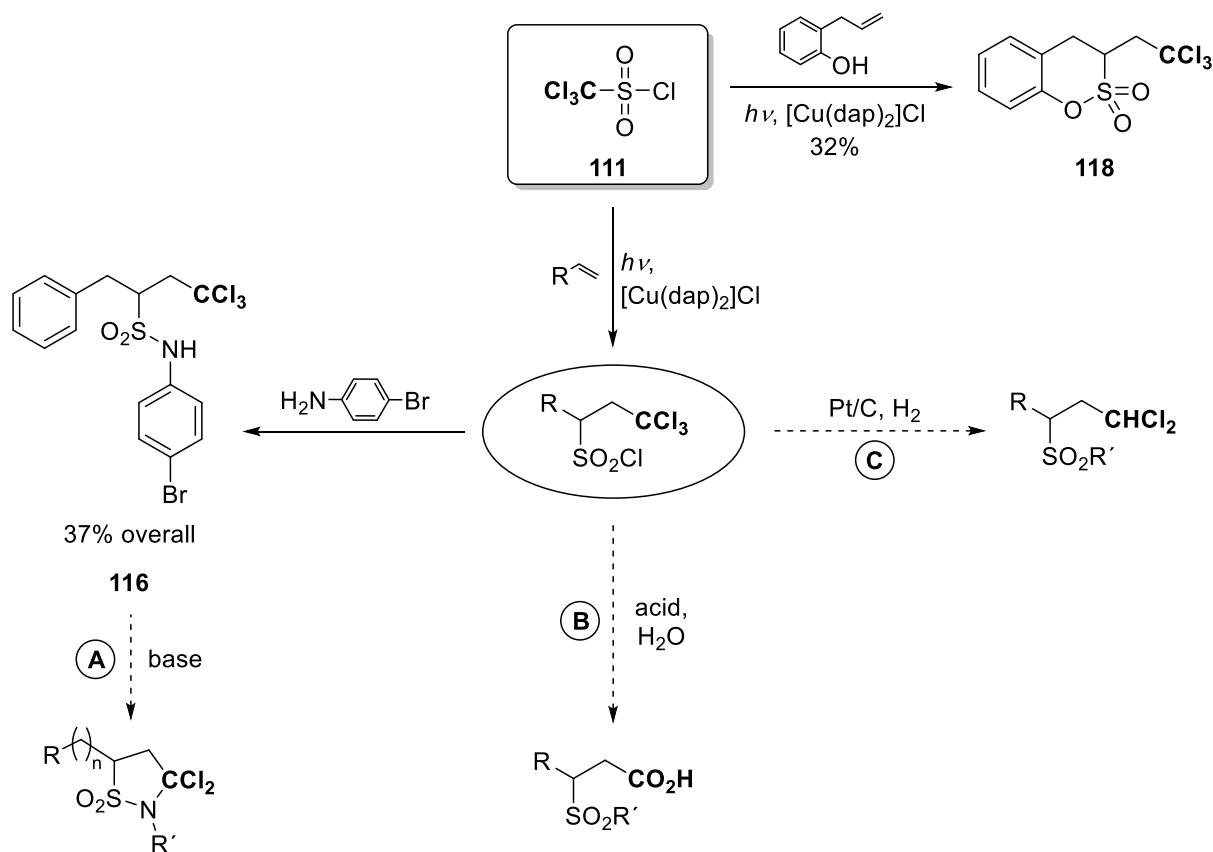
Four compounds were screened for their application as potential new ATRA reagents. First of all, Ruppert-Prakash reagent (TMSCF_3 , **88**), an established nucleophilic reagent for trifluoromethylation, was tested. This reagent proved to be unreactive in photoredox catalyzed ATRA reactions under the investigated conditions, even though, having regard to its reduction potential, it should be accessible via the oxidative quenching cycle of the applied catalysts.

As it was not clear why TMSCF_3 (**88**) was unreactive in photoredox catalyzed ATRA reactions, compounds more similar to triflyl chloride (**13**) were screened. Beginning with variation on the side of the chloride residue, readily available triflic acid (**93**) was investigated. However, triflic acid proved to be unsuitable as it undergoes undesired reactions owing to its high acidity. By identifying one of the side products as *N*-acetylamphetamine (**94**) it became clear that the strong acid properties lead to Ritter-like side reactions.

In order to inhibit the side reactions caused by the compound's acidity, the acidic proton was substituted by esterification in the next step. As phenyl trifluoromethanesulfonate (**100**) exhibits a quite high reduction potential, which is not accessible by common photoredox catalysis in theory, more easily reducible 2,4-dinitrophenyl trifluoromethanesulfonate (**103**) was tested. Surprisingly, this reagent showed no reaction with any tested theoretically suitable photoredox catalyst exhibiting sufficiently high redox potentials. A possible explanation might be a very fast back electron transfer from the substrate to the catalyst which is faster than the consecutive chemical reaction. For the investigation of such processes, further physical measurements such as Stern-Volmer analysis would be necessary.

Finally, the modification on the chloride side was unsuccessful and the modification of the trifluoromethane group was targeted. In this context, the reaction between $\text{CCl}_3\text{SO}_2\text{Cl}$ (**111**) and allylbenzene furnished the chlorosulfonylated product **112** as the main product using $[\text{Cu}(\text{dap})_2]\text{Cl}$ as the catalyst. As observed in the case of $\text{CF}_3\text{SO}_2\text{Cl}$ (**13**), the main product was formed without the extrusion of SO_2 under copper catalysis. Owing to quite low yields, the reaction conditions had to be optimized. With the optimized conditions identified, trichloromethanesulfonyl chloride (**111**) was successfully used as an ATRA reagent similar to triflyl chloride (**13**). A test reaction with styrene revealed that after loss of SO_2 only the chlorination product **114** was accessible with this substance class. In order to determine the real scope of this reagent, a screening of further substrates is necessary. Analogous to the

trifluoromethylated derivatives, the formation of important substance classes such as sulfonamides (cf. **116**) or sultones (cf. **118**) was also possible. In contrast to the CF_3 group, the CCl_3 group offers the possibility for additional derivatization (Scheme 38).



Scheme 38. Transformations originating from trichloromethanesulfonyl chloride (**111**).

With the sulfonamides so obtained, for instance, an internal cyclization after the treatment with a strong base should be possible^[147] which would open the way for new heterocycles (Scheme 38, path A). Regarding the trichloromethyl group, the formation of carboxylic acids is conceivable, for example, by hydrolysis using H_2SO_4 or HNO_3/NO_2 (path B).^[148] Another potential derivatization is the mono-hydrodechlorination of the trichloromethyl group to a *gem*-dichloromethyl group using Pt/C under hydrogen atmosphere (path C).^[149] The dichloromethyl functionality is of special interest for pharmaceuticals^[150] or can be converted to the corresponding aldehyde^[151].

D. Elucidating the Reaction Pathways of Visible-Light-Mediated Chloramination of Alkenes

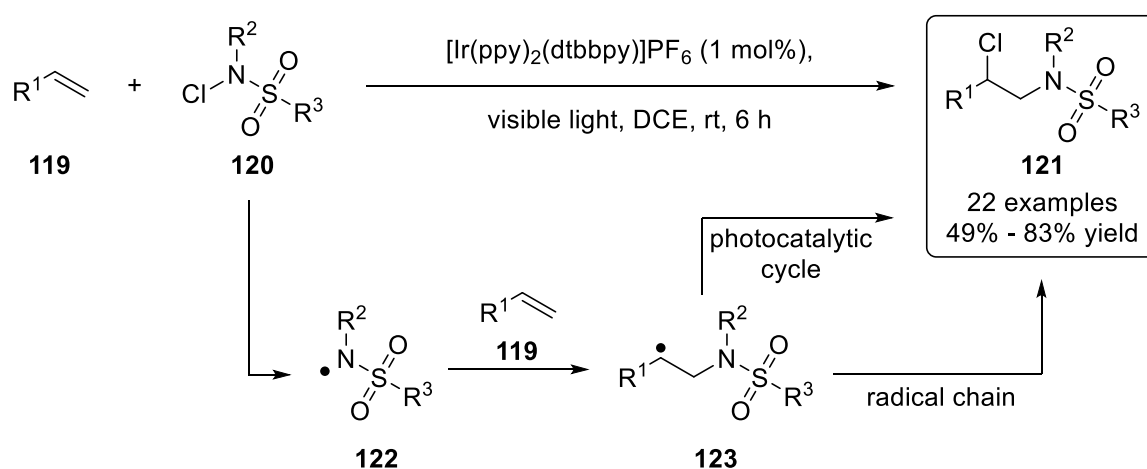
For greater clarity, catalyst $[\text{Cu}(\text{dap})_2]\text{Cl}$ (**C1-Cl**) is abbreviated as **[Cu]** and $[\text{Ir}(\text{ppy})_2(\text{dtbbpy})]\text{PF}_6$ (**C3-PF₆**) as **[Ir]** in this chapter.

1. Introduction

Photoredox catalyzed ATRA reactions are of special value for organic synthesis, being an alternative to transition metal catalyzed cross coupling reactions.^[49,152] The initial electron transfer between the catalyst and the substrate is considered to be the key step that determines the success of a given transformation. It is less recognized that subsequent reaction steps involving the photocatalyst in the course of a reaction can be equally decisive and, in particular, that the same transformation can require different photocatalysts dependent on the electronic properties of the substrates that are employed. As previously outlined in the introductory chapter A, for visible-light-mediated ATRA reactions two different mechanistic pathways, both being initiated by a single electron transfer to a halide, are well-established (cf. Scheme 7). The radical chain mechanism is plausible as many photoredox catalyzed ATRA reactions proceed equally well under thermal conditions in the presence of a radical initiator.^[33–35,37,153] On the other hand, the validity of a photocatalytic cycle has been justified owing to so-called “light/dark” experiments, demonstrating that the ATRA process is shut down and turned on again by switching the light source repeatedly off and on. However, Yoon and co-workers revealed that such “light/dark” experiments cannot be taken as clear evidence for a photocatalytic cycle in ATRA reactions, considering the fast rates of radical chain processes.^[154]

The intermolecular chloramination of alkenes **119** with *N*-chlorosulfonamides **120** (cf. Scheme 39) represents a useful transformation for the synthesis of biologically important compounds, and consequently has been intensively studied.^[155,156] Of relevance for the present study, a number of protocols have been reported that involve the initial generation of *N*-centered radicals **122** from **120** as key intermediates, which are assumed to add to an alkene **119** afterwards. Product formation runs through one of the aforementioned established pathways after formation of radical **123**. By contrast, the studies of ATRA reactions using $[\text{Cu}(\text{dap})_2]\text{Cl}$ (**[Cu]**) in Reiser’s group during the past decade revealed that with copper a potential third pathway, running via an inner-sphere mechanism, is present.^[27,28]

Recently, S. Yu and co-workers published the regioselective intermolecular visible-light-promoted chloramination of olefins **119** with *N*-chlorosulfonamides **120**, the latter serving both as the nitrogen and chlorine source (Scheme 39).^[156] This reaction is of special interest since sulfonamides play an important role in organic chemistry and find special applications for pharmaceuticals^[144,157], and the additional chlorine functionality provides a convenient handle for further synthetic transformations. Investigating different iridium- and ruthenium-based photocatalysts, [Ir(ppy)₂(dtbbpy)]PF₆ (**[Ir]**) was observed to be the most efficient catalyst for this transformation; however, only electron-rich alkenes gave rise to high yields in the process.



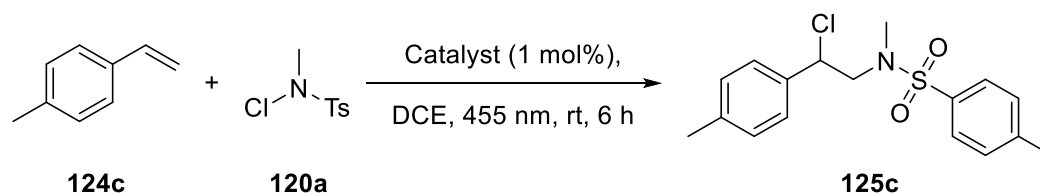
Scheme 39. 1,2-chloramination of olefins according to S. Yu *et al.*^[156]

In contrast to these results, in this chapter it is demonstrated that [Cu(dap)₂]Cl (**[Cu]**) efficiently converts electron-deficient alkenes to the corresponding chloraminated products, but is less efficient for electron-rich alkenes. Since the reaction is initiated by an electron transfer from the photoredox catalyst to the *N*-chlorosulfonamides **120** (*vide infra*), it is apparent that this initial reaction step cannot account for the catalyst dependence with respect to the alkenes **119** employed. Hence, for the chloramination reaction copper makes the significant difference as it has access to a special reaction pathway.

2. Screening of Substrate Scope

Taking *p*-methylstyrene (**124c**) as the benchmark substrate, which has been reported^[156] to give high yields in the chloramination reaction catalyzed by **[Ir]** (Table 21, entry 1), **[Cu]** was observed to promote the formation of **125c**, albeit in lower yields (entry 2). Surprisingly, carrying out a control experiment by irradiating the reaction mixture in the absence of a photocatalyst revealed that **125c** is also formed in high yields (entry 3) as long as no oxygen is present (entry 4), despite the fact that the reaction solution hardly absorbs any visible light (*vide infra*). Further controls nevertheless proved the necessity of light (entries 5 to 7), unless a catalytic amount of AIBN as a radical starter is employed at 80 °C (entry 8).

Table 21. Testing of **[Cu]**.^a



Entry	λ / nm	Catalyst, Conditions	Yield / %	
			Isolated	NMR ^b
1	455	[Ir]	83 (ref ^[156])	— ^c
2	455	[Cu]	66	79 ^d
3	455	no	85	100 ^e
4 ^f	455	no, 1 bar O ₂	-	n.r.
5	no	[Cu]	-	4
6	no	no	-	n.r.
7	no	no, 80°C	-	10
8	no	AIBN ^g , 80 °C	-	88

a) Reaction conditions: 4-methylstyrene (**124c**) (1.0 equiv, 0.30 mmol), *N*-chlorosulfonamide **120a** (1.5 equiv), catalyst (0.003 mmol, 1 mol%), anhydrous DCE (6.0 mL), degassed solution, rt, 455 nm (LED-stick), 6 h. b) Determined by ¹H-NMR using 2-nitropropane as internal standard. c) NMR yield after 1h: 50%. d) NMR yield after 1h: 80%. e) NMR yield after 1h: 44%. f) 4 h. g) 1 mol%, dark.

Due to the promising results, different electron-rich styrene derivatives **124** were screened (Table 22). The substitution pattern of methoxy substituted styrenes, as well as the choice of the catalyst used, have a dramatic influence on the reaction outcome (entries 1 to 6). While *para* substitution led to the hydroxy substituted product **125a** after workup, the expected chlorinated product was obtained with *ortho* substitution.

Table 22. Substrate scope of electron-rich styrene derivatives **124**.^a

Entry	Product	Catalyst	Yield / %	
			Isolated	NMR ^b
1	 125a	no	18 ^c	-
2		[Ir]	81 (ref ^[156]) ^c	86 (ref ^[156])
3		[Cu]	complex rxn mixture	
4	 125b	no	-	28
5		[Ir]	26	30
6		[Cu]	56	62
7	 125c	no	85	100
8		[Ir]	83 (ref ^[156])	-
9		[Cu]	66	79
10	 125d	no	-	50
11		[Ir]	53	60
12		[Cu]	40	46
13	 125e	no	-	66
14		[Ir]	72 (ref ^[156])	-
15		[Cu]	94	100
16	 125f	no	62	80 ^d
17		[Ir]	80 (ref ^[156]) ^d	-
18		[Cu]	67	84 ^d
19	 125g	no	68	76
20		[Cu]	70	80
21	 125h	no	-	40 (<i>E:Z</i> = 7:3)
22		[Ir]	-	20 (<i>E:Z</i> = 6:4)
23		[Cu]	56 ^e	72 (<i>E:Z</i> = 7:3)

a) Reaction conditions: Styrene derivative **124** (1.0 equiv, 0.30 mmol), *N*-chlorosulfonamide **120a** (1.5 equiv), catalyst (0.003 mmol, 1 mol%), anhydrous DCE (6.0 mL), degassed solution, rt, 455 nm (LED-stick), 6 h. b) Determined by ¹H-NMR using 2-nitropropane as internal standard. c) This compound had already been reported as chloro substituted. The NMR-data of the product isolated herein is in full accordance with the data reported in literature (cf. ref^[156]). However, there is clear evidence that these data correspond to the hydroxy substituted compound (see experimental part). d) dr > 99:1 (*E:Z*). e) The *E:Z* isomers were inseparable by column chromatography.

In case of *para* substitution, the chlorinated product seems to be unstable towards hydrolysis and elimination which results under copper catalysis in a complex reaction mixture. In contrast to methyl styrenes (entries 7 to 12) where the yield dropped with *ortho* substitution due to sterical hindrance independent of used catalyst, **[Cu]** was the best catalyst for *ortho*-methoxy styrene (entry 6). With styrene (**124e**), the electron-poorest substrate in this row, **[Cu]** evolved its real catalytic potential with quantitative yield and exceeded both **[Ir]** and the background reaction without catalyst (entries 13 to 15). To reveal the stereoselectivity of this process, indene and alkynes were tested as substrates. In the case of indene, only the *E*-isomer was detected and isolated, while **[Cu]** resulted in lower yields as **[Ir]** (entries 16 to 18). However, in this reaction a catalyst is not necessarily required as light irradiation alone already furnishes 62% of the product. Phenylacetylene showed moderate reactivity under **[Cu]** catalysis and the chloramination product **125h** was isolated in a 56% yield as a mixture of stereoisomers (*E:Z* = 7:3). Due to the fact that the pure *E*-isomer of this product is accessible in good yields by metal catalysis using a different copper complex^[158], as reported by Liu and co-workers, it was assumed that the *Z*-isomer might form because of radical background processes triggered by light irradiation. For this reason, the experiment was repeated without catalyst with only light irradiation; however, the *E:Z* ratio remained unchanged except for a drop in product yield. Since Liu and co-workers had not been able to transform internal alkynes or alkyl alkynes^[158], these substrates were very appealing, too. However, when converting 1-phenyl-1-propyne by using **[Cu]** as a photocatalyst, a complex reaction mixture formed which did not show any indications for the expected products. Ethyl cinnamate showed isomerization to the *Z*-isomer in 34% yield and no ATRA product was observed.

As the copper catalyst was very efficient for styrene, electron-poor styrenes were examined in the next step (Table 23). Screening such substrates showed that **[Cu]** always led to the best yields. It should be noted that, in contrast to *ortho*- and *para*-methoxy substituted styrene (Table 22, entries 1 to 6), the copper catalyst worked excellently with the *meta*-substituted one (Table 23, entries 3 and 4) where the free electron pairs of oxygen are not in conjugation with the vinyl group which reduces the electron density at the benzylic position. Comparing the results of electron-poor styrenes, a trend emerges. The more electron-poor the styrene becomes, the less efficient the iridium catalyst is and the worse the reaction works with mere light irradiation. This trend becomes evident when comparing the results of 4-chlorostyrene with 4-nitrostyrene (entries 5 to 8 and 19 to 22).

Table 23. Substrate scope of electron-poor styrene derivatives **124**.^a

124	120a		125	
Entry	Product	Catalyst	Yield / %	
			Isolated	NMR ^b
1	 125i	[Ir]	61 (ref ^[156])	-
2		[Cu]	80	90
3	 125j	[Ir]	52	52
4		[Cu]	96	97
5	 125k	no	44	47
6		[Ir]	50 (ref ^[156])	-
7		[Cu]	88	96
8		no, UV	-	66
9	 125l	[Ir]	37	42
10		[Cu]	81	86
11	 125m	no	-	30
12		[Ir]	38	44
13		[Cu]	86	92
14		AIBN ^c , 80 °C	-	40
15	 125n	no	-	7
16		[Ir]	26	30
17		[Cu]	96	100
18		AIBN ^c , 80 °C	-	16
19	 125o	no	2	8
20		[Ir]	34	37
21		[Cu]	98	100
22		AIBN ^c , 80 °C	-	6
23	 125p	no	-	< 2
24		[Ir]	19	20
25		[Cu]	60	73

a) Reaction conditions: Styrene derivative **124** (1.0 equiv, 0.30 mmol), *N*-chlorosulfonamide **120a** (1.5 equiv), catalyst (0.003 mmol, 1 mol%), anhydrous DCE (6.0 mL), degassed solution, rt, 455 nm (LED-stick), 6 h. b) Determined by ¹H-NMR using 2-nitropropane as internal standard. c) 1 mol%, dark.

Plotting the product yields of different styrene derivatives **124** in dependence on the corresponding Hammett substituent constants σ ^[159] clarifies that there is a correlation between the electron density of the substrate and the product yield, dependent on the catalyst used (Figure 19).

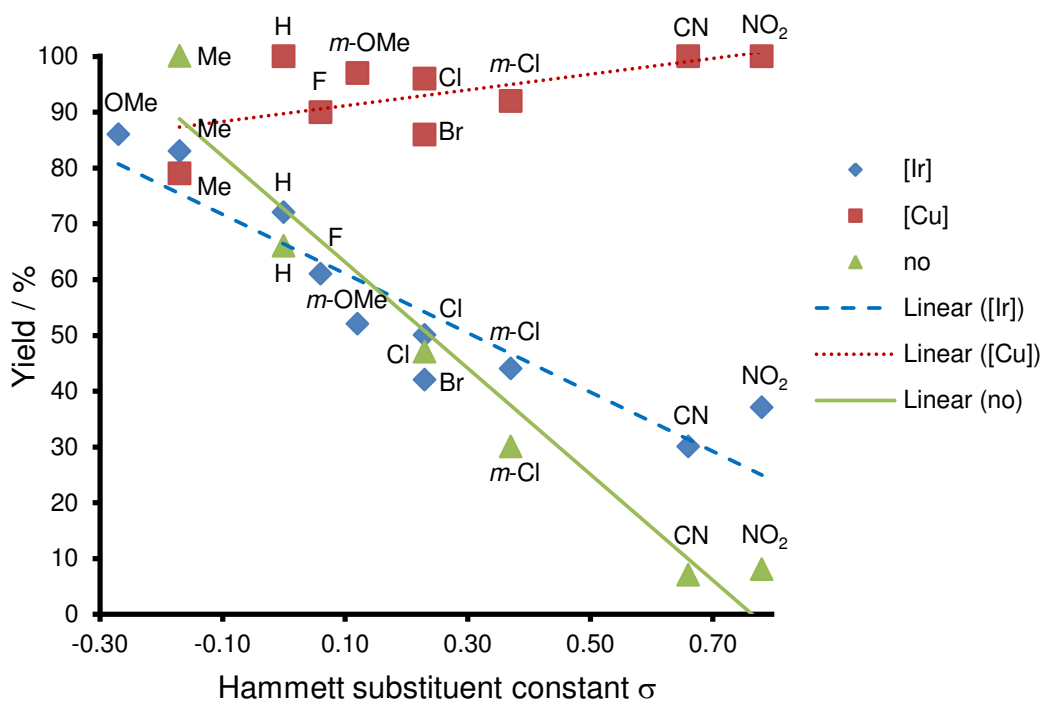
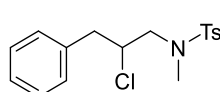
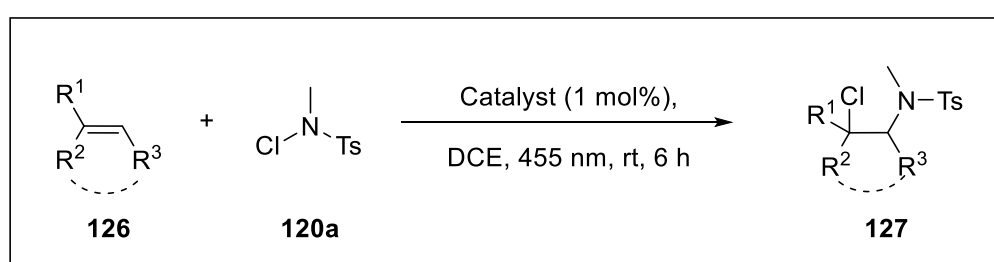
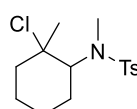
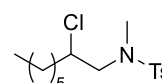


Figure 19. Product yields of different styrene derivatives **124** plotted in dependence on the corresponding Hammett substituent constants σ ^[159]. Substituents without prefix are in *para* position; substituents with prefix *m* are in *meta* position.

Encouraged by the good results of $[\text{Cu}(\text{dap})_2]\text{Cl}$ (**[Cu]**) for electron-poor styrenes, the search for the limits of this system and the screening of non vinylic alkenes was started (Scheme 40). Both allylbenzene (**126a**) and 1-methyl-1-cyclohexene (**126b**) resulted in poor yields (cf. **127a** and **127b**). With regard to **127b**, a further isomer was observed in traces by mass spectrometry of the crude reaction mixture, but it was only possible to isolate the Z-isomer by column chromatography. The structure was confirmed by X-ray analysis (see experimental part). When using 1-octene (**126c**) as a substrate, **[Ir]** was most effective and under mere irradiation with blue light no reaction occurred (cf. **127c**). Ethyl propiolate and cyclohex-2-en-1-one showed with **[Cu]** no reaction at all.

**127a****127b****127c**

		no	—	(9% NMR) ^c	no	n.r.
[Ir]	—	(15% NMR)	[Ir]	18% (19% NMR) ^c	[Ir]	64% (ref ^[156])
[Cu]	10%	(15% NMR)	[Cu]	10% (12% NMR) ^c	[Cu]	35% (41% NMR)

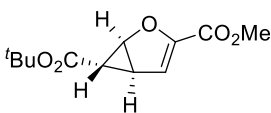
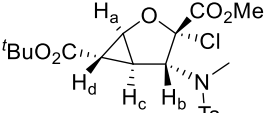
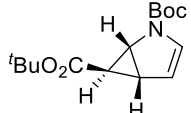
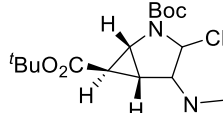

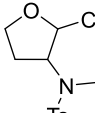
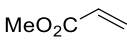
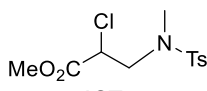
a) Reaction conditions: Olefin **126** (1.0 equiv), *N*-chlorosulfonamide **120a** (1.5 equiv), catalyst (1.0 mol%), anhydrous DCE, degassed solution, rt, 455 nm (LED-stick), 6 h. b) The yields in parenthesis were determined by ¹H-NMR using 2-nitropropane as internal standard. c) Yield of Z-Isomer.

Scheme 40. ATRA reactions with olefins.

In the next step, heterocyclic olefins were investigated, which are more challenging (Table 24). Starting with enantiopure cyclopropanated furan derivative **126d**, chloramination product **127d** was only accessible in acceptable yields using **[Cu]** (entries 1 and 2). The absolute configuration of the hydrogens on the cyclopropane ring of product **127d** is known from the starting material and remained unchanged in the course of the reaction. The preliminary assignment of the stereochemistry, which is based on the plausible attack of *N*-centered radical intermediate and of the chloride from the convex side, is supported by the existence of NOESY signals between H_b and H_d. In contrast to the cyclopropanated pyrrole derivative **126e**, which could not be successfully transformed using **[Cu]** (entry 3), the furan derivative

126d seems to have a special electron density which is beneficial for the copper catalysis. This special role becomes clear when the underlying basic structures are investigated separately. Unlike the electron-rich 2,3-dihydrofuran (**126f**), which furnishes a complex reaction mixture, methyl acrylate (**126g**) seems to be too electron-poor to show any reaction (entries 4 to 6).

Table 24. Investigation of electron-poor furan and pyrrole derivatives. ^a

Entry	Olefin	Product	Catalyst	Yield / %	
				Isolated	NMR ^b
1	 126d	 127d	[Ir]	13	16
2				40	50
3	 126e	 127e	[Cu]	complex rxn mixture	
4 ^c	 126f	 127f	[Ir]	complex rxn mixture	
5 ^c			[Cu]	complex rxn mixture	
6	 126g	 127g	[Cu]	n.r.	

a) Reaction conditions: Olefin **126** (1.0 equiv, 0.30 mmol), *N*-chlorosulfonamide **120a** (1.5 equiv), catalyst (0.003 mmol, 1 mol%), anhydrous DCE (6.0 mL), degassed solution, rt, 455 nm (LED-stick), 6 h. b) Determined by ¹H-NMR using 2-nitropropane as internal standard. c) 2,3-Dihydrofuran (2.25 mmol, 5.0 equiv), *N*-chlorosulfonamide (0.45 mmol, 1.0 equiv), catalyst (0.003 mmol).

For the application of a reaction in organic synthesis, protecting groups are often a crucial tool.^[160] As an alternative to the use of the tosyl group, there is an interest in using different protecting groups which are capable of being removed more easily. In order to provide such a protecting group, 4-nitrobenzenesulfonyl (nosyl) and *tert*-butyloxycarbonyl (Boc) were tested as protecting groups for *N*-chloromethylamine (Table 25). Regarding the Boc group, the copper catalyst was just as ineffective as [Ir(ppy)₂(dtbbpy)]PF₆ (**[Ir]**) and no reaction took place (entries 1 and 2). Using the electron-deficient nosyl group, [Cu(dap)₂]Cl (**[Cu]**) resulted in an excellent isolated yield of the corresponding chloramination product **129b**. As in the

case with electron-deficient styrene derivatives, the copper catalyst proved to be much more efficient than $[\text{Ir}(\text{ppy})_2(\text{dtbbpy})]\text{PF}_6$ (**[Ir]**).

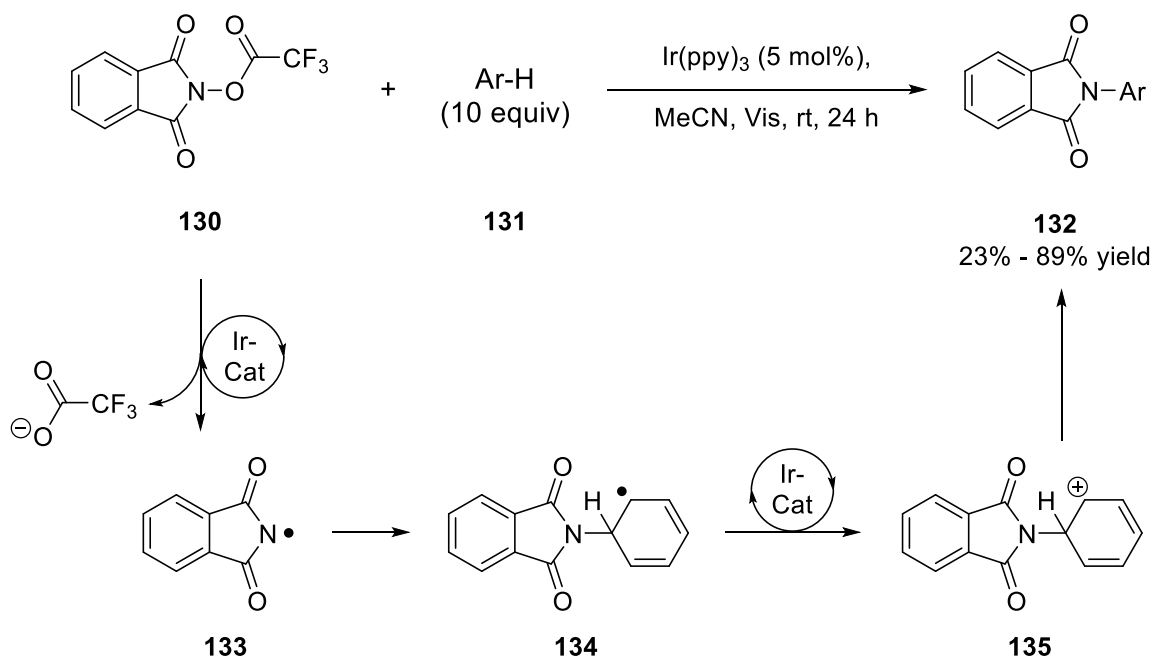
Table 25. Screening of protected *N*-chloromethylamine **128** as chloramine source. ^a

124e	128	129		
Entry	R	Product	Catalyst	Yield / %
1	Boc		[Ir]	0 (ref ^[156])
2			[Cu]	0
3	nosyl		[Ir]	50 (ref ^[156])
4			[Cu]	93

a) Reaction conditions: Styrene **124e** (1.0 equiv, 0.03 mmol), *N*-chloromethylamine **128** (1.5 equiv), catalyst (0.003 mmol, 1.0 mol%), anhydrous DCE (6.0 mL), degassed solution, rt, 455 nm (LED-stick), 6 h.

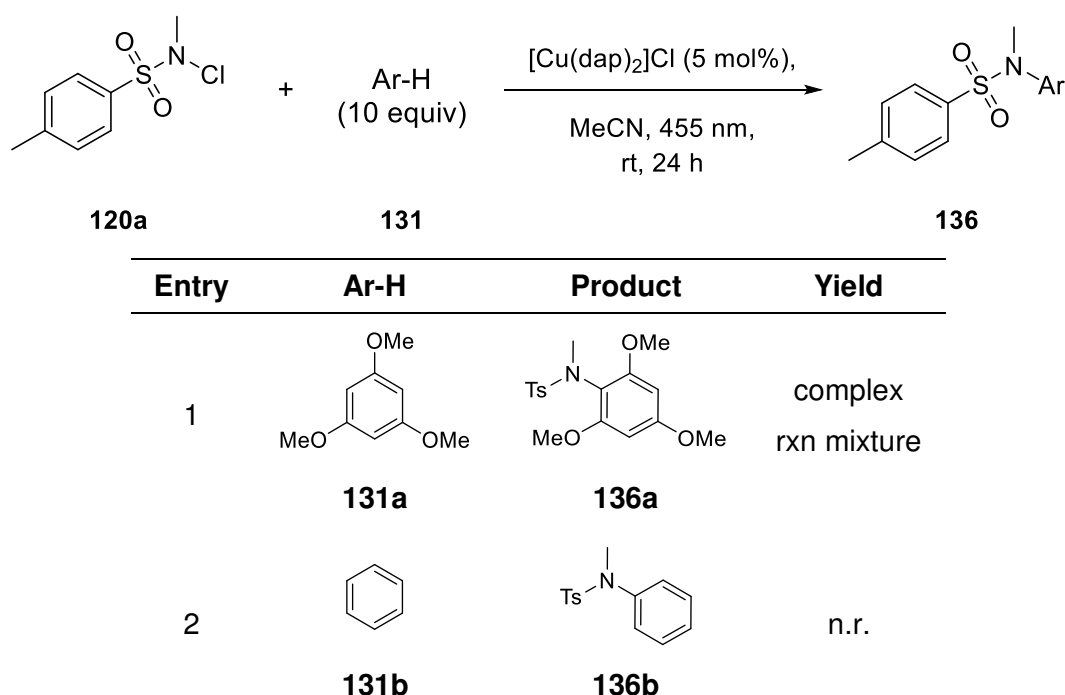
3. Reactions with *N*-Centered Radicals

Due to the fact that the 1,2-chloramination reaction is supposed to react via a *N*-centered radical **122** (cf. Scheme 39), the transformation of this intermediate in alternative reactions was targeted. In 2014, M. S. Sanford *et al.* published the C-H amination of arenes **131** with *N*-(trifluoromethyl)acyloxypthalimide (**130**) (Scheme 41).^[161] As a reaction mechanism, they propose a radical aromatic substitution mechanism where an *N*-centered phthalimidyl radical **133** forms in the initial step by a single electron transfer from the photoredox catalyst in the oxidative quenching cycle. Back electron transfer from radical intermediate **134** to the catalyst closes the photocatalytic cycle and furnishes a cationic intermediate **135** which is transferred to the product **132** by deprotonation.



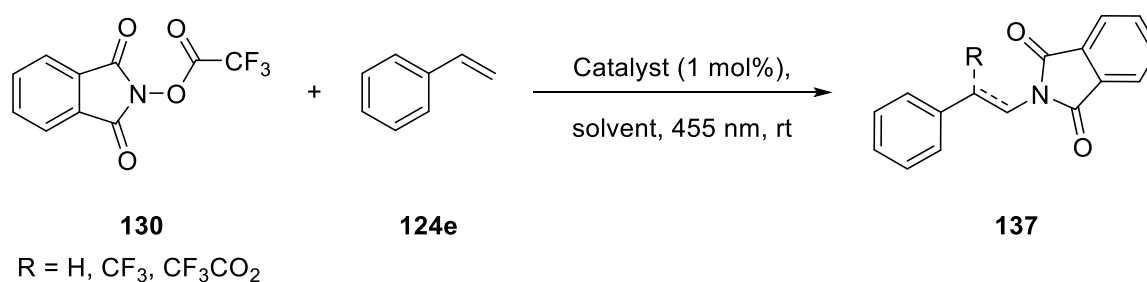
Scheme 41. C-H amination of arenes and heteroarenes according to M. S. Sanford *et al.*^[161]

N-chlorosulfonamide **120a** could therefore be a potential substrate for such transformations. Similar to M. S. Sanford's protocol, the addition of *N*-chlorosulfonamide **120a** to arenes **131** was tested (Table 26). Using electron-rich trimethoxybenzene **131a** (entry 1) furnished a complex reaction mixture in which product **136a** was identified only in traces by mass analysis. Even though the reaction was extremely unselective, this result supports the assumption that an *N*-centered radical **122** is formed from *N*-chlorosulfonamide **120a** using the copper catalyst **[Cu]**. With benzene (**131b**, entry 2), no reaction was observed.

Table 26. C-H amination of arenes **131** using *N*-chlorosulfonamide **120a**.

Reaction conditions: Arene **131** (10.0 equiv), *N*-chlorosulfonamide **120a** (1.0 equiv, 0.25 mmol), [Cu(dap)₂]Cl (**[Cu]**) (12.5 μmol, 5.0 mol%), anhydrous MeCN (2.5 mL), degassed solution, rt, 455 nm (LED-stick), 6 h.

Since *N*-(trifluoromethyl)acyloxyphthalimide (**130**) worked well in M. S. Sanford's case where a nitrogen-centered intermediate was also assumed, the next step was to test this reagent for alkenes under the chloramination conditions (Table 27).

Table 27. Testing *N*-(trifluoromethyl)acyloxyphthalimide (**130**) as a nitrogen source.^a

Entry	Time	Catalyst	Solvent	Yield of Product 138
1	23 h	[Cu]	DCE	n.r.
2	23 h	[Cu]	MeCN	37%
3 ^b	18 h	<i>fac</i> -Ir(ppy) ₃	MeCN	39%
4 ^b	23 h	[Cu]	THF	n.r.

a) Reaction conditions: *N*-(trifluoromethyl)acyloxyphthalimide (**130**) (1.5 equiv), styrene (**124e**) (1.0 equiv, 0.30 mmol), [Cu(dap)₂]Cl (**[Cu]**) (3.0 μmol, 1.0 mol%), anhydrous solvent (6.0 mL), degassed solution, rt, 455 nm (LED-stick). b) 0.60 mmol scale.

As phthalimide derivative **130** is hardly soluble in DCE (Table 27, entry 1), other solvents were applied (entries 2 to 4) as well. No reaction occurred when using DCE or THF (entries 1 and 4). Entry 2 shows that $[\text{Cu}(\text{dap})_2]\text{Cl}$ (**[Cu]**) is able to reduce *N*-(trifluoromethyl)acyloxyphthalimide (**130**). Nevertheless, it was not possible to isolate the desired ATRA-like amination products **137** in any case. However, when using acetonitrile as a solvent, double amination took place and acetamide **138** was obtained in moderate yields.

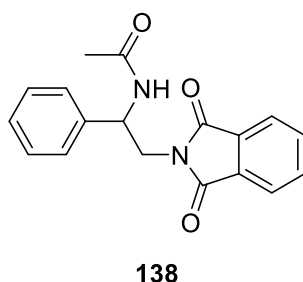
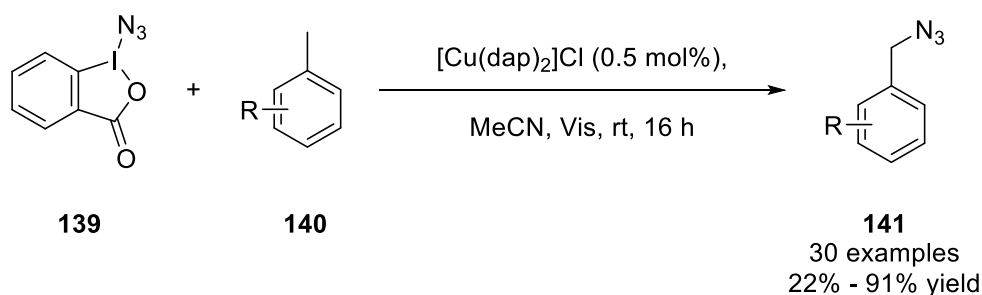
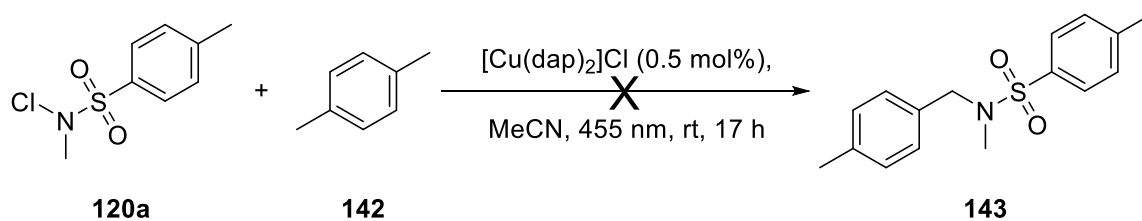


Figure 20. Isolated acetamide **138** when using acetonitrile as a solvent.

M. F. Greaney *et al.* recently reported benzylic C-H azidation with the Zhdankin Reagent (**139**) under copper photoredox catalysis (Scheme 42).^[40] Starting with the formation of azide radical under copper catalysis, a radical chain mechanism is proposed. In order to transform potentially formed radicals during the chloramination reaction, the functionalization of benzylic C-H bonds with *N*-chlorosulfonamide **120a** was tested using Greaney's conditions (Scheme 43). However, apart from the dehalogenation of *N*-chlorosulfonamide **120a**, no reaction was observed. The *N*-centered radical which is formed intermediately is probably not stable enough to perform this reaction and abstracts a hydrogen atom from the solvent instead.



Scheme 42. C-H azidation with the Zhdankin Reagent (**139**) according to M. F. Greaney *et al.*^[40]



Reaction conditions: *p*-Xylene (**142**) (40.0 equiv), *N*-chlorosulfonamide **120a** (1.0 equiv, 0.50 mmol), [Cu(dap)₂]Cl (**[Cu]**) (2.5 μmol, 0.5 mol%), anhydrous MeCN, degassed solution, rt, 455 nm (LED-stick), 17 h.

Scheme 43. Testing C-H-amination using *N*-chlorosulfonamide **120a**.

4. Investigation of UV-Absorption Spectra and Quantum Yield Measurements

With regard to the reaction mechanism, the most surprising result was that, with electron-rich substrates in particular, the 1,2-chloramination reaction presented here worked in good yields by mere light irradiation without using any catalyst. Unexpectedly, the UV-Vis absorption spectra of the substrates and product for the case of 4-methylstyrene (**124c**) (see experimental part, Figure 27) showed no clearly recognizable absorbance in the region of 455 nm which was the applied excitation wavelength. In addition, the degassed reaction mixture showed the same absorbance behavior. Thus, the formation of a possible light absorbing electron donor acceptor complex was not observable. Degassing the reaction mixture and irradiation with blue LED from outside for one or two hours had no effect on the UV-Vis absorption spectra either (see experimental part, Figure 28). The reaction outcome was checked after two hours by ^1H -NMR analysis which revealed a 21% NMR yield. As the control experiment without catalyst and light showed no reaction at all (Table 21, entry 6), it was evident that light can trigger the reaction. In the next step the UV-Vis-behavior of *N*-chlorosulfonamide **120a** was investigated under different concentrations, with the finding that there was low absorbance in the region of 450 nm which became visible when measuring a 300 mM solution in 1,2-dichloroethane (Figure 21).

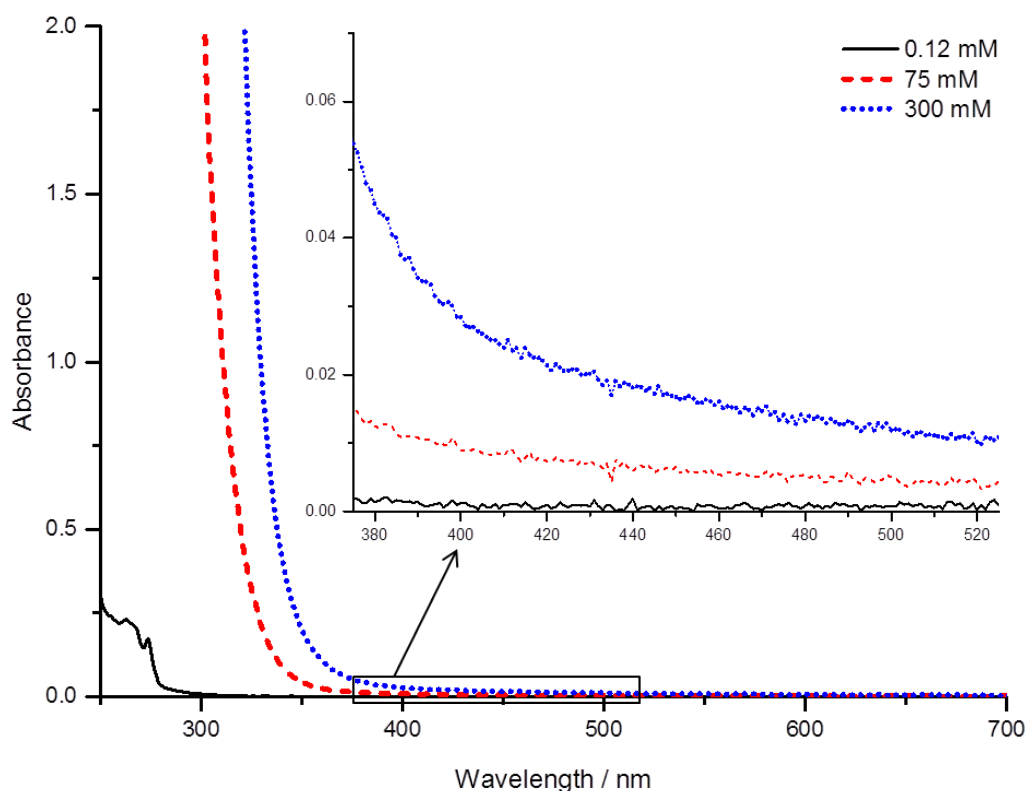


Figure 21. UV-Vis absorption spectra of different concentrations of *N*-chlorosulfonamide **120a** in anhydrous DCE.

Furthermore, this low absorbance matched with the measured low radiant powers (P_{abs}) during quantum yield determination (cf. Table 28) and the emission band of the LED used on the blue spectral side overlaps well with the absorption band of *N*-chlorosulfonamide **120a**. Since the light output power of such LEDs is very high, this small absorbance is sufficient to start chemical reactions.

In order to elucidate the different reactivities of the substrates, the quantum yields of three selected reactions were investigated (Table 28). In the case of catalyzed reactions, the yields from the quantum yield reaction setup conformed well to the yields from the standard reactions which were performed in pressure tubes with an internal irradiation setup. The non-catalyzed reactions (entries 1 and 4) were much slower than the catalyzed ones, which became evident when comparing the yields from the quantum yield determinations. This observation is supported by the reaction of 4-methylstyrene in the standard reaction setup after 1 h, where without catalyst 44%, with iridium catalyst 50%, and with copper catalyst 80% of product was formed (entries 1 to 3).

Table 28. Results of quantum yield measurements.

$\text{R-C}_6\text{H}_4\text{-CH=CH}_2$ (**124**) + Cl-N(Ts)Me_2 (**120a**) $\xrightarrow[\text{DCE, 455 nm, rt}]{\text{Catalyst (1 mol\%)}}$ $\text{R-C}_6\text{H}_4\text{-CH(Cl)-CH}_2\text{-N(Ts)Me}_2$ (**125**)

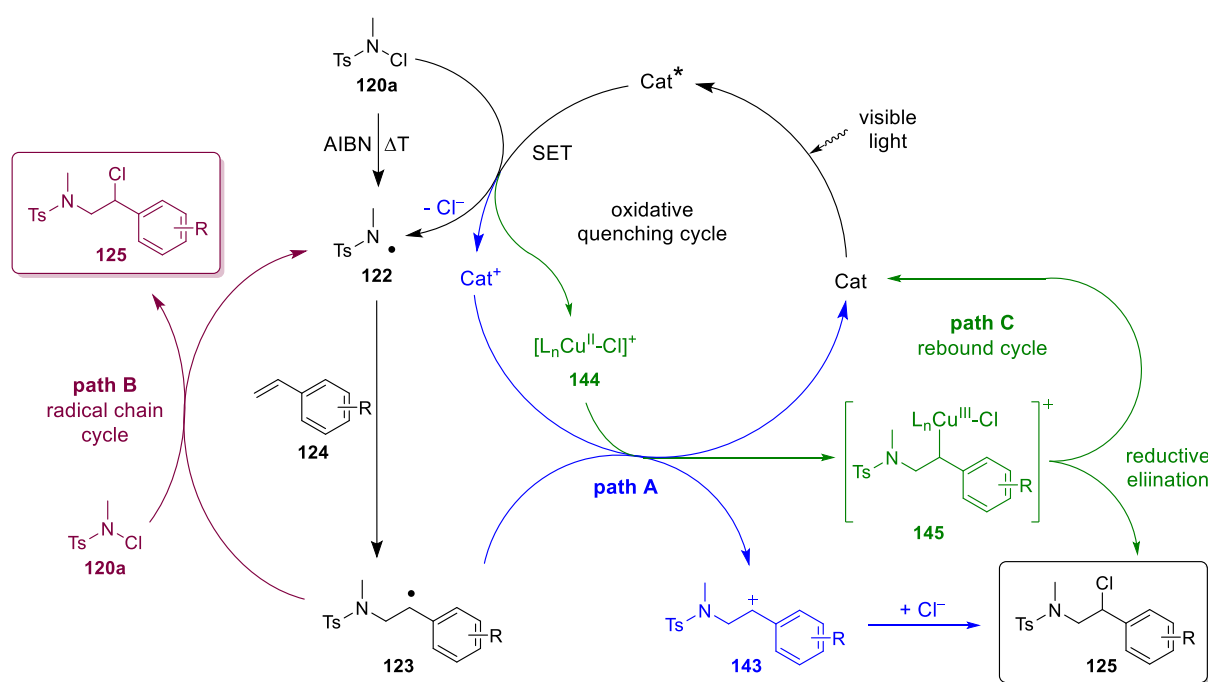
Entry	Product	Catalyst	Standard Reaction ^a (NMR Yield ^c)		Quantum Yield Determination ^b			
			6 h	1 h	Δt / h	NMR Yield ^c	P_{abs} / mW	Φ
1	 125c	no	100%	44%	6	30%	0.64	57%
2		[Ir]	83% (ref ^[156])	50%	1	39%	93.6	3%
3		[Cu]	79%	80%	1	41%	94.0	3%
4	 125k	no	47%	-	6	4%	2.36	2%
5		[Ir]	50% (ref ^[156])	-	1	27%	97.0	2%
6		[Cu]	96%	-	1	34%	97.2	3%
7	 125o	no	8%	-	-	-	-	-
8		[Ir]	37%	-	1	9%	97.3	0.7%
9		[Cu]	100%	-	1	18%	95.5	1.4%

Reaction conditions: Styrene derivative **124** (1.0 equiv), *N*-chlorosulfonamide **120a** (1.5 equiv), catalyst (1.0 mol%), anhydrous DCE, degassed solution. a) Irradiation via LED-stick (455 nm) at rt for 6 h, reaction vessel: pressure tube. b) Irradiation via LED (455 nm) in quantum yield apparatus at rt for the indicated time, reaction vessel: fluorescence cuvette. c) Determined by ¹H-NMR using 2-nitropropane as internal standard, literature yields are isolated yields.

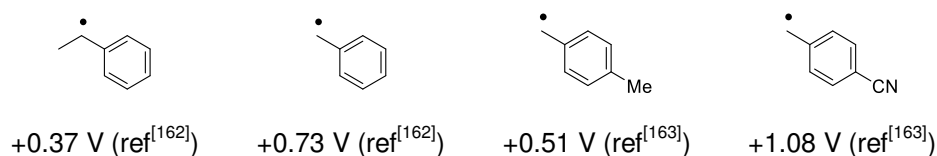
It should be noted that the light power at the sample in the quantum yield apparatus was significantly lower than in the standard reaction setup. For instance, even after 6 h reaction time in the quantum yield apparatus, only poor yields were obtained with 4-chlorostyrene because the light power is weaker (entry 4). Regarding the quantum yields, with electron-rich 4-methylstyrene (entries 1 to 3) the non-catalyzed reaction showed, with 57%, the highest value, which is a strong indication for a radical chain pathway. It has to be remarked that the overall efficiency of this reaction is nonetheless very poor because the absorbance of the reaction solution is feeble and for the calculation of the quantum yield only the absorbed photons are taken into account (cf. absorbed radiant power P_{abs}). The low quantum yields of 3% of the catalyzed reactions provide evidence that a potential radical chain mechanism plays a subordinated role here. Electron-deficient 4-chlorostyrene (entries 4 to 6) showed, with 2% to 3%, only low quantum yields in all cases. In contrast to 4-methylstyrene in the non-catalyzed reaction, both the reaction yield in the standard reaction setup (47%) and the quantum yield (2%) dropped dramatically, demonstrating that a potential radical chain mechanism becomes less efficient with electron-deficient substrates. With even more electron-deficient 4-nitrostyrene (entries 7 to 9), this effect became stronger so that the quantum yield of the non-catalyzed reaction was not determined as the yield in the standard reaction setup was already very low. Both catalyzed reactions showed, with less than 2%, a very low quantum yield; however, the copper catalyzed reaction had a value of double the amount, highlighting the better performance of **[Cu]**.

5. Reaction Mechanism

Taking the preceding results into consideration, the following reaction mechanism (Scheme 44), which is compatible with the mechanism of S. Yu *et al.*^[156], is assumed. After excitation of a photoredox catalyst by visible light, single electron transfer to *N*-chlorosulfonamide **120a** generates the nitrogen-centered radical intermediate **122** under oxidation of the catalyst. The regioselective addition of radical **122** to alkene **124** forms the carbon-centered radical intermediate **123** which can react in three different pathways to form product **125**.



Oxidation potentials vs. SCE in acetonitrile



Scheme 44. Proposed reaction mechanism for 1,2-chloramination reaction.

In pathway A, the radical intermediate **123** is oxidized to carbocation **143** by back electron transfer and regeneration of the catalyst. Path B is a conceivable radical chain mechanism which is in competition with pathway A. In this case radical **123** abstracts chlorine from *N*-chlorosulfonamide **120a** and forms product **125** by the generation of the nitrogen-centered radical **122**. When using AIBN as a radical starter under elevated temperatures, *N*-centered radical **122** is formed in the initial step and the reaction proceeds via pathway B. With electron-rich substrates, the radical chain works well which has been proven by the excellent

yield for the reaction of 4-methylstyrene and catalytic amounts of AIBN (Table 21, entry 8). When using electron-poor substrates, the carbon-centered radical intermediate **123** becomes more electrophilic and less reactive to the chloramine source **120a**. As a consequence, the radical chain mechanism slows down and the yields drop dramatically without a catalyst. In contrast to 4-methylstyrene, the reaction of 4-nitrostyrene with AIBN, for example, furnished only 6% NMR-yield (Table 23, entry 22).

The contrasting reaction behavior of **[Cu]** and **[Ir]** for electron-rich and electron-poor substrates can be explained as follows. With electron-rich substrates the oxidation of the readily oxidizable carbon-centered radical intermediate **123** is possible with both catalysts and pathway A takes place. The oxidation potential of the benzyl radical of ethylbenzene was reported as +0.37 V¹¹.^[162] This would be accessible by both **[Cu]** ($E_{1/2}(\text{Cu}^{2+}/\text{Cu}^+) = +0.62 \text{ V}^{11}$)^[19] and more strongly oxidizing **[Ir]** ($E_{1/2}(\text{Ir}^{4+}/\text{Ir}^{3+}) = +1.21 \text{ V}^{11}$)^[23]. With electron-poor substrates, the oxidation potential of the carbon-centered radical intermediate **123** increases and the potential of **[Cu]** is not high enough to oxidize it to carbocation **143** (oxidation potential of 4-methylbenzylradical: +0.51 V¹¹; oxidation potential of 4-cyanobenzylradical: +1.08 V¹¹).^[163] Thus, pathway C is favored, which involves structural reorganization and substrate coordination of the copper catalyst. After SET, the photoexcited copper complex coordinates an additional chloride and concurrently forms copper(II) species **144** and the nitrogen-centered radical intermediate **122**. As in pathways A and B, the addition of this radical to alkene **124** results in the carbon-centered radical intermediate **123**. The product could now be directly formed after combination of **123** with the coordinated chloride under regeneration of copper(I) catalyst **[Cu]** ($[\text{L}_n\text{Cu}]^+$). However, as outlined in the introductory chapter A and also proposed by S. Z. Zard^[164], it needs to be considered that a transient copper(III) species **145** is probably involved. After formation of **145** by the attack of copper(II) species **144** on radical **123**, the product would be formed by reductive elimination. In contrast to **[Cu]**, more strongly oxidizing **[Ir]** might be still able to oxidize the electron-rich carbon-centered radical **123** to the corresponding carbocation **143**. However, this electron-deficient carbocation is very unstable, and product formation is hindered. If **[Ir]** was not strong enough for oxidizing the benzyl radical, a coordination of chloride would not be possible and product formation could not take place.

¹¹ vs. SCE in MeCN

6. Conclusion

The investigation of different styrenes under various reaction conditions revealed two important aspects of the chloramination reaction. Firstly, the reaction does not always require a photocatalyst. Secondly, this chloramination works for electron-rich substrates with AIBN and there is a necessity for $[\text{Cu}(\text{dap})_2]\text{Cl}$ (**[Cu]**) when the substrates become more electron-deficient. In addition, the copper catalyst outperforms the iridium catalyst, when using the nosyl group as a protecting group. Given that the nosyl group is more easily removable than the tosyl group, **[Cu]** provides access to valuable intermediates for consecutive reactions.

Since a reaction mechanism which runs over an *N*-centered radical intermediate was assumed, *N*-chlorosulfonamide **120a** was tested for C-H amination of arenes. However, selective product formation using the copper catalyst **[Cu]** was not successful. Attempts to use the potential *N*-centered radical intermediate **122** for benzylic C-H aminations similar to M. F. Greaney and co-workers' protocol^[40] also failed, which may be due to the instability of the radical. When using *N*-(trifluoromethyl)acyloxypthalimide (**130**) as a nitrogen source for the amination of styrene, a double amination was observed in acetonitrile in moderate yields. This observation opens the door for more interesting transformations.

The reactivity of electron-poor styrenes by mere light excitation was clarified by UV-Vis spectrometry. Due to the high emission power of the LEDs used, a little absorbance of *N*-chlorosulfonamide **120a** is sufficient to drive the reaction. From a mechanistic point of view, generation of *N*-centered radicals is the initial step, irrespective of which catalytic system is used. The key steps are the subsequent reaction steps depending on the electronic properties of the substrate. Without a catalyst or when using AIBN as a radical initiator, a radical chain pathway is the only possible mechanism, whereas both, the copper and the iridium catalyst, can run in a photoredox cycle after single electron transfer via a carbon-centered radical intermediate **123** broadening the scope of the reaction. The decisive difference between the copper and iridium catalyst occurred for electron-poor substrates which could exclusively be converted in good yields with $[\text{Cu}(\text{dap})_2]\text{Cl}$ (**[Cu]**). These substrates are accessible, since **[Cu]**, in contrast to the iridium catalyst **[Ir]**, is prone to undergo structural reorganization as well as ligand exchange^[45]. Hence, **[Cu]** can run through an alternative pathway, in which copper can coordinate to intermediates under the formation of a potential copper(III) species.

E. Summary / Zusammenfassung

1. Summary

In the present thesis, the value of copper complexes for photoredox catalysis is demonstrated. In particular, new copper photoredox catalysts were developed and investigations were carried out to identify new ATRA reagents. On the basis of the visible-light-mediated chloramination of alkenes, it became particularly evident that the special reactivity of copper results in alternative reaction pathways which are crucial for the unique opportunities afforded by copper complexes.

After a brief introduction to copper catalysts in photoredox catalysis and the role of copper(III) species in organic chemistry (Chapter A), Chapter B examines the development of new copper photoredox catalysts. At first, the new copper(I) complexes, $[\text{Cu}(\text{dapacetal})_2]^+$ and $[\text{Cu}(\text{phenazino-dap})_2]^+$ were synthesized and characterized. Both complexes were inferior to the established $[\text{Cu}(\text{dap})_2]^+$ in all tested photoreactions. Finally, it was not possible to improve the catalyst performance by modifications in 5,6-position of the phenanthroline core structure. More promising for the development of more efficient copper(I)-based photoredox catalysts is the formation of heteroleptic complexes. As for copper(II) complexes, the new and readily synthesizable $[\text{Cu}(\text{dap})\text{Cl}_2]$ was observed to be an efficient photocatalyst that was even able to outperform the successful copper(I) complex $[\text{Cu}(\text{dap})_2]\text{Cl}$. With regard to the better performance of $[\text{Cu}(\text{dap})\text{Cl}_2]$, the formation of intermediary copper(III) species as key intermediates need to be taken into consideration. In order to explore the real scope of this copper(II) complex for photocatalysis and to elucidate the underlying reaction mechanism, further research, which is already ongoing, is necessary. Finally, as a new alternative to phenanthroline ligands for copper photoredox catalysts, 1,4-diaza-1,3-butadienes were investigated. In this context, $[\text{Cu}(\text{DABMes})_2]\text{BF}_4$ was for the first time successfully applied to visible-light-mediated ATRA reactions. Since this catalyst showed less efficiency it is not competitive with established $[\text{Cu}(\text{dap})_2]\text{Cl}$. However, further research of modified variants might lead to an easily accessible new class of photocatalysts.

In Chapter C, the investigation of four compounds for their potential application as new ATRA reagents in photoredox catalysis is described. Readily available trifluoromethanesulfonic acid proved to be unsuitable as it is too reactive. Owing to its high acidity, side reactions such as Ritter-like reactions occurred. The Ruppert-Prakash reagent (TMSCF_3) and 2,4-dinitrophenyl trifluoromethanesulfonate surprisingly exhibited no reactivity, even though the reduction potentials are in the accessible area of the photoredox catalysts used. Finally, after

optimizing the reaction conditions, it proved possible to use trichloromethanesulfonyl chloride ($\text{CCl}_3\text{SO}_2\text{Cl}$) as an ATRA reagent with a similar reactivity to that of trifluoromethanesulfonyl chloride ($\text{CF}_3\text{SO}_2\text{Cl}$). The use of the corresponding ATRA products was demonstrated using the formation of important substance classes such as sulfonamides or sultones as an example. The screening of further substrates would be appropriate because, in contrast to the trifluoromethyl group, the trichloromethyl group offers the potential for interesting additional derivatizations.

In the final Chapter, the reaction pathways of visible-light-mediated chloramination of alkenes with *N*-chlorosulfonamides are elucidated. This reaction was observed to be highly dependent on the type of photoredox catalyst used. While electron-rich alkenes furnished best results with iridium-based photocatalyst $[\text{Ir}(\text{ppy})_2(\text{dtbbpy})]\text{PF}_6$ but were also converted in the absence of any catalyst, electron-deficient alkenes required $[\text{Cu}(\text{dap})_2]\text{Cl}$ for this process. This behavior was explained on the basis of a mechanism, indicating the important role of photoredox catalysts beyond the initiation of a reaction by an initial electron transfer. The decisive difference between the copper and iridium catalyst was observed for electron-poor substrates, which were exclusively converted in good yields with $[\text{Cu}(\text{dap})_2]\text{Cl}$. The copper complex is the key to this reaction because, in contrast to the iridium complex, it has the ability to undergo rapid structural reorganization as well as ligand exchange.

2. Zusammenfassung

In der vorliegenden Arbeit wird die Bedeutung von Kupferkomplexen für die Photoredoxkatalyse veranschaulicht. Insbesondere wurden neue Kupfer-Photoredoxkatalysatoren entwickelt und es wurden Untersuchungen durchgeführt, um neue ATRA Reagenzien zu ermitteln. Anhand der durch sichtbares Licht vermittelten Chloraminierung von Alkenen wurde besonders deutlich, dass die spezielle Reaktivität von Kupfer zu alternativen Reaktionswegen führt, welche für die einzigartigen Möglichkeiten von Kupferkomplexen ausschlaggebend sind.

Nach einer kurzen Einleitung über Kupferkatalysatoren in der Photoredoxkatalyse und über die Rolle von Kupfer(III)-Spezies in der organischen Chemie (Kapitel A), wird in Kapitel B die Entwicklung von neuen Kupfer-Photoredoxkatalysatoren verfolgt. Dabei wurden zunächst die neuen Kupfer(I)-Komplexe, $[\text{Cu}(\text{dapacetal})_2]^+$ und $[\text{Cu}(\text{phenazino-dap})_2]^+$, synthetisiert und charakterisiert. Beide Komplexe waren dem etablierten $[\text{Cu}(\text{dap})_2]^+$ in allen getesteten Photoreaktionen unterlegen. Letztendlich war es nicht möglich, die Katalysatorleistung durch Modifikationen in der 5,6-Position der Phenanthrolinkernstruktur zu verbessern. Erfolgversprechender für die Entwicklung von effizienteren Kupfer(I)-basierten Photoredoxkatalysatoren ist die Bildung von heteroleptischen Komplexen. In Bezug auf die Kupfer(II)-Komplexe, zeigte sich der neue und leicht herstellbare $[\text{Cu}(\text{dap})\text{Cl}_2]$ als ein effizienter Photokatalysator, der sogar den erfolgreichen Kupfer(I)-Komplex $[\text{Cu}(\text{dap})_2]\text{Cl}$ übertreffen konnte. Hinsichtlich der besseren Leistung von $[\text{Cu}(\text{dap})\text{Cl}_2]$, muss die Bildung von intermediären Kupfer(III)-Spezies als entscheidende Zwischenprodukte in Betracht gezogen werden. Um das wahre Potential dieses Kupfer(II)-Komplexes für die Photokatalyse zu erforschen und um den zugrundeliegenden Reaktionsmechanismus aufzuklären, ist eine weitere Untersuchung nötig, welche bereits im Gange ist. Schließlich wurden 1,4-Diaza-1,3-butadiene als neue Alternative zu Phenanthrolinliganden in der Photoredoxkatalyse untersucht. In diesem Zusammenhang wurde $[\text{Cu}(\text{DABMes})_2]\text{BF}_4$ zum ersten Mal erfolgreich in durch sichtbares Licht vermittelte ATRA Reaktionen angewendet. Da dieser Katalysator geringere Effizienz zeigte, ist er nicht konkurrenzfähig zum bewährten $[\text{Cu}(\text{dap})_2]\text{Cl}$. Jedoch könnte eine weitere Erforschung von abgeänderten Varianten zu einer leicht zugänglichen neuen Klasse von Photokatalysatoren führen.

In Kapitel C wird die Untersuchung von vier Verbindungen auf ihre mögliche Anwendung als neue ATRA Reagenzien in der Photoredoxkatalyse beschrieben. Die leicht verfügbare Trifluormethansulfonsäure erwies sich als ungeeignet, da sie viel zu reaktiv ist. Aufgrund ihrer hohen Azidität traten Nebenreaktionen wie zum Beispiel Ritterartige Reaktionen auf. Das Ruppert-Prakash Reagenz (TMSCF_3) und 2,4-Dinitrophenyl-trifluormethansulfonat

zeigten überraschenderweise keine Reaktivität, obwohl die Reduktionspotentiale im zugänglichen Bereich der verwendeten Photoredoxkatalysatoren liegen. Schließlich war es nach Optimierung der Reaktionsbedingungen möglich, Trichlormethansulfonylchlorid ($\text{CCl}_3\text{SO}_2\text{Cl}$) als ATRA Reagenz mit einer ähnlichen Reaktivität wie Trifluormethansulfonylchlorid ($\text{CF}_3\text{SO}_2\text{Cl}$) zu verwenden. Mit der Bildung von wichtigen Substanzklassen, wie zum Beispiel von Sufonamiden oder Sultonen, wurde die Verwendung der entsprechenden ATRA Produkte veranschaulicht. Ein Austesten von weiteren Substraten ist sinnvoll, da die Trichlormethylgruppe, im Gegensatz zu der Trifluormethylgruppe, die Möglichkeit für interessante zusätzliche Derivatisierungen bietet.

Im letzten Kapitel werden die Reaktionswege der durch sichtbares Licht vermittelten Chloraminierung von Alkenen mit *N*-Chlorsulfonamiden erläutert. Diese Reaktion zeigte sich stark abhängig vom verwendeten Photoredoxkatalysator. Während elektronenreiche Alkene die besten Ergebnisse mit dem Iridiumbasierten Photokatalysator $[\text{Ir}(\text{ppy})_2(\text{dtbbpy})]\text{PF}_6$ lieferten, aber auch in Abwesenheit eines Katalysators umgesetzt wurden, erforderten elektronenarme Alkene $[\text{Cu}(\text{dap})_2]\text{Cl}$ für diesen Prozess. Dieses Verhalten konnte anhand eines Mechanismus begründet werden, der die wichtige Rolle von Photoredoxkatalysatoren aufzeigt, die über den Anstoß einer Reaktion durch einen anfänglichen Elektronentransfer hinausgeht. Der entscheidende Unterschied zwischen dem Kupfer- und Iridiumkatalysator kam bei elektronenarmen Substraten zum Vorschein, welche ausschließlich mit $[\text{Cu}(\text{dap})_2]\text{Cl}$ in guten Ausbeuten umgesetzt wurden. Dabei ist der Kupferkomplex der Schlüssel zu dieser Reaktion, weil er im Gegensatz zum Iridiumkomplex die Fähigkeit hat, schnelle strukturelle Umorganisation sowie Ligandenaustausch einzugehen.

F. Experimental Part

1. General Comments

All commercially available reagents were used without further purification unless stated otherwise. Anhydrous solvents were prepared by established laboratory procedures^[165]. Reactions with moisture or oxygen-sensitive reagents were carried out in oven-dried or flame-dried glassware under an atmosphere of predried nitrogen.

If not stated otherwise, all photochemical reactions were performed under a nitrogen atmosphere using degassed solvents. While being stirred, the reaction mixture in each case was irradiated using an internal irradiation setup, which was developed by O. Reiser *et al.*^[166] (Figure 22). The setup consists of a Schlenk pressure tube (A) and a “LED-stick” (LED (B) on top of a glass rod (C)), which channels light directly into the reaction mixture (D). A screw cap with a Teflon adaptor (E) allows tight closure of the reaction vessel. For irradiation, a blue light emitting diode (LED) (700 mA, λ_{max} = 455 nm, Osram Oslon 80) or a green LED (700 mA, λ_{max} = 530 nm, Cree XP-E) was used.

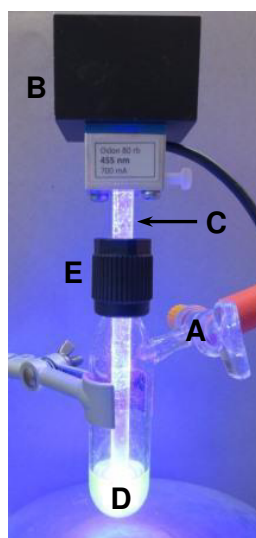


Figure 22. Irradiation setup using a LED-stick.

Column chromatography was performed on silica gel (Mesh 0.063 – 0.200 mm, Merck) or on silica gel for flash chromatography (Mesh 0.040 – 0.063 mm, Merck). Solvents for column chromatography were distilled prior to use. Thin layer chromatography (TLC) was performed on Merck TLC aluminum plates coated with silica gel 60 F254. A dual short/long wave UV lamp or treatment with suitable stains (solutions of vanillin/sulfuric acid, phosphomolybdic acid or potassium permanganate) followed by heating was used for visualization on TLC.

^1H -NMR, ^{13}C -NMR and ^{19}F -NMR measurements were recorded on a Bruker Avance 300 (300 MHz for ^1H , 75 MHz for ^{13}C , 282 MHz for ^{19}F), on a Bruker Avance III 400 MHz (400 MHz for ^1H , 101 MHz for ^{13}C , 386 MHz for ^{19}F) or on a Bruker Avance III 600 MHz (600 MHz for ^1H , 151 MHz for ^{13}C , 565 MHz for ^{19}F) spectrometer. Chemical shifts δ are reported in parts per million (ppm) relative to the solvent peak of deuterated chloroform (CDCl_3 , 7.26 ppm for ^1H , 77.16 ppm for ^{13}C) or deuterated dimethyl sulfoxide (DMSO-d_6 , 2.50 ppm for ^1H , 39.52 ppm for ^{13}C). The spectra were analyzed by first order, and the coupling constants J are reported in Hertz (Hz). The characterization of the splitting patterns of the spin multiplicity is reported as follows: s = singlet, d = doublet, t = triplet, q = quartet, m = multiplet, dd = doublet of doublets, ddd = doublet of doublet of doublets, dt = doublet of triplets, ddt = doublet of doublet of triplets, qd = quartet of doublets, quin = quintet, b = broad. DEPT-135: CH peaks up, CH_2 peaks down, CH_3 peaks up.

Infrared spectra were recorded on a Biorad Excalibur FTS 3000 spectrometer, equipped with a Specac Golden Gate Diamond Single Reflection ATR-System, or on a Cary 630 FTIR spectrometer. The wavenumbers are reported in cm^{-1} .

Mass spectrometry was performed by the Central Analytic Department of the University of Regensburg on a Finnigan MAT95, a Jeol AccuTOF GCX, a Finnigan MAT SSQ 710 A, a ThermoQuest Finnigan TSQ 7000 or an Agilent Q-TOF 6540 UHD. Elemental microanalysis was performed by the Micro Analytical Department of the University of Regensburg on a Vario MICRO cube (Elementar Analysensysteme GmbH).

Melting points (mps) were recorded on an automated system: Stanford Research Systems OptiMelt MPA 100.

X-ray crystallographic analyses were performed using an Agilent Technologies SuperNova, an Agilent Technologies Gemini R Ultra, an Agilent GV 50 or a Rigaku GV 50 diffractometer by the Central Analytic Department of the University of Regensburg.

UV-Vis absorption measurements were performed on a Varian Cary 50 Bio UV-VIS spectrophotometer or on an Agilent Cary 100 UV-VIS spectrophotometer. Luminescence spectra, excitation spectra, decay times and photoluminescence quantum yields were measured under the guidance of A. Schinabeck in the group of Prof. Dr. H. Yersin at the University of Regensburg. Luminescence and excitation spectra were recorded on a Horiba Jobin Yvon Fluorolog 3 steady-state fluorescence spectrometer or on a Horiba Jobin Yvon Fluorolog 3-22 spectrometer. For decay time measurements on the Fluorolog 3 system, a

PicoQuant LDH-P-C-375 pulsed diode laser with an excitation wavelength of 372 nm and a pulse width of 100 ps was used as the excitation source. For decay time measurements on the Fluorolog 3-22 spectrometer, a Picobrite PB-375L pulsed diode laser with an excitation wavelength of 378 nm and a pulse width < 100 ps was used as the excitation source. The emission signal was detected with a cooled photomultiplier attached to a FAST ComTec multichannel scalar card with a time resolution of 250 ps. Photoluminescence quantum yields were determined at ambient temperature with a Hamamatsu C9920-02 system equipped with a Spectralon® integrating sphere. Emission spectra of LEDs were recorded on an Ocean Optics USB4000-UV-VIS spectrometer.

For the cyclic voltammetry measurements, an Autolab PGSTAT302N (Metrohm) setup was used. The measurements were carried out by R. Hoheisel (group of Prof. Dr. B. König, University of Regensburg) in a conventional undivided electrochemical cell at 20 °C in the stated solvent under an argon atmosphere using tetrabutylammonium tetrafluoroborate (0.1 mol/L) as supporting electrolyte. The following electrodes were used: a glassy carbon working electrode, platinum wire as a counter electrode and silver wire as a reference electrode. The solvent was degassed by vigorous argon bubbling prior to the measurements. Redox potentials were referenced against ferrocene as an internal standard. The potentials of irreversible peaks were approximated by using the peak potentials. For better comparison, all values were converted using the conversion constants of A. W. Addison *et al.*^[167], and are reported in reference to the saturated calomel electrode (SCE).

2. Synthesis of Known Compounds and Reagents

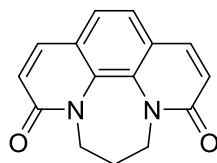
The following compounds were synthesized according to the reported procedures. The spectral data corresponded to the reported ones:

2,9-bis(para-anisyl)-1,10-phenanthroline (dap, **60**)^[25,47], 6,7-dihydro-5H-[1,4]diazepino [1,2,3,4-lmn][1,10]phenanthroline-4,8-diium bromide (**62**)^[107], 2,9-dichloro-1,10-phenanthroline (**64**)^[107], 1,10-phenanthroline-5,6-dione (**67**)^[110], 2,9-dichloro-1,10-phenanthroline-5,6-dione (**68**)^[107], 3,6-dichlorodipyrido[3,2-*a*:2',3'-*c*]phenazine (**72**)^[11], [Cu(dap)₂]Cl (**C1-Cl**)^[25,47], [Cu(dap)₂]BF₄ (**C1-BF₄**)^[25,47], [Cu(dap)₂]PF₆ (**C1-PF₆**)^[25,47], 4-nitrobenzyl bromide (**75**)^[168], *N*-Boc allylamine (**80**)^[169], *N,N'*-bis(mesityl)-1,4-diaza-1,3-butadiene (DABMes, **86**)^[170], [Cu(DABMes)₂]BF₄ (**C14**)^[109], phenyl trifluoromethanesulfonate (**100**)^[140], 3-methoxystyrene (**125j**)^[171], 1-nitro-4-vinylbenzene (**125o**)^[172], 6-(*tert*-butyl) 3-methyl (1*S*,5*S*,6*S*)-2-oxabicyclo[3.1.0]hex-3-ene-3,6-dicarboxylate (**126d**)^[173],¹² di-*tert*-butyl (1*R*,5*R*,6*R*)-2-azabicyclo[3.1.0]hex-3-ene-2,6-dicarboxylate (**126e**)^[174],¹³ *N*-(trifluoromethyl) acyloxyphthalimide (**130**)^[161].

¹² Provided by R. Eckl¹³ Provided by U. Klimczak

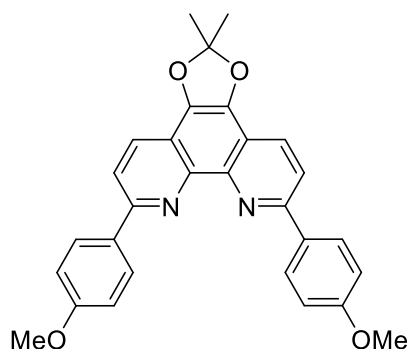
3. Chapter B: Synthesis, Characterization and Application of New Diimine-Based Copper Complexes

3.1 Compound Characterization



6,7-dihydro-5H-[1,4]diazepino[1,2,3,4-*lmn*][1,10]phenanthroline-3,9-dione (**63**)^[175]

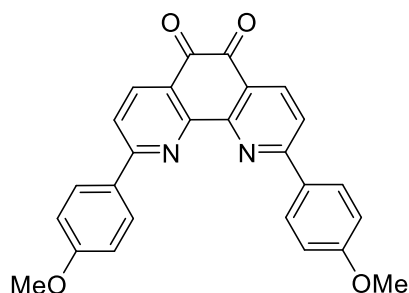
In a round-bottom flask, compound **62** (11.05 g, 28.9 mmol, 1.0 equiv) was dissolved in *tert*-butanol (180 mL). To the stirred solution, potassium *tert*-butoxide (13.62 g, 121.4 mmol, 4.2 equiv) was added at 40 °C within 10 min. After stirring at 40 °C in the open flask for 24 h, the reaction solution was saturated with oxygen using an oxygen balloon. Brine (200 mL) and chloroform (100 mL) were added and the phases were separated. The aqueous phase was extracted with chloroform (3 x 70 mL). The combined organic phases were washed with brine (100 mL), dried over Na₂SO₄, filtered and concentrated in vacuum. Compound **63** was obtained as a brown solid (6.71 g, 26.6 mmol, 92%). ¹H-NMR (400 MHz, CDCl₃) δ 7.71 (d, *J* = 9.5 Hz, 2H), 7.36 (s, 2H), 6.80 (d, *J* = 9.5 Hz, 2H), 4.32 (t, *J* = 6.6 Hz, 4H), 2.46 (quin, *J* = 6.5 Hz, 2H).



6,9-bis(4-methoxyphenyl)-2,2-dimethyl-[1,3]dioxolo[4,5-*f*][1,10]phenanthroline (dapacetal, **65**)

A two-necked Schlenk flask, fitted with a condenser, was charged with compound **69** (526 mg, 1.64 mmol, 1.0 equiv), (4-methoxyphenyl)boronic acid (550 mg, 3.62 mmol, 2.2 equiv), triphenylphosphine (17.2 mg, 0.066 mmol, 4.0 mol%) and 1,2-dimethoxyethane (6.0 mL). The mixture was degassed by two freeze-pump-thaw cycles. [Pd₂(dba)₃] (15.1 mg, 0.016 mmol, 1 mol%) as well as a mixture of K₂CO₃ (500 mg, 3.62 mmol, 2.2 equiv) in water

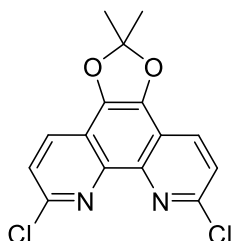
(1.2 mL) were added under slight nitrogen overpressure and the resulting mixture was degassed by two further freeze-pump-thaw cycles. The reaction mixture was stirred under a nitrogen atmosphere at 100 °C for 63 h. After cooling to room temperature, water (90 mL) and dichloromethane (60 mL) were added, and the phases were separated. The aqueous phase was extracted with dichloromethane (7 x 50 mL). The combined organic phases were washed with brine (1 x 100 mL), dried over Na₂SO₄, filtered and concentrated in vacuum. Purification by column chromatography on silica gel using mixtures of DCM:MeOH (*R*_f = 0.76 in DCM:MeOH 98:2) afforded the desired product as a yellow green solid (671 mg, 1.44 mmol, 88%). **IR** (neat, cm⁻¹) 3040, 3000, 2966, 2940, 2836, 1650, 1587, 1519, 1508, 1448, 1360, 1247, 1173, 1075, 1029, 816. **¹H-NMR** (400 MHz, CDCl₃) δ 8.41 (d, *J* = 8.8 Hz, 4H), 8.27 (d, *J* = 8.6 Hz, 2H), 8.08 (d, *J* = 8.6 Hz, 2H), 7.11 (d, *J* = 8.9 Hz, 4H), 3.92 (s, 6H), 1.89 (s, 6H). **¹³C-NMR** (101 MHz, CDCl₃) δ 160.9, 154.1, 142.2, 136.4, 132.4, 128.9, 128.9, 120.6, 119.3, 117.0, 114.3, 55.6, 26.3. **HRMS** (ESI): *m/z* calculated for C₂₉H₂₅N₂O₄ [MH⁺]: 465.1809, found: 465.1810. **mp**: 266 - 271 °C. The ¹H-NMR data are in accordance with the data reported in the literature.^[113]



2,9-bis(4-methoxyphenyl)-1,10-phenanthroline-5,6-dione (**66**)^[113]

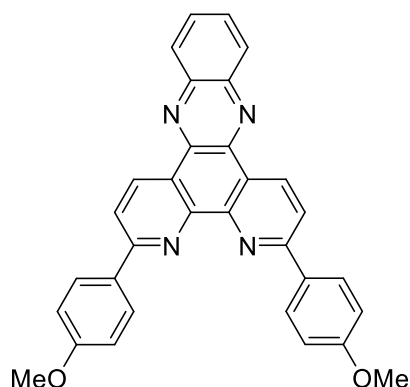
Compound **65** (300 mg, 0.65 mmol) was dissolved in a mixture of water (8.0 mL) and trifluoroacetic acid (16.3 mL) in a Schlenk flask. The reaction mixture was saturated with oxygen by using an oxygen balloon. Then, the mixture was stirred at 50 °C for 15 h under oxygen atmosphere. Trifluoroacetic acid was removed by distillation under reduced pressure. Dichloromethane (50 mL) and a solution of NaHCO₃ (1 M, 50 mL) were added, and the phases were separated. The aqueous phase was extracted with dichloromethane (7 x 50 mL). The combined organic phases were washed with water (1 x 100 mL), dried over Na₂SO₄, filtered and concentrated in vacuum. The residue was suspended in toluene (30 mL) and stirred for 10 min. The solid residue was recovered by filtration, washed with diethyl ether and dried in vacuum. This procedure afforded compound **66** as an orange solid (237 mg, 0.56 mmol, 86%). **IR** (neat, cm⁻¹) 3082, 3003, 2833, 1668, 1604, 1553, 1512, 1446, 1375, 1320, 1254, 1168, 1026, 832, 817, 769, 613. **¹H-NMR** (400 MHz, CDCl₃) δ 8.49 (d, *J* =

8.3 Hz, 2H), 8.36 (d, J = 8.8 Hz, 4H), 7.94 (d, J = 8.3 Hz, 2H), 7.11 (d, J = 8.8 Hz, 4H), 3.94 (s, 6H). **$^{13}\text{C-NMR}$** (101 MHz, CDCl_3) δ 179.0, 162.5, 162.4, 153.2, 138.0, 130.4, 129.7, 126.3, 120.5, 114.7, 55.7. **HRMS** (ESI): m/z calculated for $\text{C}_{26}\text{H}_{19}\text{N}_2\text{O}_4$ [MH^+]: 423.1339, found: 423.1342.



6,9-dichloro-2,2-dimethyl-[1,3]dioxolo[4,5-*f*][1,10]phenanthroline (69)^[107]

Compound **68** (558 mg, 2.00 mmol, 1.0 equiv) and 2-nitropropane (1.80 mL, 20.0 mmol, 10.0 equiv) were dissolved in a mixture of acetonitrile (90 mL) and water (30 mL) in a three-necked flask fitted with a condenser. The mixture was degassed by two freeze-pump-thaw cycles. A Solution of Na_2CO_3 (1.70 g, 16.0 mmol, 8.0 equiv) in water (60 mL) was degassed by two freeze-pump-thaw cycles and added. The resulting mixture was degassed by one more freeze-pump-thaw cycle and stirred at 55 °C for 15 h. After cooling to room temperature, the organic solvent was evaporated and the resulting mixture was neutralized to pH 6-7 with diluted HCl (0.5 M). The aqueous phase was extracted with dichloromethane (4 x 100 mL). The combined organic layers were dried over Na_2SO_4 , filtered and concentrated in vacuum. Purification by column chromatography on silica gel using dichloromethane (R_f = 0.42) afforded the desired product as a light yellow solid (530 mg, 1.65 mmol, 83%). **$^1\text{H-NMR}$** (300 MHz, CDCl_3) δ 8.16 (d, J = 8.6 Hz, 2H), 7.57 (d, J = 8.6 Hz, 2H), 1.86 (s, 6H).

**3,6-bis(4-methoxyphenyl)dipyrido[3,2-a:2',3'-c]phenazine (phenazino-dap, 73)¹⁴**Synthesis using condensation in the last step:

Compound **66** (350 mg, 0.83 mmol, 1.0 equiv) was suspended in ethanol (130 mL) in a round-bottom flask, 1,2-diaminobenzene (256 mg, 2.37 mmol, 2.9 equiv) was added and the suspension was refluxed at 95 °C for 3.5 h. After cooling to room temperature, the solid was filtered out and washed with ethanol and acetone. Drying in vacuum afforded compound **73** as a yellow solid (377 mg, 0.76 mmol, 92%).

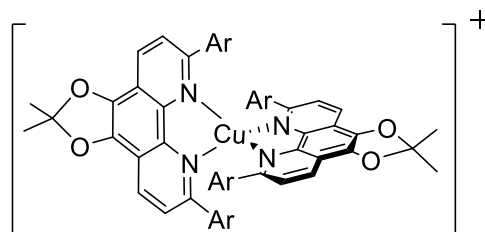
Synthesis using Suzuki coupling in the last step:

A two-necked Schlenk flask, fitted with a condenser, was charged with compound **72** (80 mg, 0.228 mmol, 1.0 equiv), (4-methoxyphenyl)boronic acid (76 mg, 0.502 mmol, 2.2 equiv), triphenylphosphine (2.4 mg, 9.1 μmol, 4.0 mol%) and toluene (4.0 mL). The mixture was degassed by two freeze-pump-thaw cycles, [Pd₂(dba)₃] (2.2 mg, 2.3 μmol, 1 mol%) as well as a mixture of K₂CO₃ (69 mg, 0.50 mmol, 2.2 equiv) in water (0.4 mL) were added under slight nitrogen overpressure and the resulting mixture was degassed by two further freeze-pump-thaw cycles. The reaction mixture was stirred under a nitrogen atmosphere at 100 °C for 63 h. After cooling to room temperature, water (30 mL) and dichloromethane (20 mL) were added, and the phases were separated. The aqueous phase was extracted with dichloromethane (4 x 20 mL). The combined organic phases were washed with brine (1 x 40 mL), dried over CaCl₂, filtered and concentrated in vacuum. Purification by column chromatography on silica gel using mixtures of DCM:MeOH (R_f = 0.54 in DCM:MeOH 99:1) afforded the crude product. After washing with ethyl acetate and acetone using a paper filter, the desired product was obtained as a yellow green solid (72 mg, 0.146 mmol, 64%).

IR (neat, cm⁻¹) 3052, 3008, 2937, 2840, 1606, 1573, 1511, 1480, 1431, 1361, 1252, 1170, 1032, 820, 760. **¹H-NMR** (600 MHz, CDCl₃) δ 9.65 (d, *J* = 8.4 Hz, 2H), 8.50 (d, *J* = 8.7 Hz,

¹⁴ The NMR spectra of this compound were measured by the Central Analytic Department of the University of Regensburg.

4H), 8.36 (dd, $J = 6.4, 3.5$ Hz, 2H), 8.24 (d, $J = 8.5$ Hz, 2H), 7.90 (dd, $J = 6.5, 3.3$ Hz, 2H), 7.15 (d, $J = 8.7$ Hz, 4H), 3.95 (s, 6H). **$^{13}\text{C-NMR}$** (151 MHz, CDCl_3) δ 161.5, 158.9, 148.3, 142.6, 141.5, 134.8, 131.7, 130.4, 129.7, 129.3, 126.0, 120.2, 114.5, 55.6. **HRMS** (ESI): m/z calculated for $\text{C}_{32}\text{H}_{23}\text{N}_4\text{O}_2$ $[\text{MH}^+]$: 495.1816, found 495.1821. **mp**: > 310 °C, decomposition.



Ar = *p*-OMe-Ph

[Cu(dapacetal)₂] BF_4 (C8-BF₄)

In a round-bottom flask, $[\text{Cu}(\text{MeCN})_4]\text{BF}_4$ (34.9 mg, 0.11 mmol, 1.0 equiv) was suspended in chloroform (1.0 mL) and sonicated at room temperature for 3 min. To the stirred solution, dapacetal (**65**) (100 mg, 0.22 mmol, 2.0 equiv) and 2.0 mL chloroform were added. The mixture was sonicated at room temperature for 3 min, and stirred at 60 °C for 25 min. After the solvent had been evaporated, the resulting solid was recrystallized from chloroform and diethyl ether. Crystallization was completed in a freezer. This procedure afforded compound **C8-BF₄** in the form of black red crystals (113 mg, 105 μmol , 95%).

[Cu(dapacetal)₂] Cl (C8-Cl)

Following the previous procedure, CuCl (6.3 mg, 0.06 mmol, 1.0 equiv) and dapacetal (**65**) (57.5 mg, 0.12 mmol, 2.0 equiv) afforded after 30 min $[\text{Cu}(\text{dapacetal})_2]\text{Cl}$ (**C8-Cl**) in the form of red brown crystals (47.5 mg, 46 μmol , 72%).

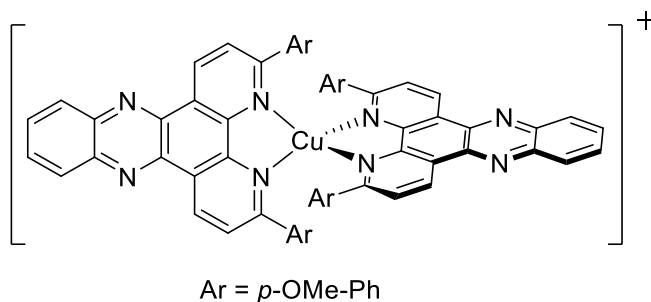
[Cu(dapacetal)₂] PF_6 (C8-PF₆)

Following the previous procedure, $[\text{Cu}(\text{MeCN})_4]\text{PF}_6$ (20.4 mg, 55 μmol , 1.0 equiv) and dapacetal (**65**) (49.7 mg, 0.11 mmol, 2.0 equiv) afforded after 30 min $[\text{Cu}(\text{dapacetal})_2]\text{PF}_6$ (**C8-PF₆**) in the form of red crystals (62.4 mg, quantitative).

Suitable crystals for X-ray structure analysis of $[\text{Cu}(\text{dapacetal})_2]\text{PF}_6$ (**C8-PF₆**) were obtained by vapor diffusion of diethyl ether into a dichloromethane solution.

IR (neat, cm^{-1}) 3069, 2994, 2932, 2840, 1652, 1606, 1585, 1505, 1445, 1372, 1247, 1178, 1034, 821. **$^1\text{H-NMR}$** (300 MHz, CDCl_3) δ 8.41 (d, $J = 8.5$ Hz, 4H), 7.87 (d, $J = 8.5$ Hz, 4H),

7.33 (d, $J = 8.6$ Hz, 8H), 6.11 (d, $J = 8.7$ Hz, 8H), 3.58 (s, 12H), 2.00 (s, 12H). **$^{13}\text{C-NMR}$** (75 MHz, CDCl_3) δ 160.0, 154.4, 139.7, 137.0, 131.6, 129.3, 129.0, 124.7, 122.5, 117.1, 112.8, 55.5, 26.2. **HRMS** (ESI): m/z calculated for $\text{C}_{58}\text{H}_{48}\text{CuN}_4\text{O}_8$ ($[\text{Cu}(\text{dapacetal})_2]^+$): 991.2763, found 991.2757. **mp**: > 272 °C, decomposition.

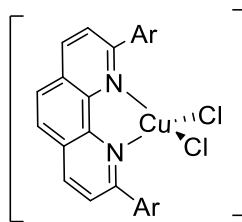


[Cu(phenazino-dap) $_2$] PF_6 (C9-PF $_6$**)¹⁵**

In a round-bottom flask, phenazino-dap (**73**) (173 mg, 0.35 mmol, 2.0 equiv) was suspended in chloroform (60 mL) and sonicated at room temperature for 5 min. To the stirred solution, tetrakis(acetonitrile)copper(I) hexafluorophosphate (67.2 mg, 0.18 mmol, 1.0 equiv) was added, the mixture was sonicated at room temperature for 5 min, and stirred at 60 °C for 30 min. After evaporation of the solvent, the resulting brown solid was dried in vacuum, washed with water (3 x) using a Büchner funnel and dissolved in acetonitrile. The solvent was evaporated and the crude product was recrystallized from dichloromethane and diethyl ether. Crystallization was completed in a freezer to afford compound **C9-PF $_6$** in the form of red crystals (159 mg, 133 μmol , 74%). **IR** (neat, cm^{-1}) 3075, 3023, 2974, 2937, 2840, 1607, 1577, 1513, 1484, 1438, 1364, 1256, 1174, 1022, 824, 753. **$^1\text{H-NMR}$** (600 MHz, DMSO-d_6) δ 9.70 (d, $J = 8.3$ Hz, 4H), 8.56 (dd, $J = 6.4, 3.4$ Hz, 4H), 8.26 (d, $J = 8.3$ Hz, 4H), 8.20 (dd, $J = 6.4, 3.4$ Hz, 4H), 7.53 (d, $J = 8.6$ Hz, 8H), 6.24 (d, $J = 8.6$ Hz, 8H), 3.12 (s, 12H). **$^{13}\text{C-NMR}$** (151 MHz, DMSO-d_6) δ 159.8, 157.7, 145.6, 142.0, 139.7, 134.2, 132.0, 130.7, 129.4, 128.9, 126.3, 125.8, 112.8, 54.6. **HRMS** (ESI): m/z calculated for $\text{C}_{64}\text{H}_{44}\text{CuN}_8\text{O}_4$ ($[\text{Cu}(\text{phenazino-dap})_2]^+$): 1051.2776, found 1051.2757. **mp**: > 290 °C, decomposition.

Suitable crystals for X-ray structure analysis of $[\text{Cu}(\text{phenazino-dap})_2]\text{PF}_6$ (**C9-PF $_6$**) were obtained by vapor diffusion of diethyl ether into a dichloromethane solution.

¹⁵ The NMR spectra of this compound were measured by the Central Analytic Department of the University of Regensburg.

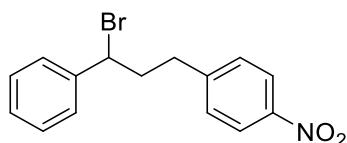


Ar = *p*-OMe-Ph

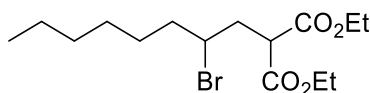
[Cu(dap)Cl₂] (C10)

In a round-bottom flask, CuCl₂ (8.8 mg, 0.065 mmol, 1.0 equiv) was suspended in chloroform (0.7 mL) and sonicated at room temperature for 3 min. To the stirred solution, 2,9-bis(para-anisyl)-1,10-phenanthroline (dap, **60**) (50.5 mg, 0.128 mmol, 2.0 equiv) and 0.3 mL chloroform were added. The mixture was sonicated at room temperature for 3 min, and stirred at 55 °C for 60 min. After the solvent had been evaporated, the resulting solid was recrystallized from chloroform and diethyl ether. Crystallization was completed in a freezer. This procedure afforded compound **C10** in the form of brownish green crystals (23.0 mg, 44 μmol, 68%). [Cu(dap)Cl₂] (**C10**) used for test reactions was synthesized in a 56% yield using the same procedure starting with a CuCl₂:dap ratio of 1:1. **IR** (neat, cm⁻¹) 3049, 2963, 2930, 2904, 2837, 1603, 1577, 1487, 1454, 1256, 1182, 1018, 842, 805, 753. **Elemental microanalysis** (%): calculated for C₂₆H₂₀Cl₂CuN₂O₂: C 59.27, H 3.83, N 5.32; found: C 59.09, H 3.83, N 5.06. **mp**: 209 °C.

Suitable crystals for X-ray analysis of [Cu(dap)Cl₂] (**C10**) were obtained by liquid diffusion of diethyl ether into a dichloromethane solution.

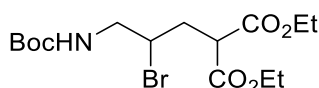
**1-(3-bromo-3-phenylpropyl)-4-nitrobenzene (76)**

An oven-dried pressure tube (6 mL size) equipped with a magnetic stir bar was charged with 4-nitrobenzyl bromide (108.0 mg, 0.50 mmol, 1.0 equiv), [Cu(dapacetal)₂]BF₄ (**C8-BF₄**) (5.4 mg, 0.005 mmol, 1 mol%) and anhydrous acetonitrile (1.0 mL). The mixture was degassed using two freeze-pump-thaw cycles. Styrene **74** (286 μ L, 2.50 mmol, 5.0 equiv) was added under slight nitrogen overpressure and the reaction mixture was degassed by one freeze-pump-thaw cycle. The tube was equipped with a light emitting LED-stick and sealed. The reaction mixture was irradiated at room temperature with a green LED (λ_{max} = 530 nm) and the reaction progress was monitored by TLC. After 24 h, the mixture was concentrated and purified by column chromatography on silica gel (hexanes:EtOAc 9:1, R_f = 0.39) to afford product **76** as a colorless oil (95.1 mg, 59%). **¹H-NMR** (300 MHz, CDCl₃) δ 8.22 – 8.11 (m, 2H), 7.41 – 7.28 (m, 7H), 4.87 (dd, J = 8.7, 6.1 Hz, 1H), 2.95 (ddd, J = 14.4, 9.1, 5.7 Hz, 1H), 2.82 (ddd, J = 13.9, 8.8, 6.6 Hz, 1H), 2.63 (ddt, J = 14.4, 8.7, 5.7 Hz, 1H), 2.44 (ddt, J = 14.3, 9.1, 6.4 Hz, 1H). **¹³C-NMR** (75 MHz, CDCl₃) δ 148.4, 146.8, 141.5, 129.5, 129.0, 128.8, 127.3, 124.0, 54.1, 40.9, 34.3. The NMR data are in accordance with the data reported in the literature.^[26]

**Diethyl 2-(2-bromooctyl)malonate (79)**

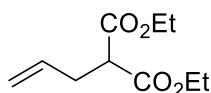
An oven-dried pressure tube (6 mL size) equipped with a magnetic stir bar was charged with diethyl bromomalonate (0.17 mL, 1.0 mmol, 2.0 equiv), [Cu(dap)₂]Cl (**C1-Cl**) (4.4 mg, 0.005 mmol, 1.0 mol%) and anhydrous acetonitrile (0.5 mL). The mixture was degassed using two freeze-pump-thaw cycles. 1-Octene **77** (79 μ L, 0.50 mmol, 1.0 equiv) was added under slight nitrogen overpressure and the reaction mixture was degassed by one freeze-pump-thaw cycle. The tube was equipped with a light emitting LED-stick and sealed. The reaction mixture was irradiated at room temperature with a blue LED (λ_{max} = 455 nm) and the reaction progress was monitored by TLC. After 24 h, the reaction was stopped by switching off the light source. The resulting mixture was concentrated and purified by column chromatography on silica gel (hexanes:EtOAc 5:1, R_f = 0.55) to afford product **79** as a colorless oil (156.4 mg, 89%). **IR** (neat, cm⁻¹) 2930, 2859, 1733, 1465, 1371, 1210, 1148,

1029, 857. **¹H-NMR** (400 MHz, CDCl₃) δ 4.25 – 4.16 (m, 4H), 4.00 (dddd, *J* = 10.7, 8.1, 5.5, 3.1 Hz, 1H), 3.78 (dd, *J* = 10.2, 4.2 Hz, 1H), 2.46 (ddd, *J* = 14.9, 10.2, 3.1 Hz, 1H), 2.25 (ddd, *J* = 14.9, 10.7, 4.2 Hz, 1H), 1.88 – 1.81 (m, 2H), 1.58 – 1.50 (m, 1H), 1.46 – 1.39 (m, 1H), 1.31 – 1.25 (m, 12H), 0.88 (t, *J* = 6.8 Hz, 3H). **¹³C-NMR** (101 MHz, CDCl₃) δ 169.2, 169.0, 61.8, 61.7, 55.2, 50.8, 39.6, 38.0, 31.8, 28.7, 27.5, 22.7, 14.2, 14.2. **HRMS** (ESI): *m/z* calculated for C₁₅H₂₈BrO₄ [MH⁺]: 351.1165, found 351.1170. The data are in accordance with the data reported in the literature.^[176]



Diethyl 2-(2-bromo-3-((*tert*-butoxycarbonyl)amino)propyl)malonate (**81**)

An oven-dried pressure tube (6 mL size) equipped with a magnetic stir bar was charged with LiBr (87 mg, 1.0 mmol, 2.0 equiv), *N*-Boc allylamine (79.0 mg, 0.50 mmol, 1.0 equiv), diethyl 2-bromomalonate (0.17 mL, 1.0 mmol, 2.0 equiv), [Cu(dap)₂]Cl (**C1-Cl**) (4.4 mg, 0.005 mmol, 1 mol%) and a mixture of DMF/H₂O (1/4 v/v, 1.0 mL). After degassing the mixture using three freeze-pump-thaw cycles, the tube was equipped with a light emitting LED-stick and sealed. The reaction mixture was irradiated at room temperature with a green LED (λ_{max} = 530 nm) and the reaction progress was monitored by TLC. After 24 h, the mixture was concentrated and purified by column chromatography on silica gel (hexanes:EtOAc 8:1, *R_f* = 0.38 in hexanes:EtOAc 4:1) to afford product **81** as a colorless oil (152.0 mg, 77%). **¹H-NMR** (400 MHz, CDCl₃) δ 4.97 (bs, 1H), 4.26 – 4.17 (m, 4H), 4.16 – 4.07 (m, 1H), 3.74 (dd, *J* = 9.5, 4.9 Hz, 1H), 3.57 – 3.45 (m, 2H), 2.47 (ddd, *J* = 14.8, 9.5, 3.7 Hz, 1H), 2.27 (ddd, *J* = 15.1, 10.2, 5.1 Hz, 1H), 1.45 (s, 9H), 1.27 (td, *J* = 7.1, 2.2 Hz, 6H). **¹³C-NMR** (101 MHz, CDCl₃) δ 169.0, 168.6, 155.7, 80.0, 62.0, 61.9, 53.4, 50.3, 47.2, 34.8, 28.5, 14.2, 14.2. The NMR data are in accordance with the data reported in the literature.^[25,31]

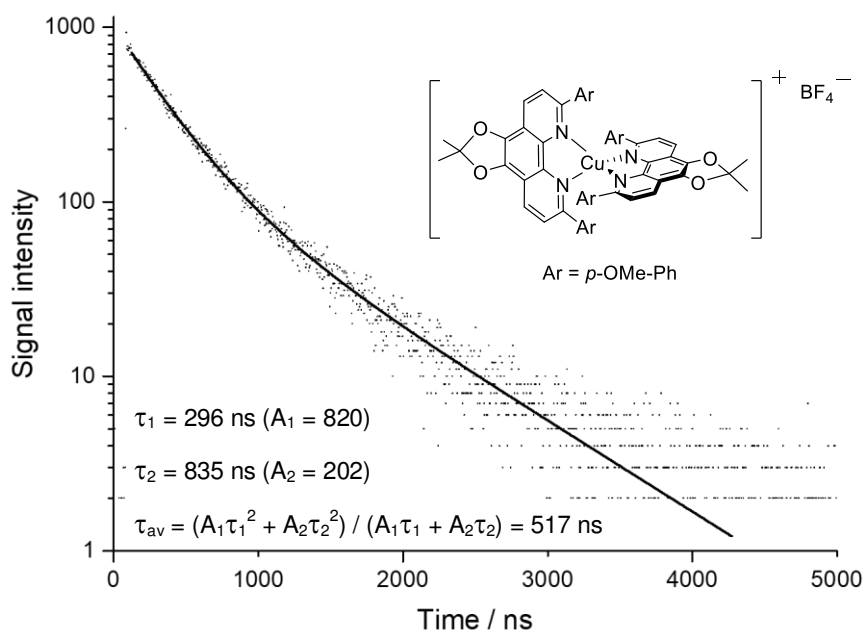


Diethyl 2-allylmalonate (**85**)

An oven-dried pressure tube (6 mL size) equipped with a magnetic stir bar was charged with diethyl bromomalonate (85 μL, 0.50 mmol, 1.0 equiv), allyltrimethylsilane (0.24 mL, 1.5 mmol, 3.0 equiv), catalyst (0.005 mmol, 1.0 mol%) and anhydrous acetonitrile (1.0 mL). After degassing the mixture using three freeze-pump-thaw cycles, the tube was equipped with

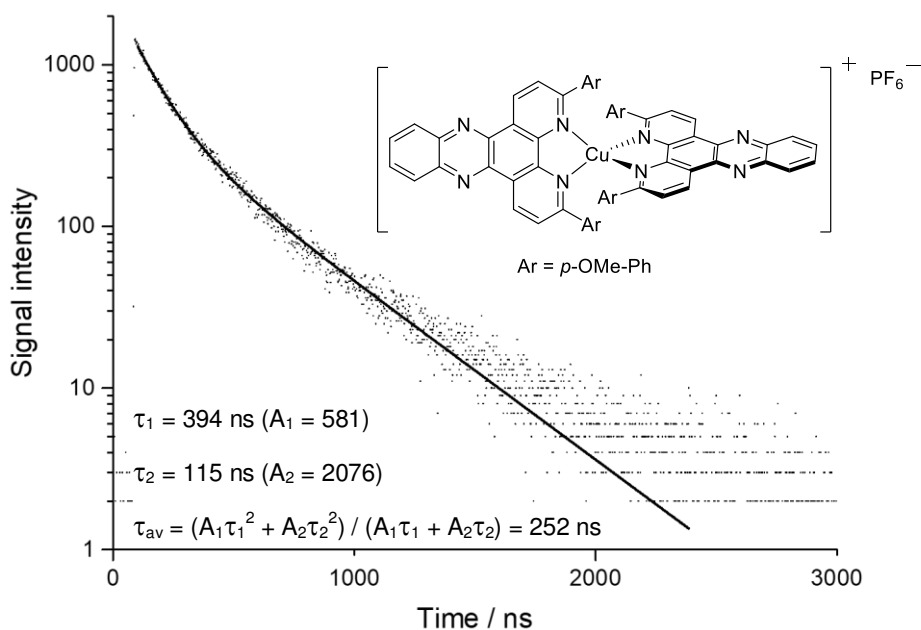
a light emitting LED-stick and sealed. The reaction mixture was irradiated at room temperature with a green LED ($\lambda_{\text{max}} = 530 \text{ nm}$) for 48 h. Using DCM, the mixture was filtrated through a short plug of silica and the solvent was removed under reduced pressure. The residue was dissolved in CDCl_3 and 1,4-dicyanobenzene (16.0 mg, 0.125 mmol, δ 7.80 (s, 4 H)) was added as internal standard. The yield was determined by ^1H -NMR by means of the characteristic product signal at 3.42 ppm (t, $J = 7.6 \text{ Hz}$, 1H). **MS** (APCI) (relative intensities): m/z 202.12 (10), 201.11 (100) [MH^+], 173.08 (5) [MH^+ , $-\text{C}_2\text{H}_4$], 109.03 (6). The product signals of the crude NMR and the mass analysis correspond to the data reported in the literature.^[20]

3.2 Luminescence Properties of $[\text{Cu}(\text{dapacetal})_2]^+$ and $[\text{Cu}(\text{phenazino-dap})_2]^+$



Measured in PMMA at ambient temperature: excitation wavelength 375 nm, detection wavelength 700 nm. The measured emission kinetics was fitted using a biexponential decay function (solid line): τ_1 and τ_2 are the individual decay times, A_1 and A_2 are the individual amplitudes and τ_{av} is the average excited state lifetime resulting from the fit.

Figure 23. Luminescence decay of $[\text{Cu}(\text{dapacetal})_2]\text{BF}_4$ (**C8-BF₄**).



Measured in PMMA at ambient temperature: excitation wavelength 375 nm, detection wavelength 723 nm. The measured emission kinetics was fitted using a biexponential decay function (solid line): τ_1 and τ_2 are the individual decay times, A_1 and A_2 are the individual amplitudes and τ_{av} is the average excited state lifetime resulting from the fit.

Figure 24. Luminescence decay of $[\text{Cu}(\text{phenazino-dap})_2]\text{PF}_6$ (**C9-PF₆**).

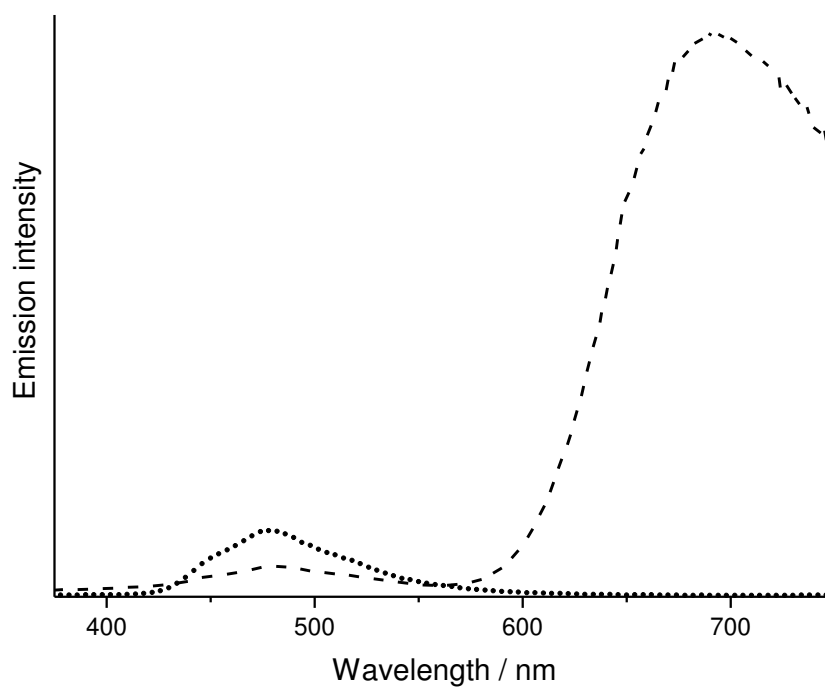


Figure 25. Luminescence spectra of [Cu(dapacetal)₂]BF₄ (**C8-BF₄**, dashed line) and dapacetal (**65**, dotted line) in PMMA at ambient temperature; excitation wavelength 300 nm.

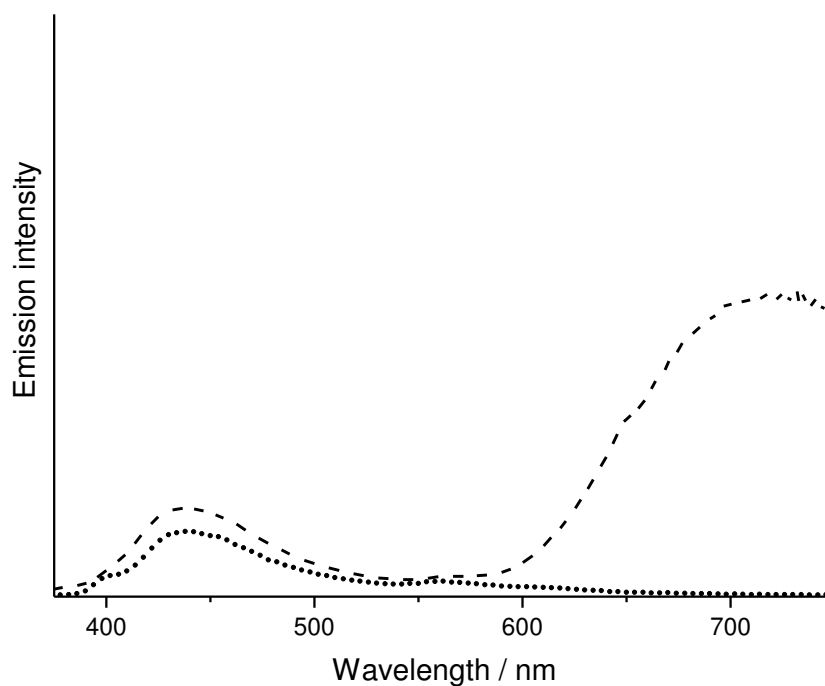
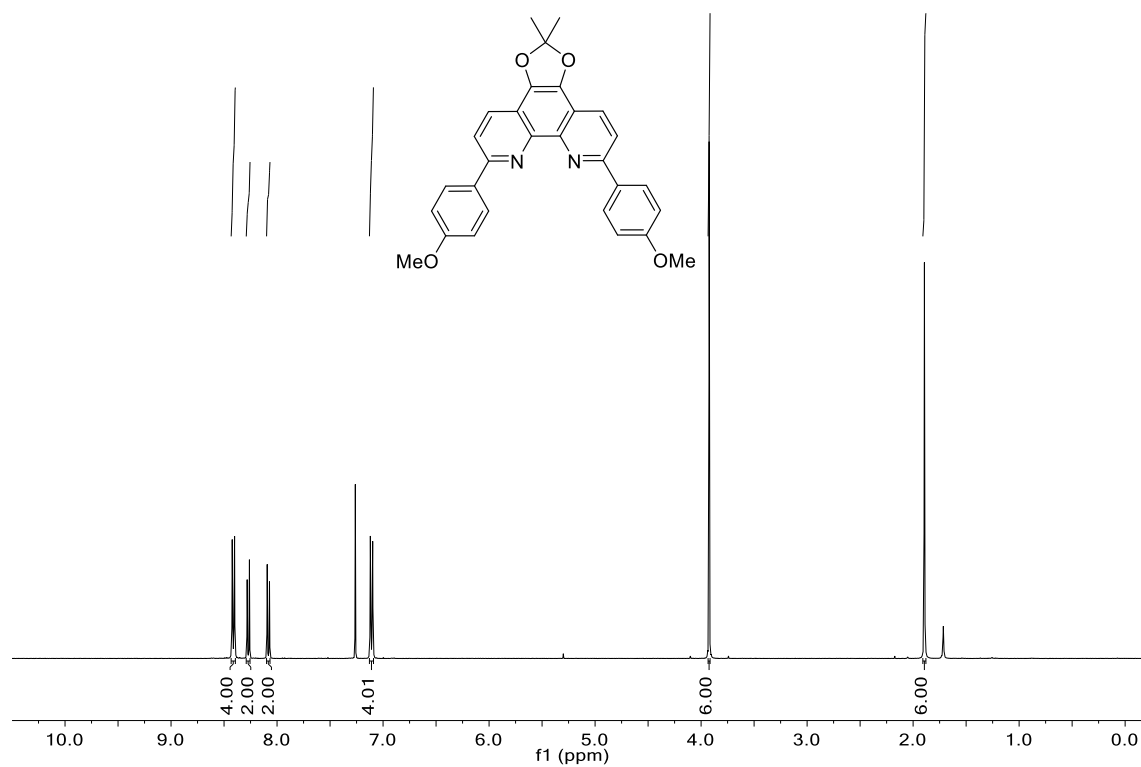


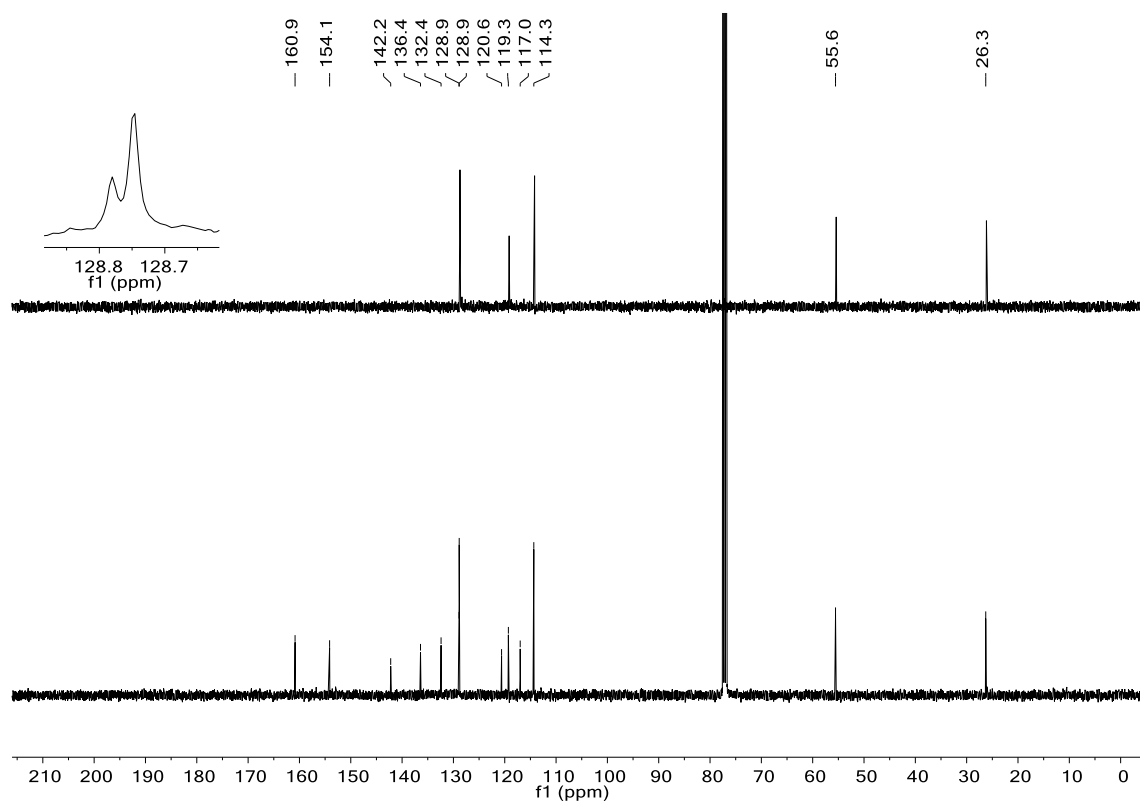
Figure 26. Luminescence spectra of [Cu(phenazino-dap)₂]PF₆ (**C9-PF₆**, dashed line) and phenazino-dap (**73**, dotted line) in PMMA at ambient temperature; excitation wavelength 330 nm.

3.3 NMR Spectra

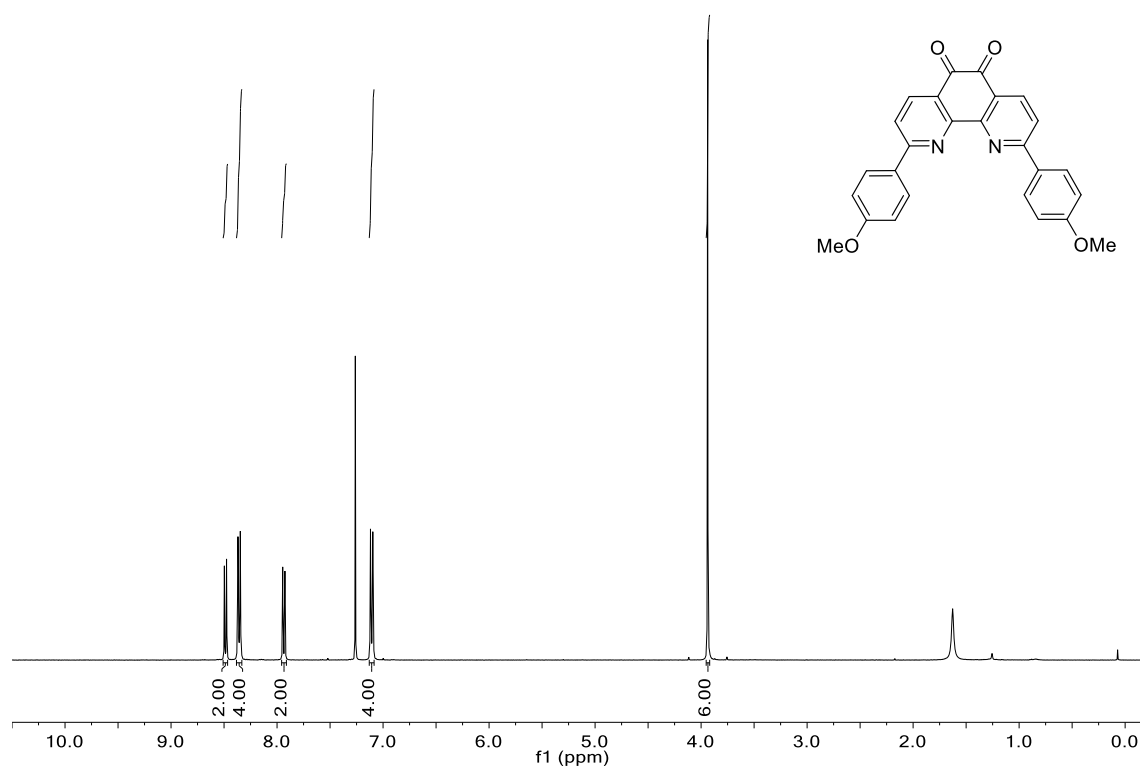
6,9-bis(4-methoxyphenyl)-2,2-dimethyl-[1,3]dioxolo[4,5-f][1,10]phenanthroline (dapacetal, 65): ^1H -NMR



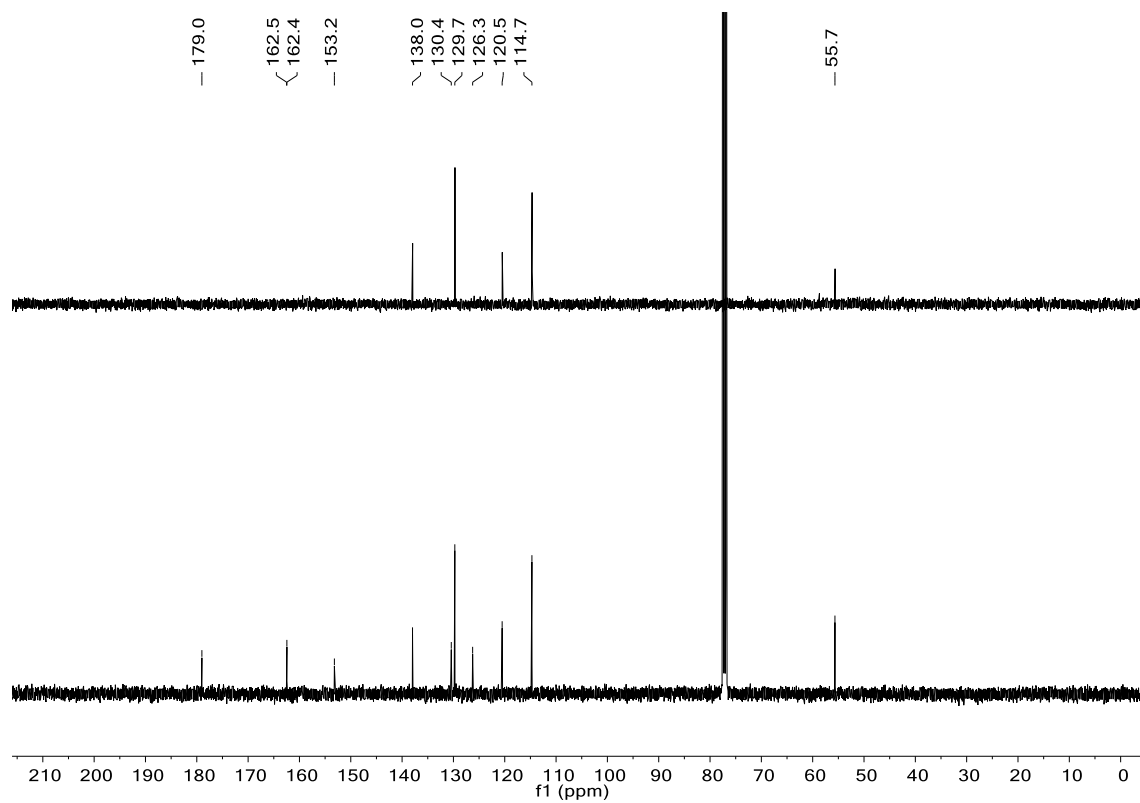
^{13}C -NMR and DEPT-135

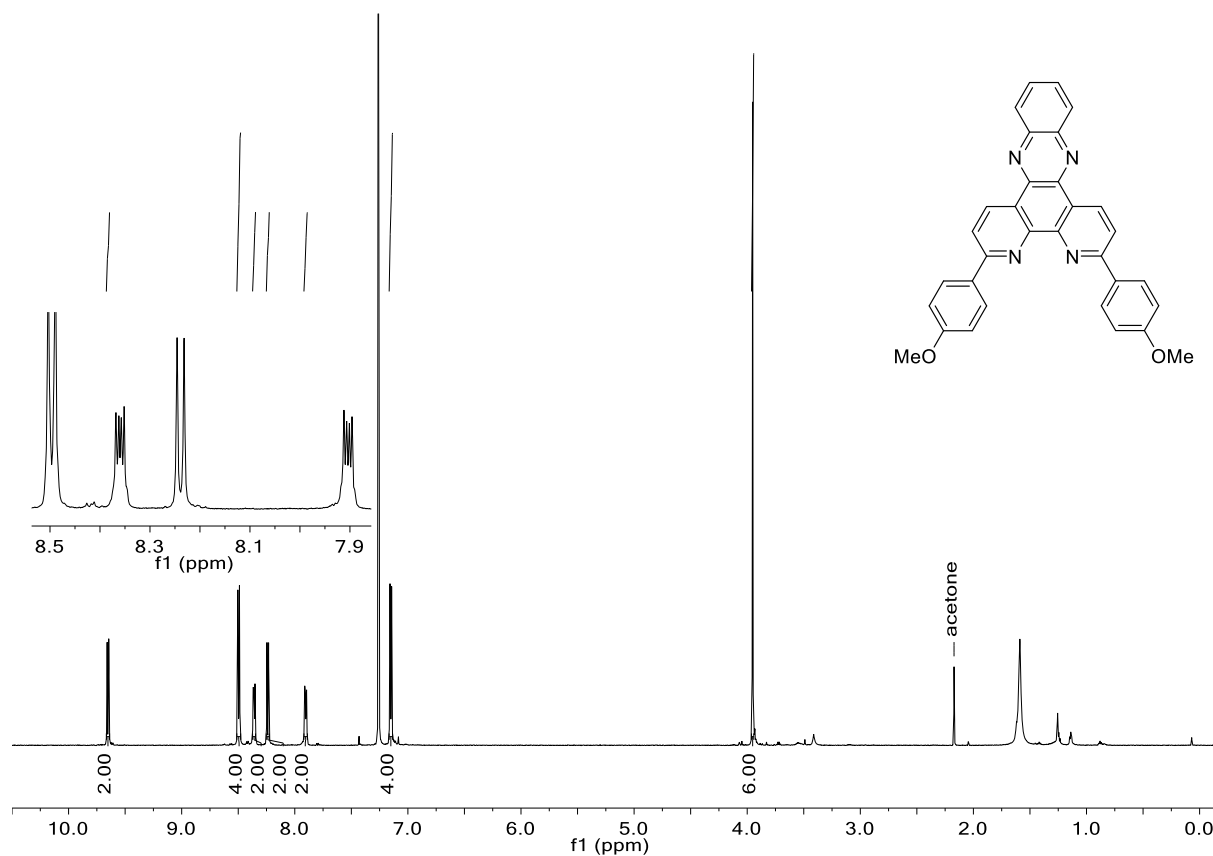
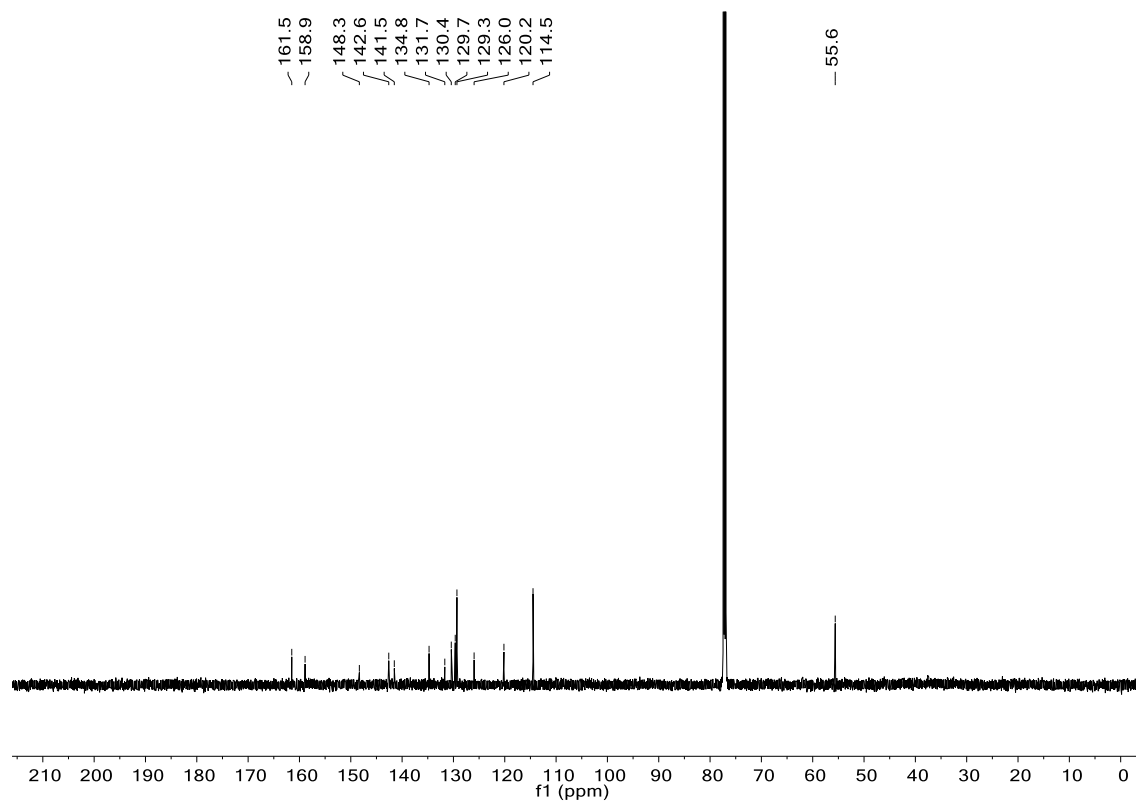


2,9-bis(4-methoxyphenyl)-1,10-phenanthroline-5,6-dione (**66**): $^1\text{H-NMR}$

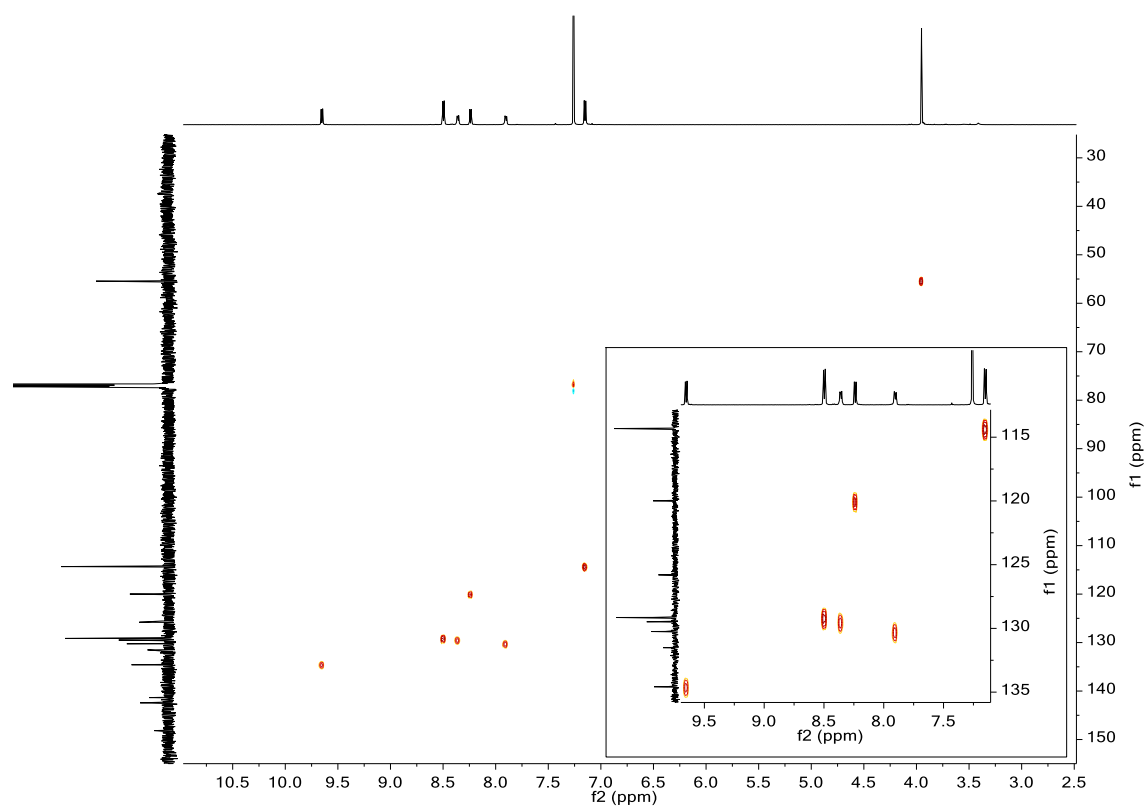


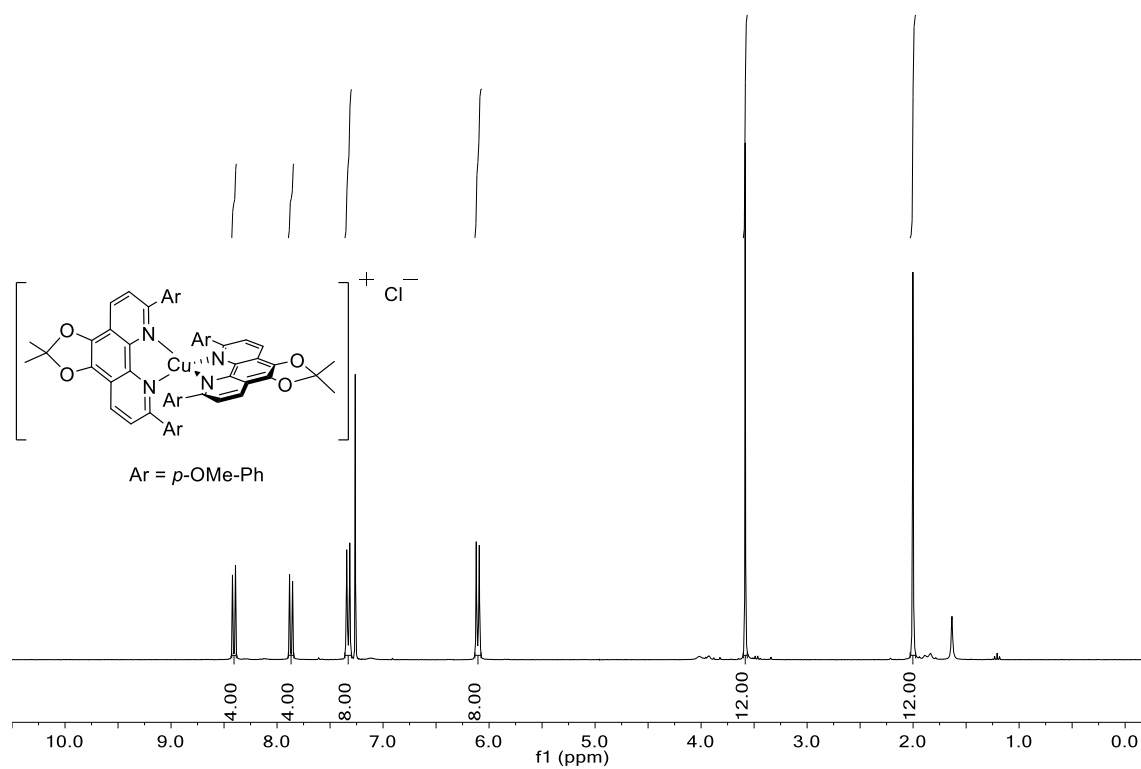
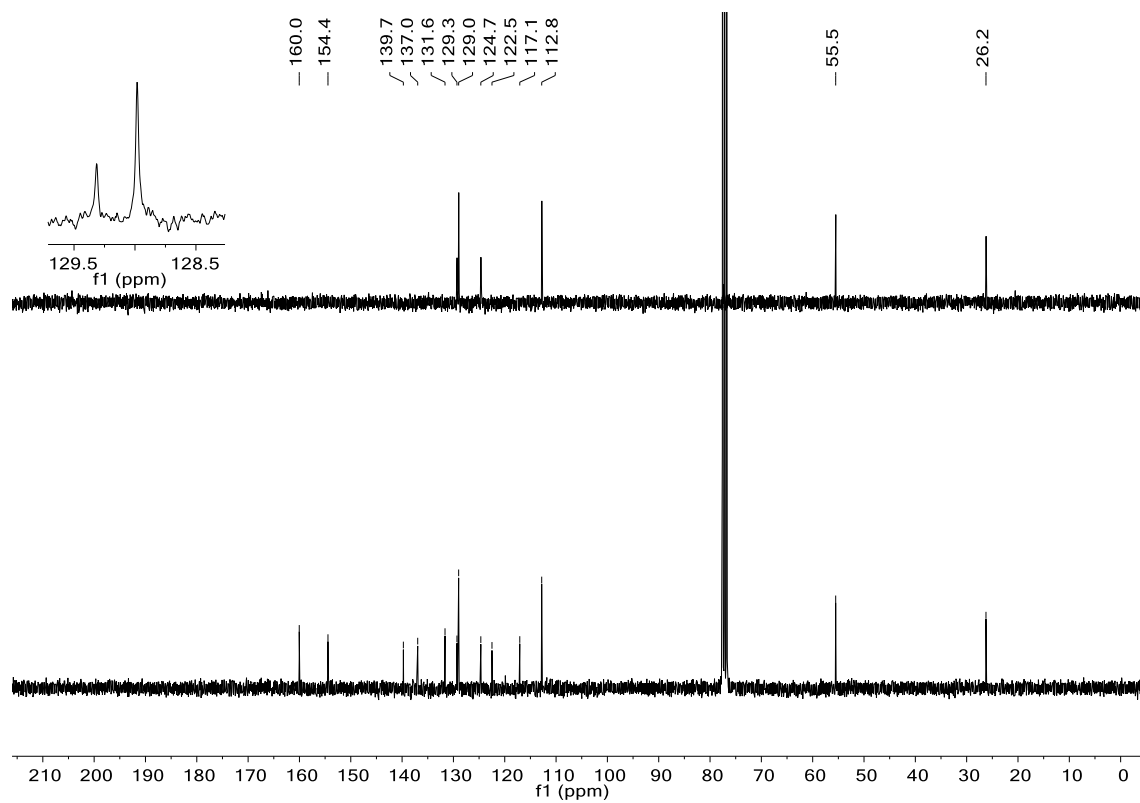
$^{13}\text{C-NMR}$ and DEPT-135



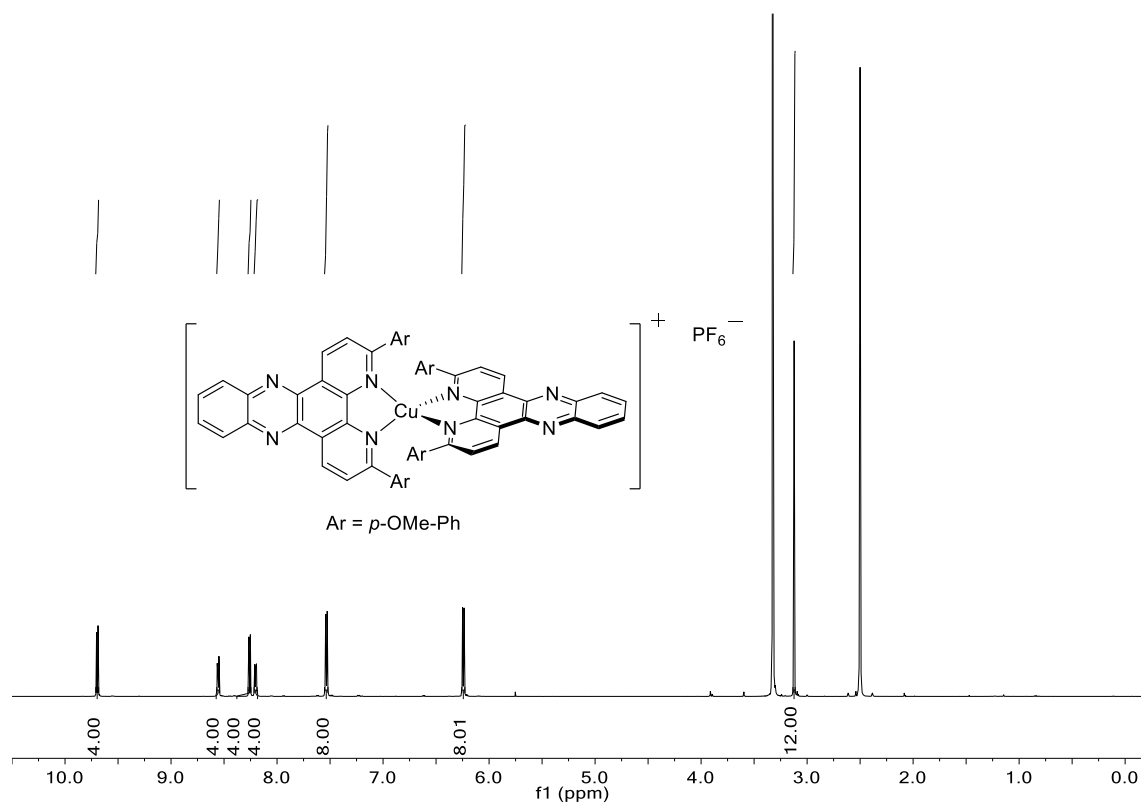
3,6-bis(4-methoxyphenyl)dipyrido[3,2-*a*:2',3'-*c*]phenazine (phenazino-dap, **73**): ^1H -NMR ^{13}C -NMR

HSQC

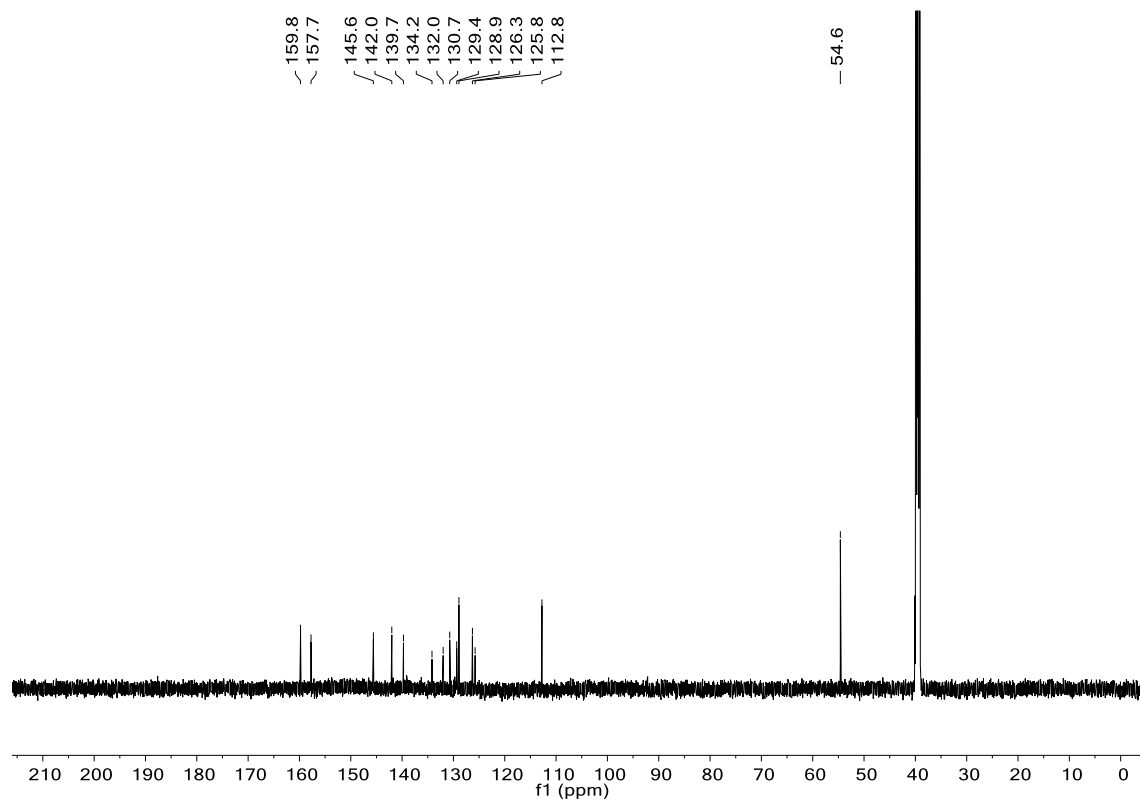


$[\text{Cu}(\text{dapacetal})_2]\text{Cl}$ (**C8-Cl**): ^1H -NMR ^{13}C -NMR

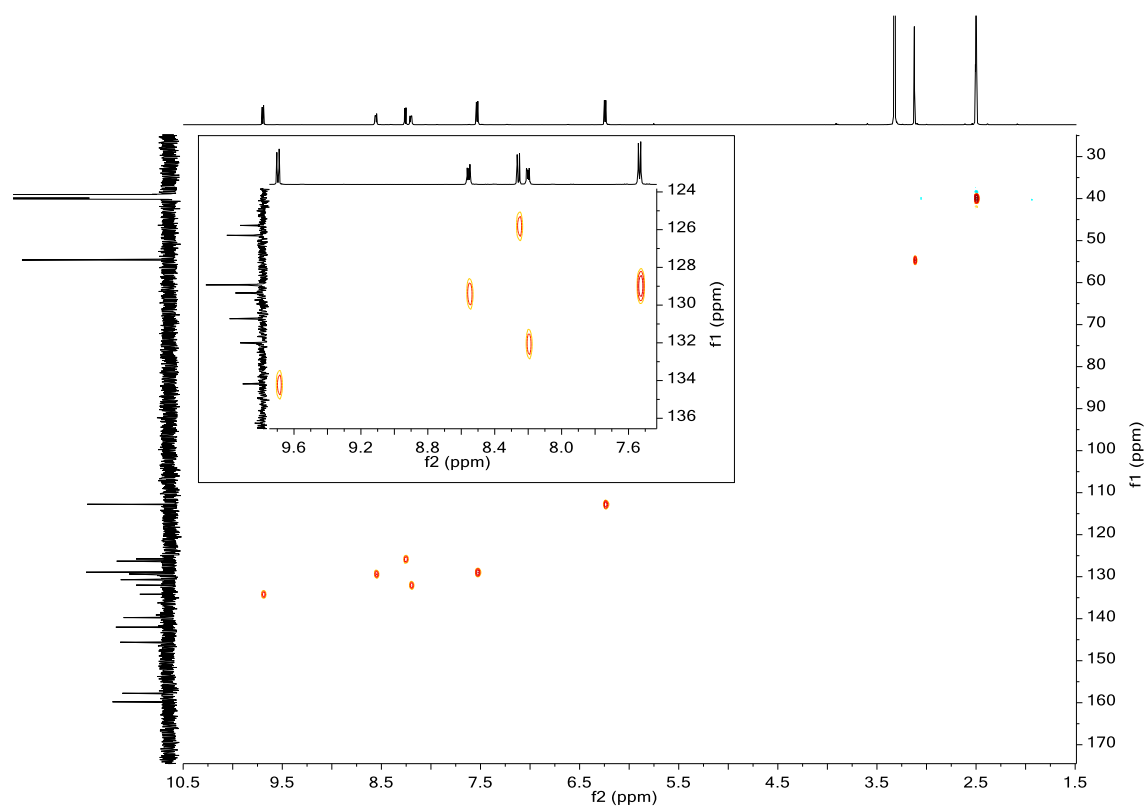
[Cu(phenazino-dap)₂](PF₆) (C9-PF₆): ¹H-NMR



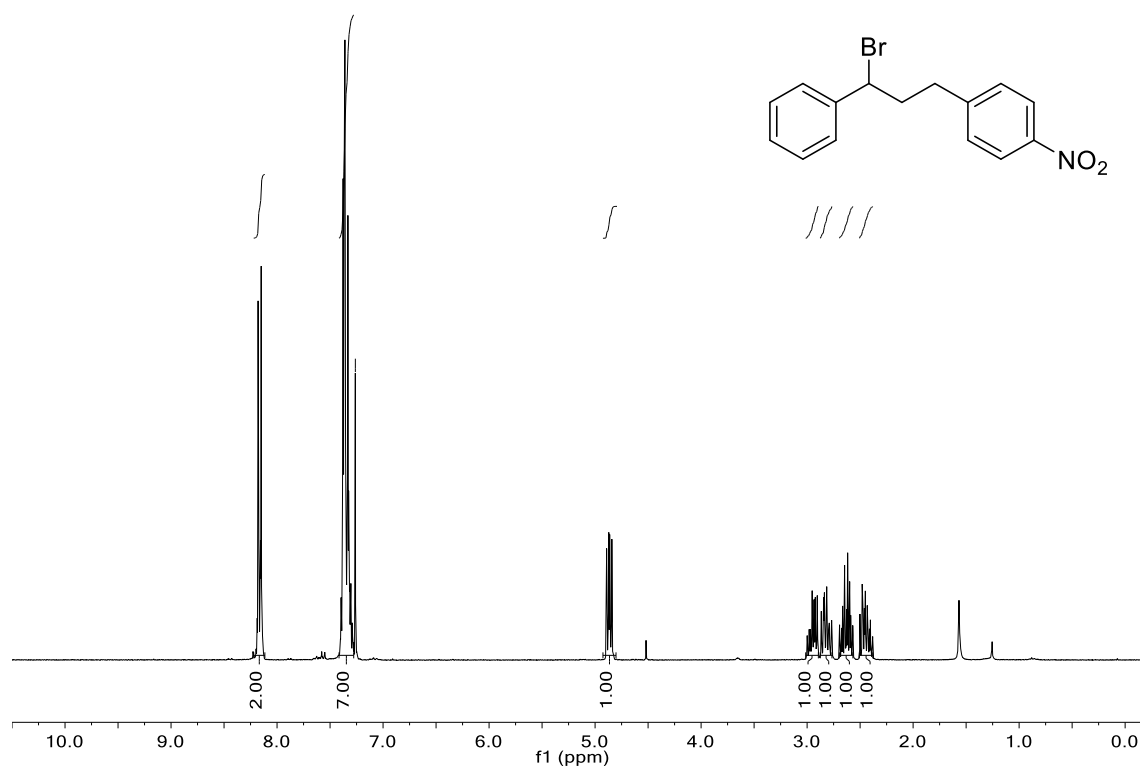
¹³C-NMR



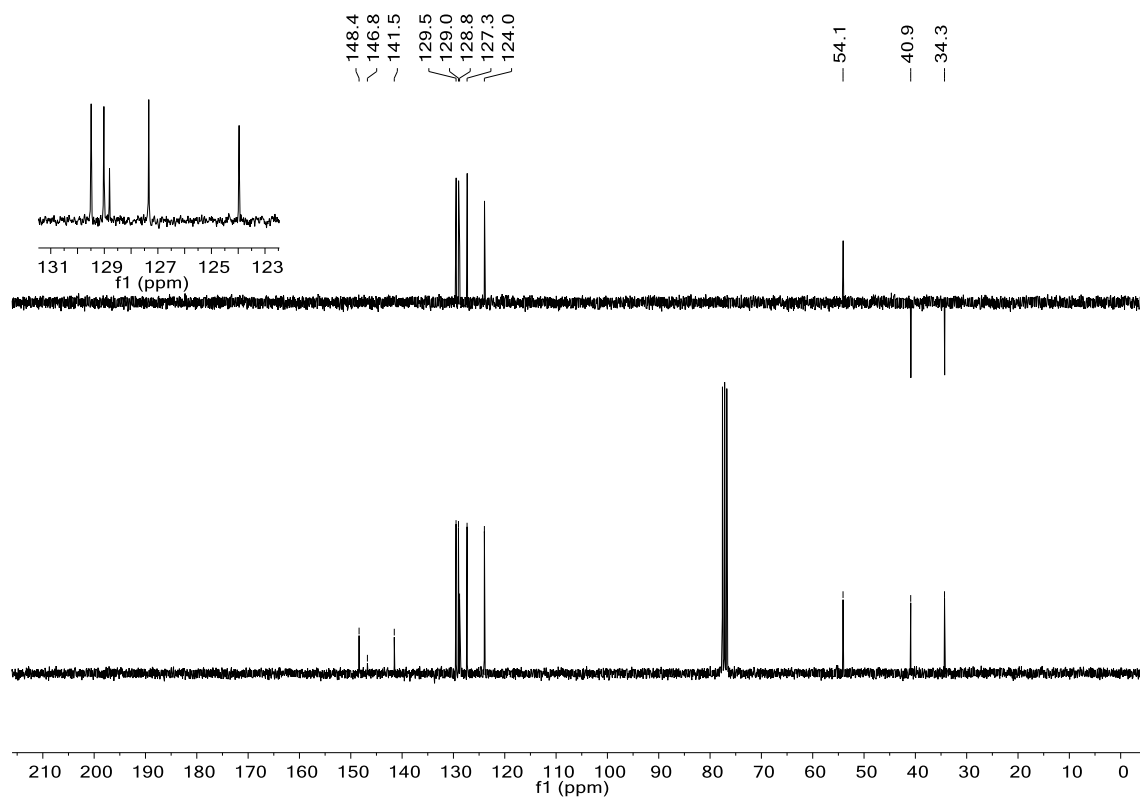
HSQC

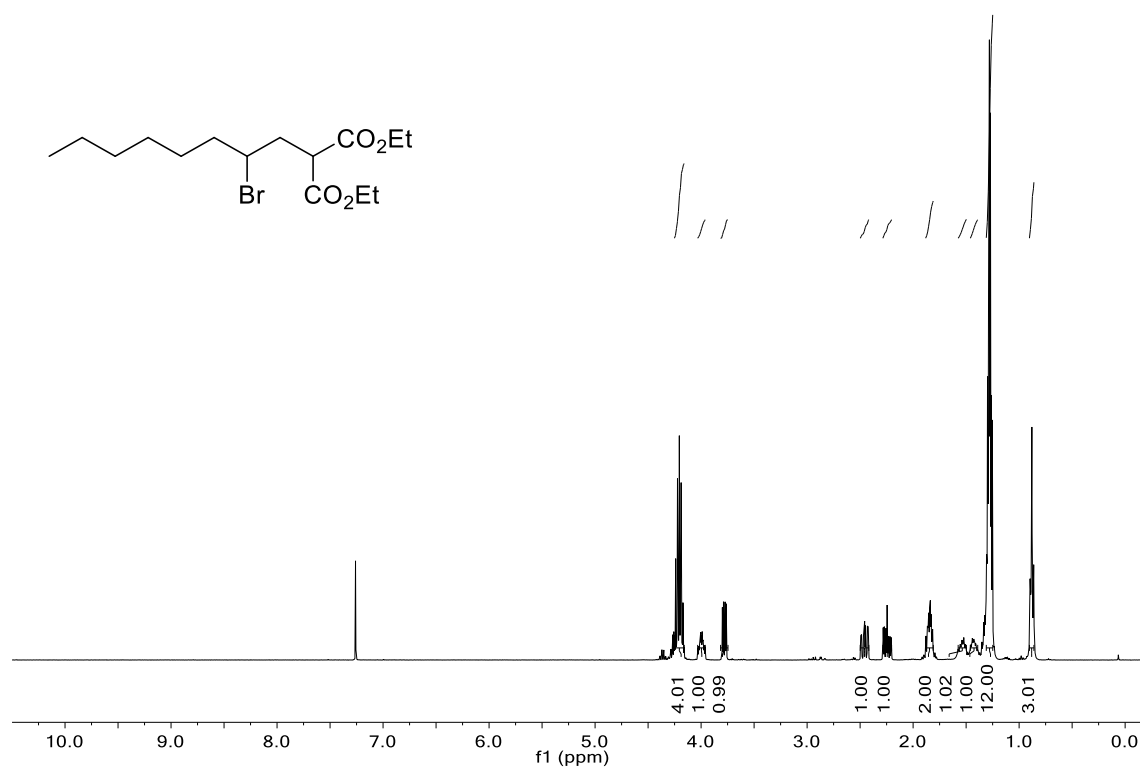
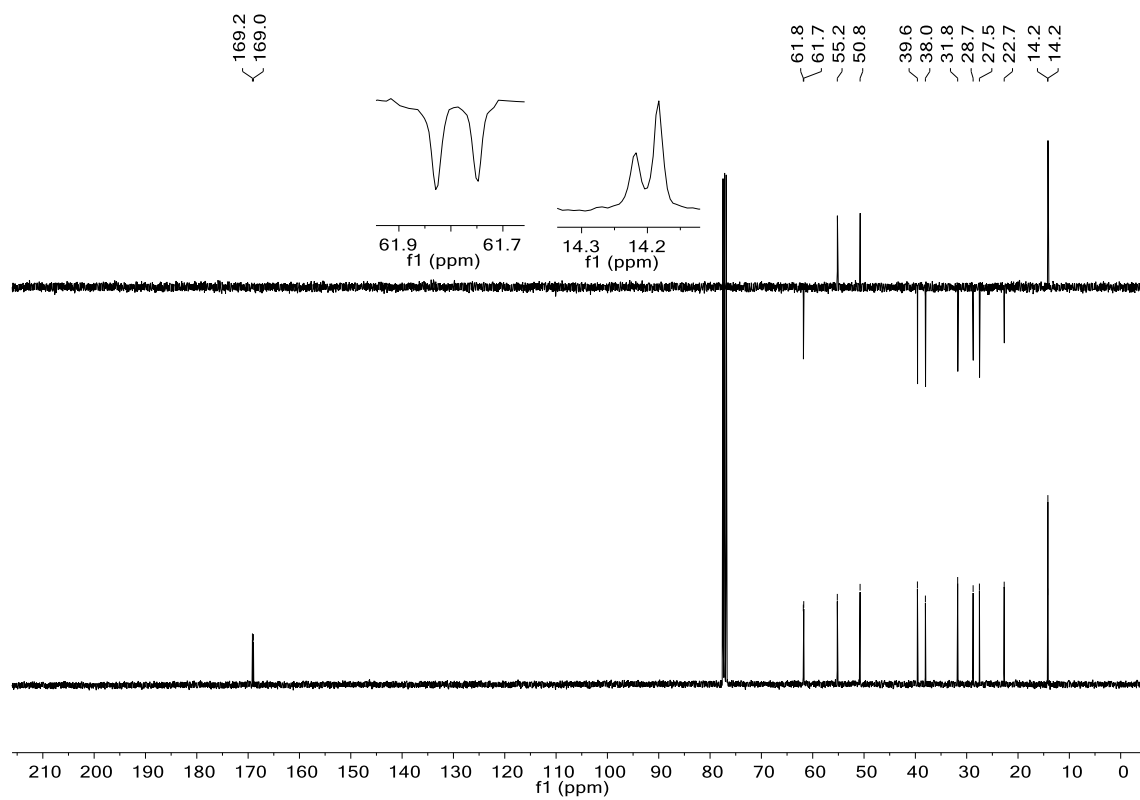


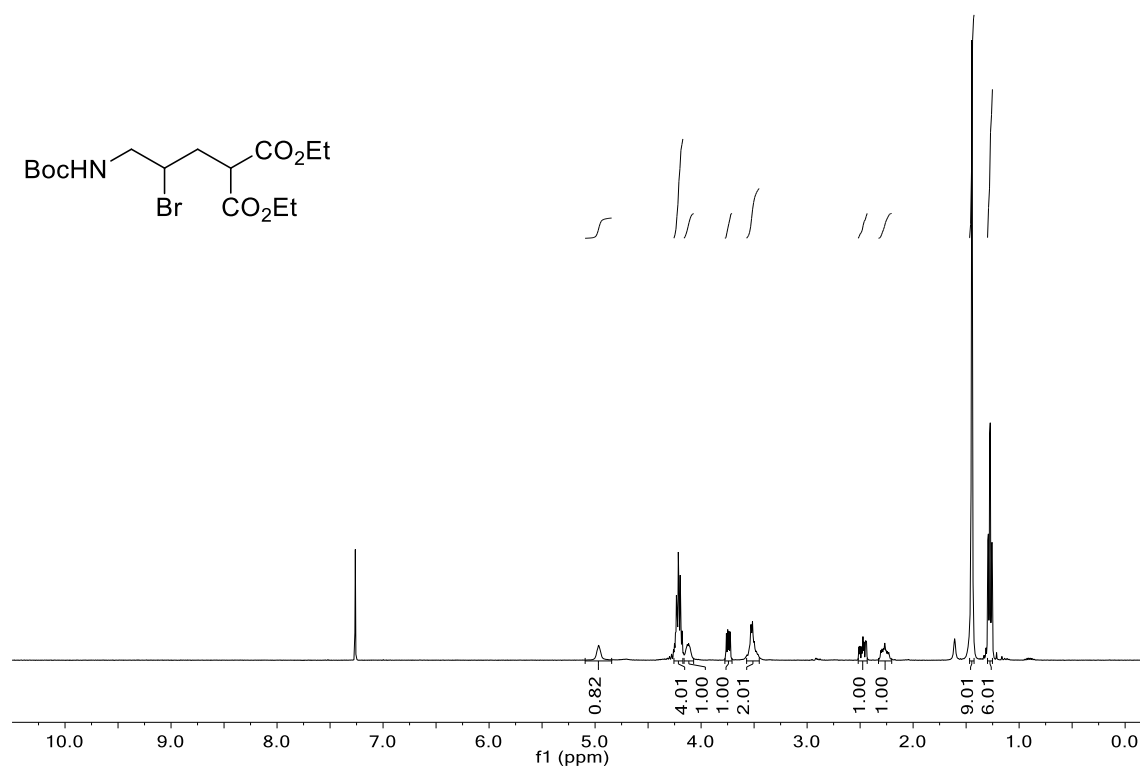
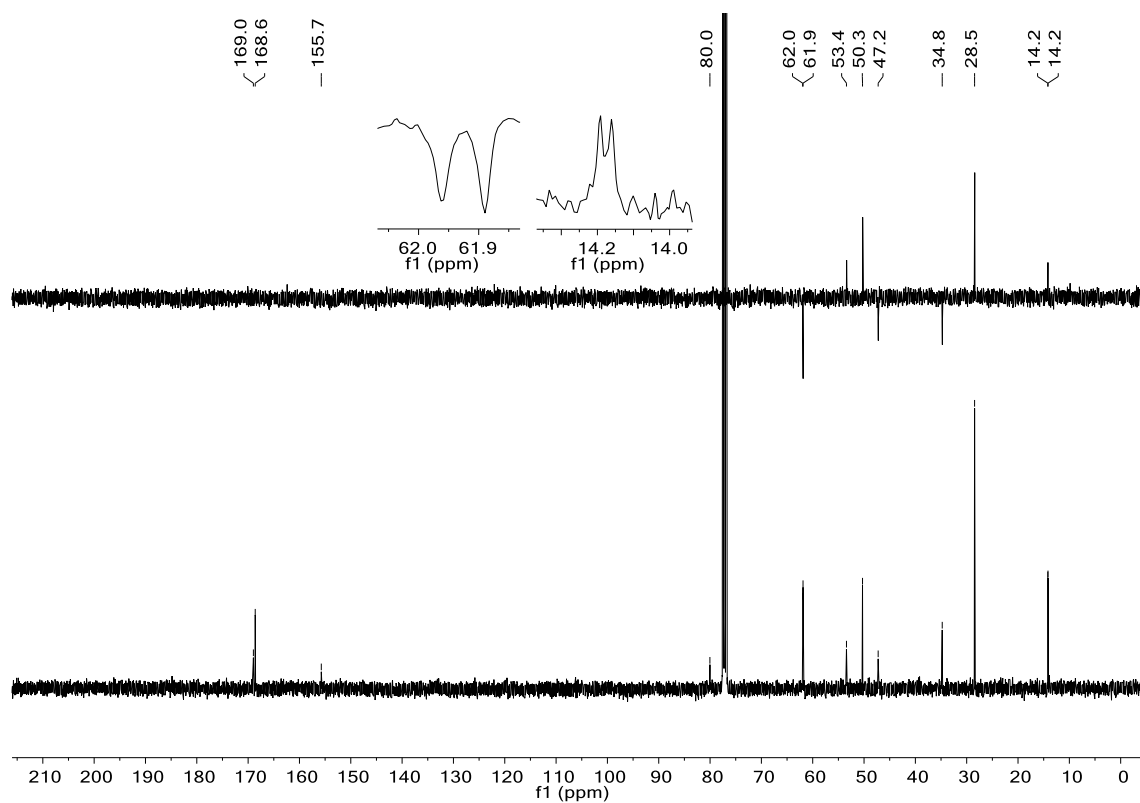
1-(3-bromo-3-phenylpropyl)-4-nitrobenzene (**76**): ^1H -NMR



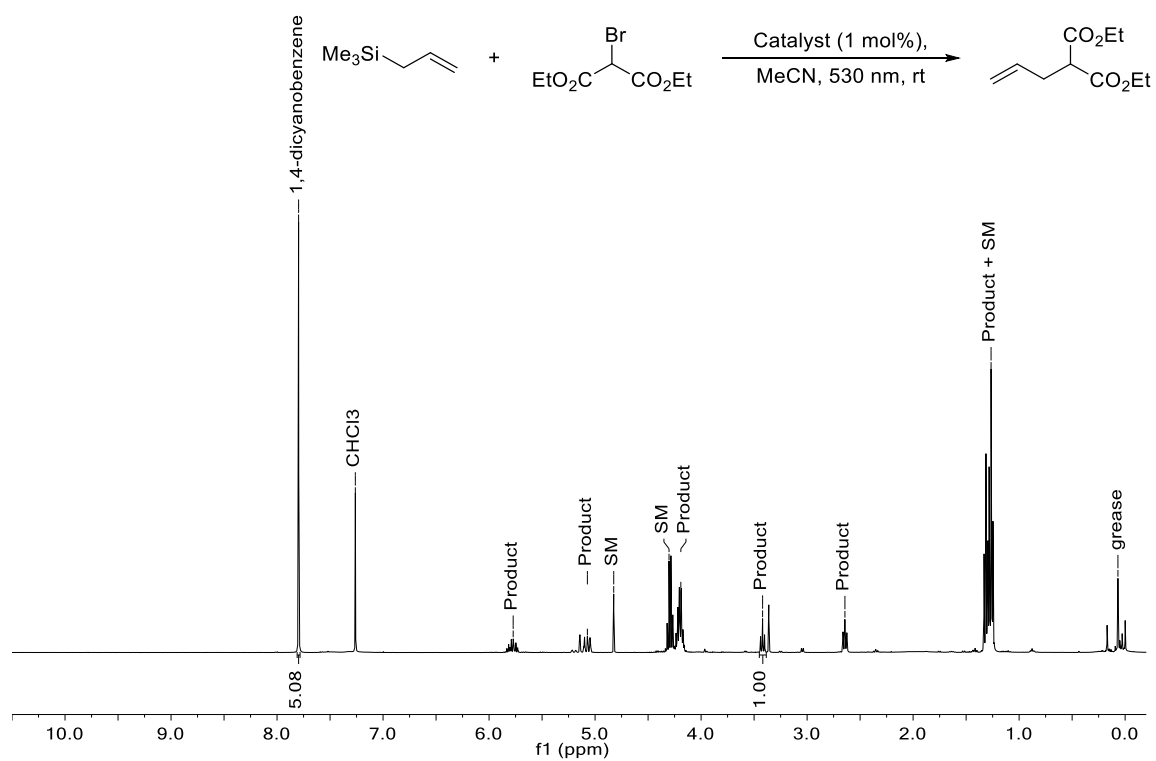
^{13}C -NMR and DEPT-135



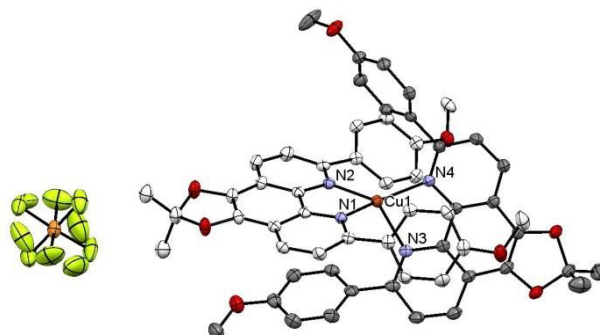
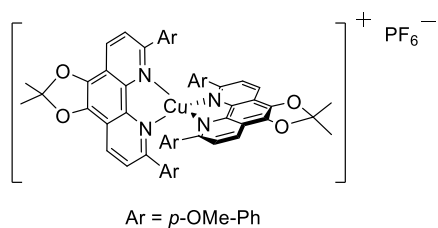
Diethyl 2-(2-bromooctyl)malonate (**79**): ^1H -NMR ^{13}C -NMR and DEPT-135

Diethyl 2-(2-bromo-3-((*tert*-butoxycarbonyl)amino)propyl)malonate (**81**): ^1H -NMR ^{13}C -NMR and DEPT-135

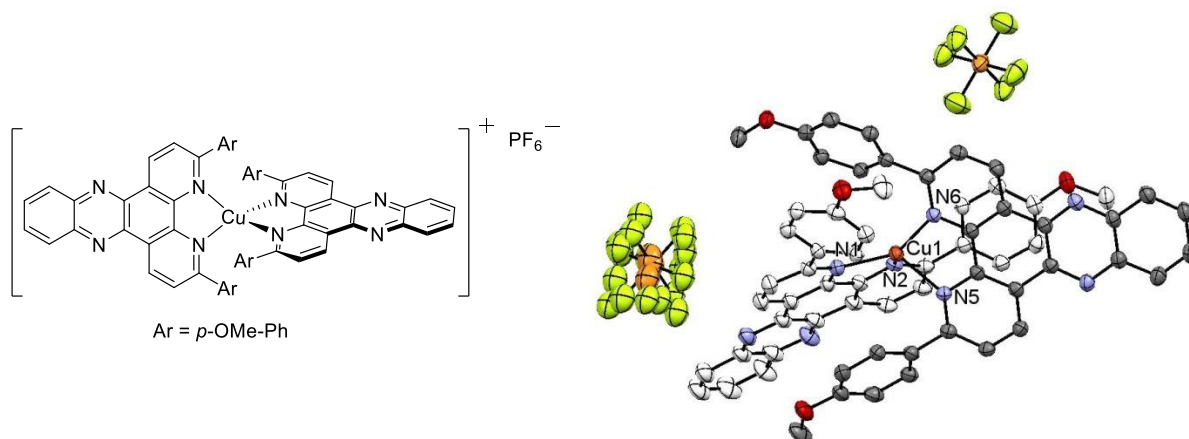
Diethyl 2-allylmalonate (**85**): ^1H -NMR (400 MHz, CDCl_3) – spectrum after filtration, containing 1,4-dicyanobenzene as internal standard



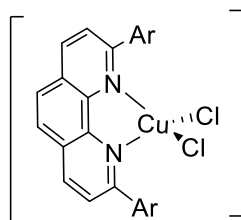
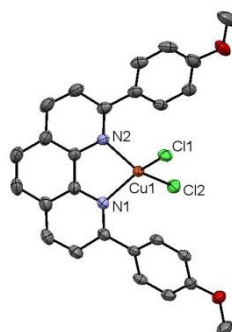
3.4 X-ray

[Cu(dapacetal)₂]⁺PF₆⁻ (**C8-PF₆**)

Formula	C ₅₈ H ₄₈ CuF ₆ N ₄ O ₈ P
$D_{\text{calc.}}/\text{g cm}^{-3}$	1.488
μ/mm^{-1}	1.631
Formula Weight	1137.51
Color	clear red
Shape	needle
Max Size/mm	0.47
Mid Size/mm	0.07
Min Size/mm	0.05
T/K	123.00(14)
Crystal System	orthorhombic
Space Group	Pbca
$a/\text{\AA}$	16.84654(14)
$b/\text{\AA}$	20.23300(16)
$c/\text{\AA}$	29.7937(2)
$\alpha/^\circ$	90
$\beta/^\circ$	90
$\gamma/^\circ$	90
$V/\text{\AA}^3$	10155.38(14)
Z	8
Z'	1
$\theta_{\text{min}}/^\circ$	3.723
$\theta_{\text{max}}/^\circ$	62.963
Measured Refl.	86664
Independent Refl.	8160
Reflections Used	7300
R_{int}	0.0375
Parameters	747
Restraints	104
Largest Peak	0.399
Deepest Hole	-0.364
GooF	1.020
wR_2 (all data)	0.0936
wR_2	0.0900
R_1 (all data)	0.0389
R_1	0.0341

[Cu(phenazino-dap)₂][PF₆] (**C9-PF₆**)

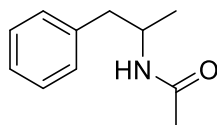
Formula	C ₆₄ H ₄₄ CuF ₆ N ₈ O ₄ P
$D_{\text{calc.}}/\text{g cm}^{-3}$	1.511
μ/mm^{-1}	1.574
Formula Weight	1197.58
Color	red
Shape	plate
Max Size/mm	0.14
Mid Size/mm	0.08
Min Size/mm	0.04
T/K	123.01(10)
Crystal System	triclinic
Space Group	P-1
$a/\text{\AA}$	7.36674(15)
$b/\text{\AA}$	12.3386(2)
$c/\text{\AA}$	29.5439(3)
$\alpha/^\circ$	81.6050(12)
$\beta/^\circ$	86.8755(12)
$\gamma/^\circ$	82.4782(16)
$V/\text{\AA}^3$	2632.05(8)
Z	2
Z'	1
$\Theta_{\text{min}}/^\circ$	3.649
$\Theta_{\text{max}}/^\circ$	73.534
Measured Refl.	27672
Independent Refl.	10260
Reflections Used	8564
R_{int}	0.0270
Parameters	924
Restraints	1215
Largest Peak	1.878
Deepest Hole	-0.594
GooF	1.048
wR_2 (all data)	0.2202
wR_2	0.2073
R_1 (all data)	0.0817
R_1	0.0707

[Cu(dap)Cl₂] (**C10**)Ar = *p*-OMe-Ph

Formula	C ₂₆ H ₂₀ Cl ₂ CuN ₂ O ₂
$D_{calc.}/\text{g cm}^{-3}$	1.512
μ/mm^{-1}	3.673
Formula Weight	526.88
Color	brownish green
Shape	n/a
Size/mm ³	0.11×0.04×0.02
T/K	123
Crystal System	monoclinic
Space Group	P2 ₁ /n
$a/\text{\AA}$	8.18335(13)
$b/\text{\AA}$	18.4690(3)
$c/\text{\AA}$	15.3943(2)
$\alpha/^\circ$	90
$\beta/^\circ$	95.7444(15)
$\gamma/^\circ$	90
$V/\text{\AA}^3$	2314.98(6)
Z	4
Z'	1
Wavelength/ \AA	1.54184
Radiation type	CuK α
$\theta_{min}/^\circ$	3.749
$\theta_{max}/^\circ$	74.034
Measured Refl.	18159
Independent Refl.	4588
Reflections Used	4076
R_{int}	0.0473
Parameters	300
Restraints	0
Largest Peak	0.339
Deepest Hole	-0.623
GooF	1.044
wR_2 (all data)	0.0861
wR_2	0.0827
R_1 (all data)	0.0370
R_1	0.0317

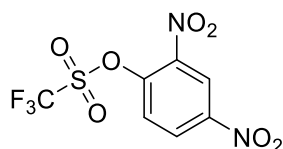
4. Chapter C: Atom Transfer Radical Addition Reactions – Investigation of New Reagents

4.1 Compound Characterization



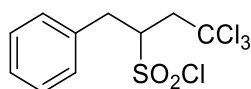
***N*-(1-phenylpropan-2-yl)acetamide (94)**

An oven-dried vial (6 mL size) equipped with a rubber septum and a magnetic stir bar was charged with CuCl (1.0 mg, 10 μ mol, 1 mol%) and anhydrous acetonitrile (2.0 mL). The mixture was degassed using three freeze-pump-thaw cycles. Allylbenzene (132 μ L, 1.0 mmol, 1.0 equiv) and triflic acid (176 μ L, 2.0 mmol, 2.0 equiv) were added under slight nitrogen overpressure. The vial was sealed, the reaction mixture was irradiated at room temperature with a green LED ($\lambda_{\text{max}} = 530$ nm, distance 1 cm) and the reaction progress was monitored by TLC. After 19 h, the mixture was filtered through a plug of Celite using DCM:MeOH 4:1. The resulting mixture was concentrated in vacuo and triethylamine (10 mL) was added. After stirring at rt for 50 min, the mixture was neutralized with diluted HCl and the aqueous phase was extracted with dichloromethane (3 x). The combined organic phases were washed with 2 M HCl (2 x) and brine (1 x), dried over Na₂SO₄, filtered and concentrated in vacuum. Purification by column chromatography on silica gel using mixtures of DCM:MeOH (98:2 and 95:5, $R_f = 0.65$ in DCM:MeOH 9:1) afforded product **94** as a pink oil (91.5 mg, 52%). **IR** (neat, cm⁻¹) 3285, 3067, 3027, 2969, 2928, 2872, 1639, 1548, 1497, 1453, 1372, 1296, 1145, 745, 698, 609. **¹H-NMR** (400 MHz, CDCl₃) δ 7.32 – 7.28 (m, 2H), 7.25 – 7.16 (m, 3H), 5.33 (bs, 1H), 4.33 – 4.19 (m, 1H), 2.84 (dd, $J = 13.5, 5.7$ Hz, 1H), 2.72 (dd, $J = 13.5, 7.1$ Hz, 1H), 1.94 (s, 3H), 1.11 (d, $J = 6.7$ Hz, 3H). **¹³C-NMR** (101 MHz, CDCl₃) δ 169.5, 138.0, 129.6, 128.5, 126.6, 46.2, 42.5, 23.6, 20.1. **MS** (CI (NH₃)) (relative intensities): m/z 178.2 (33) [MH⁺], 195.2 (100) [MNH₄⁺]. The data are in accordance with the data reported in the literature.^[136]



2,4-dinitrophenyl trifluoromethanesulfonate (**103**)^[140]

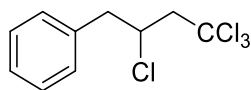
A flame-dried Schlenk flask equipped with a rubber septum was charged with 2,4-dinitrophenol (5.14 g, 27.9 mmol, 1.0 equiv), anhydrous dichloromethane (85 mL) and anhydrous pyridine (3.4 mL, 41.9 mmol, 1.5 equiv). After the mixture was cooled to 0 °C with an ice bath, trifluoromethanesulfonic anhydride (5.6 mL, 33.5 mmol, 1.2 equiv) was added dropwise to the stirred solution. The resulting mixture was warmed to room temperature and stirred for additional 20 h. Using mixtures of hexanes:EtOAc, the reaction mixture was filtered through a pad of silica and the solvent was removed under reduced pressure. Purification by column chromatography on silica gel using mixtures of hexanes:EtOAc (9:1 to 1:1, R_f = 0.40 in hexanes:EtOAc 4:1) afforded product **103** as a yellow solid (2.63 mg, 30%). **IR** (neat, cm^{-1}) 3116, 2889, 1610, 1543, 1480, 1435, 1342, 1211, 1129, 1066, 924, 865, 834, 738. **¹H-NMR** (300 MHz, CDCl_3) δ 9.04 (d, J = 2.8 Hz, 1H), 8.62 (dd, J = 9.0, 2.8 Hz, 1H), 7.72 (d, J = 9.0 Hz, 1H). **¹³C-NMR** (75 MHz, CDCl_3) δ 146.7, 145.3, 141.8, 129.8, 125.9, 122.6, 118.6 (q, J = 321.1 Hz). **¹⁹F-NMR** (282 MHz, CDCl_3) δ 73.0. **HRMS** (ESI): m/z calculated for $\text{C}_7\text{H}_3\text{F}_3\text{N}_2\text{O}_7\text{S}$ [M^+]: 315.96076, found: 315.96121. **mp**: 53 – 54 °C. The data are in accordance with the data reported in the literature.^[177]



4,4,4-trichloro-1-phenylbutane-2-sulfonyl chloride (**112**)

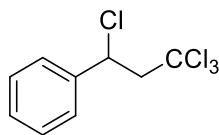
An oven-dried pressure tube (6 mL size) equipped with a magnetic stir bar was charged with $[\text{Cu}(\text{dap})_2]\text{Cl}$ (**C1-Cl**) (13.3 mg, 0.015 mmol, 1 mol%), K_2HPO_4 (523 mg, 3.00 mmol, 2.0 equiv) and anhydrous dichloromethane (1.5 mL). The mixture was degassed using two freeze-pump-thaw cycles. Allylbenzene (200 μL , 1.50 mmol, 1.0 equiv) was added and the reaction mixture was degassed by one freeze-pump-thaw cycle. Trichloromethanesulfonyl chloride (**111**) (1.31 g, 6.00 mmol, 4.0 equiv) was added under slight nitrogen overpressure, the tube was equipped with a light emitting LED-stick and sealed. The reaction mixture was irradiated at room temperature with a green LED (λ_{max} = 530 nm) while being stirred and the reaction progress was monitored by TLC. After 24 h, the reaction was stopped by switching off the light source. Water (20 mL) was added and the aqueous phase was extracted with dichloromethane (3 x 25 mL). The combined organic phases were dried over Na_2SO_4 , filtered

and concentrated. Purification by column chromatography on silica gel using mixtures of pentane:Et₂O (99:1 to 98:2, *R_f* = 0.57 in pentane:Et₂O 95:5) afforded the main product **112** as a white solid (332 mg, 66%). **IR** (neat, cm⁻¹) 3071, 3038, 2974, 2940, 2863, 1603, 1491, 1454, 1424, 1368, 1348, 1159, 1081, 1029, 932, 798, 753, 697. **¹H-NMR** (300 MHz, CDCl₃) δ 7.41 – 7.27 (m, 5H), 4.25 (qd, *J* = 6.3, 2.1 Hz, 1H), 3.67 (dd, *J* = 15.8, 2.1 Hz, 1H), 3.61 (d, *J* = 6.1 Hz, 2H), 3.24 (dd, *J* = 15.8, 6.6 Hz, 1H). **¹³C-NMR** (101 MHz, CDCl₃) δ 134.8, 129.8, 129.0, 128.0, 96.0, 74.5, 53.2, 37.7. **HRMS** (ESI): *m/z* calculated for C₁₀H₁₀Cl₄O₂S [M⁺]: 333.91501, found 333.91523. **mp**: 46 °C.

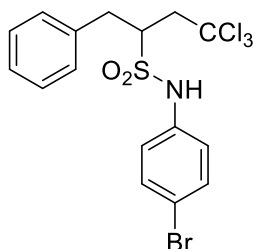


(2,4,4,4-tetrachlorobutyl)benzene (**113**)

An oven-dried pressure tube (6 mL size) equipped with a magnetic stir bar was charged with [Ru(bpy)₃]Cl₂ • 6H₂O (3.7 mg, 0.005 mmol, 1 mol%), K₂HPO₄ (174 mg, 1.00 mmol, 2.0 equiv) and anhydrous dichloromethane (0.5 mL). The mixture was degassed using two freeze-pump-thaw cycles. Allylbenzene (66 μL, 0.50 mmol, 1.0 equiv) was added and the reaction mixture was degassed by one freeze-pump-thaw cycle. Trichloromethanesulfonyl chloride (**111**) (436 mg, 2.00 mmol, 4.0 equiv) was added under slight nitrogen overpressure, the tube was equipped with a light emitting LED-stick and sealed. The reaction mixture was irradiated at room temperature with a blue LED (*λ*_{max} = 455 nm) while being stirred and the reaction progress was monitored by TLC. After 24 h, the reaction was stopped by switching off the light source and reaction mixture was diluted to 5.00 mL with DCM. For determining the yield by NMR, a sample of 0.50 mL was taken and 2-nitropropane was added as an internal standard. Water (20 mL) was added to the remaining 4.50 mL of the crude reaction mixture and the aqueous phase was extracted with dichloromethane (3 x 10 mL). The combined organic phases were dried over Na₂SO₄, filtered and concentrated. Purification by column chromatography on silica gel using mixtures of pentane:Et₂O (99:1 to 98:2, *R_f* = 0.75 in pentane:Et₂O 95:5) afforded the main product **113** as a white solid (104.3 mg, 86%). **¹H-NMR** (300 MHz, CDCl₃) δ 7.38 – 7.27 (m, 4H), 7.26 – 7.23 (m, 1H), 4.48 (ddt, *J* = 8.1, 5.9, 4.3 Hz, 1H), 3.31 – 3.22 (m, 3H), 3.14 (dd, *J* = 14.2, 8.0 Hz, 1H). **¹³C-NMR** (75 MHz, CDCl₃) δ 136.7, 129.7, 128.8, 127.4, 96.9, 61.2, 57.8, 45.4. **MS** (EI) (relative intensities): *m/z* 272.0 (8) [M⁺], 91.1 (100) [C₇H₇⁺]. The data are in accordance with the data reported in the literature.^[178]

**(1,3,3,3-tetrachloropropyl)benzene (114)**

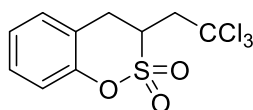
An oven-dried pressure tube (6 mL size) equipped with a magnetic stir bar was charged with $[\text{Cu}(\text{dap})_2]\text{Cl}$ (**C1-Cl**) (4.4 mg, 0.005 mmol, 1 mol%), K_2HPO_4 (174 mg, 1.00 mmol, 2.0 equiv) and anhydrous dichloromethane (0.5 mL). The mixture was degassed using two freeze-pump-thaw cycles. Distilled styrene (57 μL , 0.50 mmol, 1.0 equiv) was added and the reaction mixture was degassed by one freeze-pump-thaw cycle. Trichloromethanesulfonyl chloride (**111**) (436 mg, 2.00 mmol, 4.0 equiv) was added under slight nitrogen overpressure and the tube was equipped with a light emitting LED-stick and sealed. The reaction mixture was irradiated at room temperature with a green LED ($\lambda_{\text{max}} = 530 \text{ nm}$) while being stirred. After 24 h, the reaction was stopped by switching off the light source and the reaction mixture was diluted to 5.00 mL with DCM. For NMR-analysis, a sample of 0.50 mL was taken. Water (20 mL) was added to the remaining 4.50 mL of the crude reaction mixture and the aqueous phase was extracted with dichloromethane (3 x 10 mL). The combined organic phases were dried over Na_2SO_4 , filtered and concentrated. Purification by column chromatography on silica gel using pentane: Et_2O ($R_f = 0.70$ in pentane: Et_2O 95:5) afforded **114** as a colorless oil (100.5 mg, 87%). **IR** (neat, cm^{-1}) 3034, 3068, 2967, 2935, 1603, 1495, 1454, 1424, 1200, 1063, 1021, 969, 854, 824, 760, 693. **$^1\text{H-NMR}$** (400 MHz, CDCl_3) δ 7.47 – 7.33 (m, 5H), 5.32 (t, $J = 5.9 \text{ Hz}$, 1H), 3.64 (dd, $J = 15.3, 5.4 \text{ Hz}$, 1H), 3.55 (dd, $J = 15.3, 6.4 \text{ Hz}$, 1H). **$^{13}\text{C-NMR}$** (101 MHz, CDCl_3) δ 140.5, 129.0, 127.5, 96.3, 62.8, 58.4. The data are in accordance with the data reported in the literature.^[179]

***N*-(4-bromophenyl)-4,4,4-trichloro-1-phenylbutane-2-sulfonamide (116)**

4,4,4-trichloro-1-phenylbutane-2-sulfonyl chloride (**112**) (84.0 mg, 0.25 mmol, 1.0 equiv) and triethylamine (49 μL , 0.35 mmol, 1.4 equiv) were dissolved in dichloromethane (2.5 mL) in a round-bottom flask and cooled to 0 $^{\circ}\text{C}$. After adding 4-bromoaniline (60.2 mg, 0.35 mmol, 1.4 equiv), the reaction mixture was stirred at room temperature for 19 h. The reaction

mixture was quenched with HCl (2.5 mL, 2 M) and extracted with dichloromethane (3 x 5 mL). The combined organic phases were washed with saturated NaHCO₃ solution (1 x 10 mL) followed by brine (1 x 10 mL), dried over Na₂SO₄, filtered and concentrated in vacuum. Purification by column chromatography on silica gel using mixtures of hexanes:EtOAc (5:1 to 1:1, R_f = 0.53 in hexanes:EtOAc 5:1) afforded the desired product as a light yellow solid (63.0 mg, 54%). **IR** (neat, cm⁻¹) 3288, 3079, 3038, 2986, 2926, 2856, 1588, 1487, 1461, 1387, 1323, 1219, 1152, 928, 828, 798, 745, 701. **¹H-NMR** (400 MHz, CDCl₃) δ 7.43 – 7.29 (m, 5H), 7.26 – 7.24 (m, 2H), 6.44 – 6.33 (m, 2H), 5.29 (s, 1H), 3.75 – 3.68 (m, 2H), 3.63 (dd, *J* = 14.7, 3.0 Hz, 1H), 3.34 (dd, *J* = 14.7, 10.7 Hz, 1H), 3.00 (dd, *J* = 15.7, 7.1 Hz, 1H). **¹³C-NMR** (101 MHz, CDCl₃) δ 137.5, 135.1, 132.3, 129.7, 129.3, 128.0, 121.1, 118.1, 97.8, 61.2, 53.2, 38.3. **HRMS** (ESI): *m/z* calculated for C₁₆H₁₆BrCl₃NO₂S [MH⁺]: 469.9145, found 469.9137. **mp**: 153 - 155 °C.

Suitable crystals for X-ray structure analysis of *N*-(4-bromophenyl)-4,4,4-trichloro-1-phenylbutane-2-sulfonamide (**116**) were obtained by liquid diffusion of diethyl ether into a dichloromethane solution.

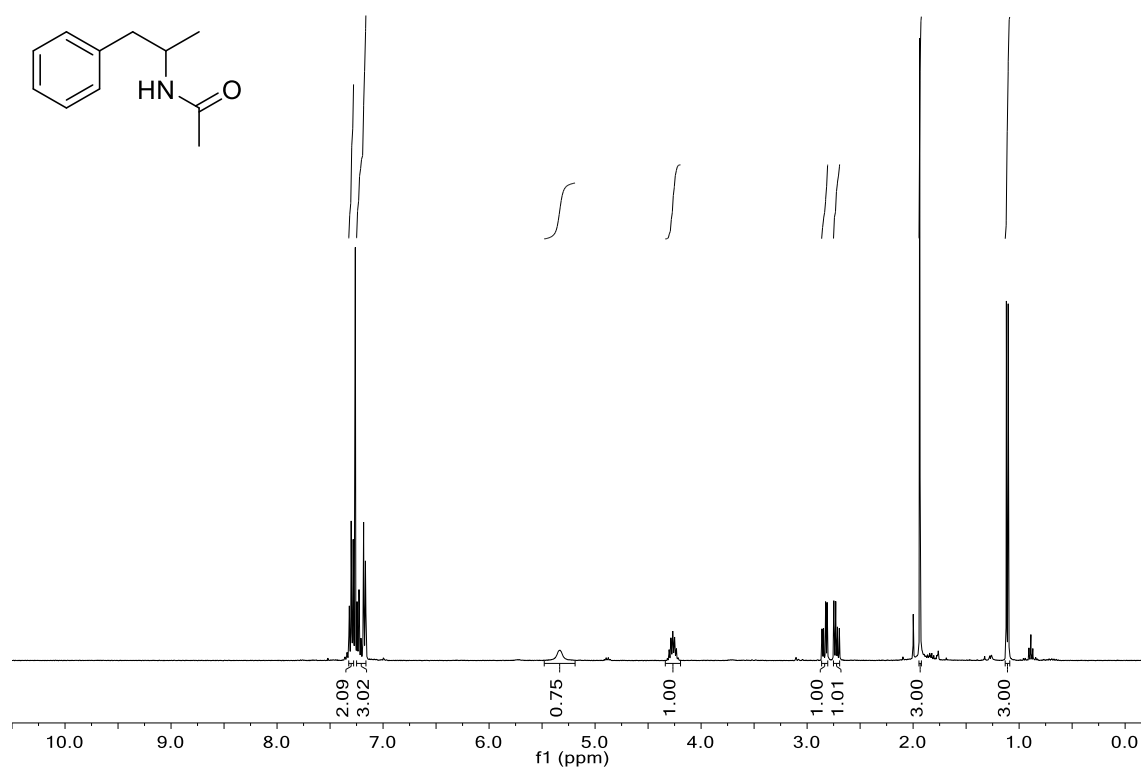
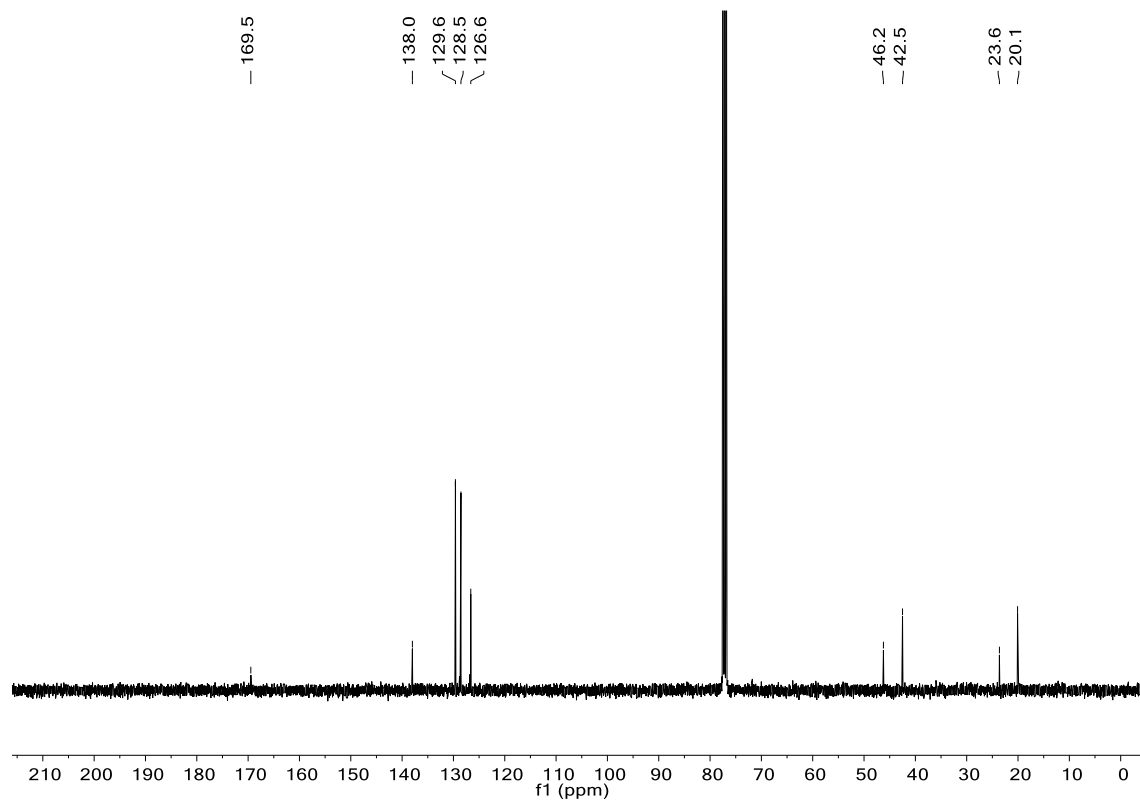


3-(2,2,2-trichloroethyl)-3,4-dihydrobenzo[e][1,2]oxathiine 2,2-dioxide (**118**)

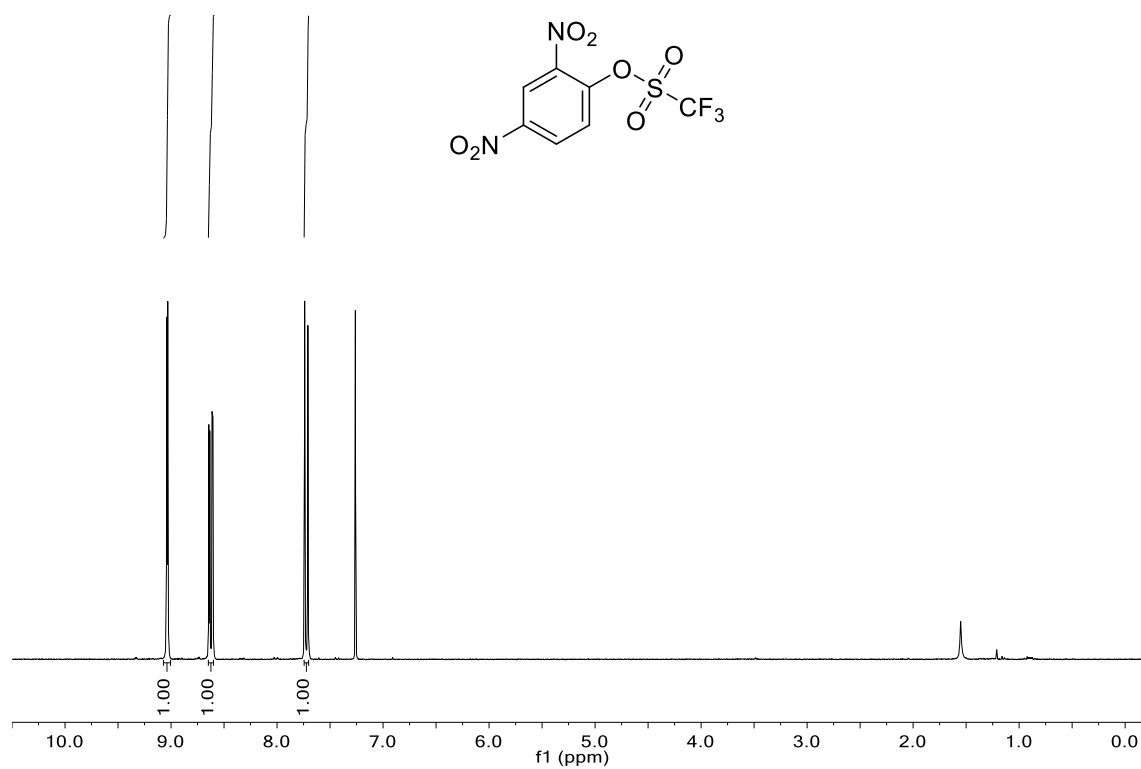
An oven-dried pressure tube (6 mL size) equipped with a magnetic stir bar was charged with allylbenzene (66 μL, 0.50 mmol, 1.0 equiv), [Cu(dap)₂]Cl (**C1-Cl**) (4.4 mg, 0.005 mmol, 1 mol%), K₂HPO₄ (174 mg, 1.00 mmol, 2.0 equiv) and anhydrous dichloromethane (0.5 mL). The mixture was degassed using two freeze-pump-thaw cycles. Trichloromethanesulfonyl chloride (**111**) (436 mg, 2.00 mmol, 4.0 equiv) was added under slight nitrogen overpressure and the reaction mixture was degassed by one freeze-pump-thaw cycle. The tube was equipped with a light emitting LED-stick and sealed. The reaction mixture was irradiated at room temperature with a green LED (λ_{max} = 530 nm) while being stirred and the reaction progress was monitored by TLC. After 3 d, the reaction was stopped by switching off the light source. Water (5 mL) was added and the aqueous phase was extracted with dichloromethane (3 x 10 mL). The combined organic phases were dried over Na₂SO₄, filtered and concentrated. Purification by column chromatography on silica gel using mixtures of pentane:DCM (R_f = 0.72 in pentane:DCM 1:1) afforded product **118** as a white solid (50.0 mg, 32%). **IR** (neat, cm⁻¹) 3067, 2974, 2934, 1584, 1487, 1453, 1431, 1361 (vs), 1238, 1182, 1155, 1100, 962, 890, 813, 753. **¹H-NMR** (300 MHz, CDCl₃) δ 7.37 – 7.29 (m, 1H),

7.25 – 7.18 (m, 2H), 7.12 – 7.01 (m, 1H), 3.99 (ddt, $J = 7.5, 5.3, 2.1$ Hz, 1H), 3.88 (dd, $J = 16.9, 5.3$ Hz, 1H), 3.69 – 3.55 (m, 2H), 3.01 (dd, $J = 15.3, 7.6$ Hz, 1H). **^{13}C -NMR** (101 MHz, CDCl_3) δ 151.1, 129.9, 129.1, 125.9, 119.5, 118.9, 96.3, 53.8, 52.0, 33.7. **HRMS** (EI): m/z calculated for $\text{C}_{10}\text{H}_9\text{Cl}_3\text{O}_3\text{S}$ [M^+]: 313.93325, found 313.93384. **mp**: 111 °C.

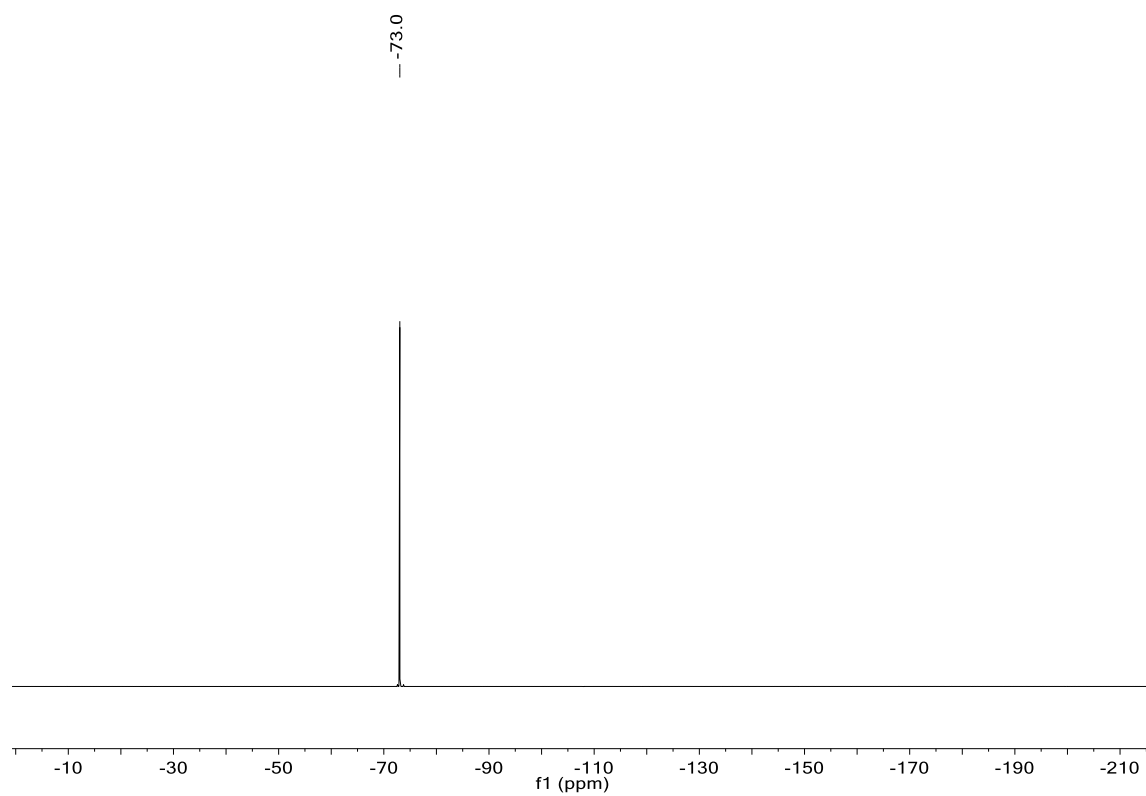
4.2 NMR Spectra

N-(1-phenylpropan-2-yl)acetamide (**94**): ^1H -NMR ^{13}C -NMR

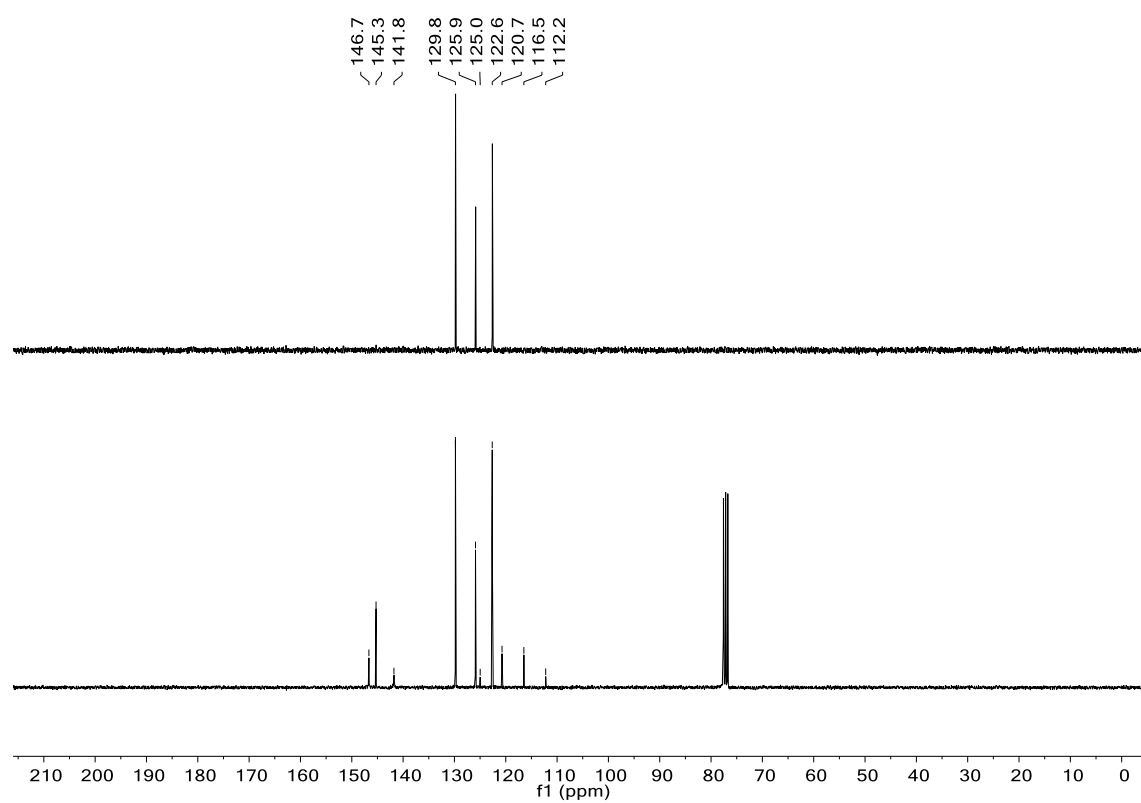
2,4-dinitrophenyl trifluoromethanesulfonate (**103**): ^1H -NMR



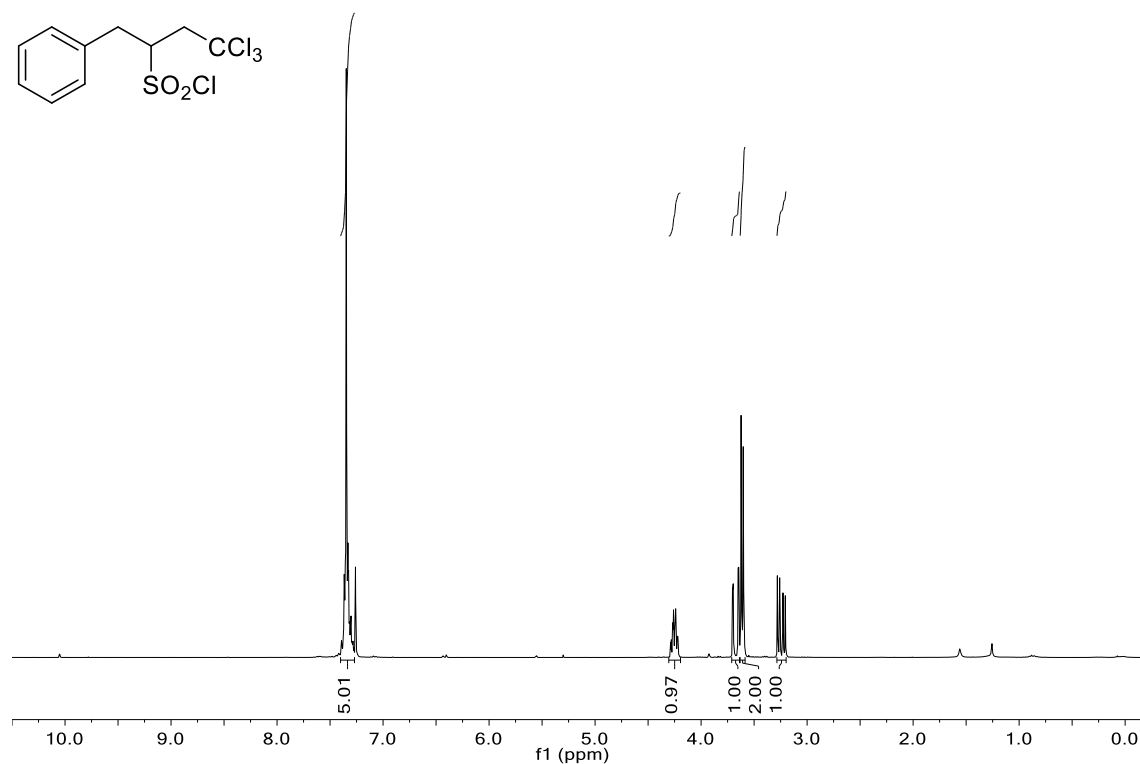
^{19}F -NMR



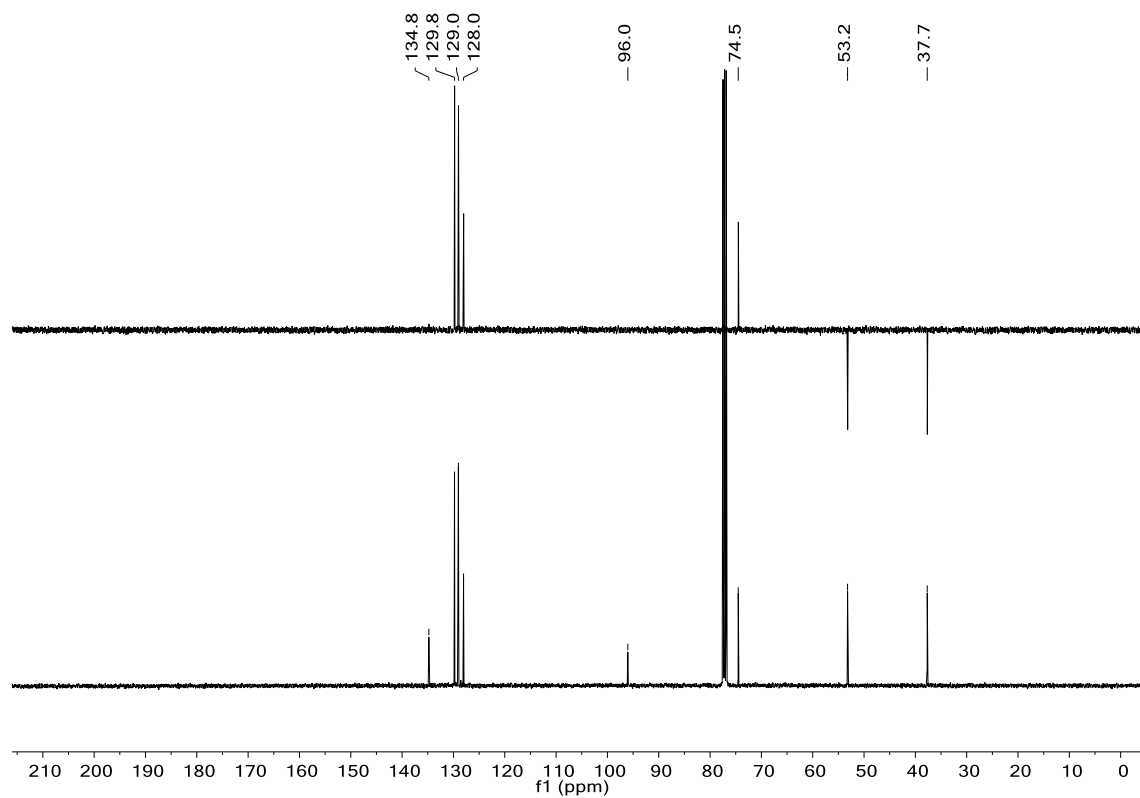
^{13}C -NMR and DEPT-135



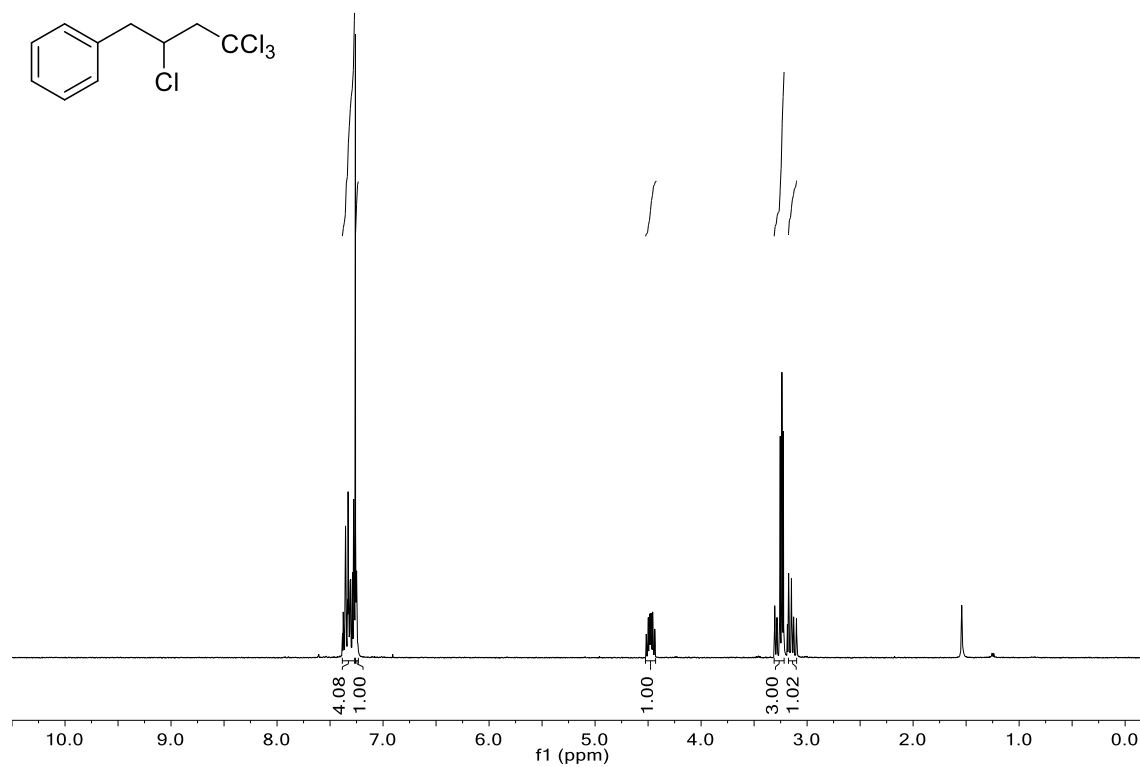
4,4,4-trichloro-1-phenylbutane-2-sulfonyl chloride (**112**): ^1H -NMR



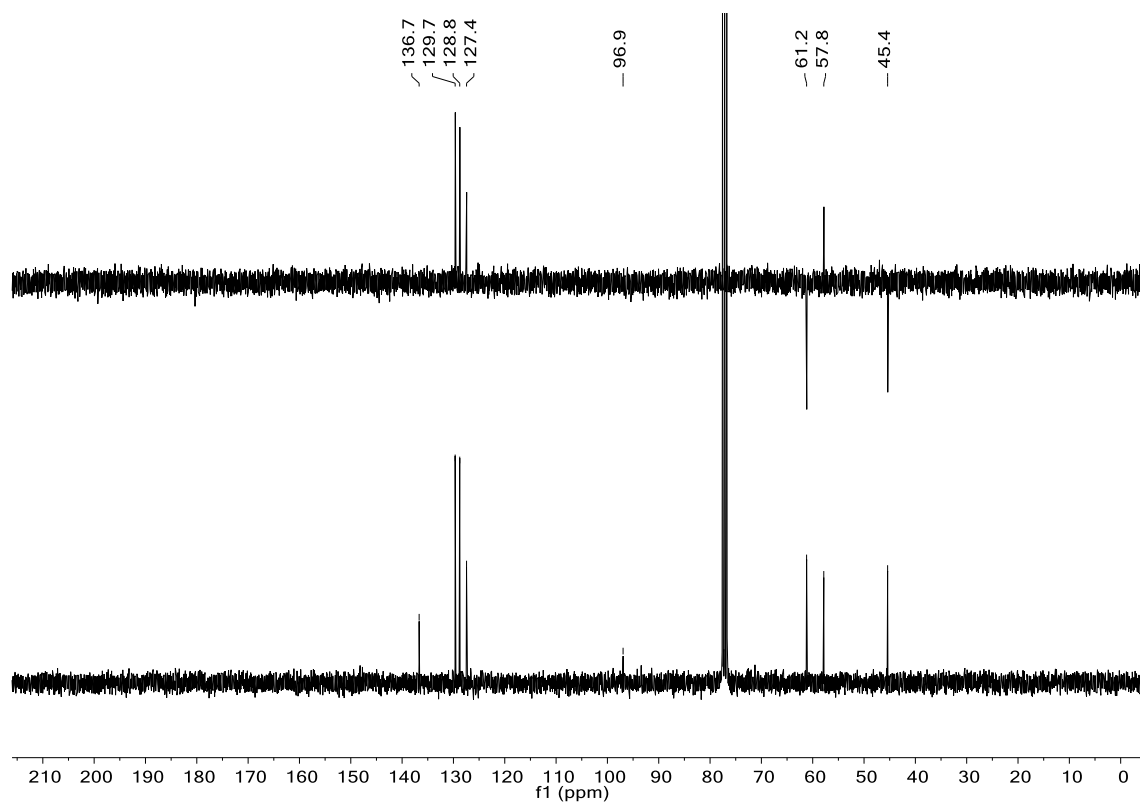
^{13}C -NMR and DEPT-135



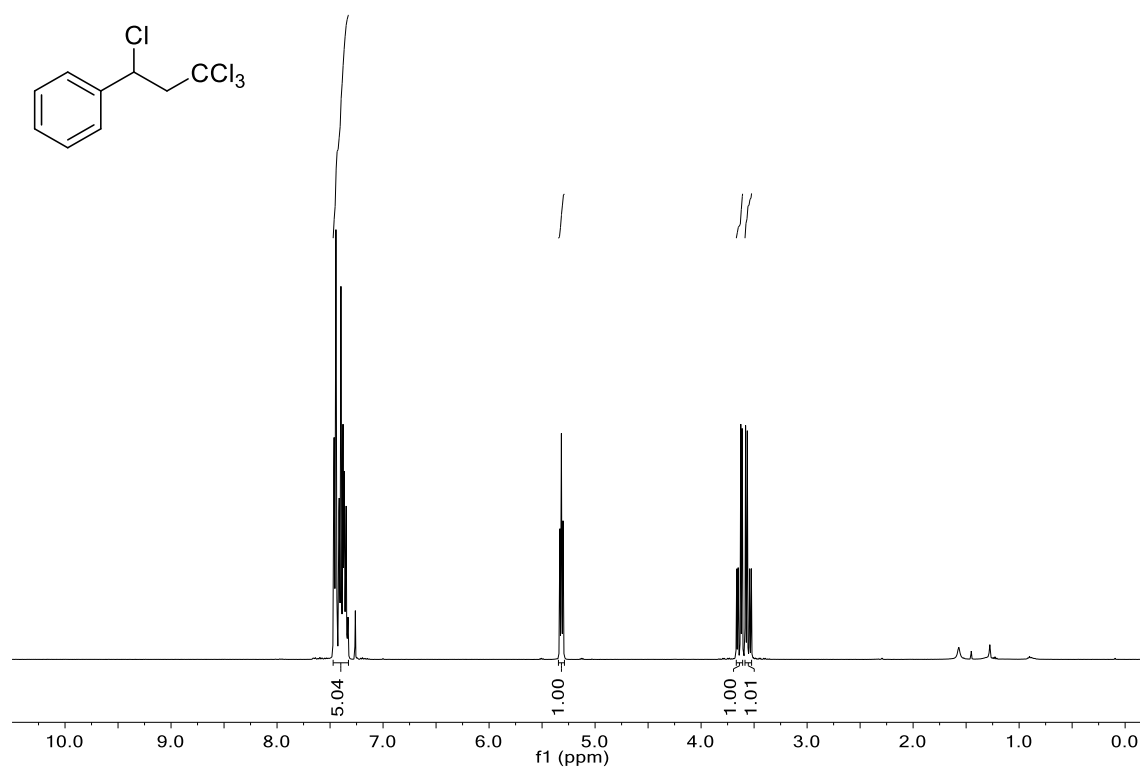
(2,4,4,4-tetrachlorobutyl)benzene (**113**): ^1H -NMR



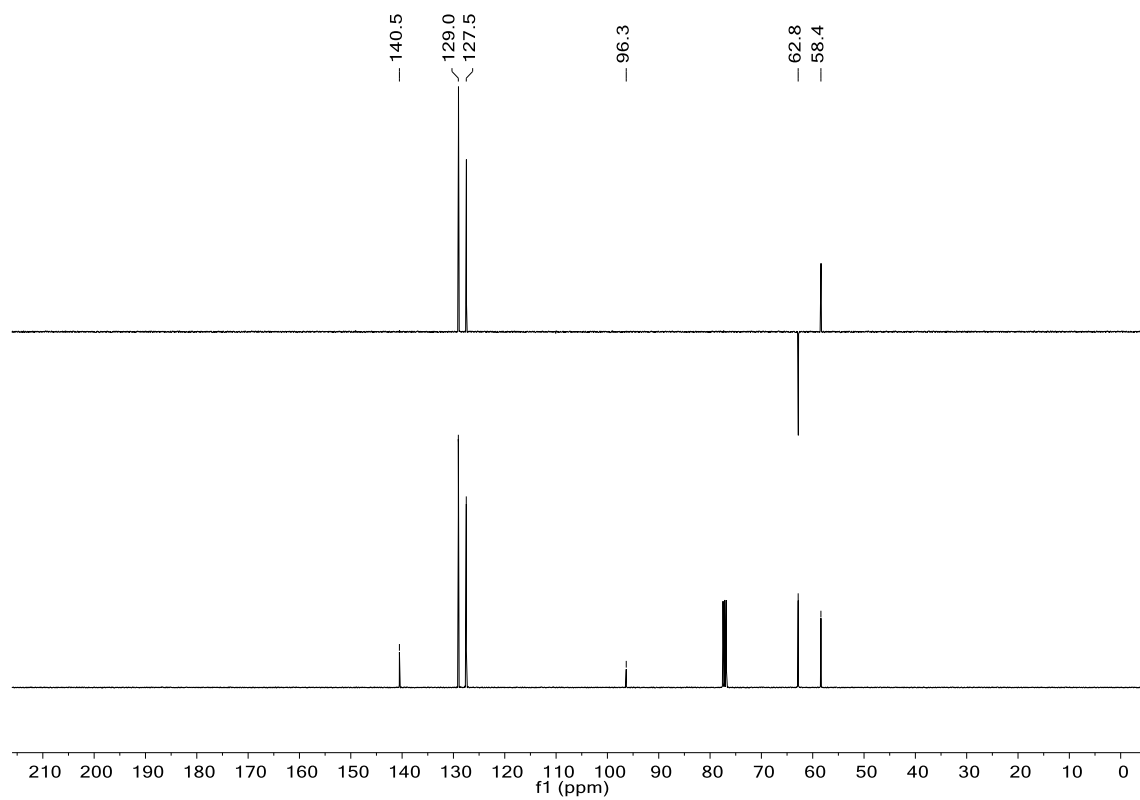
^{13}C -NMR and DEPT-135

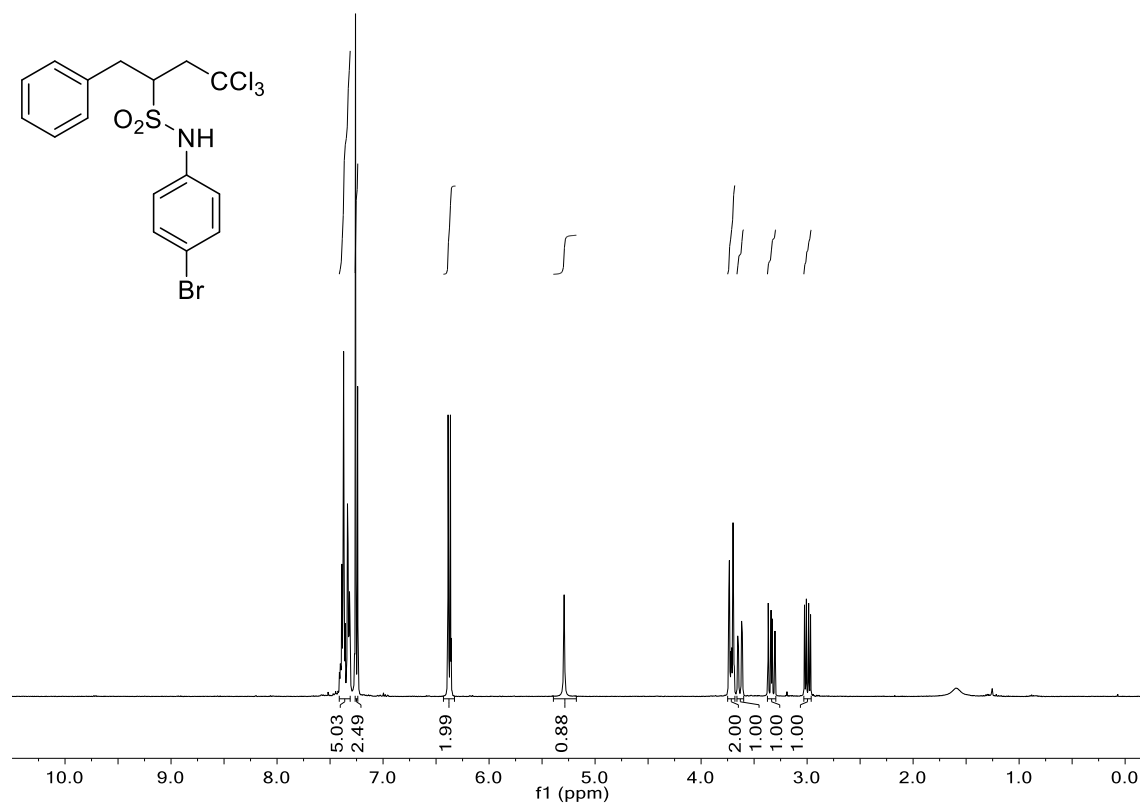
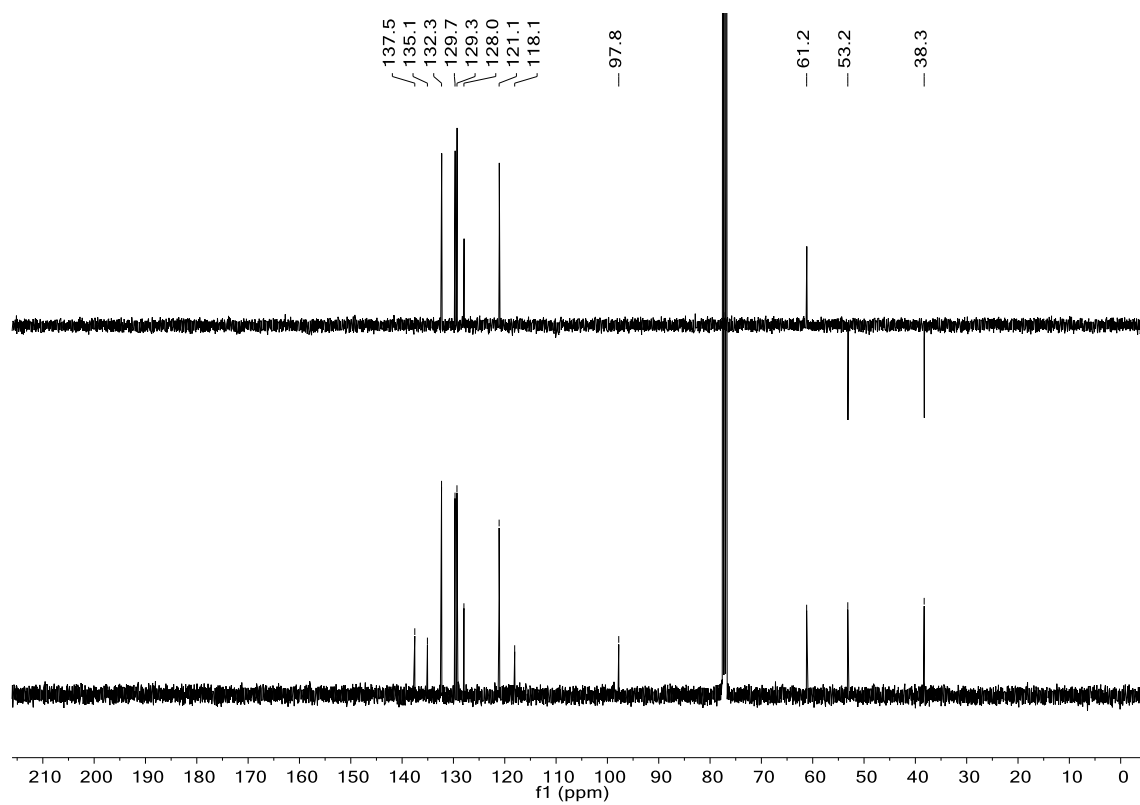


(1,3,3,3-tetrachloropropyl)benzene (**114**): ^1H -NMR

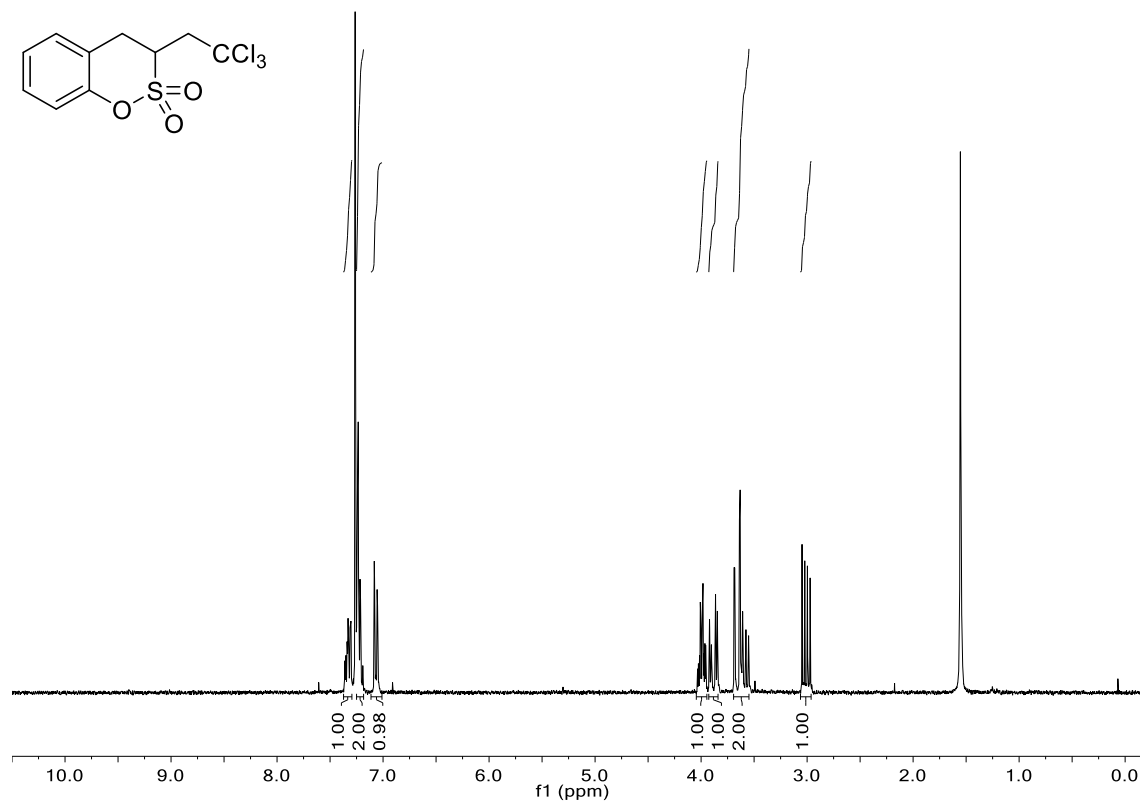


^{13}C -NMR and DEPT-135

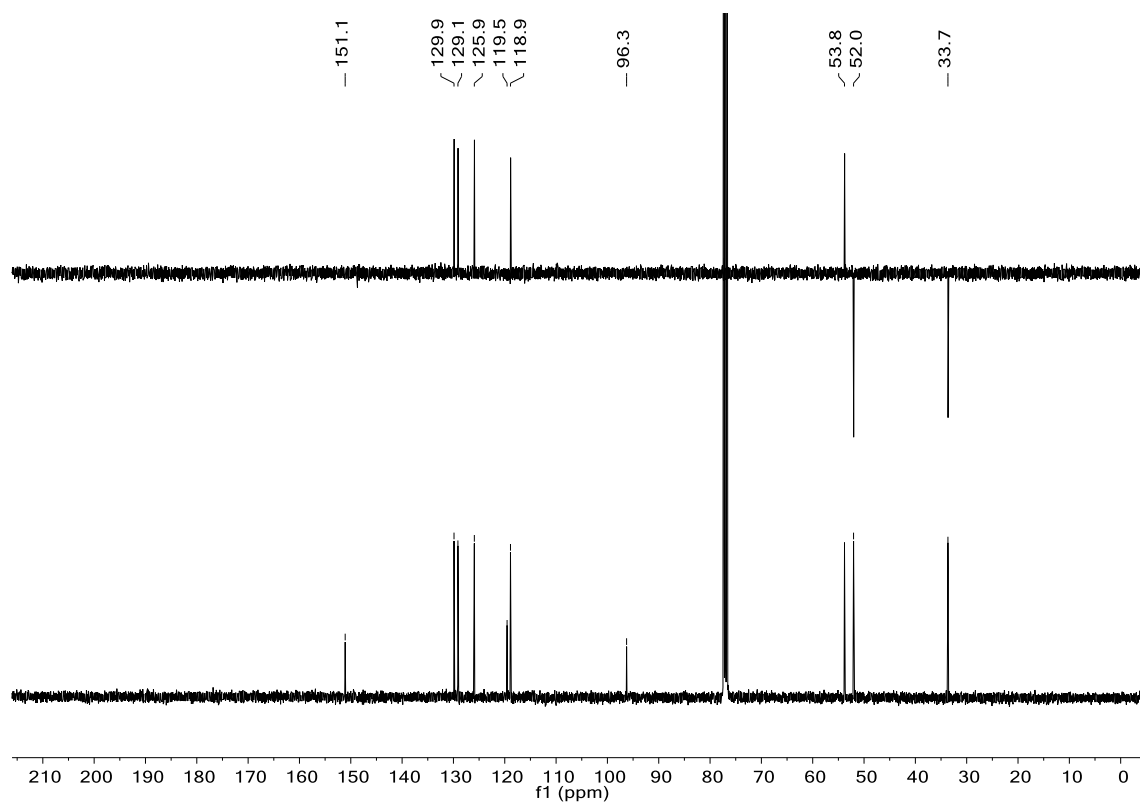


N-(4-bromophenyl)-4,4,4-trichloro-1-phenylbutane-2-sulfonamide (**116**): ^1H -NMR ^{13}C -NMR and DEPT-135

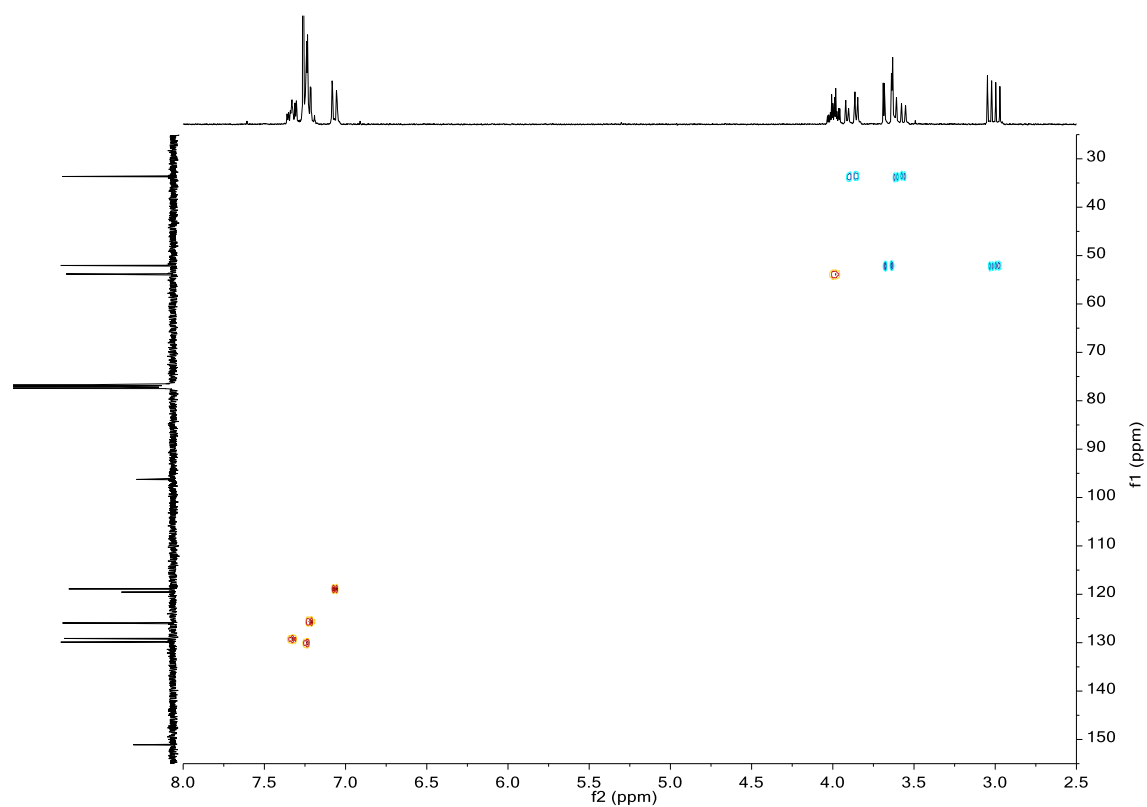
3-(2,2,2-trichloroethyl)-3,4-dihydrobenzo[e][1,2]oxathiine 2,2-dioxide (**118**): ^1H -NMR



^{13}C -NMR and DEPT-135



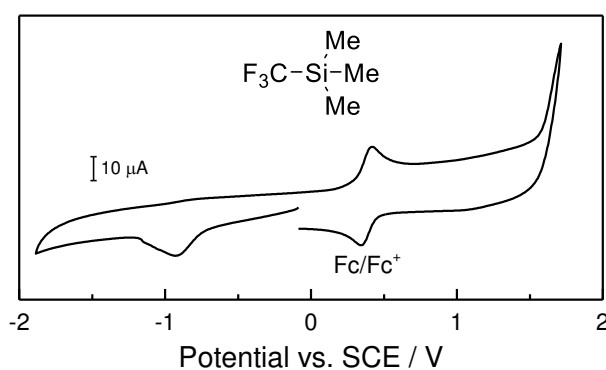
HSQC



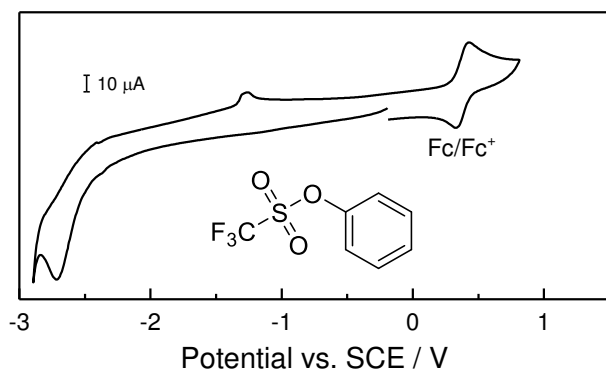
4.3 Cyclic Voltammograms

The following Cyclic voltammograms were recorded in MeCN using tetrabutylammonium tetrafluoroborate as supporting electrolyte and ferrocene as internal standard at a scan rate of $50 \text{ mV}\cdot\text{s}^{-1}$.

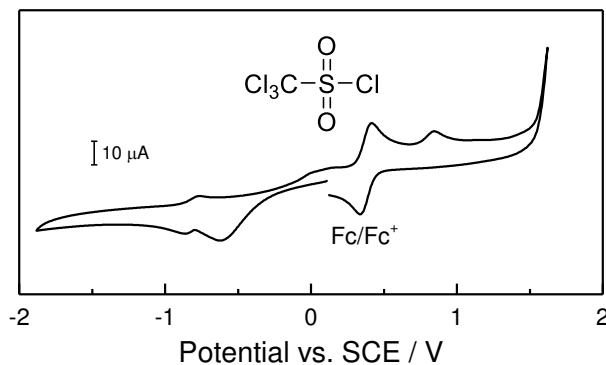
Trimethyl(trifluoromethyl)silane (TMSCF₃, **88**)



Phenyl trifluoromethanesulfonate (**100**)

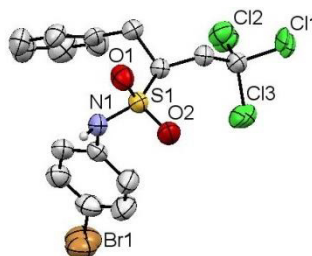
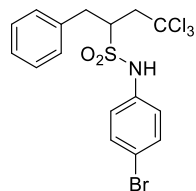


Trichloromethanesulfonyl chloride (**111**)



4.4 X-ray

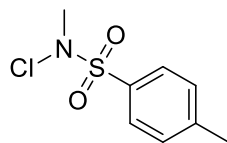
N-(4-bromophenyl)-4,4,4-trichloro-1-phenylbutane-2-sulfonamide (**116**)



Formula	C ₁₆ H ₁₅ BrCl ₃ NO ₂ S
$D_{calc.}/\text{g cm}^{-3}$	1.703
μ/mm^{-1}	8.202
Formula Weight	471.61
Color	clear colorless
Shape	prism
Size/mm ³	0.15×0.13×0.11
T/K	123.0(2)
Crystal System	monoclinic
Space Group	P2 ₁ /n
$a/\text{\AA}$	11.7170(3)
$b/\text{\AA}$	9.7941(2)
$c/\text{\AA}$	16.5349(4)
$\alpha/^\circ$	90
$\beta/^\circ$	104.195(3)
$\gamma/^\circ$	90
$V/\text{\AA}^3$	1839.57(8)
Z	4
Z'	1
Wavelength/ \AA	1.54184
Radiation type	CuK $_{\alpha}$
$\theta_{min}/^\circ$	4.182
$\theta_{max}/^\circ$	74.229
Measured Refl.	31414
Independent Refl.	3679
Reflections Used	3351
R_{int}	0.1419
Parameters	260
Restraints	34
Largest Peak	0.572
Deepest Hole	-0.723
GooF	1.031
wR_2 (all data)	0.1007
wR_2	0.0973
R_1 (all data)	0.0392
R_1	0.0359

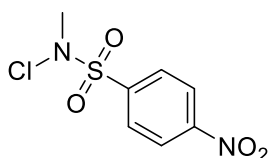
5. Chapter D: Elucidating the Reaction Pathways of Visible-Light-Mediated Chloramination of Alkenes

5.1 Synthesis of *N*-Chlorosulfonamides



Synthesis of *N*-chloro-*N*,4-dimethylbenzenesulfonamide (120a)¹⁶

To an ice-cooled mixture of *N*,4-dimethylbenzenesulfonamide (2.78 g, 15.0 mmol, 1.0 equiv) in dichloromethane (150 mL) was added 1,3,5-trichloro-1,3,5-triazinane-2,4,6-trione (TCCA, 3.84 g, 16.5 mmol, 1.1 equiv). After stirring for 4 h, the reaction was complete (judged by TLC) and the mixture was diluted with 150 mL of water. The layers were separated and the aqueous phase was extracted with dichloromethane (3 x 100 mL). The combined organic layers were dried over Na₂SO₄, filtered and concentrated in vacuum. Purification by column chromatography on silica gel using hexanes:ethyl acetate 5:1 (*R*_f = 0.42) afforded the desired product quantitatively as a white solid. **IR** (neat, cm⁻¹) 3071, 2986, 2933, 1595, 1494, 1454, 1429, 1403, 1353, 1308, 1297, 1101, 1088, 1029, 802, 779, 663. **¹H-NMR** (300 MHz, CDCl₃) δ 7.83 (d, *J* = 8.4 Hz, 2H), 7.41 (d, *J* = 8.0 Hz, 2H), 3.10 (s, 3H), 2.49 (s, 3H). **¹³C-NMR** (101 MHz, CDCl₃) δ 145.7, 130.0, 129.8, 128.7, 45.5, 21.9. **HRMS** (ESI): *m/z* calculated for C₈H₁₁ClNO₂S [MH⁺]: 220.0194, found 220.0196. **mp**: 77 °C.



Synthesis of *N*-chloro-*N*-methyl-4-nitrobenzenesulfonamide (128b)¹⁶

To an ice-cooled mixture of *N*-methyl-4-nitrobenzenesulfonamide (1.51 g, 7.0 mmol, 1.0 equiv) in dichloromethane (70 mL) was added 1,3,5-trichloro-1,3,5-triazinane-2,4,6-trione (TCCA, 1.79 g, 7.7 mmol, 1.1 equiv). After stirring for 4 h, the reaction was complete (judged by TLC) and the mixture was diluted with 70 mL of water. The layers were separated and the aqueous phase was extracted with dichloromethane (3 x 40 mL). The combined organic layers were dried over Na₂SO₄, filtered and concentrated in vacuum. Purification by column chromatography on silica gel using hexanes:EtOAc 2:1 (*R*_f = 0.55) afforded the desired

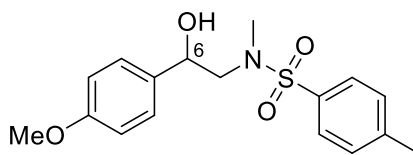
¹⁶ Conditions according to: S. Yu *et al.*, *Org. Lett.* **2015**.^[147]

product as a white solid (1.70 g, 97%). **IR** (neat, cm^{-1}) 3108, 2937, 2870, 1733 (broad), 1607, 1528 (vs), 1453, 1405, 1349, 1311, 1182, 1085, 1036, 857, 798, 738, 682. **$^1\text{H-NMR}$** (300 MHz, CDCl_3) δ 8.53 – 8.42 (m, 2H), 8.21 – 8.09 (m, 2H), 3.17 (s, 3H). **$^{13}\text{C-NMR}$** (75 MHz, CDCl_3) δ 151.3, 137.5, 131.2, 124.4, 45.4. **HRMS** (ESI): m/z calculated for $\text{C}_7\text{H}_8\text{ClN}_2\text{O}_4\text{S} [\text{MH}^+]$: 250.9888, found 250.9869. **mp**: 156 - 158 °C.

5.2 General Procedure for Chloramination of Olefins

An oven dried pressure tube (25 mL size) equipped with a magnetic stir bar was charged with *N*-chloro-*N*,4-dimethylbenzenesulfonamide (**120a**) (98.9 mg, 0.45 mmol, 1.5 equiv), [Cu(dap)₂]Cl (2.7 mg, 0.003 mmol, 1.0 mol%) and anhydrous 1,2-dichloroethane (6.00 mL). The mixture was degassed using three freeze-pump-thaw cycles. Olefin (0.30 mmol, 1.0 equiv) was added under a slight nitrogen overpressure and the tube was equipped with a light emitting LED-stick and sealed. The reaction mixture was irradiated at room temperature with a blue LED ($\lambda_{\text{max}} = 455 \text{ nm}$) while being stirred and the reaction progress was monitored by TLC. After 6 h, the reaction was stopped by switching off the light source and a sample of 0.20 mL of the crude reaction mixture was taken for measurements. For determining the yield by NMR, another sample of 1.00 mL was taken and 2-nitropropane was added as an internal standard. The remaining 4.80 mL of the crude reaction mixture were concentrated and purified by column chromatography on silica gel by using mixtures of hexanes and ethyl acetate (EtOAc) or diethyl ether (Et₂O) to afford the desired product.

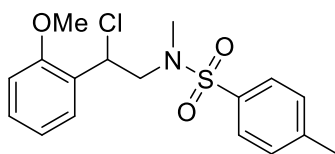
5.3 Compound Characterization

***N*-(2-hydroxy-2-(4-methoxyphenyl)ethyl)-*N*,4-dimethylbenzenesulfonamide (125a)**

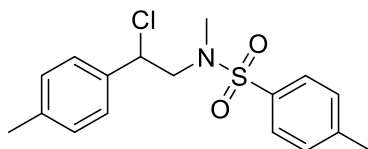
According to general procedure, **125a** was prepared from 4-methoxystyrene (**124a**) (40 μ L, 0.30 mmol, 1.0 equiv) using no catalyst. The crude product was purified by column chromatography on silica gel (hexanes:Et₂O 1:1, R_f = 0.16) to afford **125a** as a colorless oil (18.9 mg, 18% yield). After column chromatography, the product was still impurified with small amounts of *N*,4-dimethylbenzenesulfonamide (TsNMeH). **IR** (neat, cm⁻¹) 3507 (broad), 3295 (broad) 3076, 2922, 2839, 1610, 1513, 1457, 1327, 1245, 1156, 1088, 1033, 947, 813, 719. **¹H-NMR** (400 MHz, CDCl₃) δ 7.66 (d, J = 8.2 Hz, 2H), 7.30 (d, J = 8.7 Hz, 4H), 6.88 (d, J = 8.7 Hz, 2H), 4.87 (dd, J = 8.9, 3.4 Hz, 1H), 3.80 (s, 3H), 3.27 (dd, J = 14.1, 8.9 Hz, 1H), 2.98 (dd, J = 14.1, 3.5 Hz, 1H), 2.79 (s, 3H), 2.41 (s, 3H). **¹H-NMR** (400 MHz, DMSO-*d*₆) δ 7.61 (d, J = 8.2 Hz, 2H), 7.42 – 7.39 (m, 2H), 7.24 (d, J = 8.6 Hz, 2H), 6.89 (d, J = 8.6 Hz, 2H), 5.44 (d, J = 4.5 Hz, 1H), 4.67 (dt, J = 7.8, 4.8 Hz, 1H), 3.74 (s, 3H), 3.01 (qd, J = 13.5, 6.4 Hz, 2H), 2.66 (s, 3H), 2.39 – 2.38 (m, 3H). **¹³C NMR** (101 MHz, CDCl₃) δ 159.6, 143.8, 134.4, 133.3, 129.9, 127.6, 127.4, 114.1, 71.9, 58.4, 55.4, 36.9, 21.7. **HRMS** (APCI): m/z calculated for C₁₇H₂₂NO₄S [MH⁺]: 336.1264, found 336.1262.

This compound had already been reported as chloro substituted (*N*-(2-chloro-2-(4-methoxyphenyl)ethyl)-*N*,4-dimethylbenzenesulfonamide): The NMR-data of the product, which was isolated here, is in full accordance with the data reported in the literature (c.f. ref^[156]). According to the measured data of **125a** (IR, HRMS, NMR-Data in DMSO-*d*₆) there is evidence for the hydroxy substituted compound. The IR spectrum shows a typical broad O-H stretching vibration in the region of 3500 cm⁻¹.^[180] Concerning the NMR-data, the predicted ¹³C-carbon shift of carbon 6 is in the region of 71 ppm¹⁷ for the hydroxy-substituted compound, which fits well with the experimental value of 71.9 ppm. In contrast to that, for the Cl-substituted compound, this carbon shift is predicted in the region of 59 ppm¹⁷ which is in accordance with the measured values of the chloro-substituted compounds synthesized herein. Moreover, measuring the ¹H-NMR in DMSO-*d*₆ disclosed an additional doublet at 5.44 ppm which could be assigned to the proton of the hydroxy group.

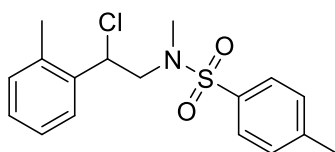
¹⁷ Data received via SciFinder: Predicted NMR data calculated using Advanced Chemistry Development, Inc. (ACD/Labs) Software V11.01 (© 1994-2017 ACD/Labs).

***N*-(2-chloro-2-(2-methoxyphenyl)ethyl)-*N*,4-dimethylbenzenesulfonamide (**125b**)**

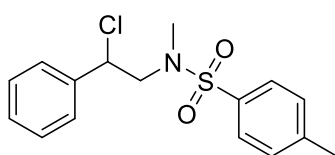
According to general procedure, (**125b**) was prepared from 2-methoxystyrene **124b** (40 μ L, 0.30 mmol, 1.0 equiv) using [Cu(dap)₂]Cl (2.7 mg, 0.003 mmol, 1.0 mol%) as a catalyst. The crude product (4.8 mL of the original reaction mixture) was purified by column chromatography on silica gel (hexanes:Et₂O 1:1, *R*_f = 0.45) to afford **125b** as a light yellow oil (47.3 mg, 56% yield). **IR** (neat, cm⁻¹) 3070, 2922, 2840, 1599, 1491, 1461, 1342, 1249, 1159, 1088, 1025, 929, 818, 752, 730. **¹H-NMR** (400 MHz, CDCl₃) δ 7.67 – 7.60 (m, 2H), 7.48 (dd, *J* = 7.6, 1.7 Hz, 1H), 7.35 – 7.27 (m, 3H), 6.99 (td, *J* = 7.5, 1.1 Hz, 1H), 6.88 (dd, *J* = 8.3, 1.0 Hz, 1H), 5.56 (dd, *J* = 7.7, 6.5 Hz, 1H), 3.85 (s, 3H), 3.62 – 3.51 (m, 2H), 2.76 (s, 3H), 2.42 (s, 3H). **¹³C-NMR** (101 MHz, CDCl₃) δ 156.7, 143.5, 135.1, 130.1, 129.8, 128.8, 127.5, 126.8, 121.1, 111.0, 56.5, 55.8, 55.2, 36.3, 21.6. **HRMS** (ESI): *m/z* calculated for C₁₇H₂₁ClNO₃S [MH⁺]: 354.0925, found 354.0935.

***N*-(2-chloro-2-(*p*-tolyl)ethyl)-*N*,4-dimethylbenzenesulfonamide (**125c**)**

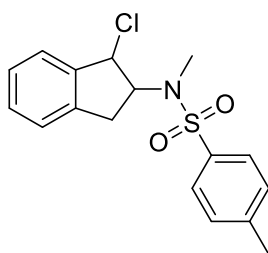
According to general procedure, **125c** was prepared from 4-methylstyrene (**124c**) (40 μ L, 0.30 mmol, 1.0 equiv) without using any catalyst. The crude product (4.8 mL of the original reaction mixture) was purified by column chromatography on silica gel (hexanes:EtOAc 15:1, *R*_f = 0.21) to afford **125c** as a white solid (68.6 mg, 85% yield). **IR** (neat, cm⁻¹) 3034, 2922, 2865, 1595, 1513, 1460, 1342, 1156, 1088, 984, 924, 857, 820, 734. **¹H-NMR** (300 MHz, CDCl₃) δ 7.64 (d, *J* = 8.3 Hz, 2H), 7.30 (dd, *J* = 8.1, 1.9 Hz, 4H), 7.17 (d, *J* = 7.7 Hz, 2H), 5.08 (t, *J* = 7.3 Hz, 1H), 3.57 (dd, *J* = 14.5, 7.4 Hz, 1H), 3.39 (dd, *J* = 14.4, 7.3 Hz, 1H), 2.63 (s, 3H), 2.42 (s, 3H), 2.36 (s, 3H). **¹³C-NMR** (75 MHz, CDCl₃) δ 143.7, 138.9, 135.9, 134.9, 129.9, 129.6, 127.5, 127.5, 61.4, 58.1, 37.1, 21.7, 21.4. **HRMS** (ESI): *m/z* calculated for C₁₇H₂₁ClNO₂S [MH⁺]: 338.0976, found 338.0985. **mp**: 91 - 94 °C. The data are in accordance with the data reported in the literature.^[156]

***N*-(2-chloro-2-(*o*-tolyl)ethyl)-*N*,4-dimethylbenzenesulfonamide (**125d**)**

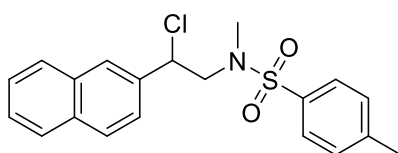
According to general procedure, **125d** was prepared from 2-methylstyrene (**124d**) (39 μ L, 0.30 mmol, 1.0 equiv) using [Ir(ppy)₂(dtbbpy)]PF₆ (2.7 mg, 0.003 mmol, 1.0 mol%) as a catalyst. The crude product (4.8 mL of the original reaction mixture) was purified by column chromatography on silica gel (hexanes:EtOAc 20:1, R_f = 0.16) to afford **125d** as a colorless oil (43.1 mg, 53% yield). **IR** (neat, cm⁻¹) 3067, 2922, 2868, 1599, 1490, 1461, 1342, 1156, 1088, 984, 924, 816, 753, 723. **¹H-NMR** (300 MHz, CDCl₃) δ 7.65 (d, J = 8.3 Hz, 2H), 7.52 – 7.41 (m, 1H), 7.31 (d, J = 7.9 Hz, 2H), 7.25 – 7.13 (m, 3H), 5.47 (t, J = 7.2 Hz, 1H), 3.59 – 3.38 (m, 2H), 2.71 (s, 3H), 2.46 (s, 3H), 2.42 (s, 3H). **¹³C-NMR** (101 MHz, CDCl₃) δ 143.8, 137.2, 136.2, 134.8, 130.9, 129.9, 128.7, 127.5, 127.2, 126.7, 58.1, 57.7, 37.5, 21.7, 19.5. **HRMS** (ESI): m/z calculated for C₁₇H₂₁ClNO₂S [MH⁺]: 338.0976, found 338.0986.

***N*-(2-chloro-2-phenylethyl)-*N*,4-dimethylbenzenesulfonamide (**125e**)**

According to general procedure, **125e** was prepared from distilled styrene (**124e**) (34 μ L, 0.30 mmol, 1.0 equiv) using [Cu(dap)₂]Cl (2.7 mg, 0.003 mmol, 1.0 mol%) as a catalyst. The crude product (4.8 mL of the original reaction mixture) was purified by column chromatography on silica gel (hexanes:EtOAc 15:1, R_f = 0.14) to afford **125e** as a light yellow oil (73.0 mg, 94% yield). **IR** (neat, cm⁻¹) 3063, 3034, 2926, 1599, 1495, 1454, 1338, 1156, 1088, 988, 932, 813, 738, 697. **¹H NMR** (300 MHz, CDCl₃) δ 7.69 – 7.61 (m, 2H), 7.45 – 7.33 (m, 5H), 7.33 – 7.28 (m, 2H), 5.11 (t, J = 7.4 Hz, 1H), 3.59 (dd, J = 14.5, 7.4 Hz, 1H), 3.40 (dd, J = 14.5, 7.3 Hz, 1H), 2.62 (s, 3H), 2.43 (s, 3H). **¹³C NMR** (101 MHz, CDCl₃) δ 143.8, 138.9, 134.9, 129.9, 129.0, 128.9, 127.7, 127.5, 61.5, 58.2, 37.1, 21.7. **HRMS** (ESI): m/z calculated for C₁₆H₁₉ClNO₂S [MH⁺]: 324.0820, found 324.0823. The data are in accordance with the data reported in the literature.^[156]

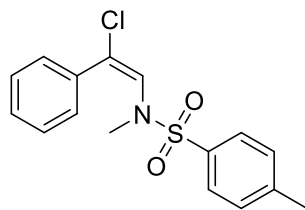
***N*-(1-chloro-2,3-dihydro-1*H*-inden-2-yl)-*N*,4-dimethylbenzenesulfonamide (**125f**)**

According to general procedure, **125f** was prepared from 1*H*-indene (**124f**) (35 μ L, 0.30 mmol, 1.0 equiv) using [Cu(dap)₂]Cl (2.7 mg, 0.003 mmol, 1.0 mol%) as a catalyst. The crude product (4.8 mL of the original reaction mixture) was purified by column chromatography on silica gel (hexanes:EtOAc 15:1, *R*_f = 0.13) to afford **125f** as a light yellow oil (53.7 mg, 67% yield). **IR** (neat, cm⁻¹) 3030, 2955, 2922, 2857, 1599, 1492, 1461, 1338, 1156, 1088, 965, 816, 746, 701. **¹H-NMR** (300 MHz, CDCl₃, *E*-isomer) δ 7.79 (d, *J* = 8.3 Hz, 2H), 7.35 (d, *J* = 8.2 Hz, 3H), 7.32 – 7.24 (m, 1H), 7.29 – 7.22 (m, 1H), 7.22 – 7.13 (m, 1H), 5.08 (d, *J* = 5.6 Hz, 1H), 4.95 (dt, *J* = 8.2, 5.9 Hz, 1H), 3.20 (dd, *J* = 16.5, 8.2 Hz, 1H), 2.83 (dd, *J* = 16.4, 6.4 Hz, 1H), 2.68 (s, 3H), 2.46 (s, 3H). **¹³C-NMR** (75 MHz, CDCl₃, *E*-isomer) δ 143.7, 140.2, 139.6, 136.3, 129.9, 129.5, 127.9, 127.6, 125.1, 124.7, 67.0, 62.8, 33.4, 29.9, 21.8. **HRMS** (ESI): *m/z* calculated for C₁₇H₁₉ClNO₂S [MH⁺]: 336.0822, found 336.0820. The data are in accordance with the data reported in the literature.^[156]

***N*-(2-chloro-2-(naphthalen-2-yl)ethyl)-*N*,4-dimethylbenzenesulfonamide (**125g**)**

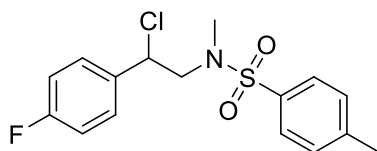
According to general procedure, **125g** was prepared from 2-vinylnaphthalene (**124g**) (46.3 mg, 0.30 mmol, 1.0 equiv) using [Cu(dap)₂]Cl (2.7 mg, 0.003 mmol, 1.0 mol%) as a catalyst. The crude product (4.8 mL of the original reaction mixture) was purified by column chromatography on silica gel (hexanes:EtOAc 15:1, *R*_f = 0.09) to afford **125g** as a colorless oil (62.4 mg, 70% yield). **IR** (neat, cm⁻¹) 3056, 2922, 2851, 1599, 1495, 1443, 1342, 1156, 1088, 988, 932, 820, 779, 723. **¹H-NMR** (300 MHz, CDCl₃) δ 7.92 – 7.78 (m, 4H), 7.63 (d, *J* = 8.3 Hz, 2H), 7.59 – 7.46 (m, 3H), 7.31 – 7.27 (m, 1H), 7.26 – 7.22 (m, 1H), 5.28 (t, *J* = 7.4 Hz, 1H), 3.69 (dd, *J* = 14.5, 7.2 Hz, 1H), 3.52 (dd, *J* = 14.5, 7.5 Hz, 1H), 2.63 (s, 3H), 2.41 (s, 3H). **¹³C-NMR** (75 MHz, CDCl₃) δ 143.8, 136.0, 134.9, 133.5, 133.1, 129.9, 129.0,

128.3, 127.9, 127.4, 127.3, 126.9, 126.8, 124.6, 61.7, 58.0, 37.2, 21.7. **HRMS** (ESI): m/z calculated for $C_{20}H_{21}ClNO_2S$ [MH^+]: 374.0983, found 374.0976.



***N*-(1-chloro-1-phenylprop-1-en-2-yl)-*N*,4-dimethylbenzenesulfonamide (125h)**

According to general procedure, **125h** was prepared from phenylacetylene (**124h**) (33 μ L, 0.30 mmol, 1.0 equiv) using $[Cu(dap)_2]Cl$ (2.7 mg, 0.003 mmol, 1.0 mol%) as a catalyst. The crude product (4.8 mL of the original reaction mixture) was purified by column chromatography on silica gel (hexanes:EtOAc 15:1, R_f = 0.10) to afford **125h** as a colorless oil (43.0 mg, 56% yield of a mixture of non-separable diastereomers: *E*:*Z* = 7:3). **1H -NMR** (300 MHz, $CDCl_3$, *E*-isomer) δ 7.71 (d, J = 8.2 Hz, 2H), 7.38 (d, J = 7.8 Hz, 2H), 7.30 – 7.24 (m, 2H), 7.26 – 7.18 (m, 3H), 6.67 (s, 1H), 2.58 (s, 3H), 2.48 (s, 3H). **1H -NMR** (300 MHz, $CDCl_3$, *Z*-isomer) δ 7.74 (d, J = 8.1 Hz, 2H), 7.56 – 7.46 (m, 2H), 7.36 – 7.31 (m, 5H), 6.90 (s, 1H), 3.23 (s, 3H), 2.45 (s, 3H). **^{13}C -NMR** (101 MHz, $CDCl_3$, *E*-isomer) δ 144.4, 135.5, 134.1, 130.1, 129.4, 128.9, 128.3, 127.6, 127.4, 127.2, 126.1, 36.7, 21.8. **^{13}C -NMR** (101 MHz, $CDCl_3$, *Z*-isomer) δ 144.2, 136.5, 135.2, 130.0, 129.4, 129.2, 128.6, 127.4, 126.8, 126.7, 125.1, 36.5, 21.8. **HRMS** (ESI, *E*-isomer): m/z calculated for $C_{16}H_{17}ClNO_2S$ [MH^+]: 322.0663, found 322.0668. The data of the *E*-isomer are in accordance with the data reported in the literature.^[158]

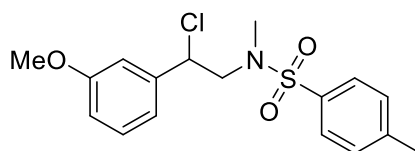


***N*-(2-chloro-2-(4-fluorophenyl)ethyl)-*N*,4-dimethylbenzenesulfonamide (125i)¹⁸**

According to general procedure, **125i** was prepared from 4-fluorostyrene (**124i**) (36 μ L, 0.30 mmol, 1.0 equiv) using $[Cu(dap)_2]Cl$ (2.7 mg, 0.003 mmol, 1.0 mol%) as a catalyst. The crude product (4.8 mL of the original reaction mixture) was purified by column

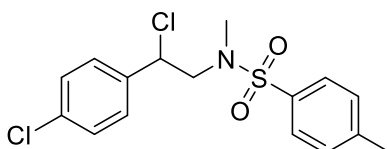
¹⁸ The NMR spectra of this compound were measured by the Central Analytic Department of the University of Regensburg.

chromatography on silica gel (hexanes:EtOAc 15:1, R_f = 0.18) to afford **125i** as a colorless oil (65.3 mg, 80% yield). **IR** (neat, cm^{-1}) 3049, 2926, 2827, 1603, 1513, 1457, 1338, 1226, 1159, 1088, 988, 932, 839, 734. **$^1\text{H-NMR}$** (400 MHz, CDCl_3) δ 7.69 – 7.60 (m, 2H), 7.43 – 7.37 (m, 2H), 7.34 – 7.28 (m, 2H), 7.12 – 7.01 (m, 2H), 5.10 (t, J = 7.4 Hz, 1H), 3.55 (dd, J = 14.5, 7.1 Hz, 1H), 3.39 (dd, J = 14.5, 7.6 Hz, 1H), 2.63 (s, 3H), 2.43 (s, 3H). **$^{13}\text{C-NMR}$** (101 MHz, CDCl_3) δ 163.0 (d, $J_{\text{C-F}}$ = 248.0 Hz), 143.9, 134.8, 134.7 (d, $J_{\text{C-F}}$ = 3.3 Hz), 130.0, 129.5 (d, $J_{\text{C-F}}$ = 8.3 Hz), 127.5, 115.9 (d, $J_{\text{C-F}}$ = 21.9 Hz), 60.6, 58.2, 37.2, 21.7. **$^{19}\text{F-NMR}$** (282 MHz, CDCl_3) δ -113.0. **HRMS** (ESI): m/z calculated for $\text{C}_{16}\text{H}_{18}\text{ClFNO}_2\text{S}$ [MH^+]: 342.0725, found 342.0739. The data are in accordance with the data reported in the literature.^[156]



***N*-(2-chloro-2-(3-methoxyphenyl)ethyl)-*N*,4-dimethylbenzenesulfonamide (**125j**)**

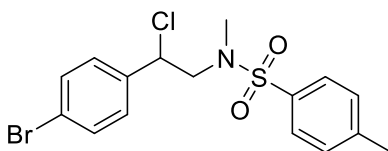
According to general procedure, **125j** was prepared from 3-methoxystyrene (**124j**) (42 μL , 0.30 mmol, 1.0 equiv) using $[\text{Cu}(\text{dap})_2]\text{Cl}$ (2.7 mg, 0.003 mmol, 1.0 mol%) as a catalyst. The crude product (4.8 mL of the original reaction mixture) was purified by column chromatography on silica gel (hexanes:Et₂O 1:1, R_f = 0.38) to afford **125j** as a light yellow oil (81.9 mg, 96% yield). **IR** (neat, cm^{-1}) 3067, 2930, 2840, 1599, 1491, 1457, 1342, 1260, 1156, 1088, 1040, 936, 768, 731, 697. **$^1\text{H-NMR}$** (400 MHz, CDCl_3) δ 7.69 – 7.60 (m, 2H), 7.34 – 7.27 (m, 3H), 7.03 – 6.95 (m, 1H), 6.95 (t, J = 2.1 Hz, 1H), 6.87 (ddd, J = 8.3, 2.6, 0.9 Hz, 1H), 5.07 (t, J = 7.3 Hz, 1H), 3.82 (s, 3H), 3.57 (dd, J = 14.5, 7.4 Hz, 1H), 3.41 (dd, J = 14.5, 7.2 Hz, 1H), 2.65 (s, 3H), 2.42 (s, 3H). **$^{13}\text{C-NMR}$** (101 MHz, CDCl_3) δ 159.9, 143.8, 140.3, 134.9, 130.0, 129.9, 127.4, 119.9, 114.6, 113.1, 61.4, 58.1, 55.5, 37.1, 21.6. **HRMS** (ESI): m/z calculated for $\text{C}_{17}\text{H}_{21}\text{ClNO}_3\text{S}$ [MH^+]: 354.0925, found 354.0930.



***N*-(2-chloro-2-(4-chlorophenyl)ethyl)-*N*,4-dimethylbenzenesulfonamide (**125k**)**

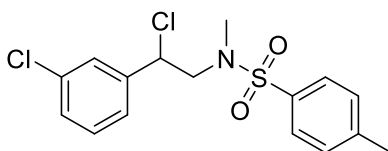
According to general procedure, **125k** was prepared from 4-chlorostyrene (**124k**) (36 μL , 0.30 mmol, 1.0 equiv) using $[\text{Cu}(\text{dap})_2]\text{Cl}$ (2.7 mg, 0.003 mmol, 1.0 mol%) as a catalyst. The

crude product (5.0 mL of the original reaction mixture) was purified by column chromatography on silica gel (hexanes:EtOAc 15:1, R_f = 0.11) to afford **125k** as a colorless oil (78.0 mg, 88% yield). **IR** (neat, cm^{-1}) 3034, 2968, 2922, 1596, 1491, 1457, 1342, 1156, 1088, 988, 928, 813, 749, 686. **^1H NMR** (300 MHz, CDCl_3) δ 7.63 (d, J = 8.3 Hz, 2H), 7.35 (s, 4H), 7.36 – 7.26 (m, 2H), 5.08 (t, J = 7.4 Hz, 1H), 3.54 (dd, J = 14.5, 7.1 Hz, 1H), 3.37 (dd, J = 14.4, 7.7 Hz, 1H), 2.63 (s, 3H), 2.43 (s, 3H). **^{13}C NMR** (75 MHz, CDCl_3) δ 143.9, 137.3, 134.9, 134.6, 130.0, 129.1, 129.1, 127.4, 60.5, 58.1, 37.2, 21.7. **HRMS** (ESI): m/z calculated for $\text{C}_{16}\text{H}_{18}\text{Cl}_2\text{NO}_2\text{S}$ [MH^+]: 358.0430, found 358.0436. The data are in accordance with the data reported in the literature.^[156]



***N*-(2-(4-bromophenyl)-2-chloroethyl)-*N*,4-dimethylbenzenesulfonamide (125l)**

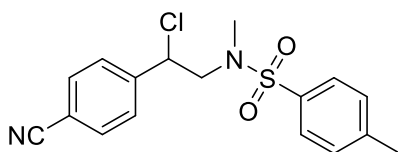
According to general procedure, **125l** was prepared from 4-bromostyrene (**124l**) (39 μL , 0.30 mmol, 1.0 equiv) using $[\text{Cu}(\text{dap})_2]\text{Cl}$ (2.7 mg, 0.003 mmol, 1.0 mol%) as a catalyst. The crude product (4.8 mL of the original reaction mixture) was purified by column chromatography on silica gel (hexanes:EtOAc 15:1, R_f = 0.10) to afford **125l** as a colorless oil (78.3 mg, 81% yield). **IR** (neat, cm^{-1}) 3053, 2952, 2922, 2848, 1596, 1491, 1462, 1445, 1405, 1346, 1156, 1088, 988, 924, 824, 746, 667. **^1H -NMR** (300 MHz, CDCl_3) δ 7.63 (d, J = 8.3 Hz, 2H), 7.56 – 7.45 (m, 2H), 7.36 – 7.28 (m, 4H), 5.07 (t, J = 7.4 Hz, 1H), 3.53 (dd, J = 14.5, 7.1 Hz, 1H), 3.37 (dd, J = 14.4, 7.7 Hz, 1H), 2.63 (s, 3H), 2.43 (s, 3H). **^{13}C -NMR** (75 MHz, CDCl_3) δ 143.9, 137.8, 134.6, 132.1, 130.0, 129.4, 127.4, 123.0, 60.5, 58.0, 37.2, 21.7. **HRMS** (ESI): m/z calculated for $\text{C}_{16}\text{H}_{18}\text{BrClNO}_2\text{S}$ [MH^+]: 401.9925, found 401.9929.



***N*-(2-chloro-2-(3-chlorophenyl)ethyl)-*N*,4-dimethylbenzenesulfonamide (125m)**

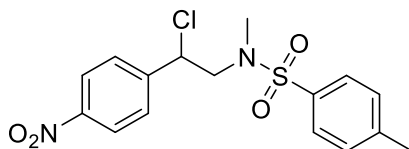
According to general procedure, **125m** was prepared from 3-chlorostyrene (**124m**) (38 μL , 0.30 mmol, 1.0 equiv) using $[\text{Cu}(\text{dap})_2]\text{Cl}$ (2.7 mg, 0.003 mmol, 1.0 mol%) as a catalyst. The crude product (4.8 mL of the original reaction mixture) was purified by column

chromatography on silica gel (hexanes:EtOAc 15:1, R_f = 0.13) to afford **125m** as a colorless oil (74.0 mg, 86% yield). **IR** (neat, cm^{-1}) 3064, 2922, 2818, 1595, 1576, 1476, 1431, 1338, 1156, 1088, 992, 932, 816, 753, 727, 690. **$^1\text{H-NMR}$** (400 MHz, CDCl_3) δ 7.64 (d, J = 8.3 Hz, 2H), 7.41 – 7.36 (m, 1H), 7.36 – 7.27 (m, 5H), 5.07 (t, J = 7.3 Hz, 1H), 3.54 (dd, J = 14.6, 7.3 Hz, 1H), 3.40 (dd, J = 14.5, 7.3 Hz, 1H), 2.66 (s, 3H), 2.43 (s, 3H). **$^{13}\text{C-NMR}$** (101 MHz, CDCl_3) δ 143.9, 140.8, 134.8, 134.8, 130.2, 130.0, 129.2, 127.8, 127.5, 125.9, 60.5, 58.1, 37.3, 21.7. **HRMS** (ESI): m/z calculated for $\text{C}_{16}\text{H}_{18}\text{Cl}_2\text{NO}_2\text{S}$ [MH^+]: 358.0430, found 358.0438.



***N*-(2-chloro-2-(4-cyanophenyl)ethyl)-*N*,4-dimethylbenzenesulfonamide (**125n**)**

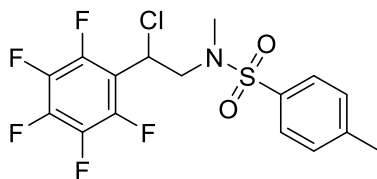
According to general procedure, **125n** was prepared from 4-cyanostyrene (**124n**) (39 μL , 0.30 mmol, 1.0 equiv) using $[\text{Cu}(\text{dap})_2]\text{Cl}$ (2.7 mg, 0.003 mmol, 1.0 mol%) as a catalyst. The crude product (4.8 mL of the original reaction mixture) was purified by column chromatography on silica gel (mixtures of hexanes:EtOAc 8:1 to 3:1, R_f = 0.29 in hexanes:EtOAc 3:1) to afford **125n** as a colorless oil (80.0 mg, 96% yield). **IR** (neat, cm^{-1}) 3065, 3027, 2926, 2823, 2229, 1599, 1495, 1457, 1338, 1156, 1088, 988, 932, 816, 760, 720. **$^1\text{H-NMR}$** (400 MHz, CDCl_3) δ 7.68 (d, J = 8.4 Hz, 2H), 7.63 (d, J = 8.3 Hz, 2H), 7.56 (d, J = 8.3 Hz, 2H), 7.32 (d, J = 8.0 Hz, 2H), 5.15 (t, J = 7.4 Hz, 1H), 3.52 (dd, J = 14.5, 7.0 Hz, 1H), 3.41 (dd, J = 14.5, 7.8 Hz, 1H), 2.63 (s, 3H), 2.43 (s, 3H). **$^{13}\text{C-NMR}$** (101 MHz, CDCl_3) δ 144.1, 143.8, 134.4, 132.7, 130.0, 128.6, 127.4, 118.4, 112.9, 60.1, 58.1, 37.4, 21.7. **HRMS** (ESI): m/z calculated for $\text{C}_{17}\text{H}_{18}\text{ClN}_2\text{O}_2\text{S}$ [MH^+]: 349.0772, found 349.0773.



***N*-(2-chloro-2-(4-nitrophenyl)ethyl)-*N*,4-dimethylbenzenesulfonamide (**125o**)**

According to general procedure, **125o** was prepared from 4-nitrostyrene (**124o**) (45 mg, 0.30 mmol, 1.0 equiv) using $[\text{Cu}(\text{dap})_2]\text{Cl}$ (2.7 mg, 0.003 mmol, 1.0 mol%) as a catalyst. The crude product (5.0 mL of the original reaction mixture) was purified by column chromatography on silica gel (hexanes:Et₂O 1:1, R_f = 0.30) to afford **125o** as a yellow oil

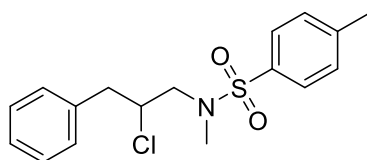
(90.0 mg, 98% yield). **IR** (neat, cm^{-1}) 3112, 3083, 2926, 2866, 1599, 1521 (vs), 1457, 1342, 1156, 1092, 932, 857, 813, 742. **^1H NMR** (400 MHz, CDCl_3) δ 8.24 (d, J = 8.7 Hz, 2H), 7.69 – 7.56 (m, 4H), 7.32 (d, J = 8.0 Hz, 2H), 5.21 (t, J = 7.4 Hz, 1H), 3.54 (dd, J = 14.5, 6.9 Hz, 1H), 3.44 (dd, J = 14.5, 7.8 Hz, 1H), 2.65 (s, 3H), 2.43 (s, 3H). **^{13}C -NMR** (101 MHz, CDCl_3) δ 148.2, 145.7, 144.1, 134.4, 130.1, 128.8, 127.5, 124.1, 59.7, 58.1, 37.4, 21.7. **HRMS** (ESI): m/z calculated for $\text{C}_{16}\text{H}_{18}\text{ClN}_2\text{O}_4\text{S}$ [MH^+]: 369.0670; found: 369.0674.



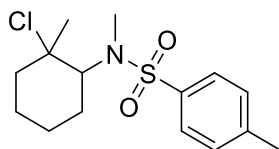
***N*-(2-chloro-2-(perfluorophenyl)ethyl)-*N*,4-dimethylbenzenesulfonamide (125p)**¹⁹

According to general procedure, **125p** was prepared from distilled 2,3,4,5,6-pentafluorostyrene (**124p**) (41 μL , 0.30 mmol, 1.0 equiv) using $[\text{Cu}(\text{dap})_2]\text{Cl}$ (2.7 mg, 0.003 mmol, 1.0 mol%) as a catalyst. The crude product (4.8 mL of the original reaction mixture) was purified by column chromatography on silica gel (mixtures of hexanes:EtOAc 5:1 to 3:1, R_f = 0.57 in hexanes:EtOAc 3:1) to afford **125p** as a colorless oil (58.5 mg, 60% yield). **IR** (neat, cm^{-1}) 3032, 2929, 2847, 1655, 1599, 1523, 1506 (vs), 1457, 1349, 1162, 1133, 1021, 980, 949, 816, 734. **^1H -NMR** (300 MHz, CDCl_3) δ 7.64 (d, J = 8.3 Hz, 2H), 7.36 – 7.30 (m, 2H), 5.48 – 5.35 (m, 1H), 3.93 (dd, J = 14.4, 9.1 Hz, 1H), 3.40 (dd, J = 14.4, 6.3 Hz, 1H), 2.82 (s, 3H), 2.44 (s, 3H). **^{13}C -NMR** (151 MHz, CDCl_3) δ 145.5 (d, $J_{\text{C-F}}$ = 252.7 Hz), 144.2, 141.9 (d, $J_{\text{C-F}}$ = 256.8 Hz), 137.8 (d, $J_{\text{C-F}}$ = 252.9 Hz), 134.2, 130.0, 127.5, 112.5 (td, $J_{\text{C-F}}$ = 14.5, 3.8 Hz), 55.0, 48.1, 37.0, 21.6. **^{19}F -NMR** (282 MHz, CDCl_3) δ -140.8 (d, J = 20.9 Hz), -152.4 (tt, J = 21.1, 2.8 Hz), -161.3 (td, J = 21.9, 8.1 Hz). **HRMS** (ESI): m/z calculated for $\text{C}_{16}\text{H}_{14}\text{ClF}_5\text{NO}_2\text{S}$ [MH^+]: 414.0348, found 414.0351.

¹⁹ The NMR spectra of this compound were measured by the Central Analytic Department of the University of Regensburg.

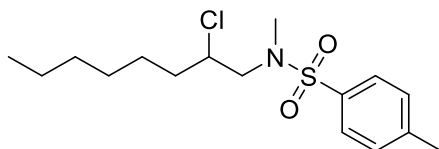
***N*-(2-chloro-3-phenylpropyl)-*N*,4-dimethylbenzenesulfonamide (**127a**)**

According to general procedure, **127a** was prepared from allylbenzene (**126a**) (40 μ L, 0.30 mmol, 1.0 equiv) using $[\text{Cu}(\text{dap})_2]\text{Cl}$ (2.7 mg, 0.003 mmol, 1.0 mol%) as a catalyst. The crude product (4.8 mL of the original reaction mixture) was purified by column chromatography on silica gel (hexanes:EtOAc 15:1, R_f = 0.08) to afford **127a** as a colorless oil (8.3 mg, 10% yield). **IR** (neat, cm^{-1}) 3064, 3030, 2922, 2855, 1599, 1495, 1454, 1342, 1159, 1088, 943, 816, 738, 701. **$^1\text{H-NMR}$** (400 MHz, CDCl_3) δ 7.62 (d, J = 8.2 Hz, 2H), 7.38 – 7.25 (m, 5H), 7.26 – 7.23 (m, 2H), 4.30 (dtd, J = 9.0, 6.6, 4.8 Hz, 1H), 3.46 (dd, J = 14.4, 6.4 Hz, 1H), 3.28 (dd, J = 14.4, 4.8 Hz, 1H), 3.09 (dd, J = 14.3, 7.0 Hz, 1H), 2.94 (dd, J = 14.4, 9.0 Hz, 1H), 2.85 (s, 3H), 2.43 (s, 3H). **$^{13}\text{C-NMR}$** (101 MHz, CDCl_3) δ 143.8, 137.3, 134.4, 129.9, 129.5, 128.6, 127.6, 127.1, 61.1, 56.8, 42.1, 37.3, 21.7. **HRMS** (ESI): m/z calculated for $\text{C}_{17}\text{H}_{21}\text{ClNO}_2\text{S}$ [MH^+]: 338.0976, found 338.0981.

***N*-(2-chloro-2-methylcyclohexyl)-*N*,4-dimethylbenzenesulfonamide (**127b**)**

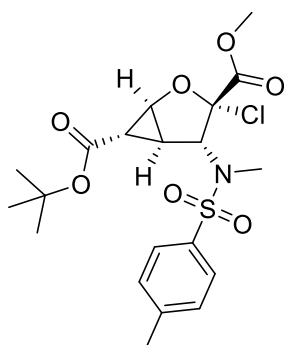
According to general procedure, **127b** was prepared from 1-methylcyclohex-1-ene (**126b**) (107 μ L, 0.90 mmol, 1.0 equiv) in DCE (18.0 mL) using $[\text{Ir}(\text{ppy})_2(\text{dtbbpy})]\text{PF}_6$ (8.2 mg, 0.009 mmol, 1.0 mol%) as a catalyst and *N*-chloro-*N*,4-dimethylbenzenesulfonamide (**120a**) (296.6 mg, 1.35 mmol, 1.5 equiv). The crude product (17.0 mL of the original reaction mixture) was purified by column chromatography on silica gel (hexanes:EtOAc 15:1, R_f = 0.19) to afford **127b** as a white solid (49.0 mg, 18% yield of *Z*-isomer). **IR** (neat, cm^{-1} , *Z*-isomer) 3068, 2997, 2930, 2863, 1595, 1495, 1446, 1338, 1163, 973, 928, 865, 775. **$^1\text{H-NMR}$** (300 MHz, CDCl_3 , *Z*-isomer) δ 7.66 (d, J = 8.3 Hz, 2H), 7.31 (d, J = 7.9 Hz, 1H), 3.79 (dd, J = 12.2, 3.6 Hz, 1H), 2.86 (s, 3H), 2.43 (s, 3H), 2.08 – 1.96 (m, 1H), 1.78 – 1.65 (m, 7H), 1.59 – 1.49 (m, 1H), 1.29 – 1.23 (m, 1H), 1.01 – 0.89 (m, 1H). **$^{13}\text{C-NMR}$** (101 MHz, CDCl_3 , *Z*-isomer) δ 143.4, 136.1, 129.8, 127.3, 76.3, 63.6, 43.1, 31.4, 31.1, 26.0, 25.6, 21.7, 21.7. **HRMS** (ESI, *Z*-isomer): m/z calculated for $\text{C}_{15}\text{H}_{23}\text{ClNO}_2\text{S}$ [MH^+]: 316.1133, found 316.1138. **mp**: 76 – 81 $^\circ\text{C}$.

Suitable crystals for X-ray analysis of **127b** were obtained by liquid diffusion of Et₂O into a hexanes solution.



***N*-(2-chlorooctyl)-*N*,4-dimethylbenzenesulfonamide (**127c**)**

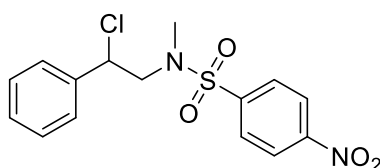
According to general procedure, **127c** was prepared from distilled 1-octene (**126c**) (47 μ L, 0.30 mmol, 1.0 equiv) using [Cu(dap)₂]Cl (2.7 mg, 0.003 mmol, 1.0 mol%) as a catalyst. The crude product (4.8 mL of the original reaction mixture) was purified by column chromatography on silica gel (hexanes:EtOAc 15:1, *R*_f = 0.32) to afford **127c** as a colorless oil (28.3 mg, 35% yield). **IR** (neat, cm⁻¹) 2957, 2930, 2859, 1599, 1494, 1457, 1341, 1159, 1088, 973, 932, 816, 738. **¹H-NMR** (400 MHz, CDCl₃) δ 7.68 (d, *J* = 8.3 Hz, 2H), 7.33 (d, *J* = 7.9 Hz, 2H), 4.11 – 4.00 (m, 1H), 3.37 (dd, *J* = 14.2, 6.7 Hz, 1H), 3.08 (dd, *J* = 14.2, 6.8 Hz, 1H), 2.83 (s, 3H), 2.43 (s, 3H), 1.96 – 1.86 (m, 1H), 1.69 – 1.53 (m, 2H), 1.46 – 1.26 (m, 7H), 0.92 – 0.87 (m, 3H). **¹³C-NMR** (101 MHz, CDCl₃) δ 143.8, 134.6, 129.9, 127.6, 61.0, 57.0, 37.1, 35.5, 31.8, 28.9, 26.2, 22.7, 21.7, 14.2. **LRMS** (ESI) (relative intensities): *m/z* 332.15 (100) [MH⁺], 296.17 (36) [MH⁺, -HCl]. The data are in accordance with the data reported in the literature.^[156]



6-(*tert*-butyl) 3-methyl (1*S*,3*S*,4*R*,5*R*,6*S*)-3-chloro-4-((*N*,4-dimethylphenyl)sulfonamido)-2-oxabicyclo [3.1.0]hexane-3,6-dicarboxylate (127d**)**

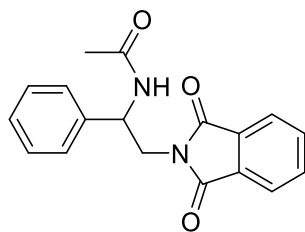
According to general procedure, **127d** was prepared from 6-(*tert*-butyl) 3-methyl (1*S*,5*S*,6*S*)-2-oxabicyclo[3.1.0]hex-3-ene-3,6-dicarboxylate (**126d**) (72.1 mg, 0.30 mmol, 1.0 equiv) using [Cu(dap)₂]Cl (2.7 mg, 0.003 mmol, 1.0 mol%) as a catalyst. The crude product (4.8 mL of the original reaction mixture) was purified by column chromatography on silica gel (hexanes:Et₂O

1:1, $R_f = 0.32$) to afford **127d** as a white solid (43.7 mg, 40% yield). The assignment of the stereochemistry is preliminary. **IR** (neat, cm^{-1}) 3071, 2978, 2933, 1759, 1715, 1596, 1495, 1456, 1439, 1401, 1370, 1353, 1320, 1297, 1167, 1115, 1096, 943, 872, 840, 723. **$^1\text{H-NMR}$** (400 MHz, CDCl_3) δ 7.70 (d, $J = 8.3$ Hz, 2H), 7.33 (d, $J = 8.0$ Hz, 2H), 5.32 (s, 1H), 4.60 (dd, $J = 5.2, 1.1$ Hz, 1H), 3.88 (s, 3H), 3.00 (dd, $J = 4.0, 1.1$ Hz, 1H), 2.63 (s, 3H), 2.43 (s, 3H), 1.66 (dd, $J = 5.2, 4.0$ Hz, 1H), 1.43 (s, 9H). **$^{13}\text{C-NMR}$** (101 MHz, CDCl_3) δ 168.7, 165.0, 144.3, 135.0, 130.1, 127.5, 104.1, 82.3, 69.9, 68.0, 54.1, 30.3, 28.2, 24.6, 23.5, 21.7. **HRMS** (ESI): m/z calculated for $\text{C}_{20}\text{H}_{27}\text{ClNO}_7\text{S}$ [MH^+]: 460.1191, found 460.1196. **mp**: 122 - 124 °C.



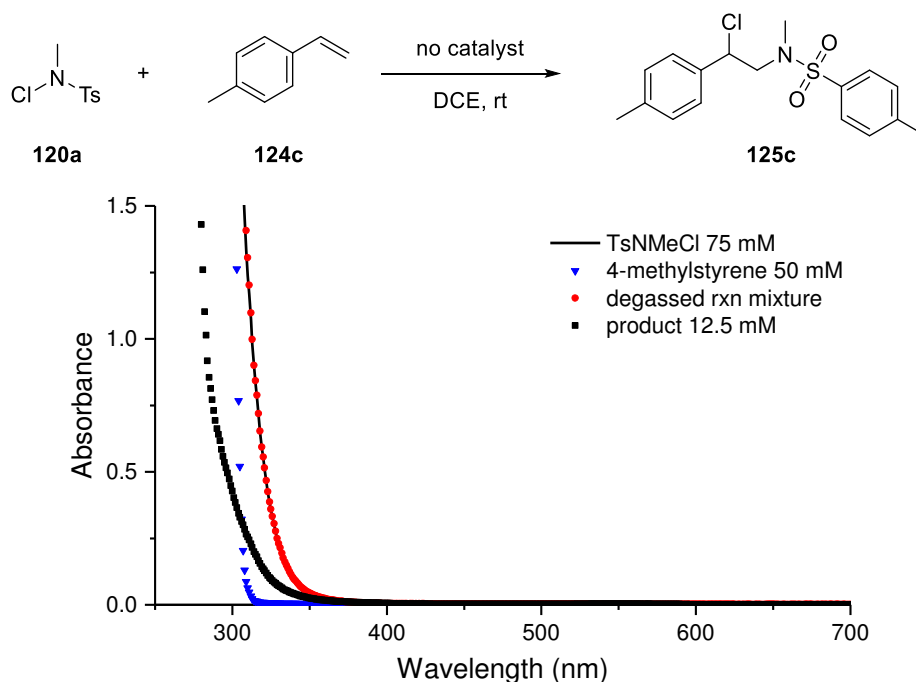
***N*-(2-chloro-2-phenylethyl)-*N*-methyl-4-nitrobenzenesulfonamide (**129b**)**

According to general procedure, **129b** was prepared from distilled styrene (**124e**) (34 μL , 0.30 mmol, 1.0 equiv) and *N*-chloro-*N*-methyl-4-nitrobenzenesulfonamide (**128b**) (112.8 mg, 0.45 mmol, 1.5 equiv) using $[\text{Cu}(\text{dap})_2]\text{Cl}$ (2.7 mg, 0.003 mmol, 1.0 mol%) as a catalyst. The crude product (4.8 mL of the original reaction mixture) was purified by column chromatography on silica gel (hexanes:EtOAc 15:1, $R_f = 0.09$) to afford **129b** as a light yellow oil (79.2 mg, 93% yield). **IR** (neat, cm^{-1}) 3105, 3034, 2930, 2868, 1606, 1528 (vs), 1454, 1349, 1311, 1163, 1088, 932, 857, 758, 742, 697. **$^1\text{H-NMR}$** (400 MHz, CDCl_3) δ 8.34 (d, $J = 8.7$ Hz, 2H), 7.93 (d, $J = 8.7$ Hz, 2H), 7.48 – 7.32 (m, 5H), 5.10 (t, $J = 7.3$ Hz, 1H), 3.66 (dd, $J = 14.6, 7.6$ Hz, 1H), 3.51 (dd, $J = 14.5, 7.1$ Hz, 1H), 2.73 (s, 3H). **$^{13}\text{C-NMR}$** (101 MHz, CDCl_3) δ 150.3, 144.0, 138.3, 129.3, 129.1, 128.6, 127.6, 124.6, 61.0, 58.1, 36.9. **HRMS** (ESI): m/z calculated for $\text{C}_{15}\text{H}_{16}\text{ClN}_2\text{O}_4\text{S}$ [MH^+]: 355.0514, found 355.0517. The data are in accordance with the data reported in the literature.^[156]

***N*-(2-(1,3-dioxoisindolin-2-yl)-1-phenylethyl)acetamide (**138**)**

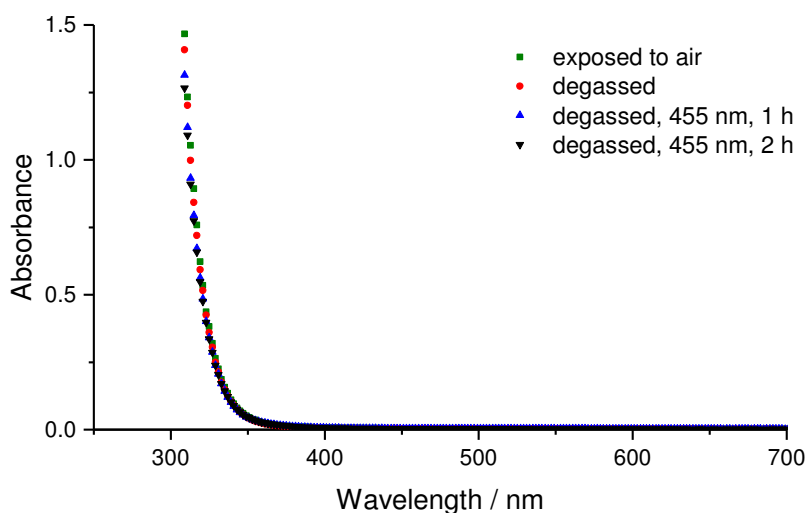
An oven dried pressure tube (25 mL size) equipped with a magnetic stir bar was charged with *N*-(trifluoromethyl)acyloxypthalimide (**130**) (233.2 mg, 0.90 mmol, 1.5 equiv), *fac*-Ir(ppy)₃ (3.9 mg, 0.006 mmol, 1.0 mol%) and anhydrous acetonitrile (12.0 mL). The mixture was degassed using three freeze-pump-thaw cycles. Distilled styrene (**124e**) (69 μ L, 0.60 mmol, 1.0 equiv) was added under a slight nitrogen overpressure and the tube was equipped with a light emitting LED-stick and sealed. The reaction mixture was irradiated at room temperature with a blue LED (λ_{max} = 455 nm) while being stirred and the reaction progress was monitored by TLC. After 18 h, the reaction was stopped by switching off the light source and a sample of 0.20 mL of the crude reaction mixture was taken for measurements. For determining the yield by NMR, another sample of 1.00 mL was taken and 2-nitropropane was added as an internal standard. The remaining 10.80 mL of the crude reaction mixture were concentrated and the remaining brownish solid was diluted with 25 mL of saturated NaHCO₃ solution. The aqueous phase was extracted with EtOAc (3 x 25 mL). The combined organic layers were dried over Na₂SO₄, filtered and concentrated in vacuum. Purification by column chromatography on silica gel (mixtures of hexanes:EtOAc 2:1 to pure EtOAc, R_f = 0.37 in hexanes:EtOAc 1:3) afforded **138** as a white solid (65.0 mg, 39%). **IR** (neat, cm⁻¹) 3310, 3060, 2937, 1774, 1707, 1648, 1539, 1428, 1394, 1372, 1297, 1118, 1040, 957, 723, 701. **¹H-NMR** (400 MHz, CDCl₃) δ 7.85 (dd, J = 5.5, 3.1 Hz, 2H), 7.73 (dd, J = 5.5, 3.0 Hz, 2H), 7.41 – 7.31 (m, 4H), 7.33 – 7.27 (m, 1H), 6.51 (d, J = 7.7 Hz, 1H), 5.34 (ddd, J = 9.6, 8.0, 4.2 Hz, 1H), 4.05 – 3.93 (m, 2H), 1.94 (s, 3H). **¹³C-NMR** (75 MHz, CDCl₃) δ 170.0, 168.8, 138.9, 134.4, 131.8, 129.0, 128.1, 126.5, 123.7, 53.6, 43.0, 23.5. **HRMS** (ESI): m/z calculated for C₁₈H₁₇N₂O₃ [MH⁺]: 309.1234, found 309.1236. **mp**: 202 - 207 °C.

5.4 Absorption Spectra



All compounds were measured in concentrations used for the standard reaction conditions. Product **125c** was measured in a lower concentration of 12.5 mmol/L corresponding to a theoretical yield of 25%.

Figure 27. UV-Vis absorption spectra of *N*-chlorosulfonamide **120a** (TsNMeCl, black line), 4-methylstyrene (**124c**) (blue triangles), degassed reaction mixture of compound **125c** before irradiation with blue LED (455 nm) (red dots) and product **125c** (black squares) in DCE.



Mixture of TsNMeCl (**120a**) (75 mM) and 4-methylstyrene (**124c**) (50 mM) in DCE. Conditions: mixture exposed to air, no light irradiation (green squares); degassed mixture before light irradiation (red dots); degassed mixture after irradiation with blue LED (455 nm) for 1 h (blue triangles); degassed mixture after irradiation with blue LED for 2 h (black triangles).

Figure 28. UV-Vis absorption spectra of the reaction mixture of compound **125c** under different conditions.

5.5 Quantum Yield Determination

The quantum yield Φ of the visible light driven chloramination of various substituted styrenes with *N*-chloro-*N*,4-dimethylbenzenesulfonamide (**120a**) was determined using a method developed by E. Riedle *et al.*^[181] For irradiation, a blue LED (950 mA operating current, $\lambda_{\text{max}} = 455$ nm, OSRAM LD-CQ7P-1U3U) was used. The radiant power was measured with a commercial power meter (PowerMax USB - PS19Q Power Sensor from Coherent) using computer-aided read out with PowerMax software.

An oven-dried pressure tube was charged with *N*-chloro-*N*,4-dimethylbenzenesulfonamide (**120a**) (66.0 mg, 0.30 mmol, 1.5 equiv) and [Cu(dap)₂]Cl (1.8 mg, 2.0 μ mol, 1.0 mol%) under nitrogen atmosphere. Anhydrous 1,2-dichloroethane (4.00 mL) was added and the reaction mixture was degassed by three pump-freeze-thaw cycles. Styrene derivative **124** (0.20 mmol, 1.0 equiv) was added under a slight nitrogen overpressure. An oven dried fluorescence cuvette equipped with a magnetic stir bar and a septum was flushed with nitrogen. Immediately prior to the quantum yield measurement, 2.00 mL of the reaction solution (corresponding to 0.10 mmol of styrene derivative) was transferred to the measuring cuvette under a nitrogen atmosphere. In order to minimize ambient light, the measurement was accomplished in a dark room. The radiant power of light transmitted by the cuvette with a blank solution (P_{ref}) was measured. The cuvette with the blank solution was exchanged by the cuvette containing the reaction mixture and the transmitted radiant power (P_{sample}) was determined. The transmitted radiant power was monitored during the whole irradiation and remained constant. The sample was irradiated for the indicated time while being stirred (cf. Table 29) and the yield was determined by ¹H-NMR analysis using 2-nitropropane as internal standard. It should be noted that the light power at the sample was significantly lower than in the standard reaction setup with the irradiation via LED-stick.

The quantum yield Φ was calculated as follows:

$$\Phi = \frac{N_{\text{prod}}}{N_{\text{ph,abs}}} = \frac{n_{\text{prod}} * N_A * h * c}{P_{\text{abs}} * \Delta t * \lambda} = \frac{n_{\text{prod}} * N_A * h * c}{(P_{\text{ref}} - P_{\text{sample}}) * f * \Delta t * \lambda}$$

Here, Φ is the quantum yield, N_{prod} is the number of molecules created, $N_{\text{ph,abs}}$ is the number of photons absorbed, N_A is Avogadro's constant in mol⁻¹, n_{prod} is the molar amount of product molecules created in mol, P_{abs} is the radiant power absorbed in Watt, Δt is the irradiation time in seconds, h is Planck's constant in Js, c is the speed of light in ms⁻¹, λ is the wavelength of the irradiation source in meters, P_{ref} is the radiant power transmitted by a blank cuvette in

Watt, P_{sample} is the radiant power transmitted by the cuvette with the reaction mixture in Watt and f is a correction factor. The correction factor f depends on the reflection coefficient R of the air-glass-interface. Neglecting second order effects, f can be calculated from:

$$f = \frac{1 + R * \frac{P_{\text{sample}}}{P_{\text{ref}}}}{1 - R}$$

For a fused silica cuvette and $\lambda = 443 \text{ nm}$, $R = 0.0357$.

$$P_{\text{abs}} = (P_{\text{ref}} - P_{\text{sample}}) * f$$

Example using the data of entry 1, Table 29:

$$f = \frac{1 + R * \frac{P_{\text{sample}}}{P_{\text{ref}}}}{1 - R} = \frac{1 + 0.0357 * \frac{99.9\text{mW}}{100.5\text{mW}}}{1 - 0.0357} = 1.0738$$

$$\begin{aligned}\Phi &= \frac{n_{\text{prod}} * N_{\text{A}} * h * c}{(P_{\text{ref}} - P_{\text{sample}}) * f * \Delta t * \lambda} = \\ &= \frac{0.030 * 10^{-3} \text{mol} * 6.022 * 10^{23} \text{mol}^{-1} * 6.626 * 10^{-34} \text{Js} * 2.998 * 10^8 \text{ms}^{-1}}{(100.5 - 99.9) * 10^{-3} \text{Js}^{-1} * 1.0738 * 21600 \text{s} * 455 * 10^{-9} \text{m}} = 0.567 \\ &\cong 57\%\end{aligned}$$

Table 29. Results of quantum yield measurements.

R -C₆H₄-CH=CH₂ + Cl-N(CH₃)₂-C₆H₄-CH₃

Catalyst (1 mol%),
 DCE, 455 nm, rt

R -C₆H₄-CH(Cl)-CH₂-N(CH₃)₂-C₆H₄-CH₃

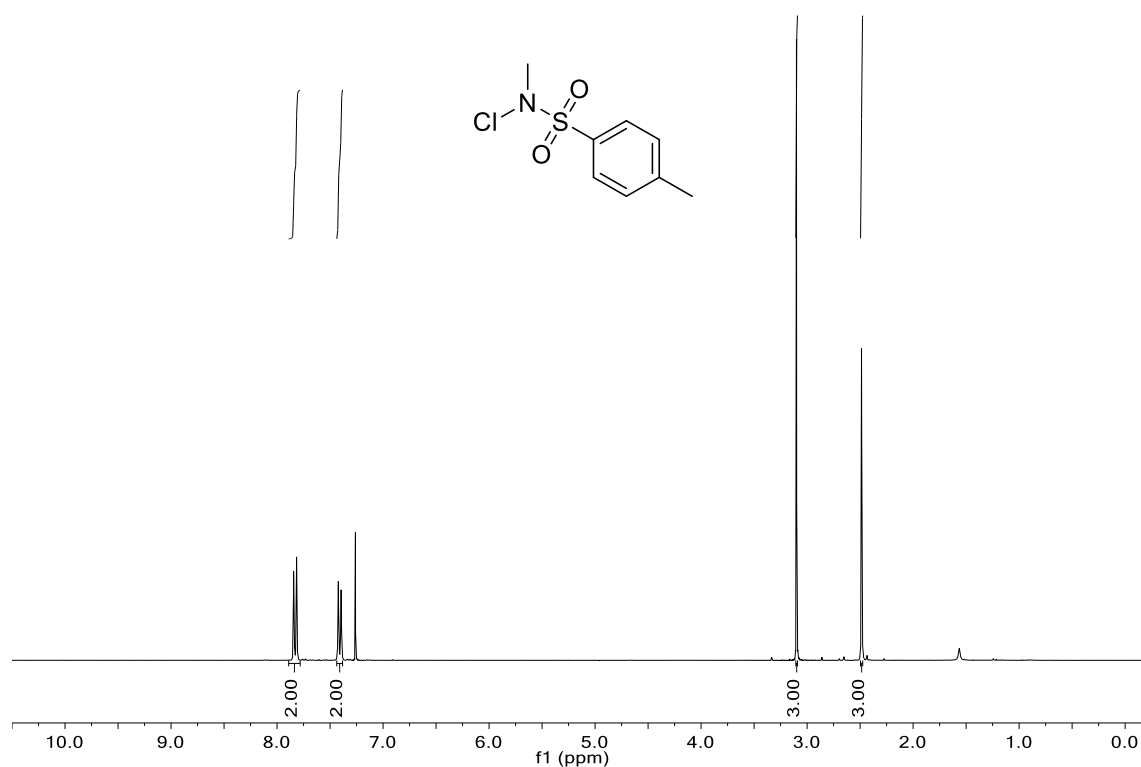
124 **120a** **125**

Entry	Product	Catalyst	Δt / h	P_{ref} / mW	P_{sample} / mW	P_{abs} / mW	NMR Yield	Φ
1	 125c	no	6	100.5	99.9	0.64	30%	57%
2		[Ir]	1	97.6	7.6	93.6	39%	3%
3		[Cu]	1	96.6	6.2	94.0	41%	3%
4	 125k	no	6	102.0	99.8	2.36	4%	2%
5		[Ir]	1	99.7	6.4	97.0	27%	2%
6		[Cu]	1	99.6	6.1	97.2	34%	3%
7	 125o	[Ir]	1	99.7	6.1	97.3	9%	0.7%
8		[Cu]	1	99.4	7.6	95.5	18%	1.4%

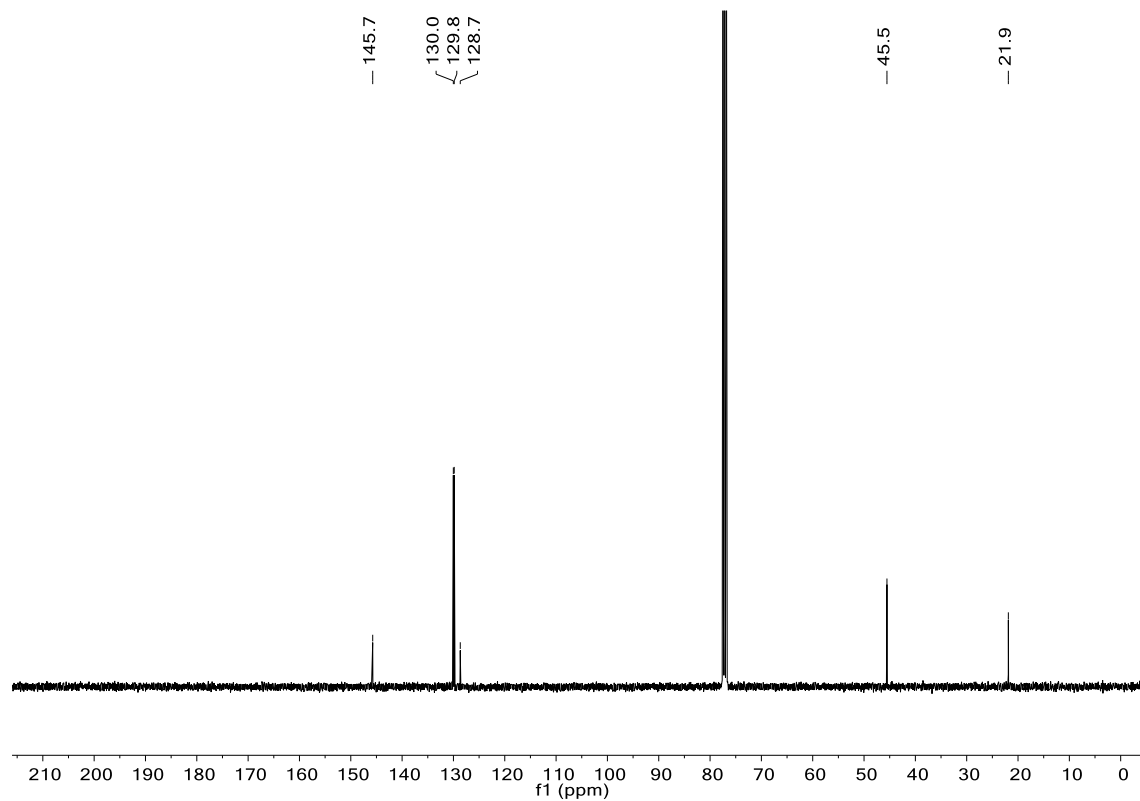
Reaction conditions: *N*-chloro-*N*,4-dimethylbenzenesulfonamide (**120a**) (1.5 equiv, 0.15 mmol), catalyst (1.0 mol%), anhydrous DCE (2.00 mL), degassed solution, alkene (0.10 mmol, 1.0 equiv), rt, irradiation with blue LED (455 nm), stirred reaction mixture. The NMR yields were determined by ^1H -NMR using 2-nitropropane as internal standard. Used catalysts: $[\text{Cu}(\text{dap})_2]\text{Cl}$ (**[Cu]**), $[\text{Ir}(\text{ppy})_2(\text{dtbbpy})]\text{PF}_6$ (**[Ir]**) or no catalyst (no).

5.6 NMR and IR Spectra

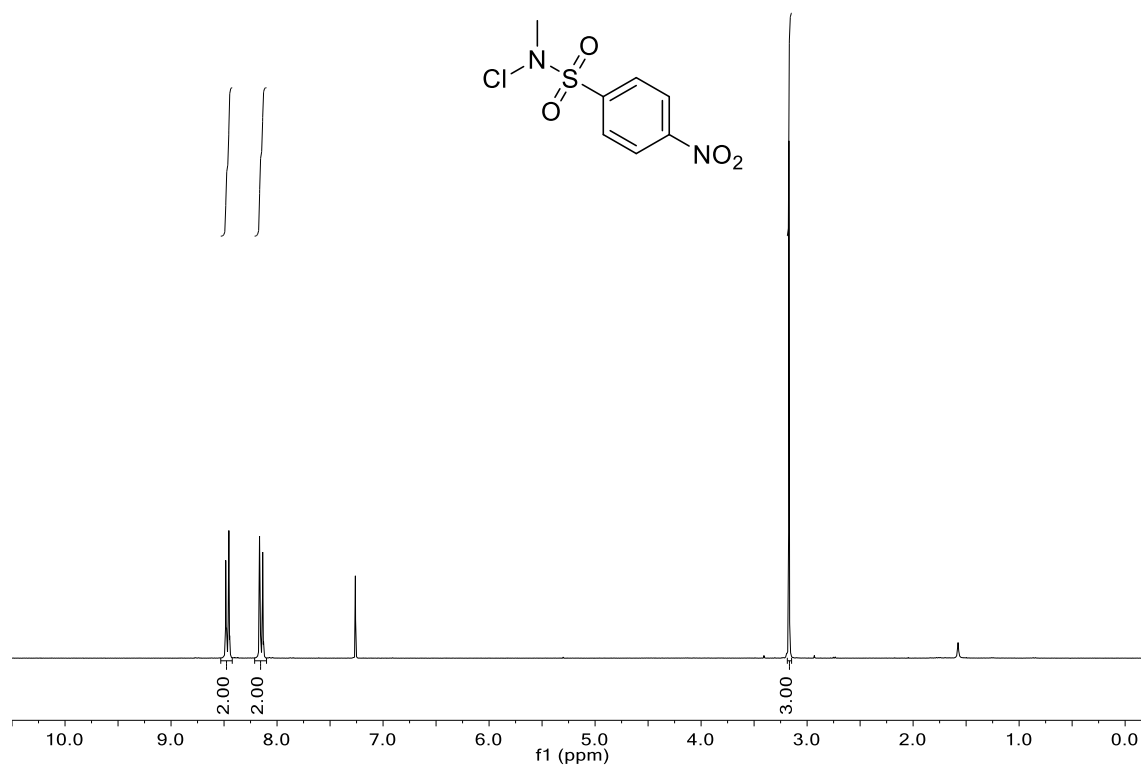
N-chloro-*N*,4-dimethylbenzenesulfonamide (**120a**): ^1H -NMR



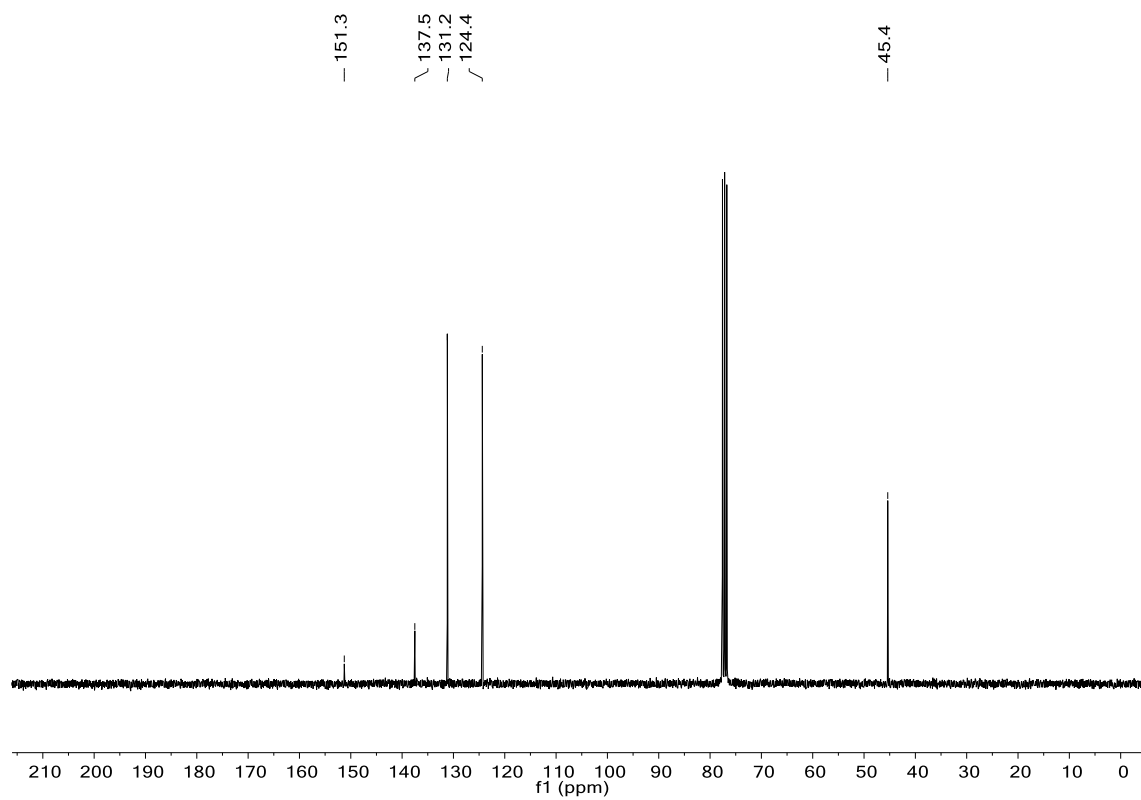
^{13}C -NMR



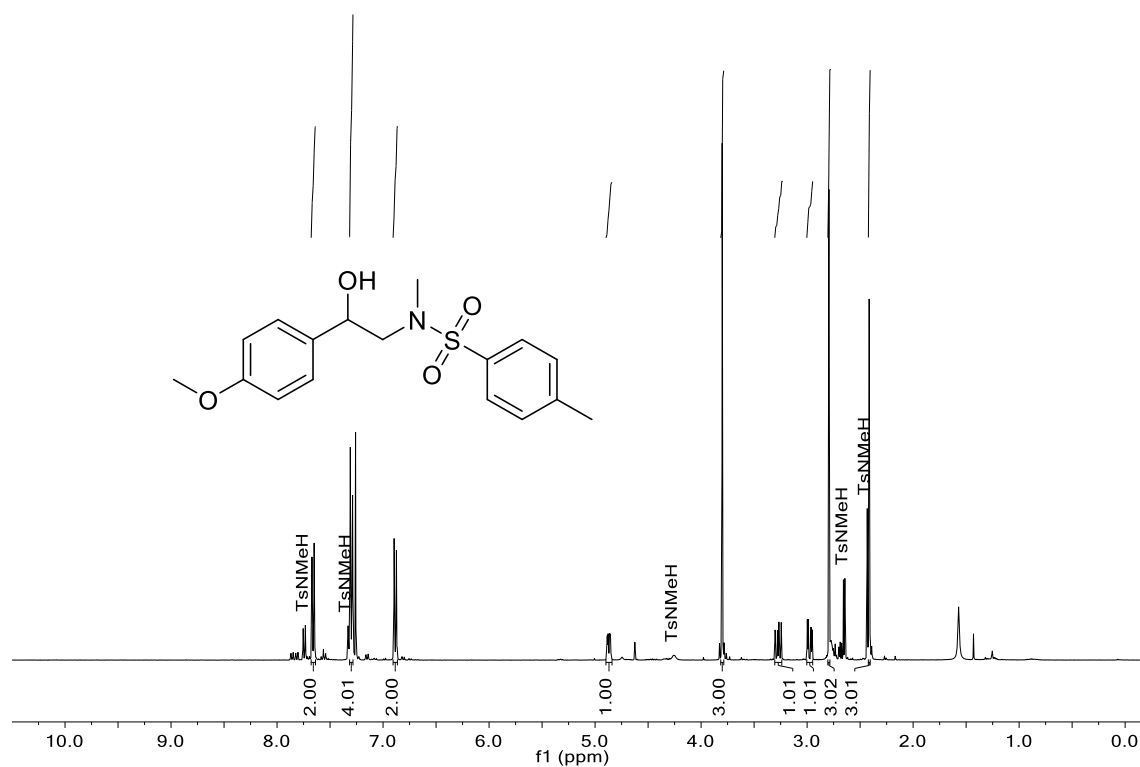
N-chloro-*N*-methyl-4-nitrobenzenesulfonamide (**128b**): ^1H -NMR



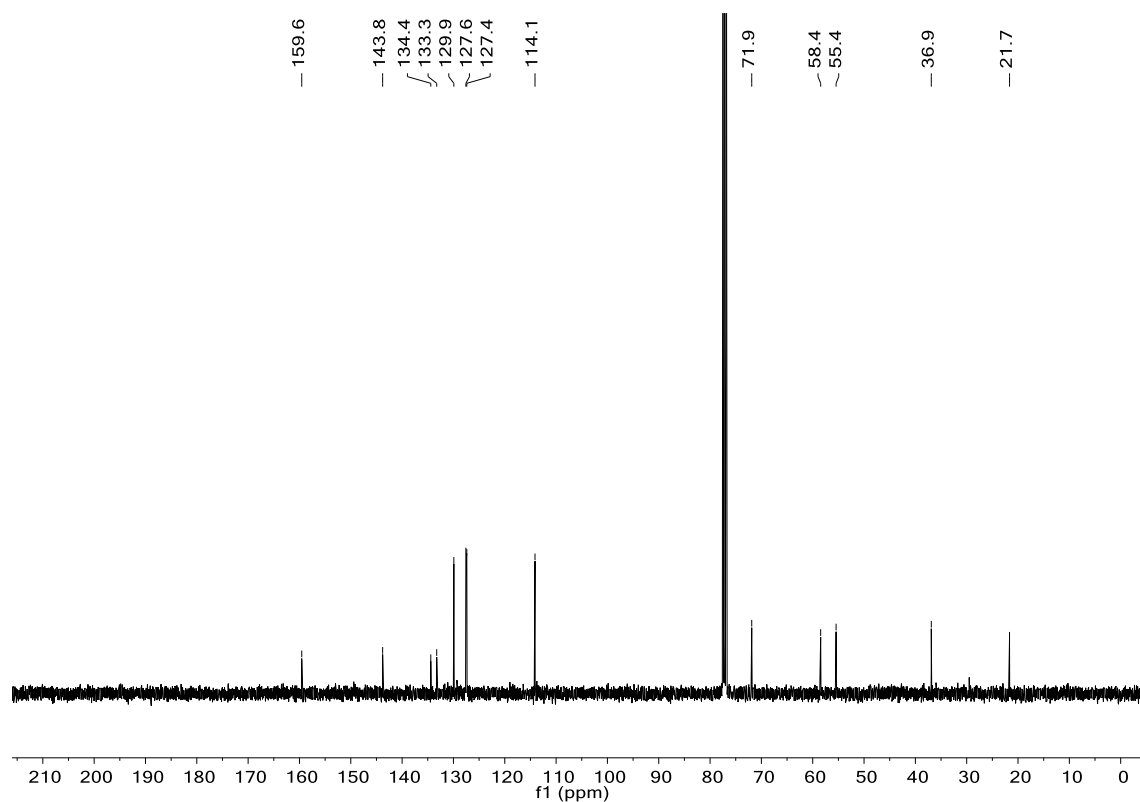
^{13}C -NMR

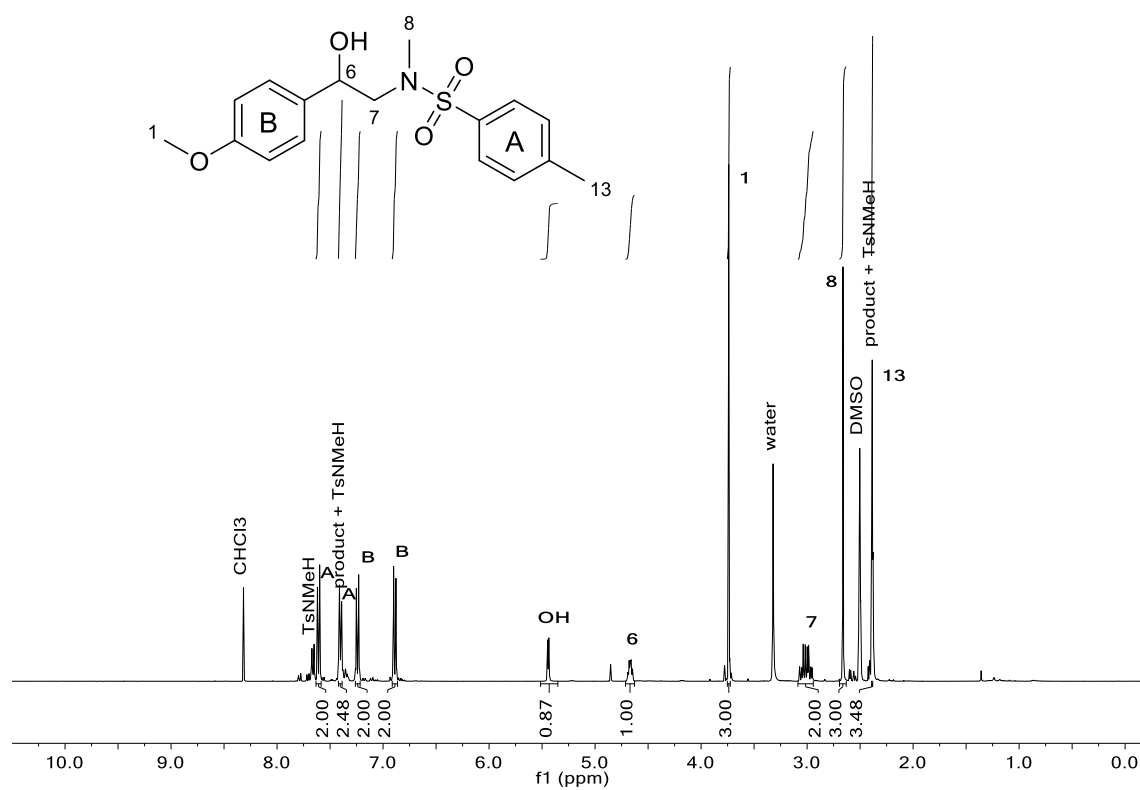
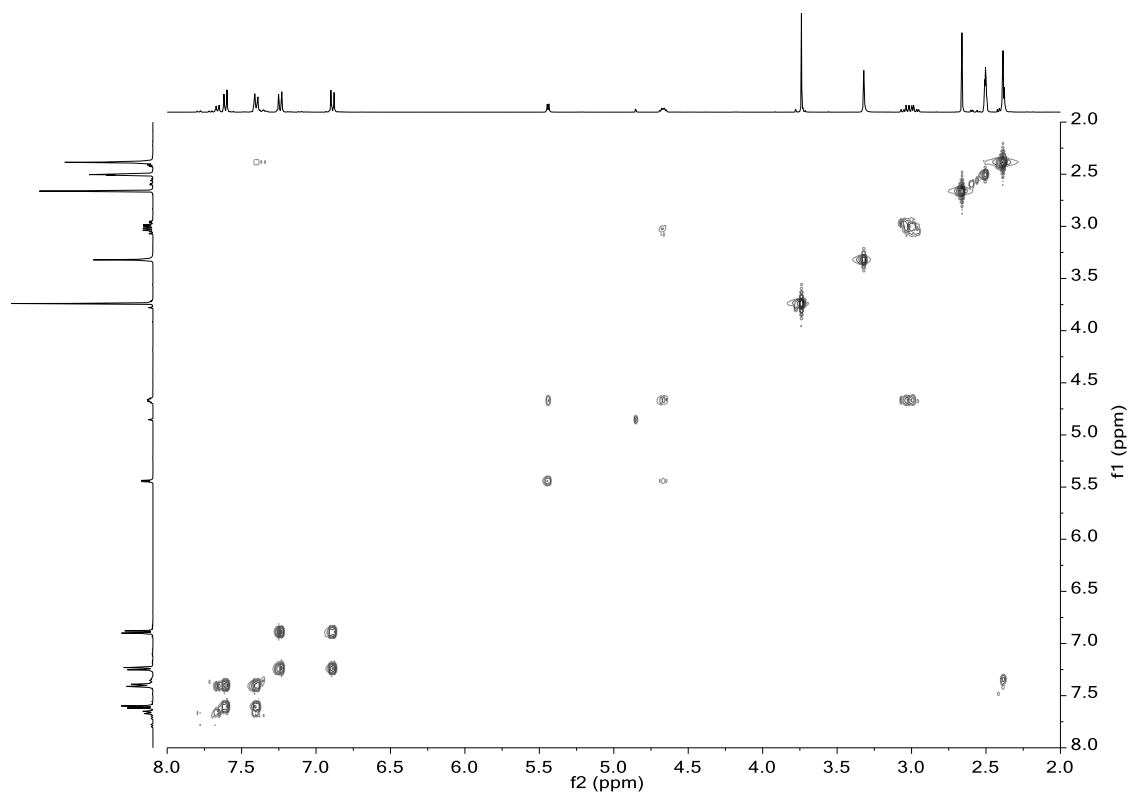


N-(2-hydroxy-2-(4-methoxyphenyl)ethyl)-*N*,4-dimethylbenzenesulfonamide (**125a**): ^1H -NMR (CDCl_3)

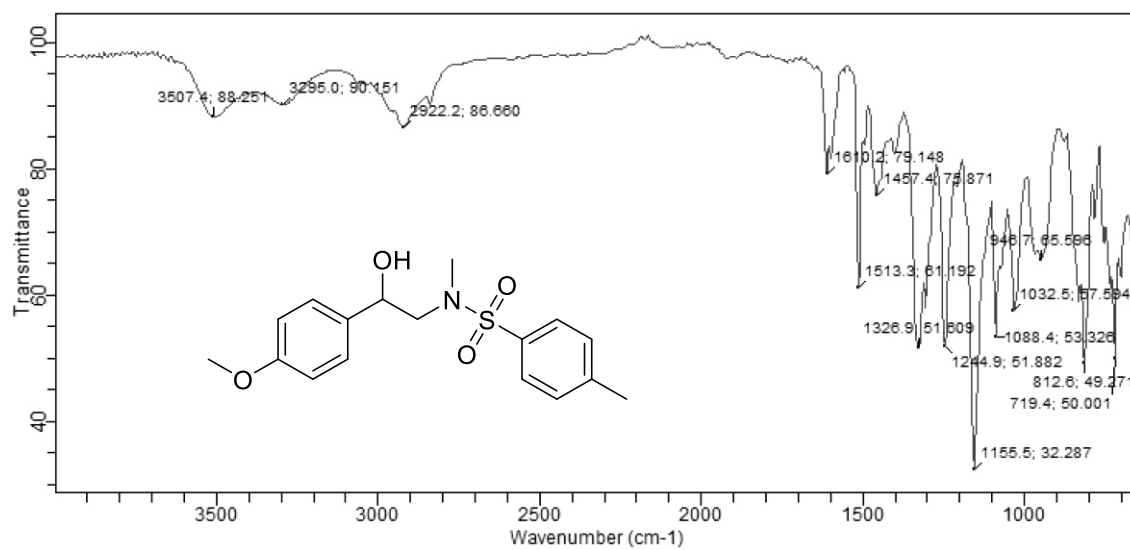


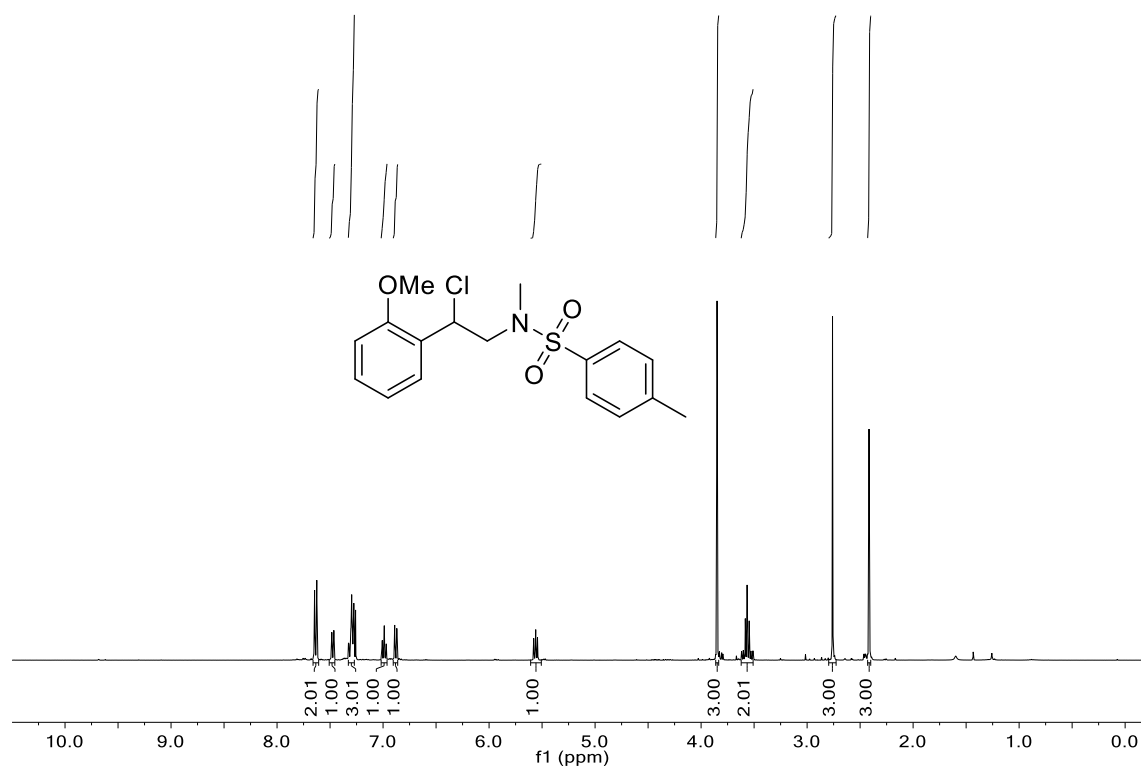
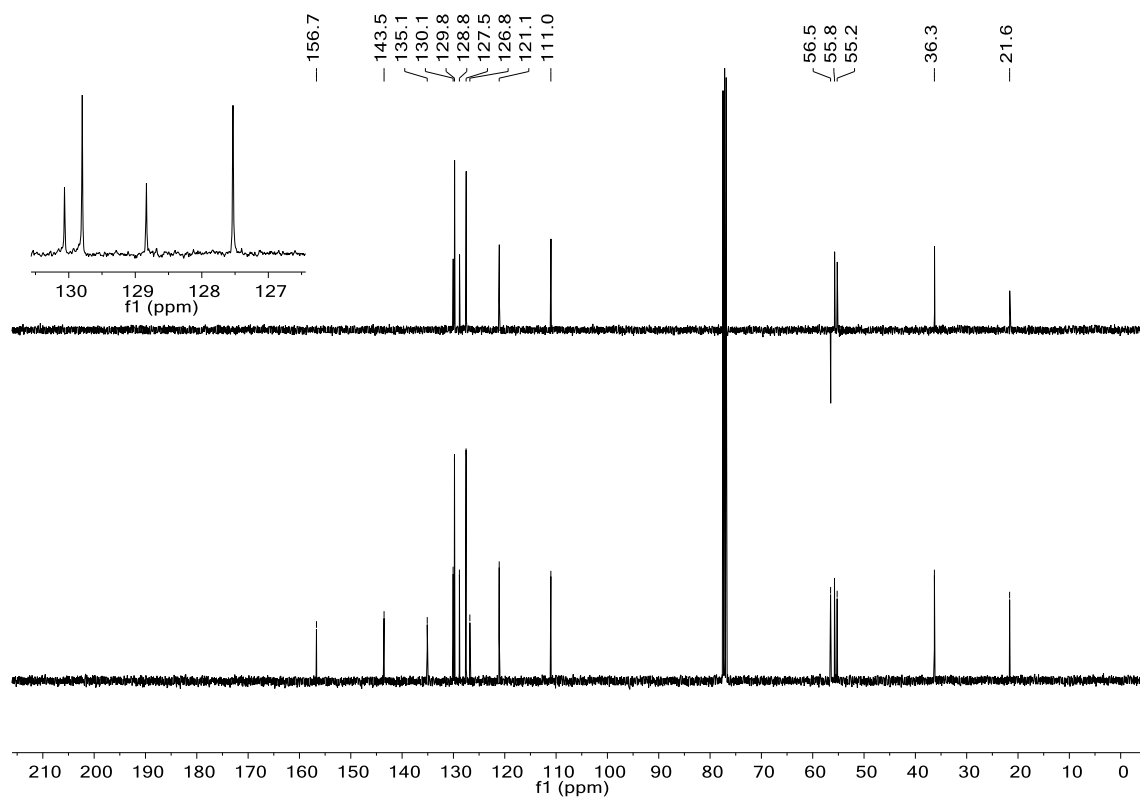
^{13}C -NMR (CDCl_3)

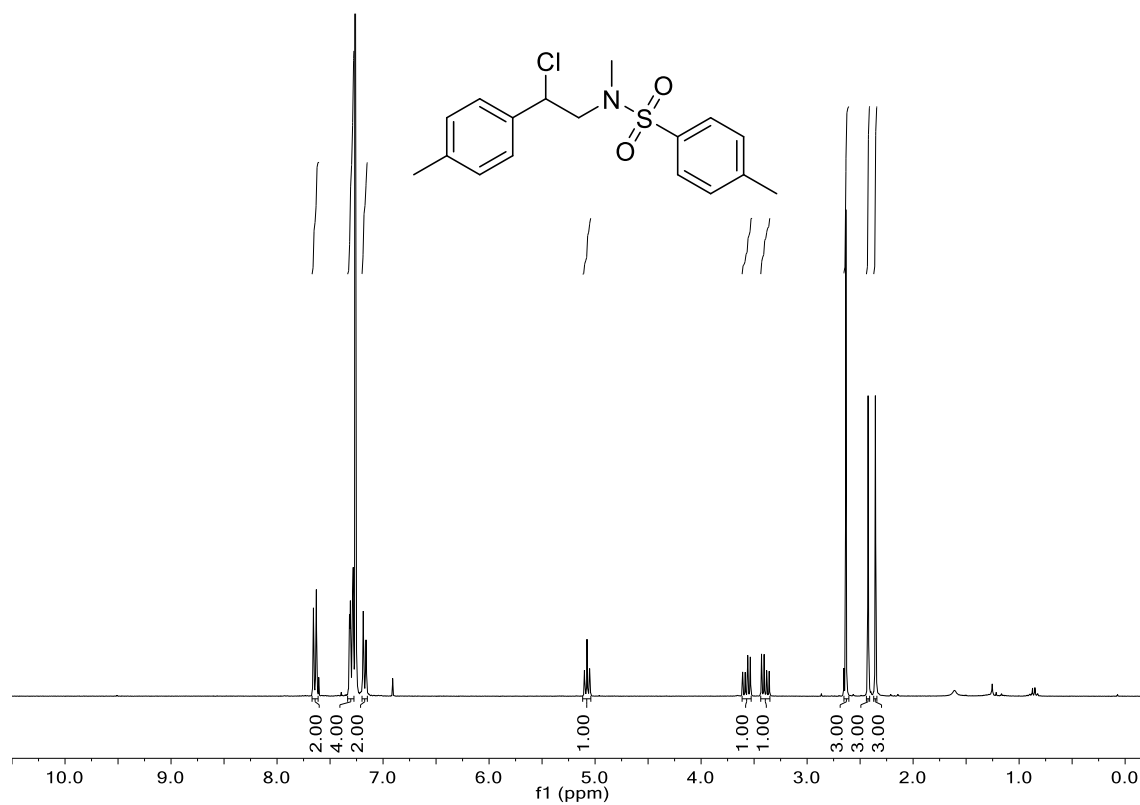
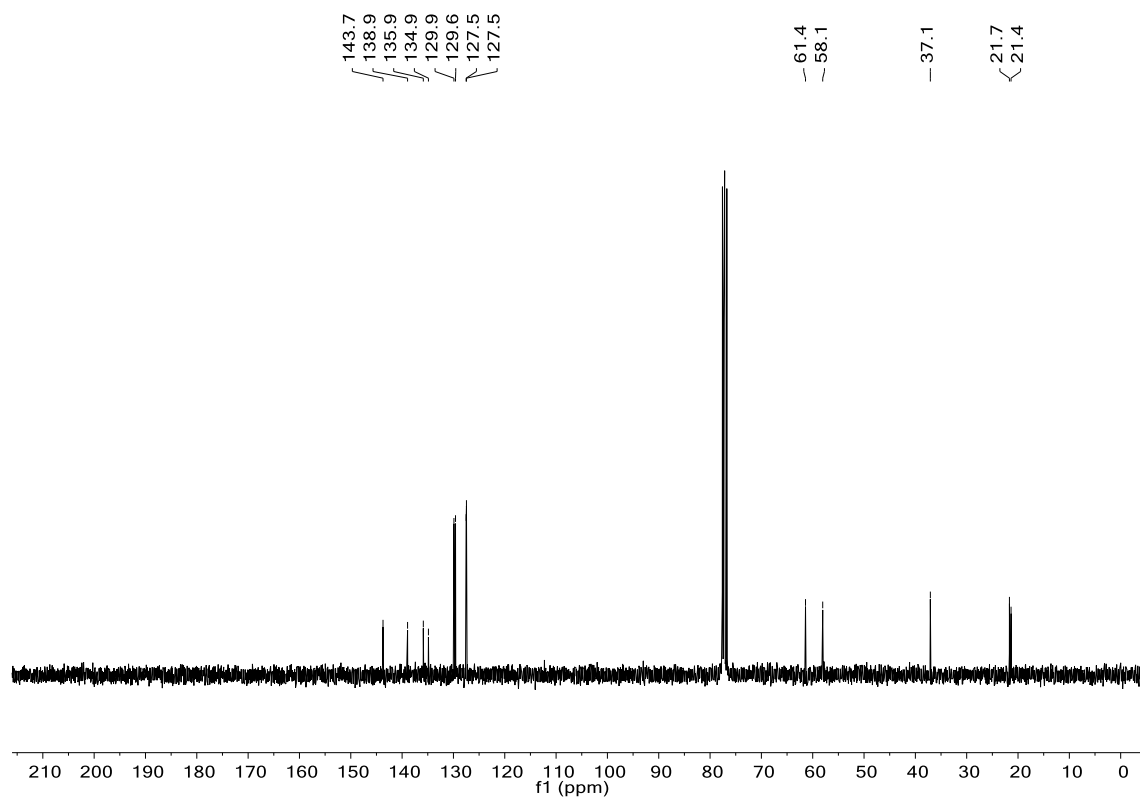


$^1\text{H-NMR}$ (DMSO-d_6)COSY (DMSO-d_6)

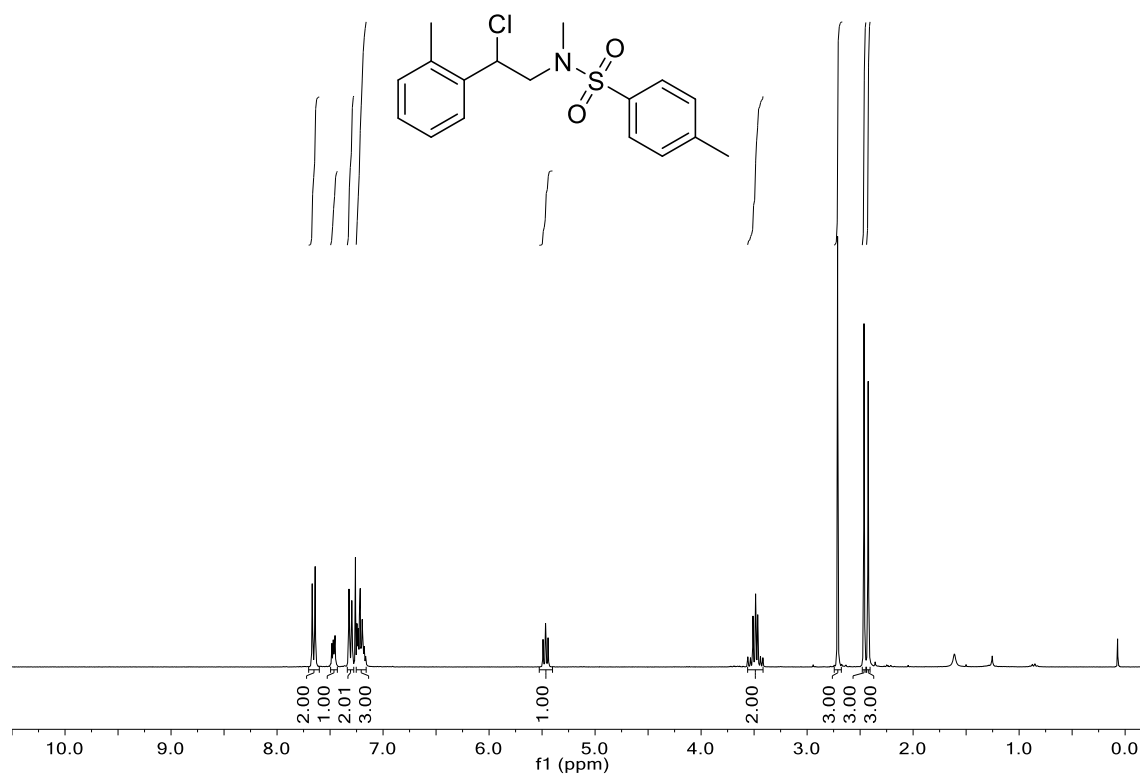
IR Spectrum



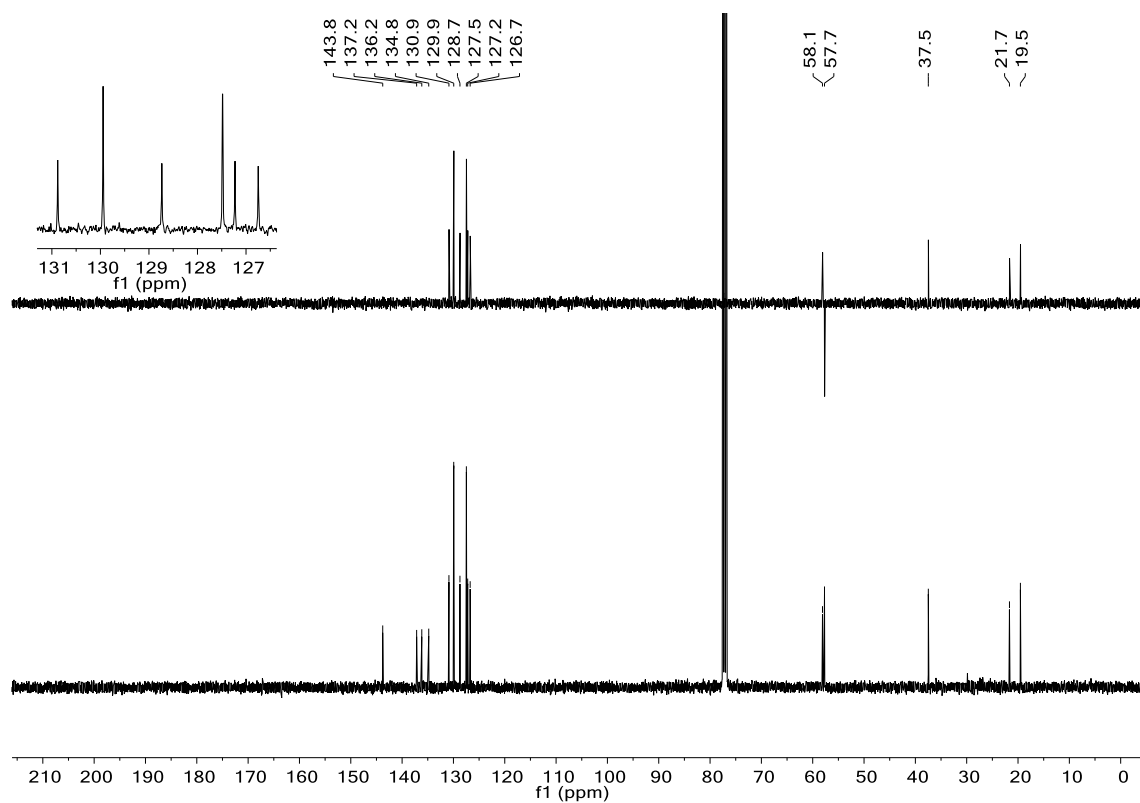
N-(2-chloro-2-(2-methoxyphenyl)ethyl)-*N*,4-dimethylbenzenesulfonamide (**125b**): ^1H -NMR ^{13}C -NMR and DEPT-135

N-(2-chloro-2-(*p*-tolyl)ethyl)-*N*,4-dimethylbenzenesulfonamide (**125c**): ^1H -NMR ^{13}C -NMR

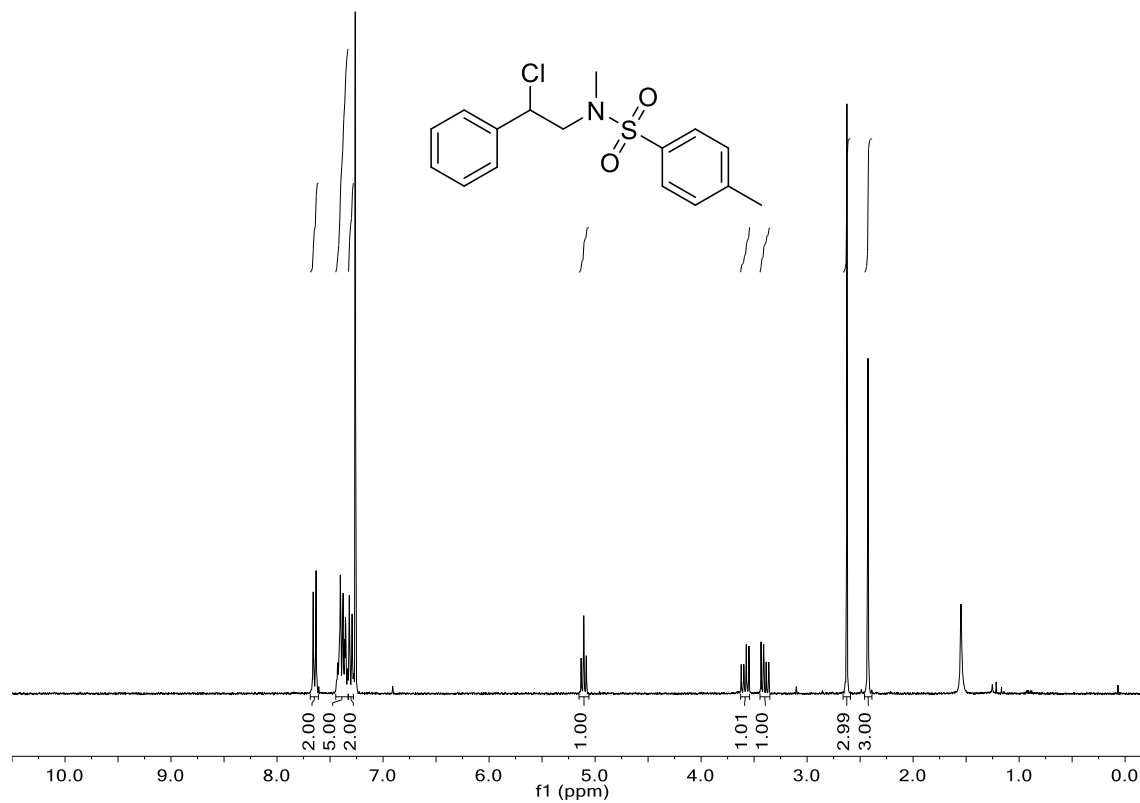
N-(2-chloro-2-(*o*-tolyl)ethyl)-*N*,4-dimethylbenzenesulfonamide (**125d**): ^1H -NMR



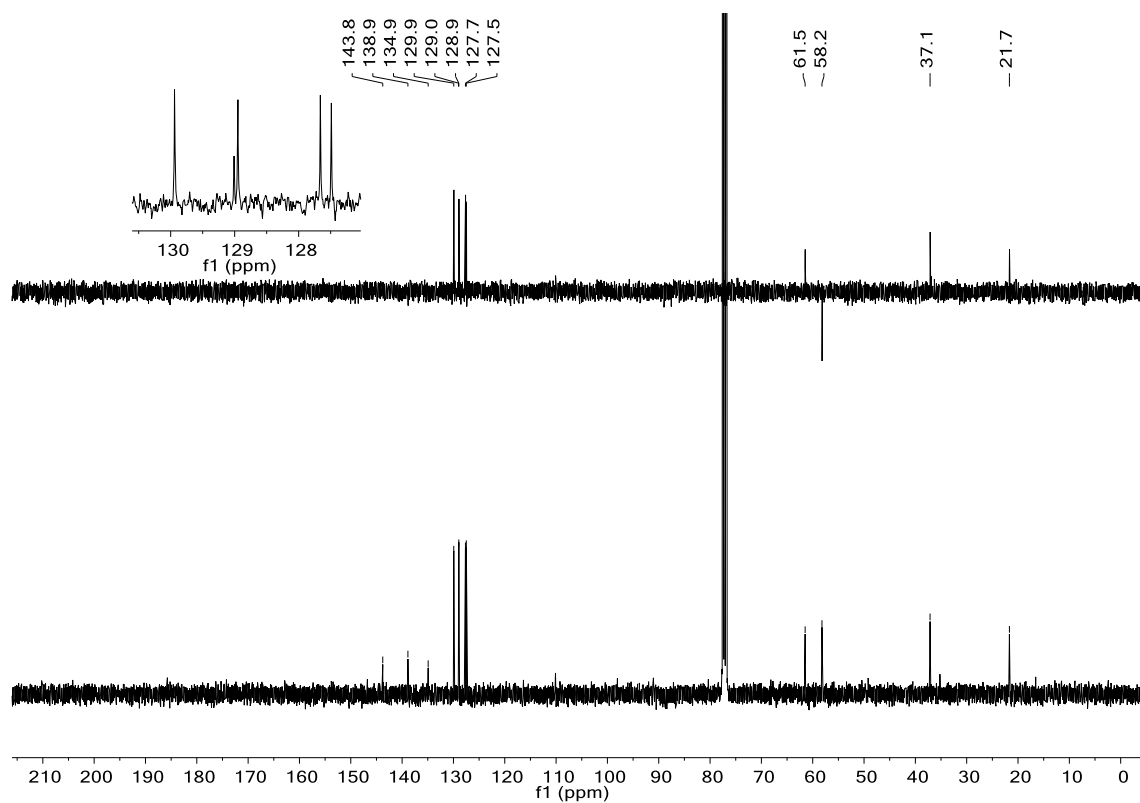
^{13}C -NMR and DEPT-135

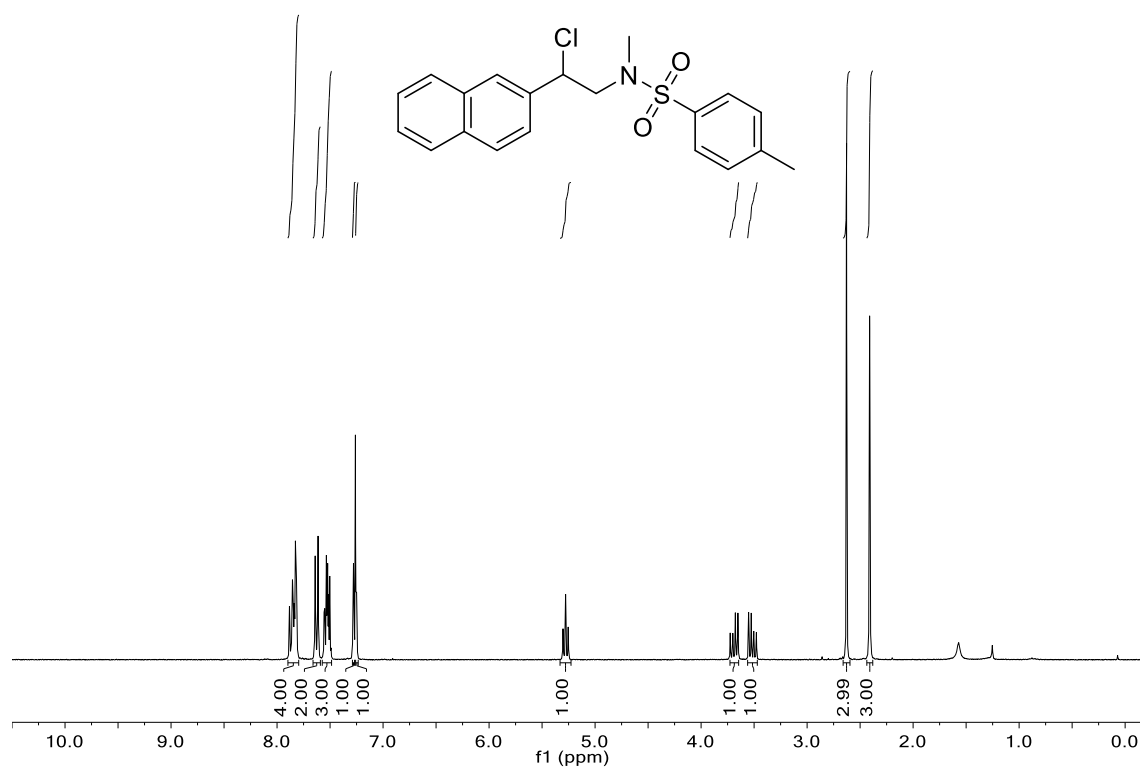
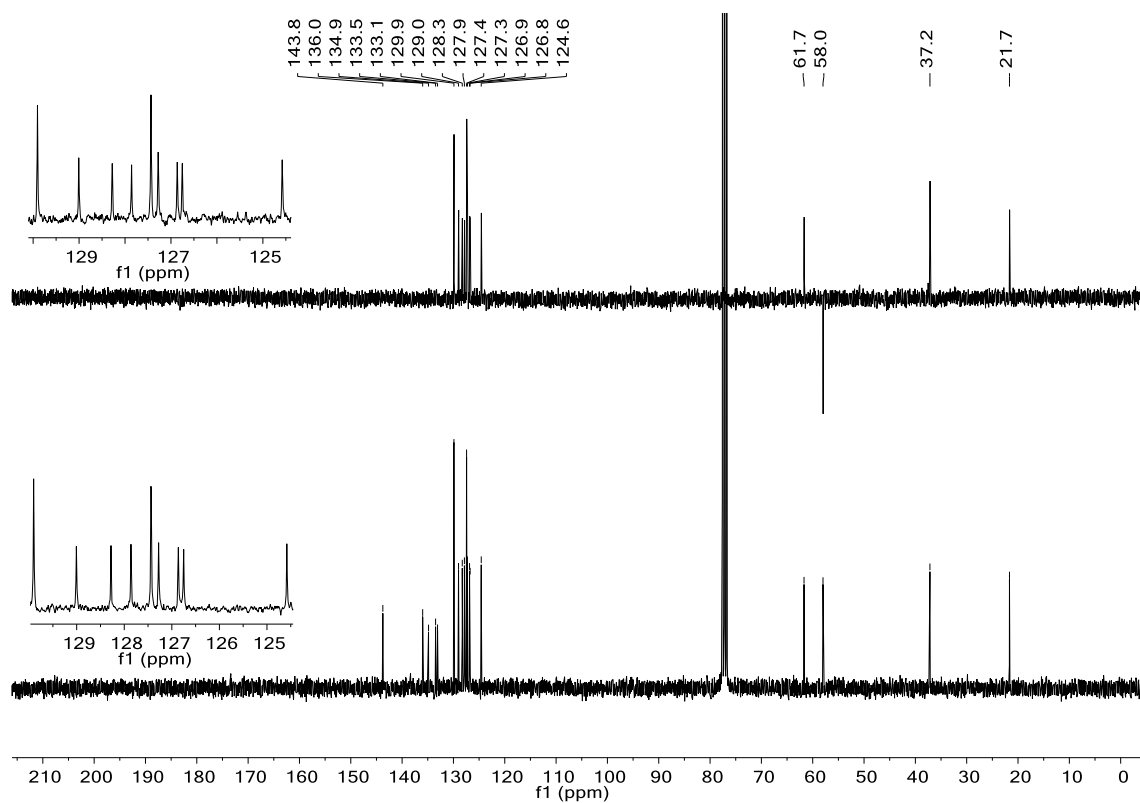


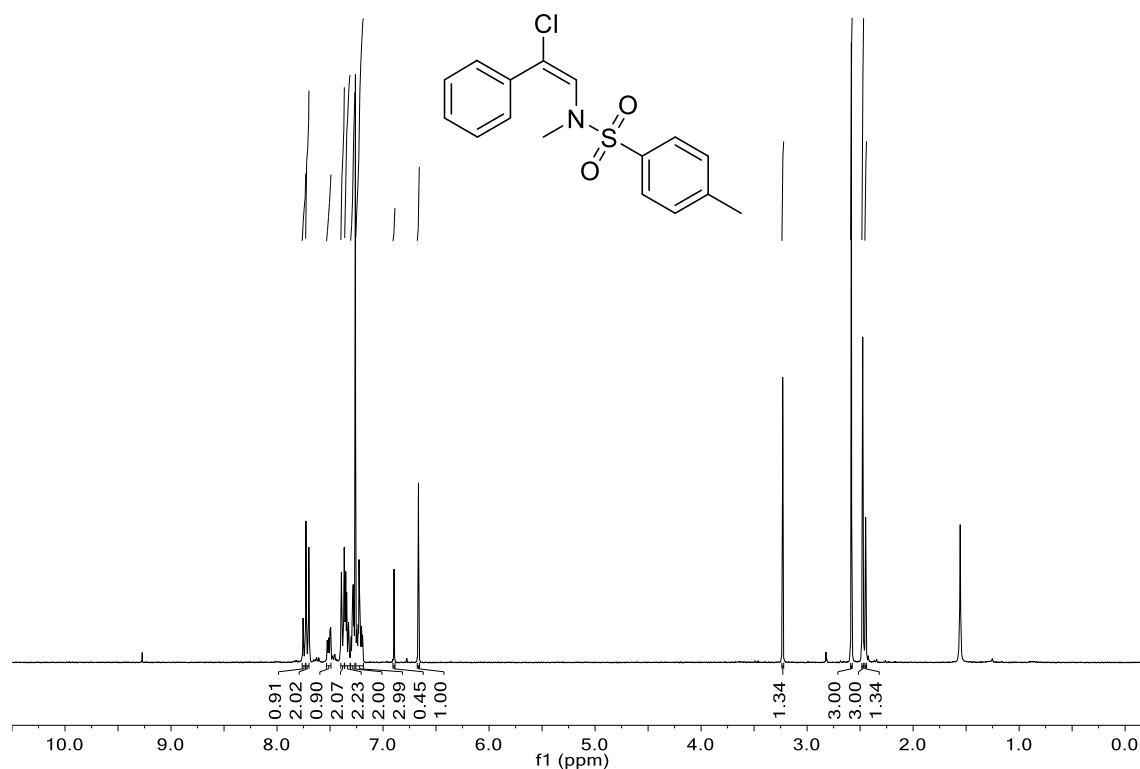
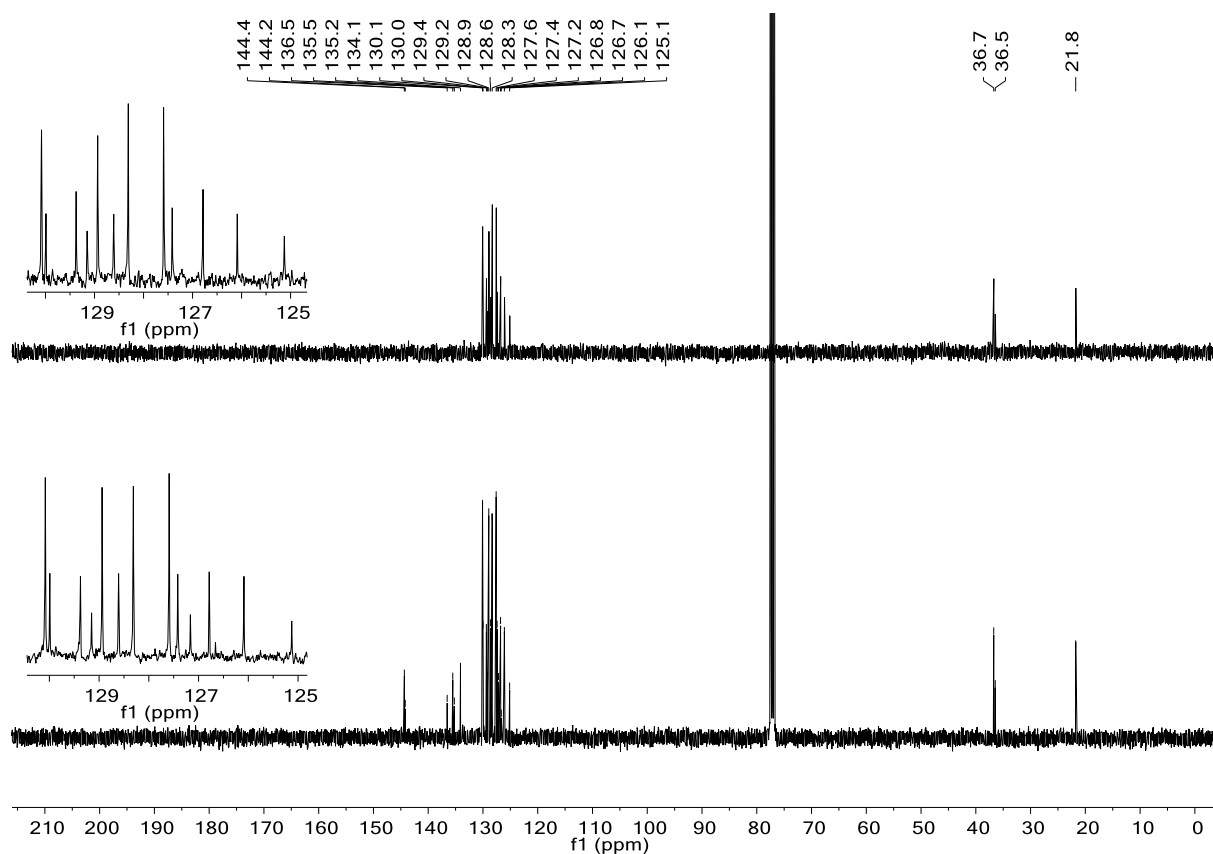
N-(2-chloro-2-phenylethyl)-*N*,4-dimethylbenzenesulfonamide (**125e**): ^1H -NMR



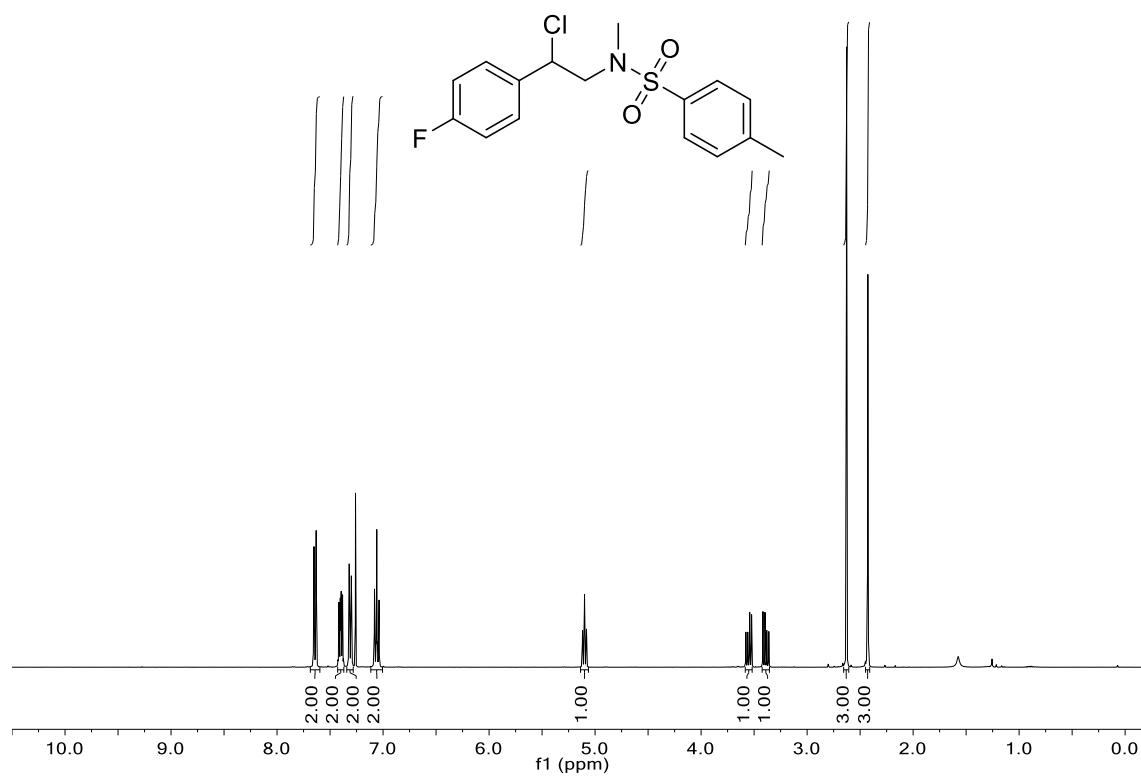
^{13}C -NMR and DEPT-135



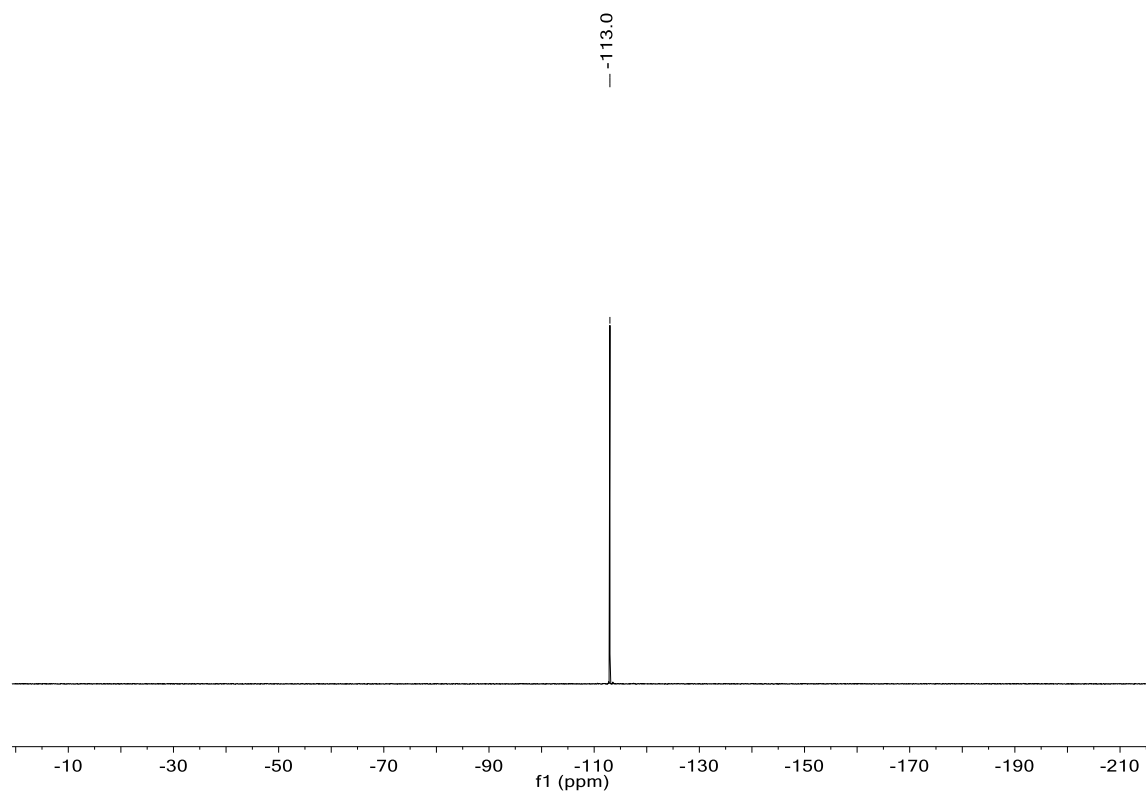
N-(2-chloro-2-(naphthalen-2-yl)ethyl)-*N*,4-dimethylbenzenesulfonamide (**125g**): ^1H -NMR ^{13}C -NMR and DEPT-135

N-(1-chloro-1-phenylprop-1-en-2-yl)-*N*,4-dimethylbenzenesulfonamide (**125h**): ^1H -NMR ^{13}C -NMR and DEPT-135

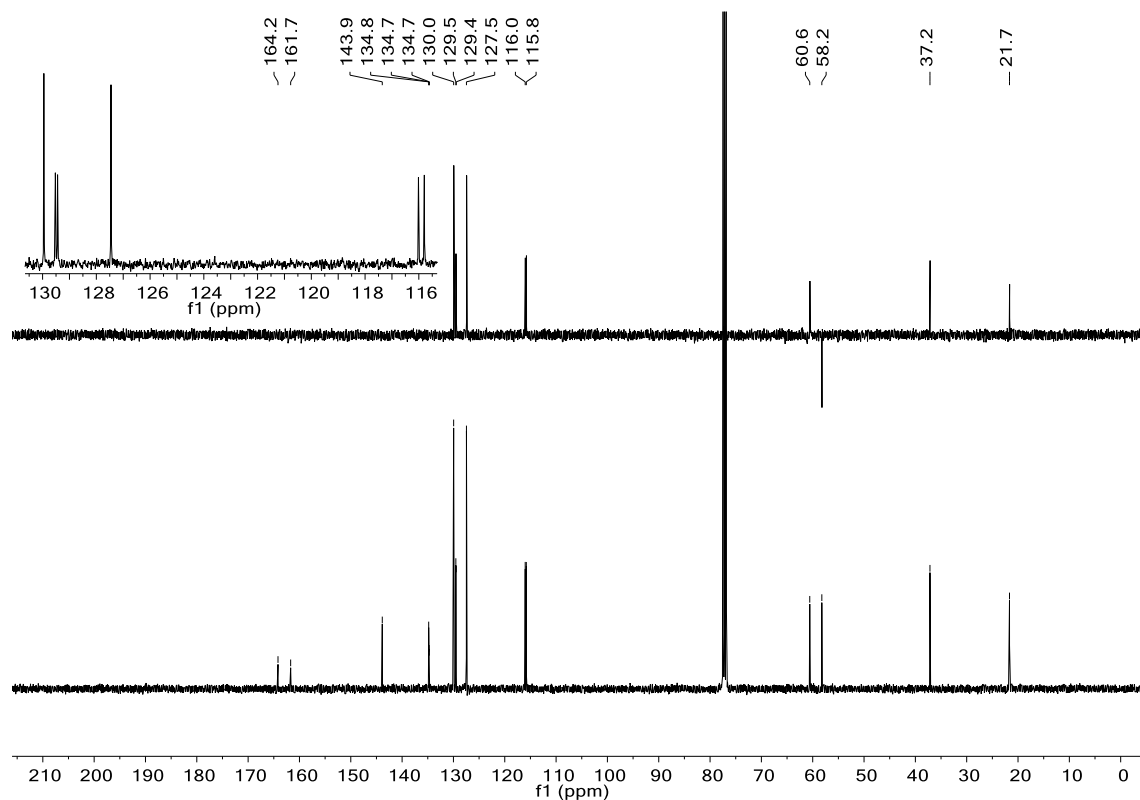
N-(2-chloro-2-(4-fluorophenyl)ethyl)-*N*,4-dimethylbenzenesulfonamide (**125i**): ^1H -NMR

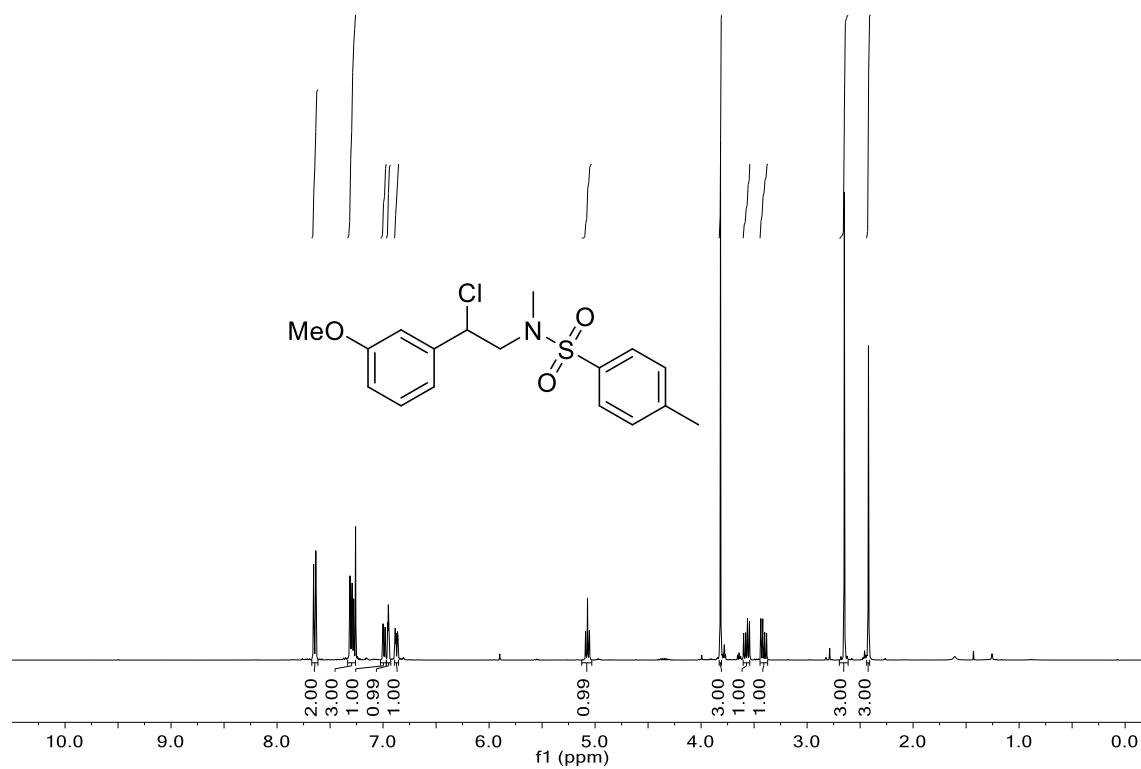
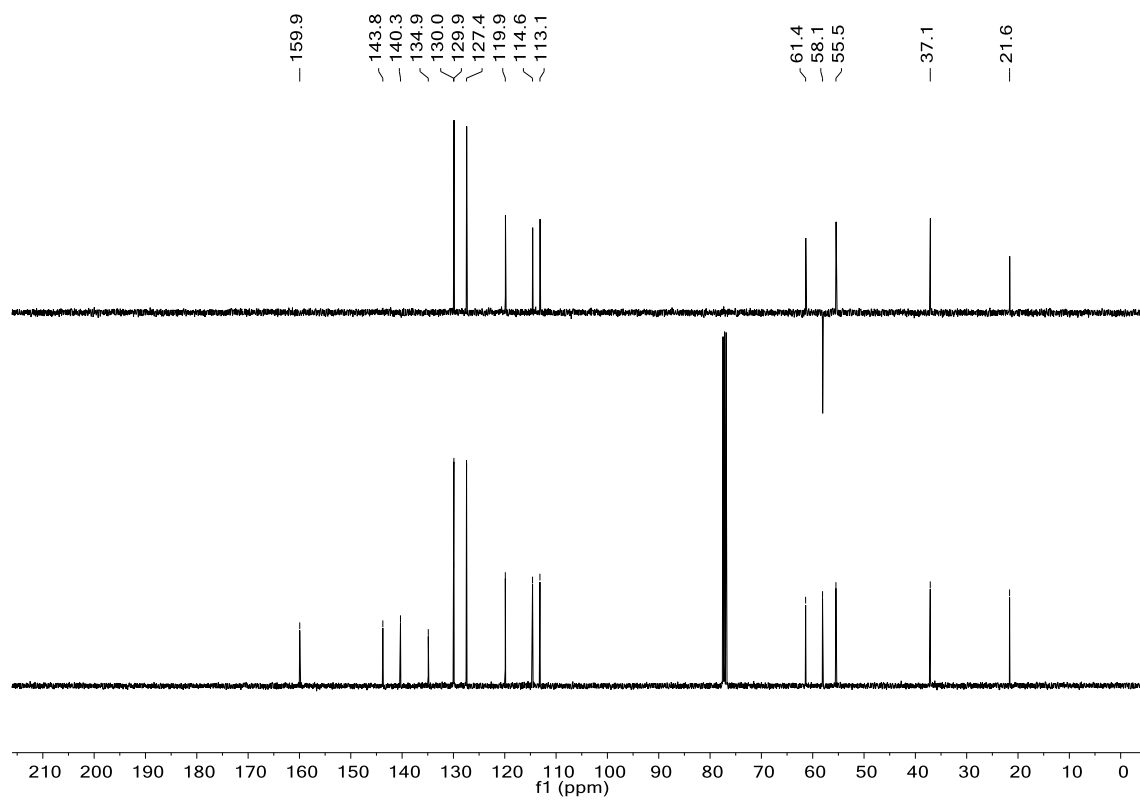


^{19}F -NMR

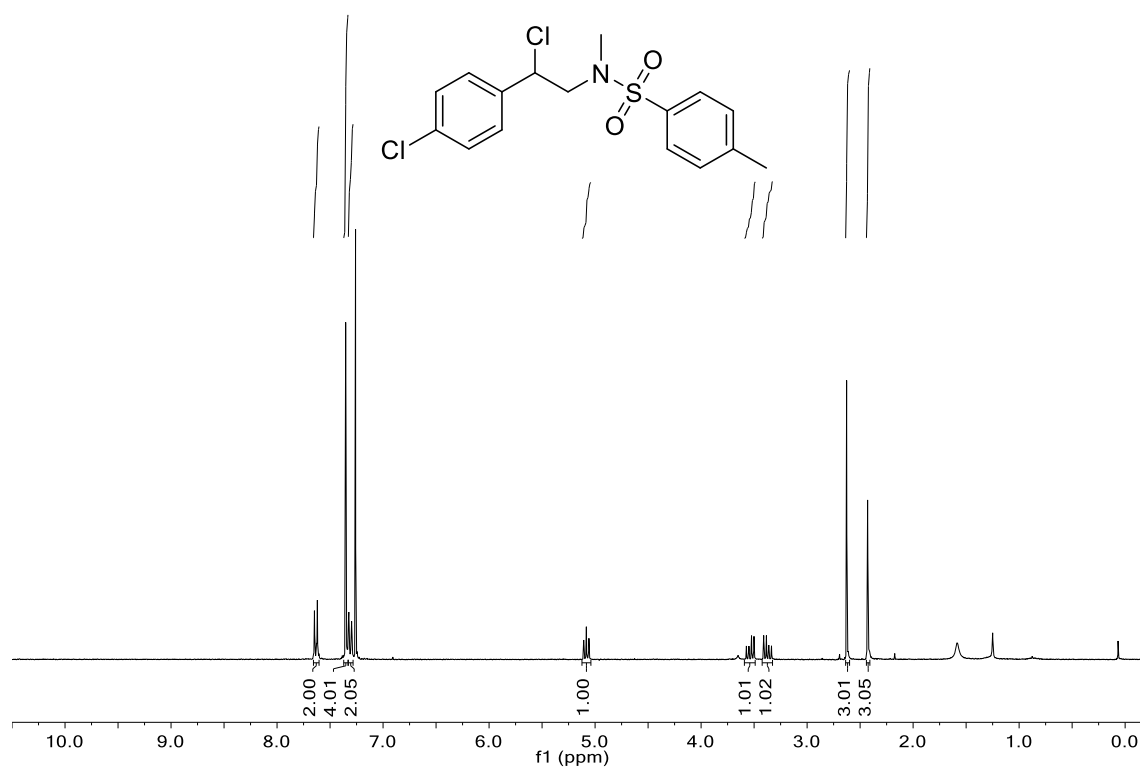


^{13}C -NMR and DEPT-135

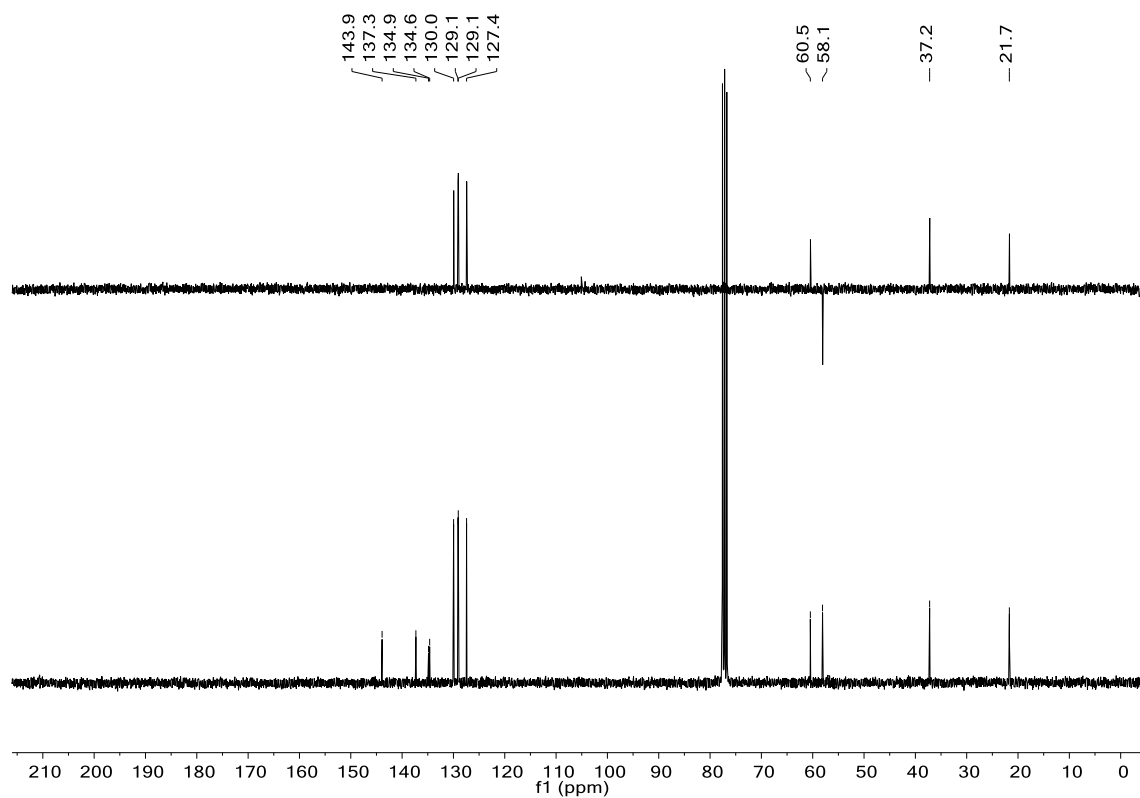


N-(2-chloro-2-(3-methoxyphenyl)ethyl)-*N*,4-dimethylbenzenesulfonamide (**125j**): ^1H -NMR ^{13}C -NMR and DEPT-135

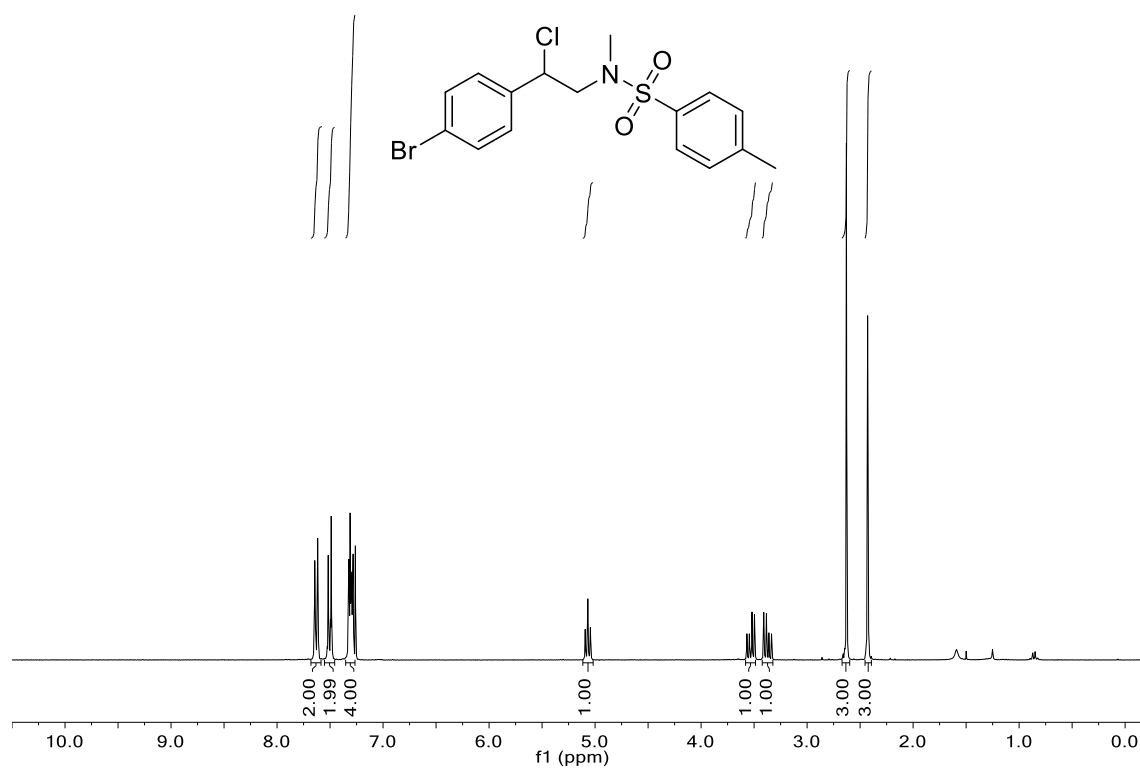
N-(2-chloro-2-(4-chlorophenyl)ethyl)-*N*,4-dimethylbenzenesulfonamide (**125k**): ^1H -NMR



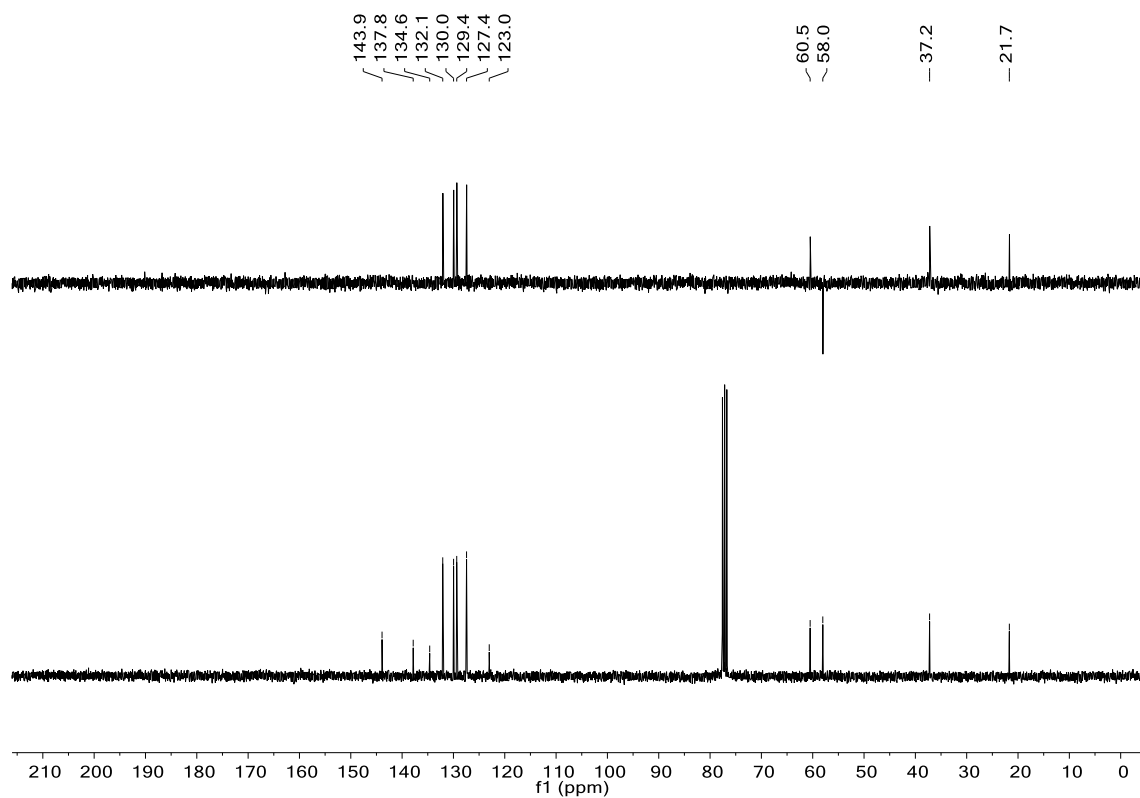
^{13}C -NMR and DEPT-135



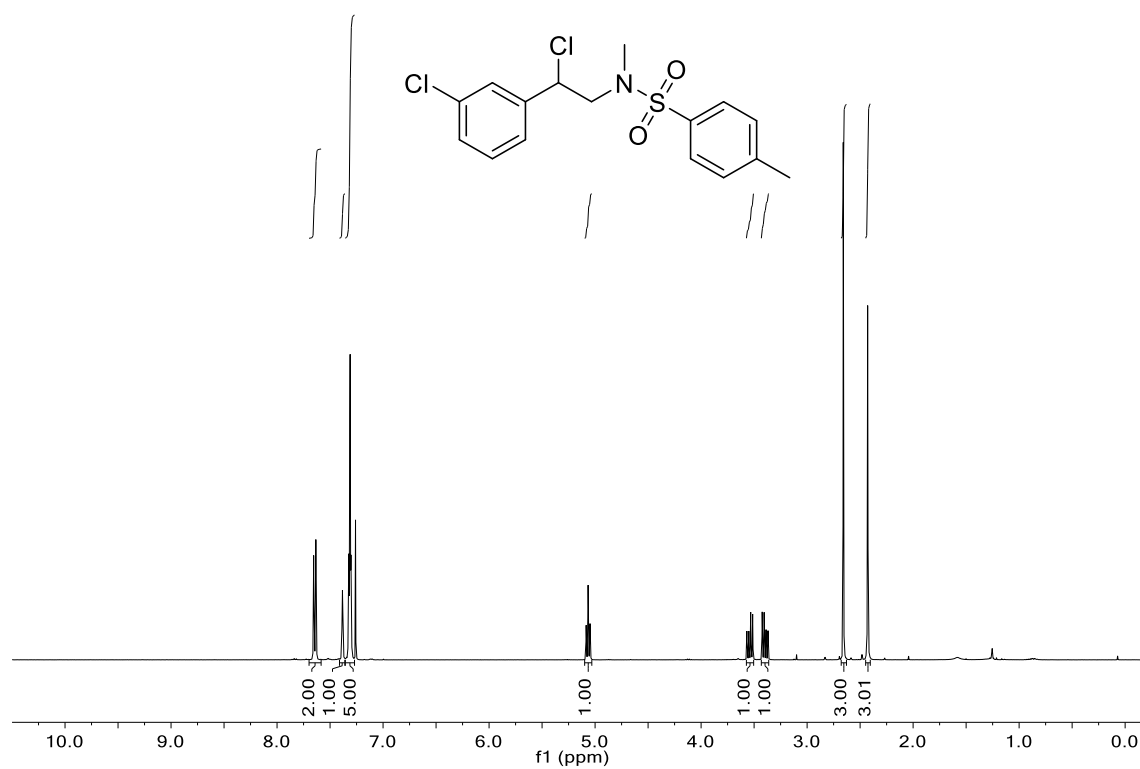
N-(2-(4-bromophenyl)-2-chloroethyl)-*N*,4-dimethylbenzenesulfonamide (**125I**): ^1H -NMR



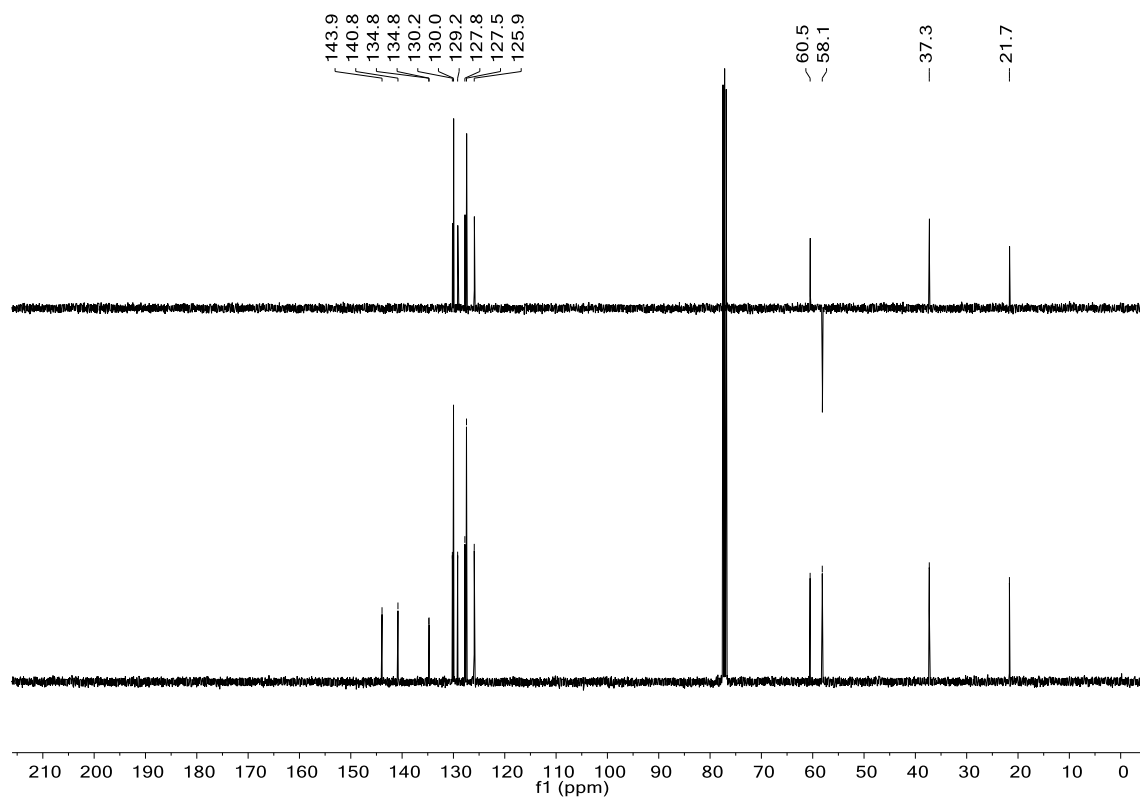
^{13}C -NMR and DEPT-135



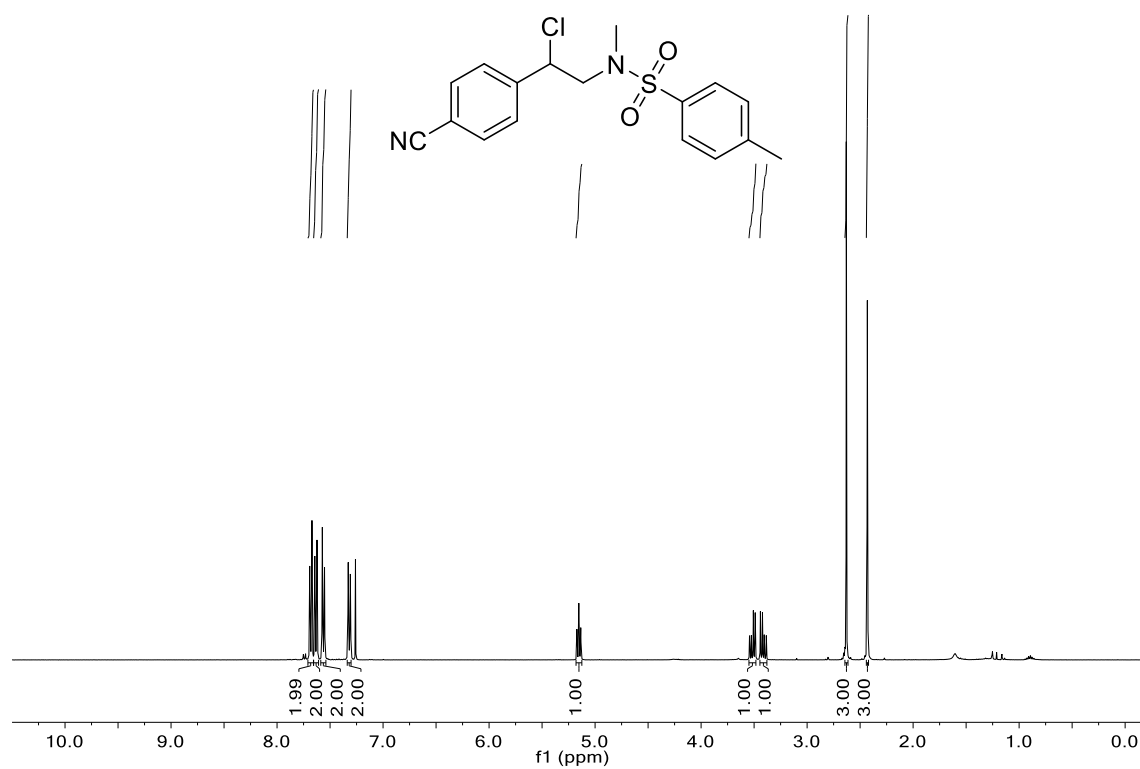
N-(2-chloro-2-(3-chlorophenyl)ethyl)-*N*,4-dimethylbenzenesulfonamide (**125m**): ^1H -NMR



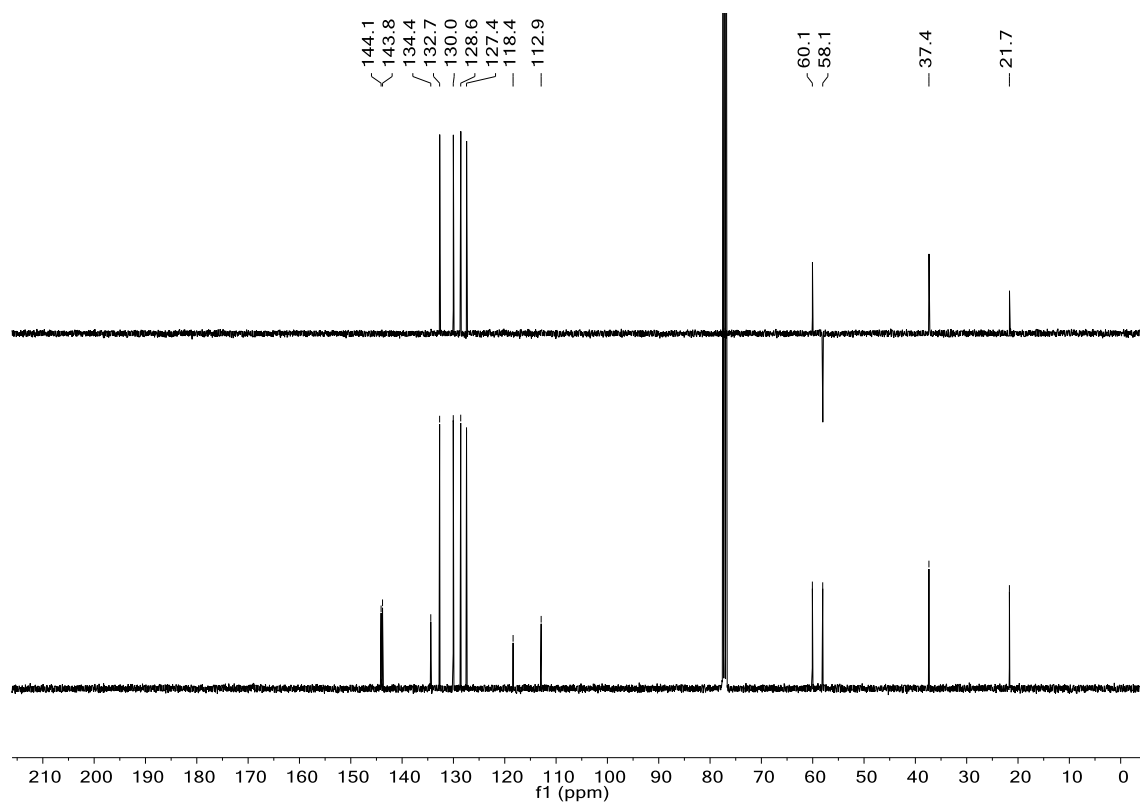
^{13}C -NMR and DEPT-135

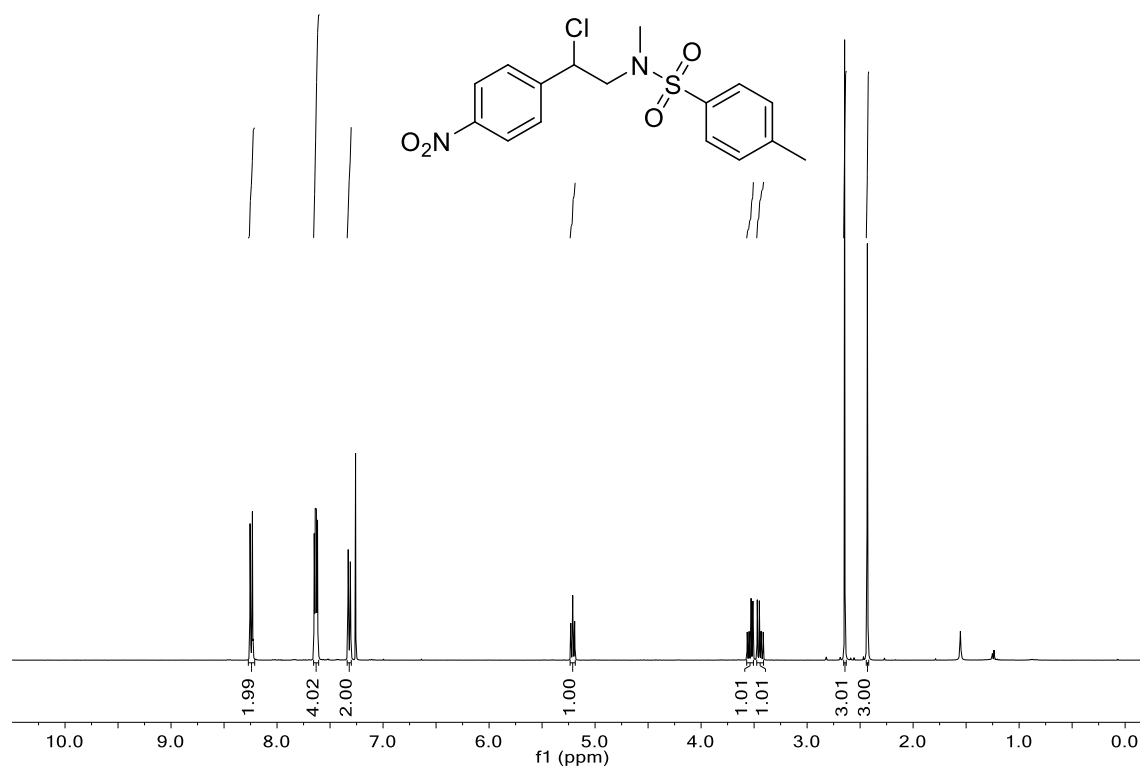
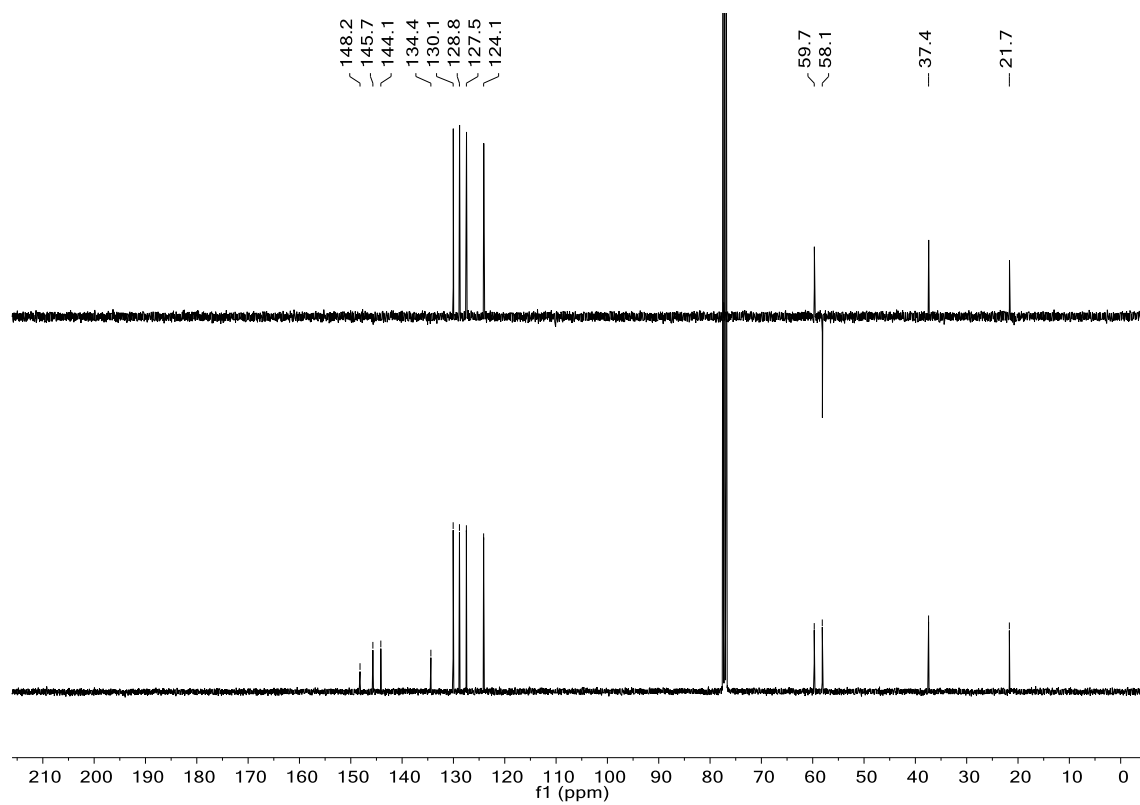


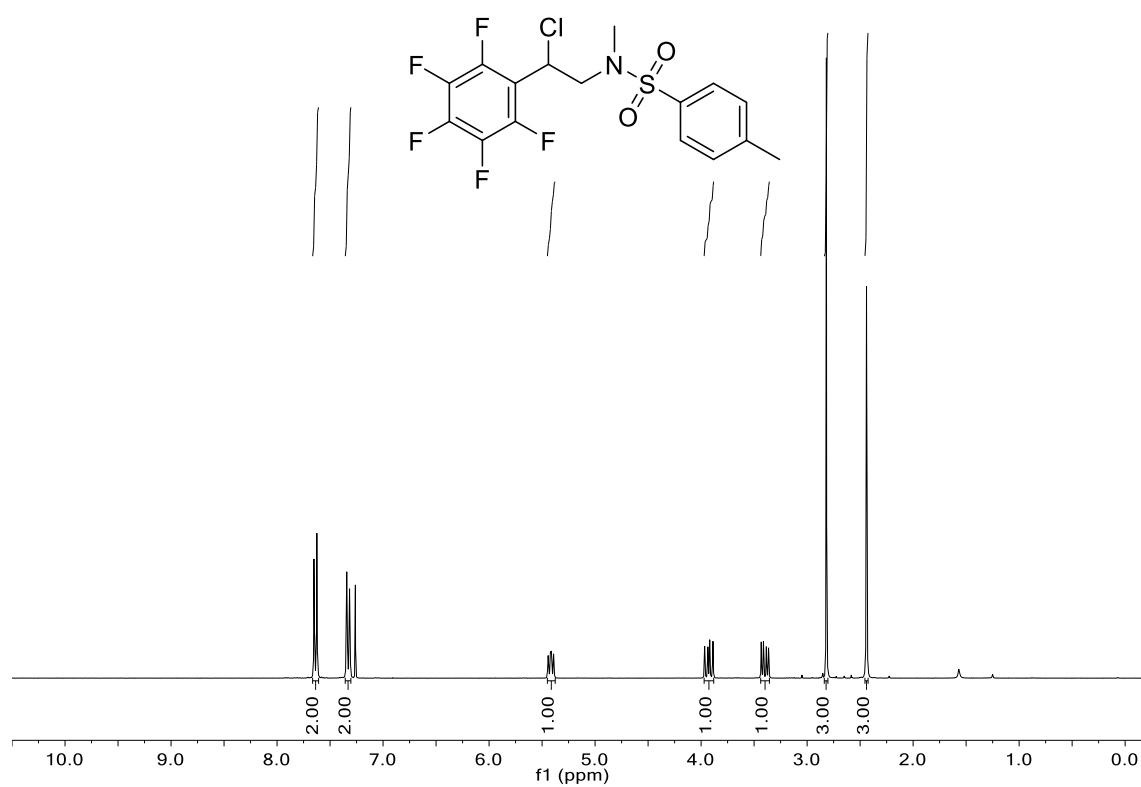
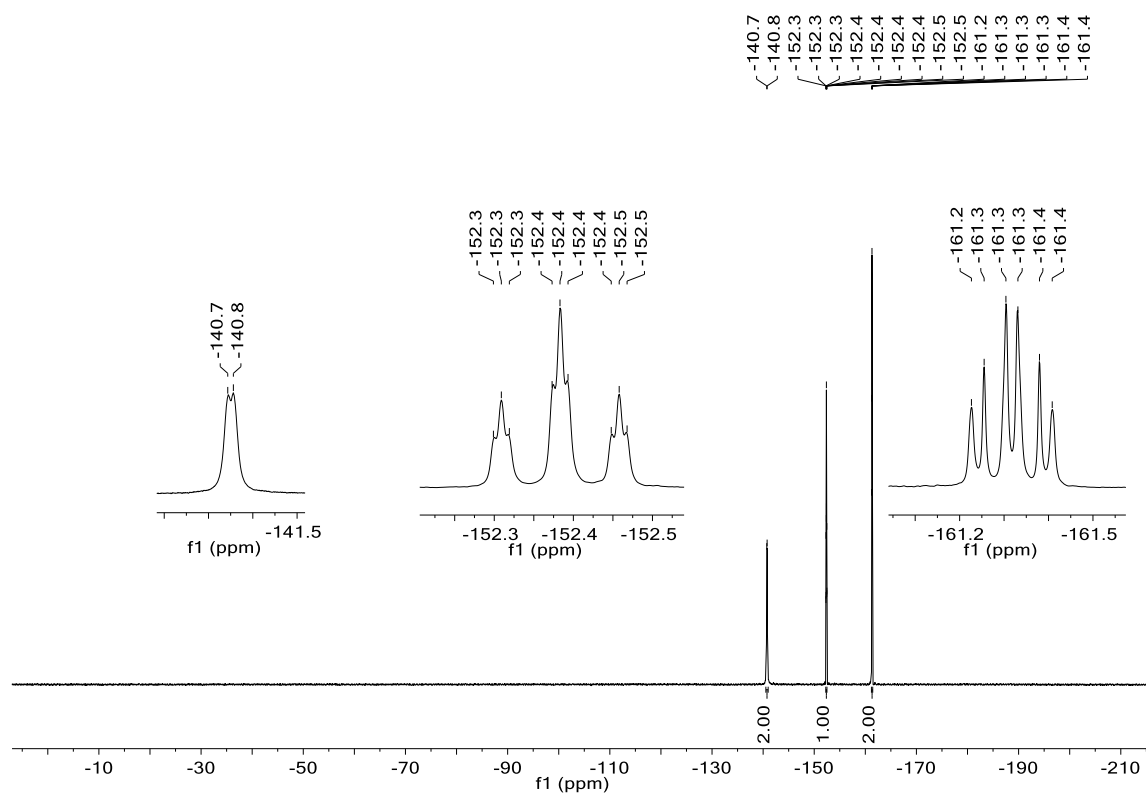
N-(2-chloro-2-(4-cyanophenyl)ethyl)-*N*,4-dimethylbenzenesulfonamide (**125n**): ^1H -NMR



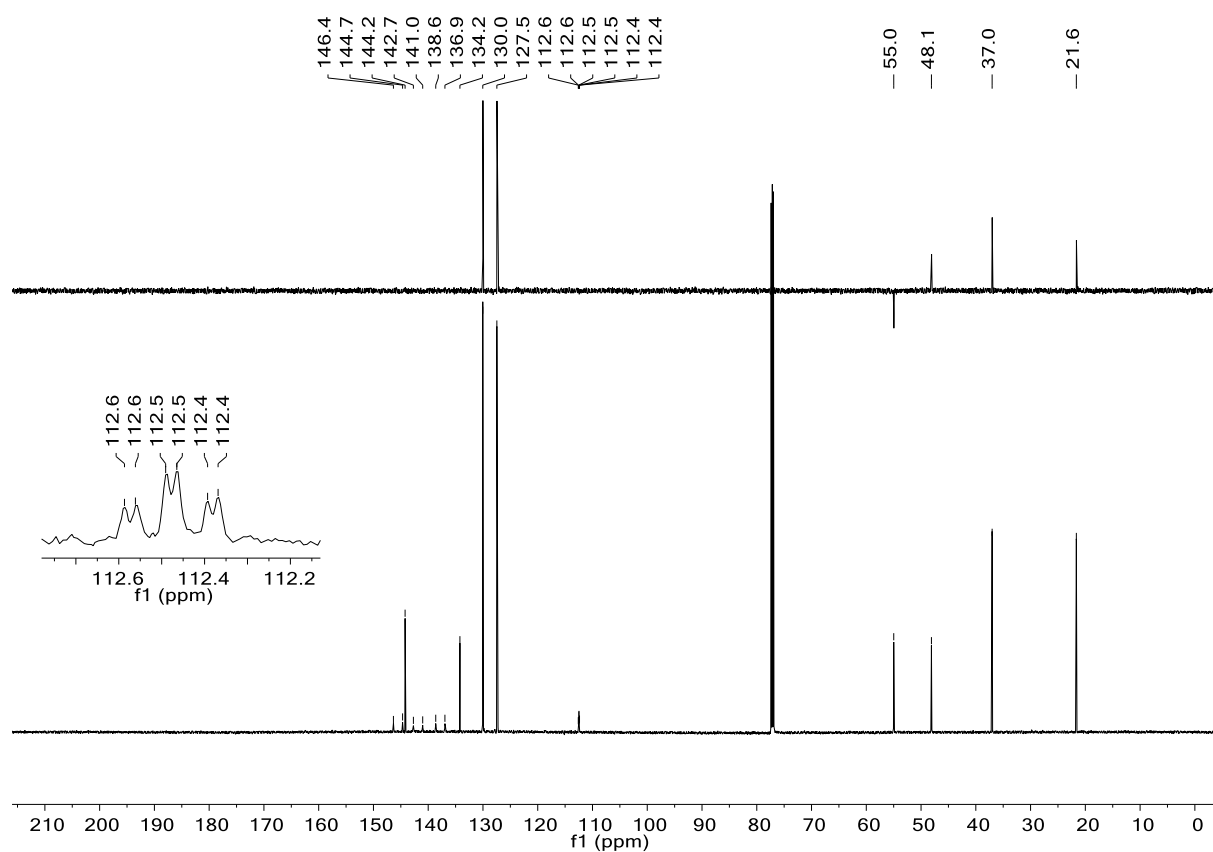
^{13}C -NMR and DEPT-135

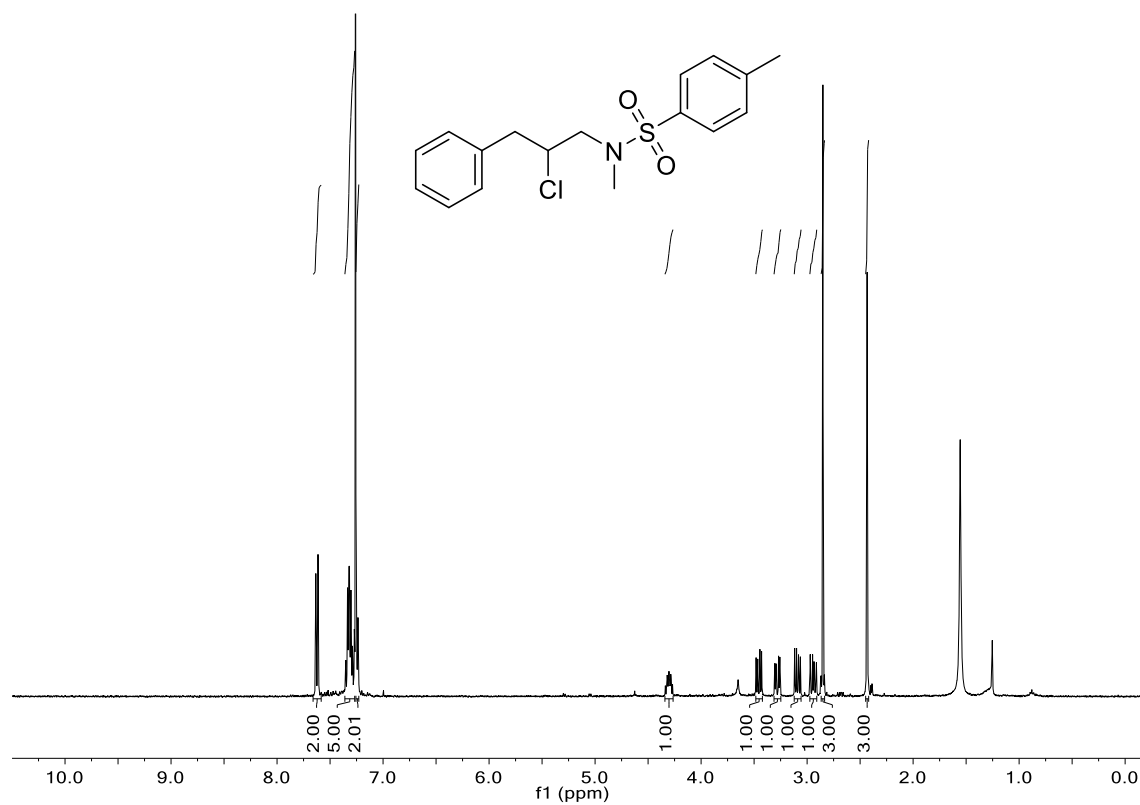
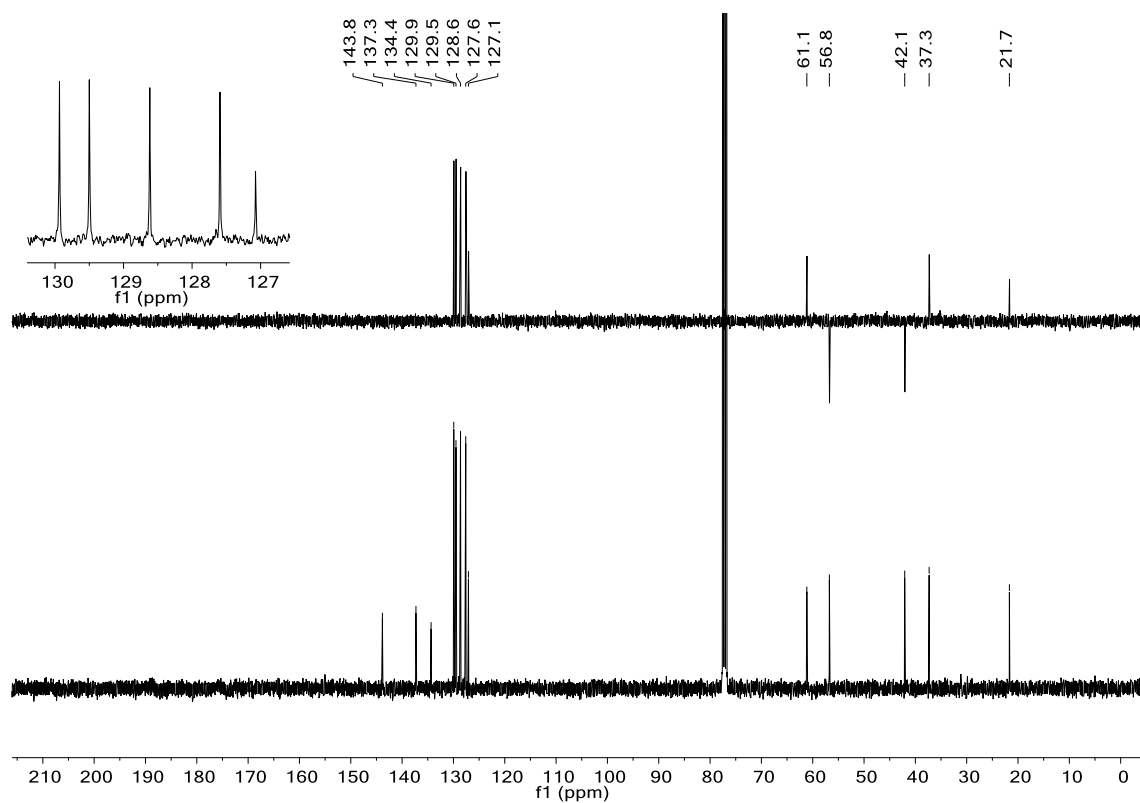


N-(2-chloro-2-(4-nitrophenyl)ethyl)-*N*,4-dimethylbenzenesulfonamide (**125o**): ^1H -NMR ^{13}C -NMR and DEPT-135

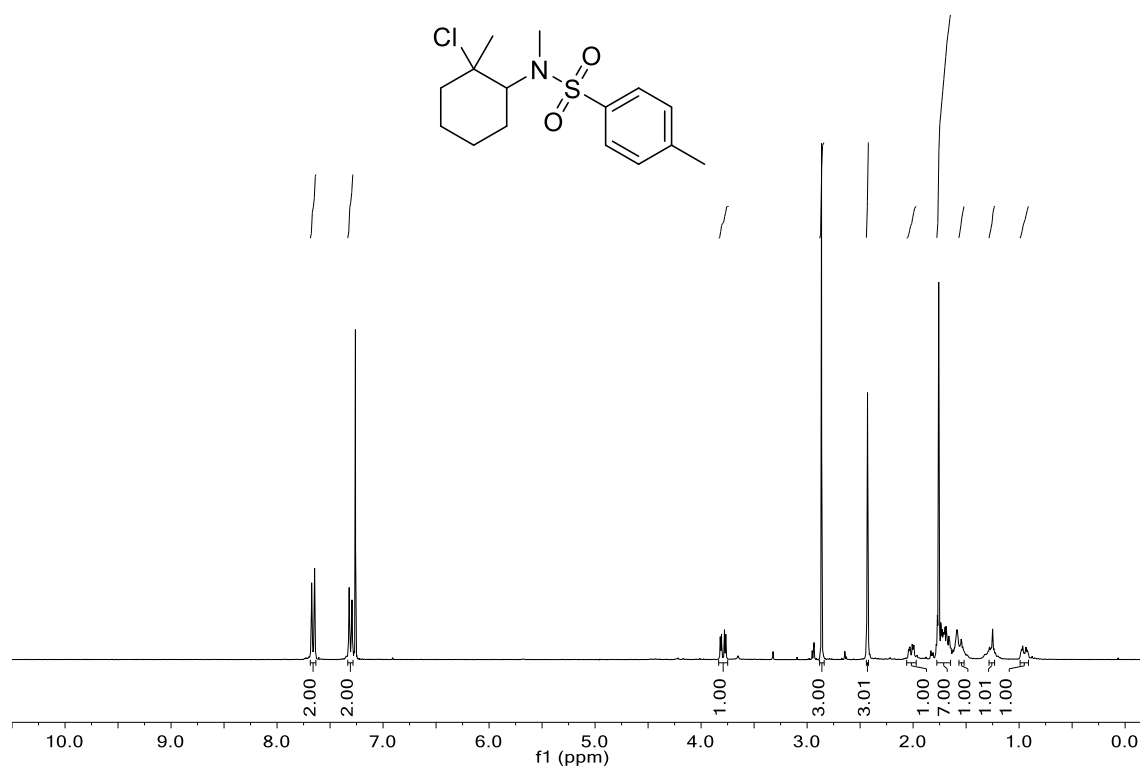
N-(2-chloro-2-(perfluorophenyl)ethyl)-*N*,4-dimethylbenzenesulfonamide (**125p**): ^1H -NMR ^{19}F -NMR

^{13}C -NMR and DEPT-135

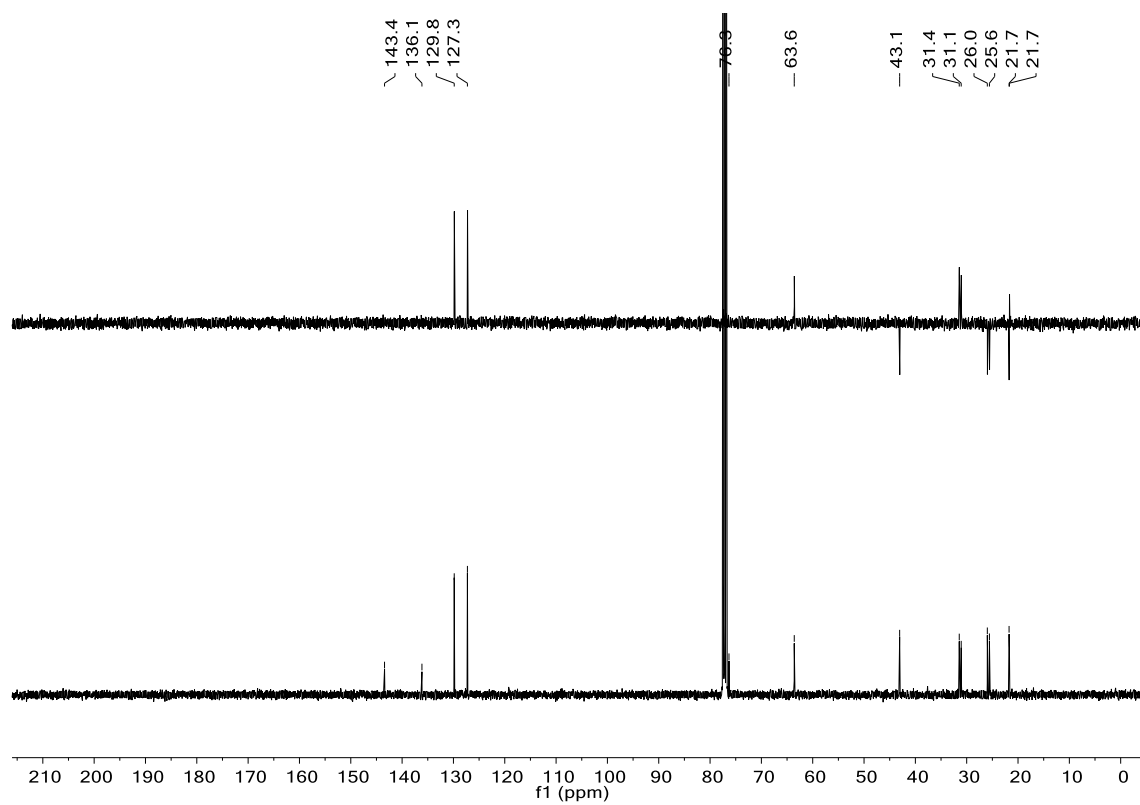


N-(2-chloro-3-phenylpropyl)-*N*,4-dimethylbenzenesulfonamide (**127a**): ^1H -NMR ^{13}C -NMR and DEPT-135

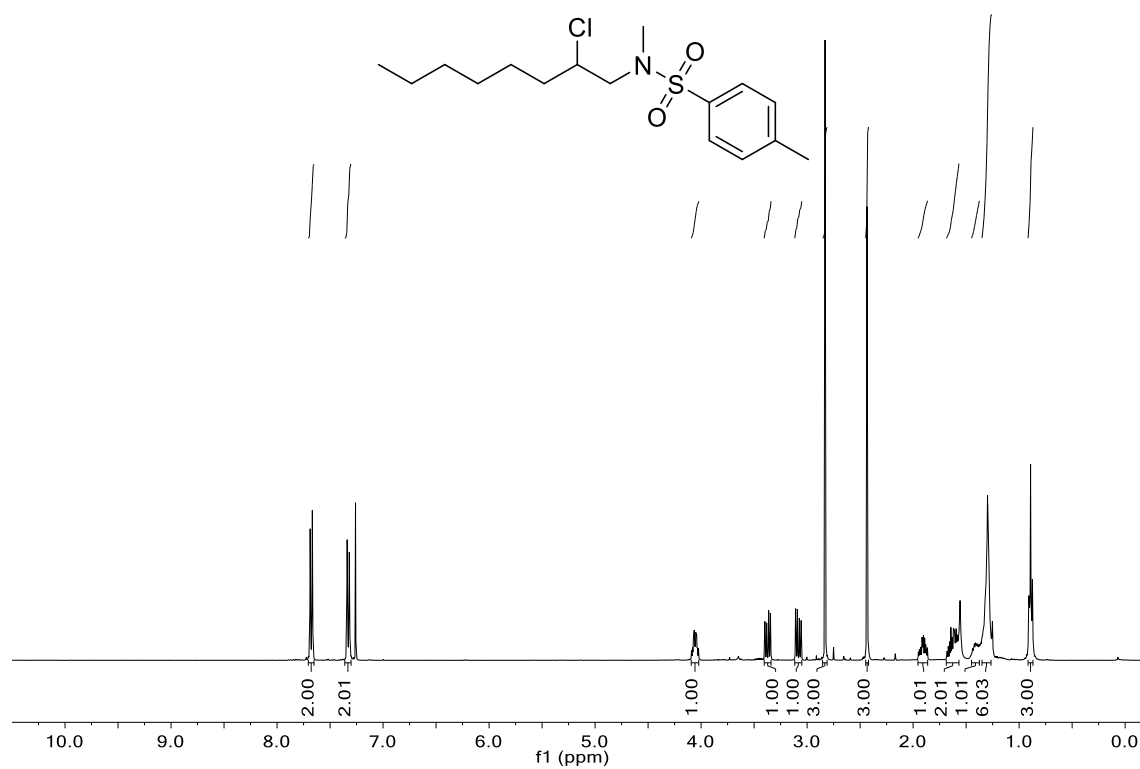
N-(2-chloro-2-methylcyclohexyl)-*N*,4-dimethylbenzenesulfonamide (**127b**): ^1H -NMR



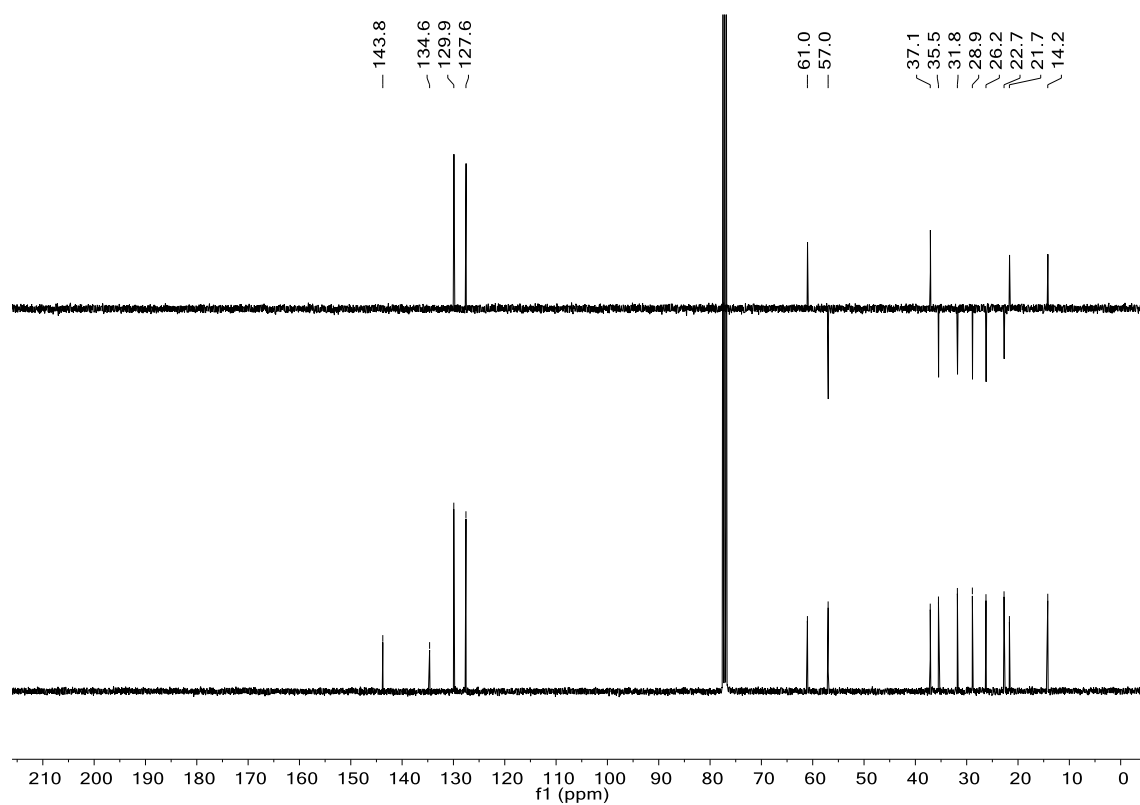
^{13}C -NMR and DEPT-135



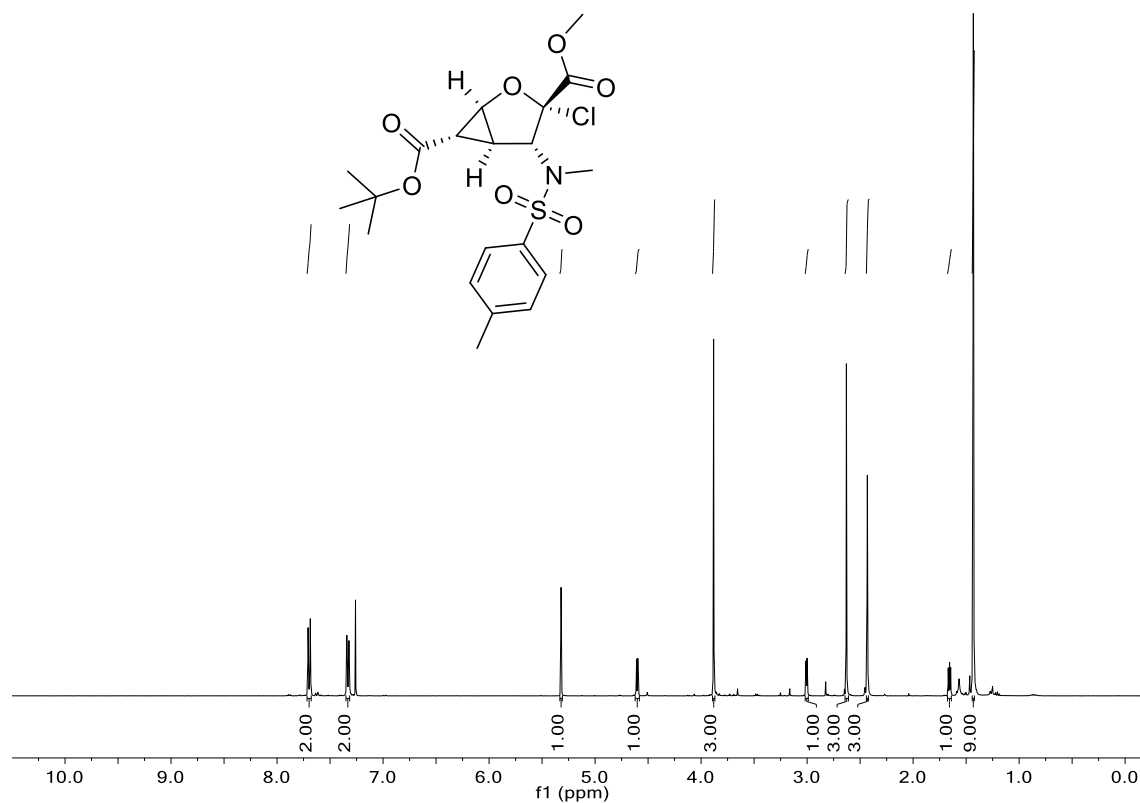
N-(2-chlorooctyl)-*N*,4-dimethylbenzenesulfonamide (**127c**): ^1H -NMR



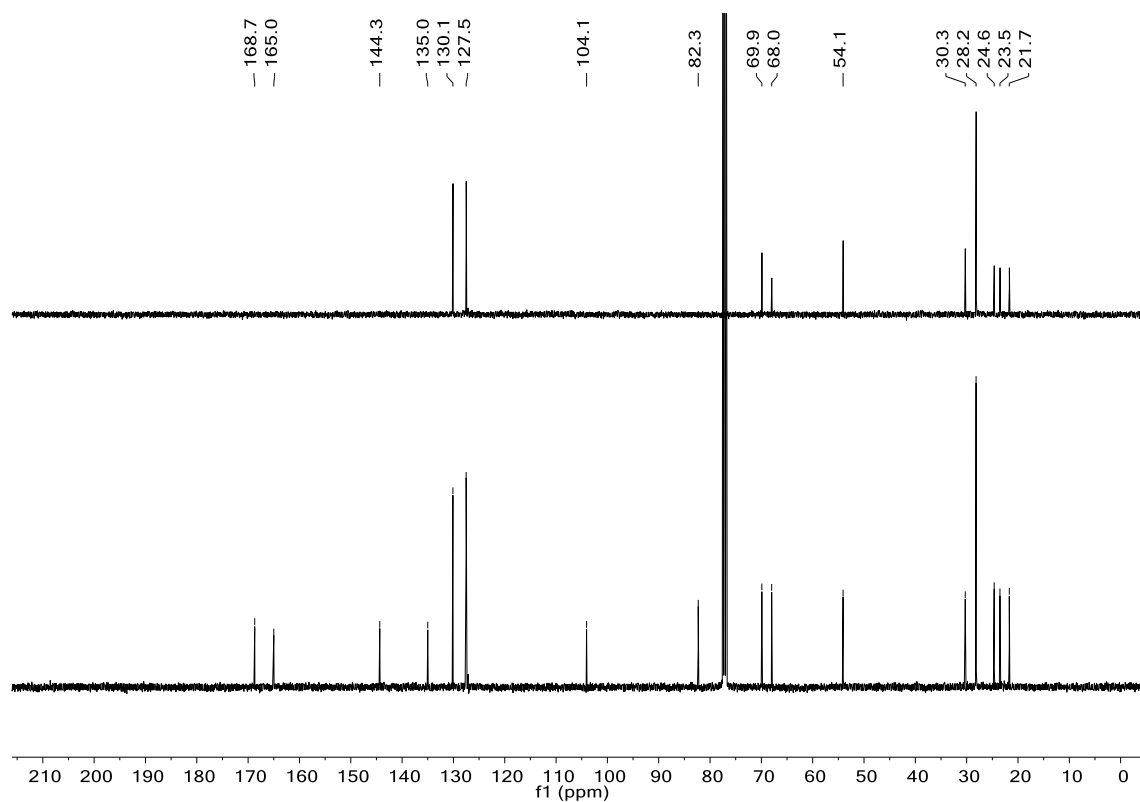
^{13}C -NMR and DEPT-135



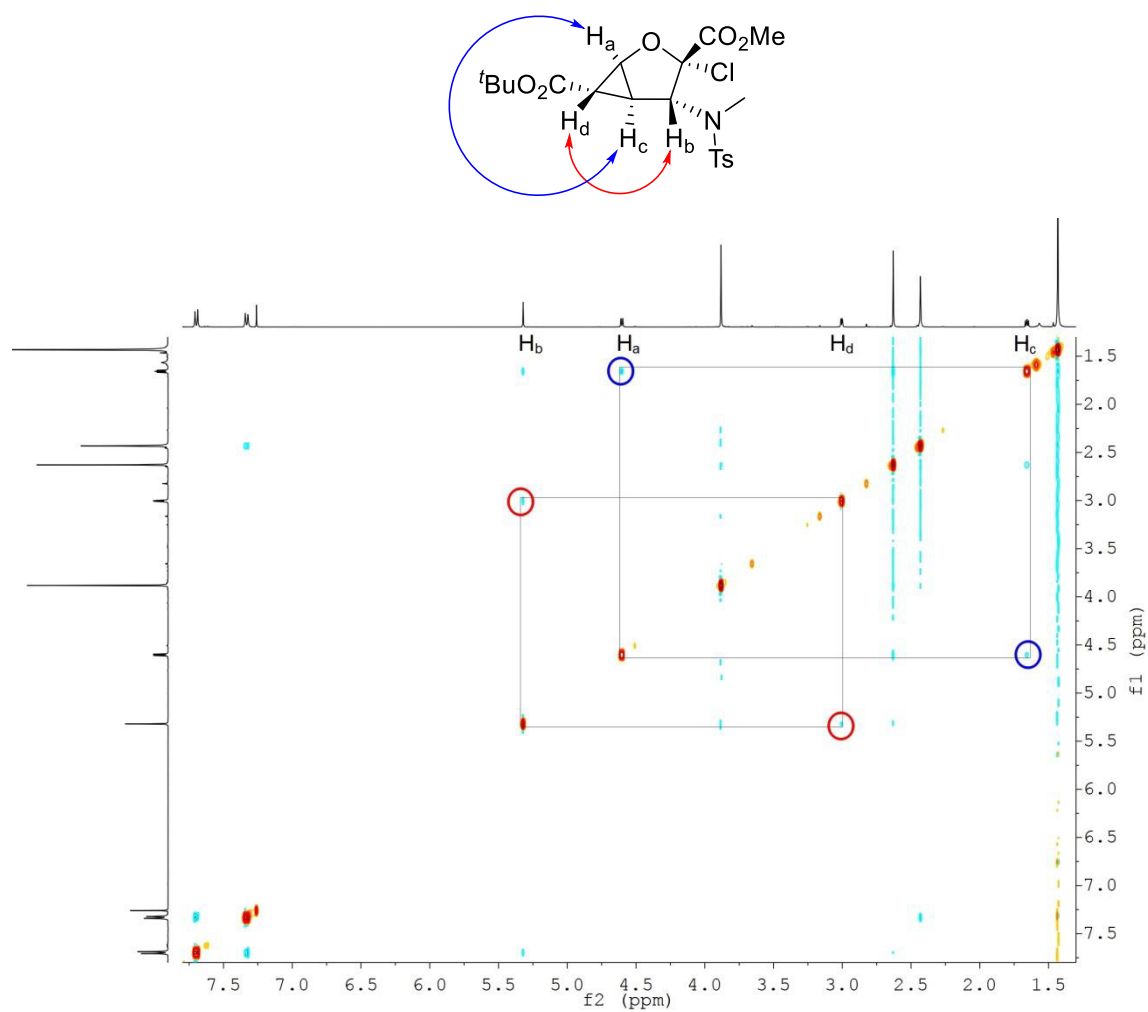
6-(*tert*-butyl) 3-methyl (1*S*,3*S*,4*R*,5*R*,6*S*)-3-chloro-4-((*N*,4-dimethylphenyl)sulfonamido)-2-oxabicyclo[3.1.0] hexane-3,6-dicarboxylate (**127d**): ^1H -NMR



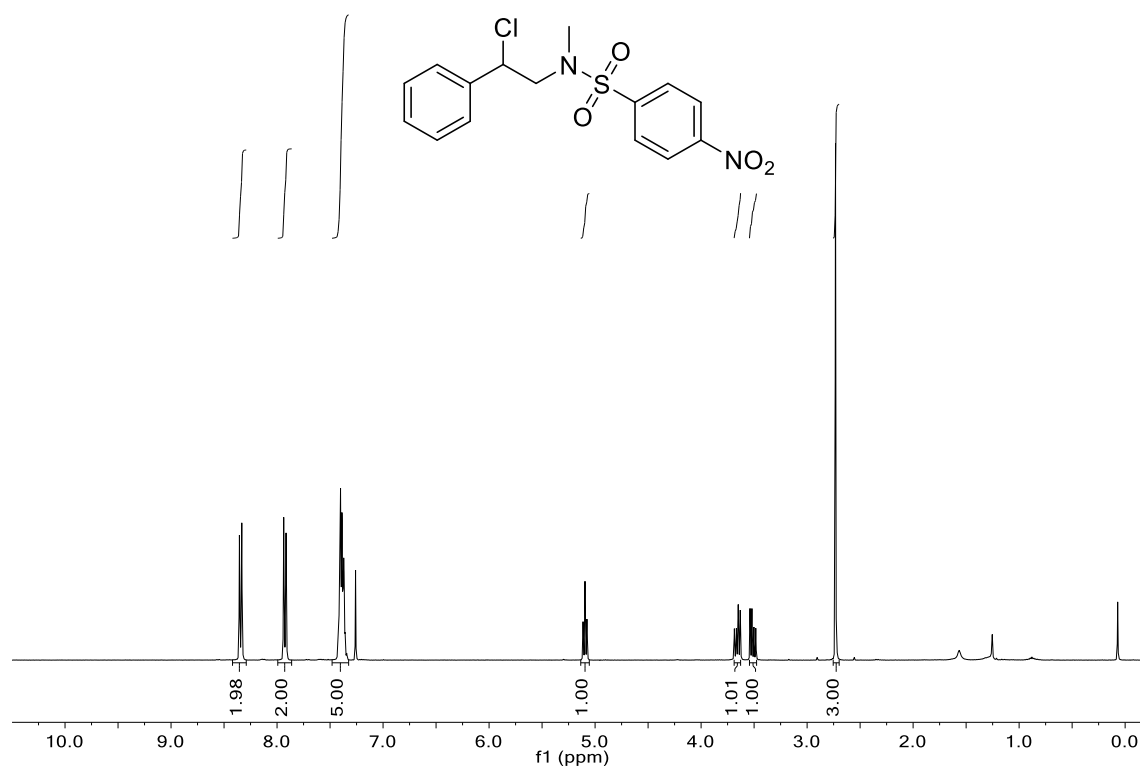
^{13}C -NMR and DEPT-135



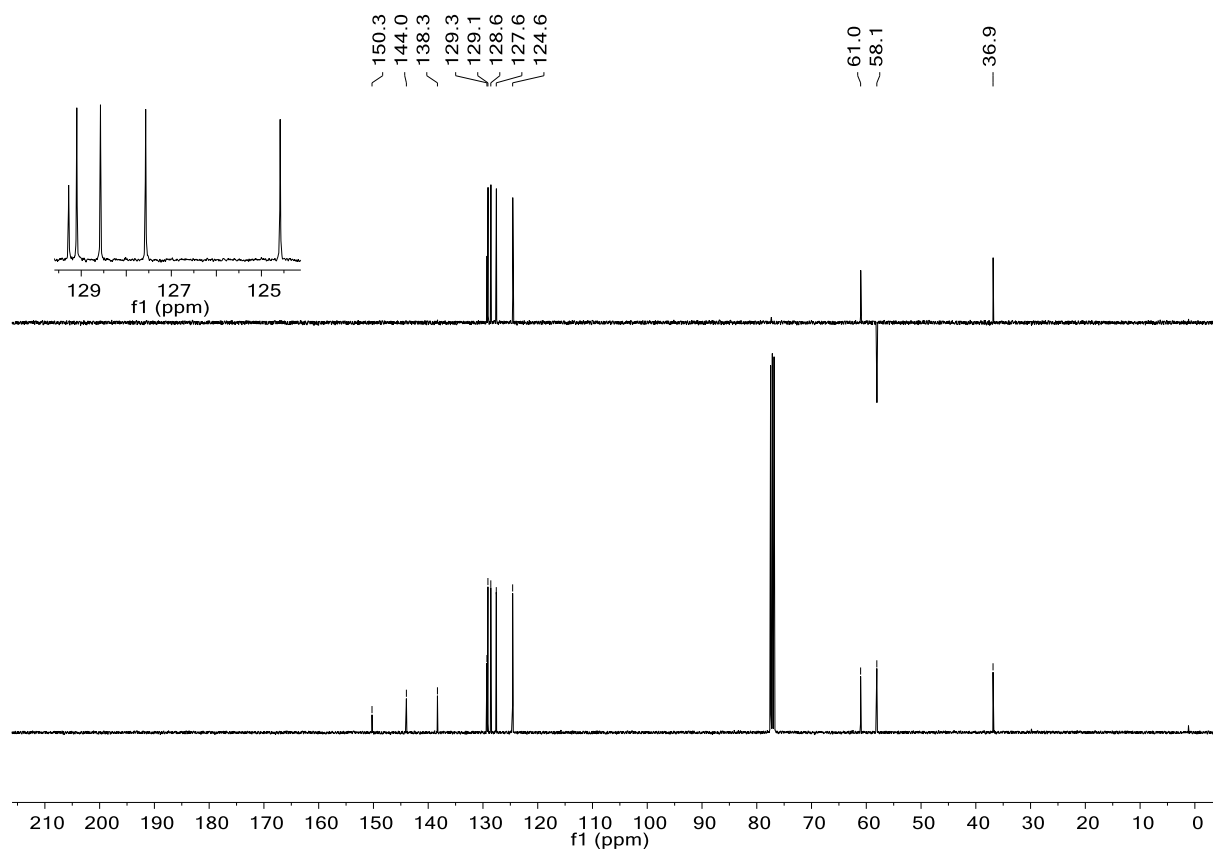
NOESY



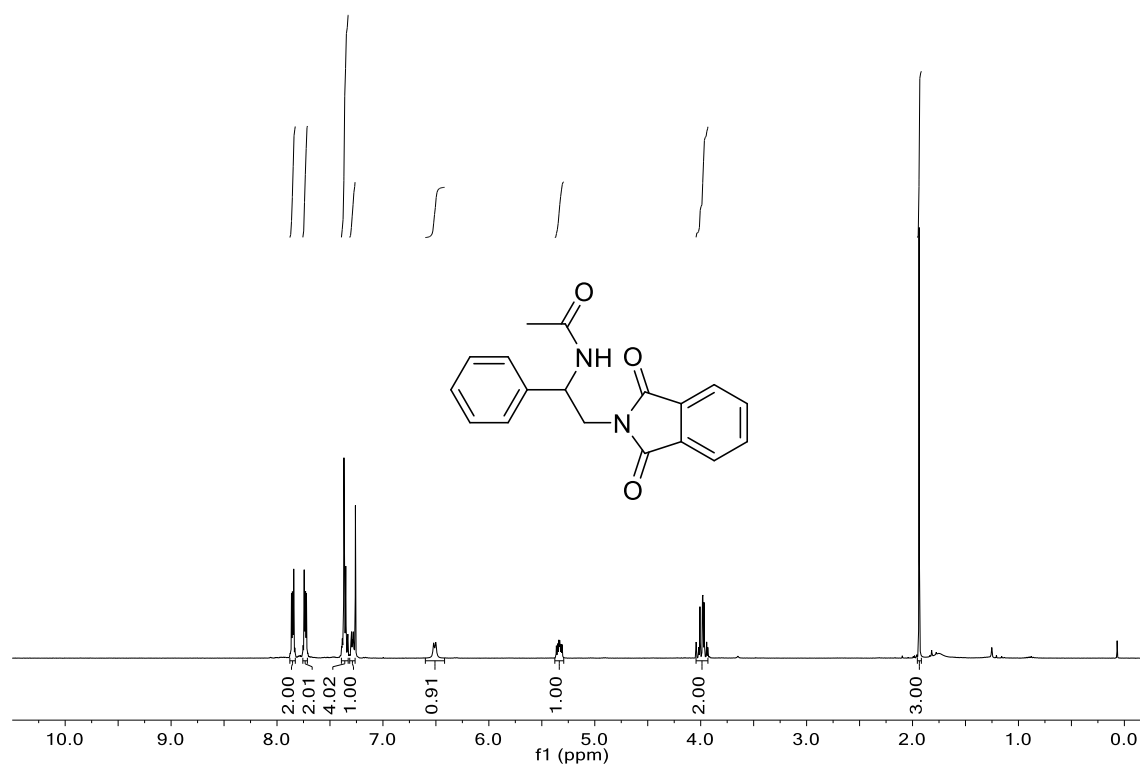
N-(2-chloro-2-phenylethyl)-*N*-methyl-4-nitrobenzenesulfonamide (**129b**): ^1H -NMR



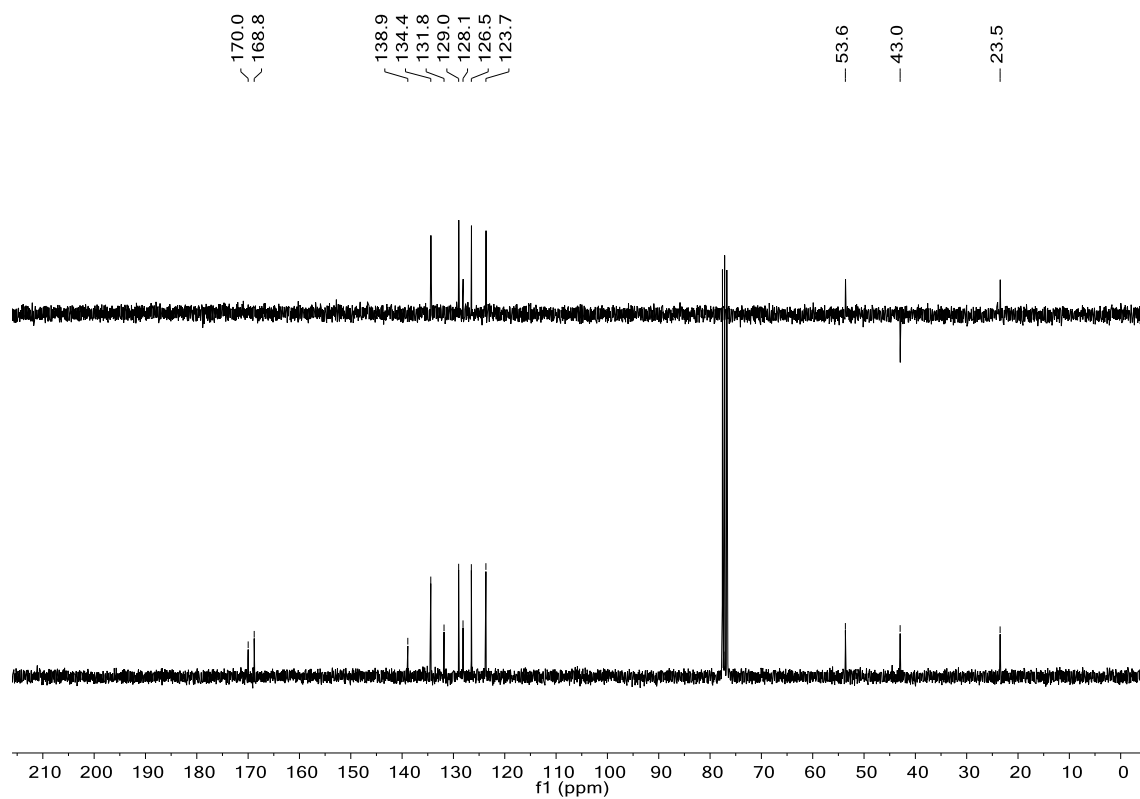
^{13}C -NMR and DEPT-135



N-(2-(1,3-dioxoisindolin-2-yl)-1-phenylethyl)acetamide (**138**): ^1H -NMR

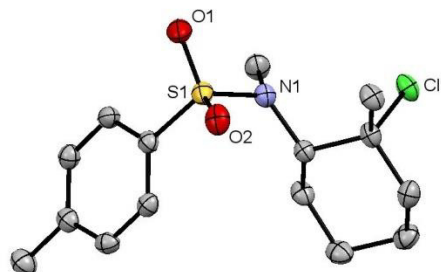
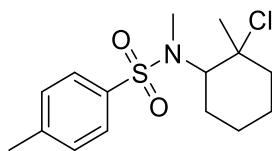


^{13}C -NMR and DEPT-135



5.7 X-ray

N-(2-chloro-2-methylcyclohexyl)-*N*,4-dimethylbenzenesulfonamide (**127b**)



Formula	C ₁₅ H ₂₂ ClNO ₂ S
$D_{\text{calc.}}/\text{g cm}^{-3}$	1.341
μ/mm^{-1}	3.414
Formula Weight	315.84
Color	clear colorless
Shape	plate
Size/mm ³	0.45×0.16×0.07
T/K	123.02(10)
Crystal System	orthorhombic
Space Group	Pbca
$a/\text{\AA}$	16.7808(3)
$b/\text{\AA}$	9.47060(16)
$c/\text{\AA}$	19.6889(3)
$\alpha/^\circ$	90
$\beta/^\circ$	90
$\gamma/^\circ$	90
$V/\text{\AA}^3$	3129.04(9)
Z	8
Z'	1
Wavelength/ \AA	1.54184
Radiation type	CuK α
$\theta_{\text{min}}/^\circ$	4.491
$\theta_{\text{max}}/^\circ$	76.251
Measured Refl.	20844
Independent Refl.	3275
Reflections Used	3033
R_{int}	0.0306
Parameters	184
Restraints	0
Largest Peak	0.388
Deepest Hole	-0.394
GooF	1.043
wR_2 (all data)	0.0867
wR_2	0.0844
R_1 (all data)	0.0338
R_1	0.0312

G. References

- [1] P. U. Clark, J. D. Shakun, S. A. Marcott, A. C. Mix, M. Eby, S. Kulp, A. Levermann, G. A. Milne, P. L. Pfister, B. D. Santer, D. P. Schrag, S. Solomon, T. F. Stocker, B. H. Strauss, A. J. Weaver, R. Winkelmann, D. Archer, E. Bard, A. Goldner, K. Lambeck, R. T. Pierrehumbert, G.-K. Plattner, *Nature Climate Change* **2016**, *6*, 360–369.
- [2] Population Reference Bureau, *2017 World Population Data Sheet*; <http://www.prb.org/Publications/Datasheets/2017/2017-world-population-data-sheet.aspx> [18 September 2017].
- [3] a) P. Anastas, N. Eghbali, *Chem. Soc. Rev.* **2010**, *39*, 301–312; b) N. S. Lewis, D. G. Nocera, *Proc. Natl. Acad. Sci. USA* **2006**, *103*, 15729–15735.
- [4] G. Ciamician, *Science* **1912**, *36*, 385–394.
- [5] a) V. Balzani, A. Credi, M. Venturi, *ChemSusChem* **2008**, *1*, 26–58; b) N. T. R. N. Kumara, A. Lim, C. M. Lim, M. I. Petra, P. Ekanayake, *Renewable and Sustainable Energy Reviews* **2017**, *78*, 301–317; c) S. Chu, Y. Cui, N. Liu, *Nat Mater* **2017**, *16*, 16–22; d) M. A. Green, S. P. Bremner, *Nat Mater* **2017**, *16*, 23–34.
- [6] a) A. J. Esswein, D. G. Nocera, *Chem. Rev.* **2007**, *107*, 4022–4047; b) E.-M. Aro, *Ambio* **2015**, *45*, 24–31; c) C. D. Botero Gutiérrez, D. L. Restrepo Serna, C. A. Cardona Alzate, *BRJ* **2017**, *4*, 691–703.
- [7] K. Zeitle, *Angew. Chem. Int. Ed.* **2009**, *48*, 9785–9789.
- [8] D. M. Schultz, T. P. Yoon, *Science* **2014**, *343*.
- [9] A. D. McNaught, A. Wilkinson; photocatalyst. M. Nič, J. Jirá, B. Košata, Jenkins (Eds.), *IUPAC Compendium of Chemical Terminology, 2nd ed. (the "Gold Book")*, Blackwell Scientific Publications, Oxford **1997**.
- [10] C. K. Prier, D. A. Rankic, D. W. C. MacMillan, *Chem. Rev.* **2013**, *113*, 5322–5363.
- [11] M. Yamada, Y. Tanaka, Y. Yoshimoto, S. Kuroda, I. Shimao, *Bull. Chem. Soc. Jpn.* **1992**, *65*, 1006–1011.
- [12] a) J. M. R. Narayanam, C. R. J. Stephenson, *Chem. Soc. Rev.* **2011**, *40*, 102–113; b) D. Ravelli, D. Dondi, M. Fagnoni, A. Albini, *Chem. Soc. Rev.* **2009**, *38*, 1999–2011; c) B. König, *Chemical Photocatalysis*, De Gruyter, Berlin **2013**.
- [13] J. W. Tucker, C. R. J. Stephenson, *J. Org. Chem.* **2012**, *77*, 1617–1622.
- [14] F. Teplý, *Collect. Czech. Chem. Commun.* **2011**, *76*, 859–917.
- [15] Y. Pellegrin, F. Odobel, *Comptes Rendus Chimie* **2017**, *20*, 283–295.
- [16] Leading reviews on visible light photoredox catalysis: a) K. Zeitle, *Angew. Chem. Int. Ed.* **2009**, *48*, 9785–9789; b) F. Teplý, *Collect. Czech. Chem. Commun.* **2011**, *76*, 859–917; c) J. M. R. Narayanam, C. R. J. Stephenson, *Chem. Soc. Rev.* **2011**, *40*, 102–113; d) J. W. Tucker, C. R. J. Stephenson, *J. Org. Chem.* **2012**, *77*, 1617–1622; e) M.

- Reckenthäler, A. G. Griesbeck, *Adv. Synth. Catal.* **2013**, *355*, 2727–2744; f) C. K. Prier, D. A. Rankic, D. W. C. MacMillan, *Chem. Rev.* **2013**, *113*, 5322–5363; g) D. M. Schultz, T. P. Yoon, *Science* **2014**, *343*; h) D. Ravelli, S. Protti, M. Fagnoni, *Chem. Rev.* **2016**, *116*, 9850–9913; i) M. H. Shaw, J. Twilton, D. W. C. MacMillan, *J. Org. Chem.* **2016**, *81*, 6898–6926; j) N. A. Romero, D. A. Nicewicz, *Chem. Rev.* **2016**, *116*, 10075–10166.
- [17] Leading reviews on copper in visible light photoredox catalyzed reactions: a) S. Paria, O. Reiser, *ChemCatChem* **2014**, *6*, 2477–2483; b) O. Reiser, *Acc. Chem. Res.* **2016**, *49*, 1990–1996.
- [18] For applications of $[\text{Cu}(\text{dap})_2]^+$ in photoredox catalysis see: a) J.-M. Kern, J.-P. Sauvage, *J. Chem. Soc., Chem. Commun.* **1987**, 546–548; b) M. Pirtsch, S. Paria, T. Matsuno, H. Isobe, O. Reiser, *Chem. Eur. J.* **2012**, *18*, 7336–7340; c) S. Paria, M. Pirtsch, V. Kais, O. Reiser, *Synthesis* **2013**, *45*, 2689–2698; d) A. Baralle, L. Fensterbank, J.-P. Goddard, C. Ollivier, *Chem. Eur. J.* **2013**, *19*, 10809–10813; e) D. B. Bagal, G. Kachkovskyi, M. Knorn, T. Rawner, B. M. Bhanage, O. Reiser, *Angew. Chem. Int. Ed.* **2015**, *54*, 6999–7002; f) M. Knorn, T. Rawner, R. Czerwieniec, O. Reiser, *ACS Catal* **2015**, *5*, 5186–5193; g) X.-J. Tang, W. R. Dolbier, *Angew. Chem. Int. Ed.* **2015**, *54*, 4246–4249; h) Z. Zhang, X. Tang, C. S. Thomason, W. R. Dolbier, *Org. Lett.* **2015**, *17*, 3528–3531; i) G. Fumagalli, P. T. G. Rabet, S. Boyd, M. F. Greaney, *Angew. Chem. Int. Ed.* **2015**, *54*, 11481–11484; j) T. Rawner, M. Knorn, E. Lutsker, A. Hossain, O. Reiser, *J. Org. Chem.* **2016**, *81*, 7139–7147; k) S. K. Pagire, S. Paria, O. Reiser, *Org. Lett.* **2016**, *18*, 2106–2109; l) T. P. Nicholls, G. E. Constable, J. C. Robertson, M. G. Gardiner, A. C. Bissember, *ACS Catal* **2016**, *6*, 451–457; m) W. Ma, D. Chen, Y. Ma, L. Wang, C. Zhao, W. Yang, *Polym. Chem.* **2016**, *7*, 4226–4236; n) P. T. G. Rabet, G. Fumagalli, S. Boyd, M. F. Greaney, *Org. Lett.* **2016**, *18*, 1646–1649.
- [19] J.-M. Kern, J.-P. Sauvage, *J. Chem. Soc., Chem. Commun.* **1987**, 546–548.
- [20] M. Knorn, T. Rawner, R. Czerwieniec, O. Reiser, *ACS Catal* **2015**, *5*, 5186–5193.
- [21] a) K. Kalyanasundaram, *Coord. Chem. Rev.* **1982**, *46*, 159–244; b) A. Juris, V. Balzani, P. Belser, A. von Zelewsky, *Helv. Chim. Acta* **1981**, *64*, 2175–2182.
- [22] J. D. Slinker, A. A. Gorodetsky, M. S. Lowry, J. Wang, S. Parker, R. Rohl, S. Bernhard, G. G. Malliaras, *J. Am. Chem. Soc.* **2004**, *126*, 2763–2767.
- [23] M. S. Lowry, J. I. Goldsmith, J. D. Slinker, R. Rohl, R. A. Pascal, G. G. Malliaras, S. Bernhard, *Chem. Mater.* **2005**, *17*, 5712–5719.
- [24] C. O. Dietrich-Buchecker, J. P. Sauvage, *Tetrahedron Lett.* **1983**, *24*, 5091–5094.
- [25] M. Pirtsch, S. Paria, T. Matsuno, H. Isobe, O. Reiser, *Chem. Eur. J.* **2012**, *18*, 7336–7340.
- [26] S. Paria, M. Pirtsch, V. Kais, O. Reiser, *Synthesis* **2013**, *45*, 2689–2698.

- [27] D. B. Bagal, G. Kachkovskyi, M. Knorn, T. Rawner, B. M. Bhanage, O. Reiser, *Angew. Chem. Int. Ed.* **2015**, *54*, 6999–7002.
- [28] T. Rawner, M. Knorn, E. Lutscher, A. Hossain, O. Reiser, *J. Org. Chem.* **2016**, *81*, 7139–7147.
- [29] S. K. Pagire, S. Paria, O. Reiser, *Org. Lett.* **2016**, *18*, 2106–2109.
- [30] B. M. Trost, *Science* **1991**, *254*, 1471–1477.
- [31] J. D. Nguyen, J. W. Tucker, M. D. Konieczynska, C. R. J. Stephenson, *J. Am. Chem. Soc.* **2011**, *133*, 4160–4163.
- [32] C.-J. Wallentin, J. D. Nguyen, P. Finkbeiner, C. R. J. Stephenson, *J. Am. Chem. Soc.* **2012**, *134*, 8875–8884.
- [33] M. S. Kharasch, E. V. Jensen, W. H. Urry, *Science* **1945**, *102*, 128.
- [34] M. S. Kharasch, P. S. Skell, P. Fisher, *J. Am. Chem. Soc.* **1948**, *70*, 1055–1059.
- [35] D. P. Curran, *Synthesis* **1988**, *1988*, 489–513.
- [36] J. M. Muñoz-Molina, T. R. Belderrain, P. J. Pérez, *Eur. J. Inorg. Chem.* **2011**, 3155–3164.
- [37] T. Pintauer, K. Matyjaszewski, *Chem. Soc. Rev.* **2008**, *37*, 1087–1097.
- [38] A. C. Hernandez-Perez, A. Vlassova, S. K. Collins, *Org. Lett.* **2012**, *14*, 2988–2991.
- [39] G. Fumagalli, P. T. G. Rabet, S. Boyd, M. F. Greaney, *Angew. Chem. Int. Ed.* **2015**, *54*, 11481–11484.
- [40] P. T. G. Rabet, G. Fumagalli, S. Boyd, M. F. Greaney, *Org. Lett.* **2016**, *18*, 1646–1649.
- [41] Z. Zhang, X. Tang, C. S. Thomason, W. R. Dolbier, *Org. Lett.* **2015**, *17*, 3528–3531.
- [42] T. P. Nicholls, G. E. Constable, J. C. Robertson, M. G. Gardiner, A. C. Bissember, *ACS Catal* **2016**, *6*, 451–457.
- [43] D. G. Cuttall, S.-M. Kuang, P. E. Fanwick, D. R. McMillin, R. A. Walton, *J. Am. Chem. Soc.* **2002**, *124*, 6–7.
- [44] a) B. Michelet, C. Deldaele, S. Kajouj, C. Moucheron, G. Evano, *Org. Lett.* **2017**, 3576–3579; b) A. C. Hernandez-Perez, S. K. Collins, *Angew. Chem. Int. Ed.* **2013**, 12696.
- [45] O. Reiser, *Acc. Chem. Res.* **2016**, *49*, 1990–1996.
- [46] B. Wang, D. P. Shelar, X.-Z. Han, T.-T. Li, X. Guan, W. Lu, K. Liu, Y. Chen, W.-F. Fu, C.-M. Che, *Chem. Eur. J.* **2015**, *21*, 1184–1190.
- [47] T. Rawner, *Copper(I) Phenanthrolines in Photocatalysis*; Dissertation, Universität Regensburg, **2016**.
- [48] S. H. Oh, Y. R. Malpani, N. Ha, Y.-S. Jung, S. B. Han, *Org. Lett.* **2014**, *16*, 1310–1313.
- [49] T. Courant, G. Masson, *J. Org. Chem.* **2016**, *81*, 6945–6952.
- [50] M. Mitani, I. Kato, K. Koyama, *J. Am. Chem. Soc.* **1983**, *105*, 6719–6721.
- [51] N. Krause, *Modern Organocopper Chemistry*. 1st ed., Wiley-VCH, Weinheim **2002**.

- [52] A. F. Holleman, E. Wiberg, N. Wiberg, *Lehrbuch der anorganischen Chemie*. 102., stark umgearb. u. verb. Aufl., De Gruyter, Berlin **2007**.
- [53] A. Casitas, X. Ribas, *Chem. Sci.* **2013**, 4, 2301–2318.
- [54] R. Santo, R. Miyamoto, R. Tanaka, T. Nishioka, K. Sato, K. Toyota, M. Obata, S. Yano, I. Kinoshita, A. Ichimura, T. Takui, *Angew. Chem. Int. Ed.* **2006**, 45, 7611–7614.
- [55] M. Melník, M. Kabešová, *J. Coord. Chem.* **2000**, 50, 323–338.
- [56] A. Casitas, A. E. King, T. Parella, M. Costas, S. S. Stahl, X. Ribas, *Chem. Sci.* **2010**, 1, 326–330.
- [57] A. M. Romine, N. Nebra, A. I. Konovalov, E. Martin, J. Benet-Buchholz, V. V. Grushin, *Angew. Chem. Int. Ed.* **2015**, 54, 2745–2749.
- [58] S.-L. Zhang, W.-F. Bie, *RSC Adv.* **2016**, 6, 70902–70906.
- [59] K. K. Gurjar, R. K. Sharma, *ChemCatChem* **2017**, 9, 862–869.
- [60] C. Krebs, T. Glaser, E. Bill, T. Weyhermüller, W. Meyer-Klaucke, K. Wieghardt, *Angew. Chem. Int. Ed.* **1999**, 38, 359–361.
- [61] D. W. Margerum, K. L. Chellappa, F. P. Bossu, G. L. Burce, *J. Am. Chem. Soc.* **1975**, 97, 6894–6896.
- [62] M. A. Willert-Porada, D. J. Burton, N. C. Baenziger, *J. Chem. Soc., Chem. Commun.* **1989**, 1633–1634.
- [63] H. Furuta, H. Maeda, A. Osuka, *J. Am. Chem. Soc.* **2000**, 122, 803–807.
- [64] X. Ribas, D. A. Jackson, B. Donnadieu, J. Mahía, T. Parella, R. Xifra, B. Hedman, K. O. Hodgson, A. Llobet, T. D. P. Stack, *Angew. Chem. Int. Ed.* **2002**, 41, 2991–2994.
- [65] B. Yao, D.-X. Wang, Z.-T. Huang, M.-X. Wang, *Chem. Commun.* **2009**, 2899–2901.
- [66] T. D. Lash, *Chem. Rev.* **2017**, 117, 2313–2446.
- [67] R. E. Marsh, *Acta Cryst.* **1997**, B53, 317–322.
- [68] A. J. Hickman, M. S. Sanford, *Nature* **2012**, 484, 177–185.
- [69] L. M. Huffman, S. S. Stahl, *J. Am. Chem. Soc.* **2008**, 130, 9196–9197.
- [70] M. Rovira, M. Font, F. Acuña-Parés, T. Parella, J. M. Luis, J. Lloret-Fillol, X. Ribas, *Chem. Eur. J.* **2014**, 20, 10005–10010.
- [71] H. Zhang, B. Yao, L. Zhao, D.-X. Wang, B.-Q. Xu, M.-X. Wang, *J. Am. Chem. Soc.* **2014**, 136, 6326–6332.
- [72] a) C. Long, L. Zhao, J.-S. You, M.-X. Wang, *Organometallics* **2014**, 33, 1061–1067; b) B. Yao, Y. Liu, L. Zhao, D.-X. Wang, M.-X. Wang, *J. Org. Chem.* **2014**, 79, 11139–11145.
- [73] a) E. R. Bartholomew, S. H. Bertz, S. Cope, D. C. Dorton, M. Murphy, C. A. Ogle, *Chem. Commun.* **2008**, 1176–1177; b) E. R. Bartholomew, S. H. Bertz, S. K. Cope, M. D. Murphy, C. A. Ogle, A. A. Thomas, *Chem. Commun.* **2010**, 46, 1253–1254.

- [74] S. H. Bertz, S. Cope, M. Murphy, C. A. Ogle, B. J. Taylor, *J. Am. Chem. Soc.* **2007**, *129*, 7208–7209.
- [75] S. H. Bertz, S. Cope, D. Dorton, M. Murphy, C. A. Ogle, *Angew. Chem. Int. Ed.* **2007**, *46*, 7082–7085.
- [76] T. Gärtner, W. Henze, R. M. Gschwind, *J. Am. Chem. Soc.* **2007**, *129*, 11362–11363.
- [77] E. R. Bartholomew, S. H. Bertz, S. Cope, M. Murphy, C. A. Ogle, *J. Am. Chem. Soc.* **2008**, *130*, 11244–11245.
- [78] P. J. Donoghue, J. Tehranchi, C. J. Cramer, R. Sarangi, E. I. Solomon, W. B. Tolman, *J. Am. Chem. Soc.* **2011**, *133*, 17602–17605.
- [79] C. Citek, J. B. Gary, E. C. Wasinger, T. D. P. Stack, *J. Am. Chem. Soc.* **2015**, *137*, 6991–6994.
- [80] a) S. Itoh, *Acc. Chem. Res.* **2015**, *48*, 2066–2074; b) C. E. Elwell, N. L. Gagnon, B. D. Neisen, D. Dhar, A. D. Spaeth, G. M. Yee, W. B. Tolman, *Chem. Rev.* **2017**, *117*, 2059–2107; c) W. Keown, J. B. Gary, T. D. P. Stack, *J. Biol. Inorg. Chem.* **2017**, *22*, 289–305.
- [81] N. Yoshikai, E. Nakamura, *Chem. Rev.* **2012**, *112*, 2339–2372.
- [82] X.-X. Guo, D.-W. Gu, Z. Wu, W. Zhang, *Chem. Rev.* **2015**, *115*, 1622–1651.
- [83] N. V. Tzouras, I. K. Stamatopoulos, A. T. Papastavrou, A. A. Liori, G. C. Vougioukalakis, *Coord. Chem. Rev.* **2017**, *343*, 25–138.
- [84] S. D. McCann, S. S. Stahl, *Acc. Chem. Res.* **2015**, *48*, 1756–1766.
- [85] a) D. A. Evans, J. L. Katz, T. R. West, *Tetrahedron Lett.* **1998**, *39*, 2937–2940; b) P. Y. S. Lam, C. G. Clark, S. Saubern, J. Adams, M. P. Winters, D. M. T. Chan, A. Combs, *Tetrahedron Lett.* **1998**, *39*, 2941–2944.
- [86] A. E. King, T. C. Brunold, S. S. Stahl, *J. Am. Chem. Soc.* **2009**, *131*, 5044–5045.
- [87] a) J. X. Qiao, P. Y. S. Lam, *Synthesis* **2011**, *2011*, 829–856; b) A. E. King, B. L. Ryland, T. C. Brunold, S. S. Stahl, *Organometallics* **2012**, *31*, 7948–7957.
- [88] W.-J. Yoo, T. Tsukamoto, S. Kobayashi, *Angew. Chem. Int. Ed.* **2015**, *54*, 6587–6590.
- [89] F. Ullmann, J. Bielecki, *Ber. Dtsch. Chem. Ges.* **1901**, *34*, 2174–2185.
- [90] a) J. Lindley, *Tetrahedron* **1984**, *40*, 1433–1456; b) G. Evano, N. Blanchard, M. Toumi, *Chem. Rev.* **2008**, *108*, 3054–3131.
- [91] C. Sambhagio, S. P. Marsden, A. J. Blacker, P. C. McGowan, *Chem. Soc. Rev.* **2014**, *43*, 3525–3550.
- [92] a) G. O. Jones, P. Liu, K. N. Houk, S. L. Buchwald, *J. Am. Chem. Soc.* **2010**, *132*, 6205–6213; b) H.-Z. Yu, Y.-Y. Jiang, Y. Fu, L. Liu, *J. Am. Chem. Soc.* **2010**, *132*, 18078–18091.
- [93] S. E. Creutz, K. J. Lotito, G. C. Fu, J. C. Peters, *Science* **2012**, *338*, 647–651.

- [94] a) L. M. Huffman, A. Casitas, M. Font, M. Canta, M. Costas, X. Ribas, S. S. Stahl, *Chem. Eur. J.* **2011**, *17*, 10643–10650; b) M. Font, T. Parella, M. Costas, X. Ribas, *Organometallics* **2012**, *31*, 7976–7982.
- [95] Y. Ye, M. S. Sanford, *J. Am. Chem. Soc.* **2012**, *134*, 9034–9037.
- [96] X. Zhu, S. Chiba, *Chem. Soc. Rev.* **2016**, *45*, 4504–4523.
- [97] R. J. Phipps, N. P. Grimster, M. J. Gaunt, *J. Am. Chem. Soc.* **2008**, *130*, 8172–8174.
- [98] R. J. Phipps, M. J. Gaunt, *Science* **2009**, *323*, 1593–1597.
- [99] D. A. Koch, B. J. Henne, D. E. Bartak, *J. Electrochem. Soc.* **1987**, *134*, 3062–3067.
- [100] A. A. Isse, C. Y. Lin, M. L. Coote, A. Gennaro, *J. Phys. Chem. B* **2010**, *115*, 678–684.
- [101] D. A. Nicewicz, D. W. C. MacMillan, *Science* **2008**, *322*, 77–80.
- [102] H. G. Roth, N. A. Romero, D. A. Nicewicz, *Synlett* **2016**, *27*, 714–723.
- [103] J. G. Lawless, D. E. Bartak, M. D. Hawley, *J. Am. Chem. Soc.* **1969**, *91*, 7121–7127.
- [104] M. Knorn, *Metal-Isonitriles*; Dissertation, Universität Regensburg, **2015**.
- [105] N. Armaroli, *Chem. Soc. Rev.* **2001**, *30*, 113–124.
- [106] M. S. Lazorski, F. N. Castellano, *Polyhedron* **2014**, *82*, 57–70.
- [107] J. Frey, T. Kraus, V. Heitz, J.-P. Sauvage, *Chem. Eur. J.* **2007**, *13*, 7584–7594.
- [108] A. Lavie-Cambot, M. Cantuel, Y. Leydet, G. Jonusauskas, D. M. Bassani, N. D. McClenaghan, *Coord. Chem. Rev.* **2008**, *252*, 2572–2584.
- [109] B. Zelenay, R. Frutos-Pedreño, J. Markalain-Barta, E. Vega-Isa, A. J. P. White, S. Díez-González, *Eur. J. Inorg. Chem.* **2016**, *2016*, 4649–4658.
- [110] S. Kümmel, *Chemical Photocatalysis with Flavins*; Dissertation, Universität Regensburg, **2012**.
- [111] Y. Pellegrin, M. Sandroni, E. Blart, A. Planchat, M. Evain, N. C. Bera, M. Kayanuma, M. Sliwa, M. Rebarz, O. Poizat, C. Daniel, F. Odobel, *Inorg. Chem.* **2011**, *50*, 11309–11322.
- [112] M. Pirtsch, *Photokatalyse mit [Cu(dap)₂Cl] und sichtbarem Licht*; Dissertation, Universität Regensburg, **2013**.
- [113] M. G. Pfeffer, L. Zedler, S. Kupfer, M. Paul, M. Schwalbe, K. Peuntinger, D. M. Guldi, J. Guthmuller, J. Popp, S. Grafe, B. Dietzek, S. Rau, *Dalton Trans* **2014**, *43*, 11676–11686.
- [114] N. Herron, M. A. Guidry, V. Rostovtsev, W. Gao, Y. Wang, Y. Shen, J. A. Merlo, *Electronic device including phenanthroline derivative*, WO2010075379A2, **2010**.
- [115] a) C. Dietrich-Buchecker, J. P. Sauvage, J. M. Kern, *J. Am. Chem. Soc.* **1989**, *111*, 7791–7800; b) M. Geoffroy, M. Wermeille, C. O. Buchecker, J.-P. Sauvage, G. Bernardinelli, *Inorg. Chim. Acta* **1990**, *167*, 157–164.
- [116] P. Yang, X.-J. Yang, B. Wu, *Eur. J. Inorg. Chem.* **2009**, 2951–2958.

- [117] B. Wu, P. Yang, X. Huang, Y. Liu, X. Liu, C. Xia, *Z. Anorg. Allg. Chem.* **2006**, *632*, 684–688.
- [118] C. T. Cunningham, J. J. Moore, K. L. H. Cunningham, P. E. Fanwick, D. R. McMillin, *Inorg. Chem.* **2000**, *39*, 3638–3644.
- [119] M. Gelbert, C. Körber, O. Friedrich, F. Fahrenkrug, M. Keller, U. Lüning, *Supramolecular Chemistry* **2002**, *14*, 199–210.
- [120] a) P. M. Bush, J. P. Whitehead, C. C. Pink, E. C. Gramm, J. L. Eglin, S. P. Watton, L. E. Pence, *Inorg. Chem.* **2001**, *40*, 1871–1877; b) P. Kulkarni, S. Padhye, E. Sinn, C. E. Anson, A. K. Powell, *Inorg. Chim. Acta* **2002**, *332*, 167–175.
- [121] M. Julliard, M. Chanon, *Chem. Rev.* **1983**, *83*, 425–506.
- [122] C. L. Foster, C. A. Kilner, M. Thornton-Pett, M. A. Halcrow, *Acta Cryst.* **2000**, *C56*, 319–320.
- [123] a) H. tom Dieck, L. Stamp, *Z. Naturforsch. B* **1990**, *45*, 1369–1382; b) L. Stamp, H. tom Dieck, *Inorg. Chim. Acta* **1987**, *129*, 107–114; c) H. tom Dieck, I. W. Renk, *Ber. Dtsch. Chem. Ges.* **1971**, *104*, 92–109; d) H. Ayranci, C. Daul, M. Zobrist, A. von Zelewsky, *Helv. Chim. Acta* **1975**, *58*, 1732–1735.
- [124] G. van Koten, K. Vrieze, *Adv. Organomet. Chem.* **1982**, *21*, 151–239.
- [125] a) S. Anga, R. K. Kottalanka, T. Pal, T. K. Panda, *J. Mol. Struct.* **2013**, *1040*, 129–138; b) K. Vrieze, *J. Organomet. Chem.* **1986**, *300*, 307–326.
- [126] a) J. Reinhold, R. Benedix, P. Birner, H. Hennig, *Inorg. Chim. Acta* **1979**, *33*, 209–213; b) J. Reinhold, R. Benedix, P. Birner, H. Hennig, *Z. Chem.* **1977**, *17*, 115–116.
- [127] C. J. Allan, B. F. T. Cooper, H. J. Cowley, J. M. Rawson, C. L. B. Macdonald, *Chem. Eur. J.* **2013**, *19*, 14470–14483.
- [128] a) W. Kaim, *Inorg. Chem.* **2011**, *50*, 9752–9765; b) R. E. Piau, T. Guillon, E. Lebon, N. Perrot, F. Alary, M. Boggio-Pasqua, J.-L. Heully, A. Juris, P. Sutra, A. Igau, *New J. Chem.* **2012**, *36*, 2484–2492.
- [129] I. Ruppert, K. Schlich, W. Volbach, *Tetrahedron Lett.* **1984**, *25*, 2195–2198.
- [130] G. K. S. Prakash, R. Krishnamurti, G. A. Olah, *J. Am. Chem. Soc.* **1989**, *111*, 393–395.
- [131] G. K. S. Prakash, A. K. Yudin, *Chem. Rev.* **1997**, *97*, 757–786.
- [132] X. Liu, C. Xu, M. Wang, Q. Liu, *Chem. Rev.* **2015**, *115*, 683–730.
- [133] A. Olejniczak, A. Katrusiak, A. Vij, *J. Fluorine Chem.* **2008**, *129*, 1090–1095.
- [134] A. Streitwieser Jr., C. L. Wilkins, E. Kiehlmann, *J. Am. Chem. Soc.* **1968**, *90*, 1598–1601.
- [135] R. D. Howells, J. D. Mc Cown, *Chem. Rev.* **1977**, *77*, 69–92.
- [136] L. Aalberg, K. Andersson, C. Bertler, H. Borén, M. D. Cole, J. Dahlén, Y. Finnon, H. Huizer, K. Jalava, E. Kaa, E. Lock, A. Lopes, A. Poortman-van der Meer, E. Sippola, *Forensic Science International* **2005**, *149*, 219–229.

- [137] a) J. J. Ritter, P. P. Minieri, *J. Am. Chem. Soc.* **1948**, *70*, 4045–4048; b) L. I. Krimen, D. J. Cota, *Org. React.* **1969**, *17*, 213–325.
- [138] E. Raamat, K. Kaupmees, G. Ovsjannikov, A. Trummal, A. Kütt, J. Saame, I. Koppel, I. Kaljurand, L. Lipping, T. Rodima, V. Pihl, I. A. Koppel, I. Leito, *J. Phys. Org. Chem.* **2013**, *26*, 162–170.
- [139] A. Jutand, A. Mosleh, *J. Org. Chem.* **1997**, *62*, 261–274.
- [140] S. J. Zhou, Z. Huang, *Chiral Phosphines for Palladium-Catalyzed Asymmetric Alpha-Arylation of Ester Enolates to Produce Tertiary Stereocenters in High enantioselectivity*, WO 2013/028132 A1, **2013**.
- [141] R. Chaudhary, P. Natarajan, *ChemistrySelect* **2017**, *2*, 6458–6479.
- [142] a) X.-J. Tang, C. S. Thomason, W. R. Dolbier, *Org. Lett.* **2014**, *16*, 4594–4597; b) X.-J. Tang, W. R. Dolbier, *Angew. Chem. Int. Ed.* **2015**, *54*, 4246–4249; c) Z. Zhang, H. Martinez, W. R. Dolbier, *J. Org. Chem.* **2017**, *82*, 2589–2598.
- [143] D. A. Nagib, D. W. C. MacMillan, *Nature* **2011**, *480*, 224–228.
- [144] F. Carta, A. Scozzafava, C. T. Supuran, *Expert Opin. Ther. Pat.* **2012**, *22*, 747–758.
- [145] H. Erdmann, *Liebigs Ann. Chem.* **1888**, *247*, 306–366.
- [146] a) A. Mustafa, *Chem. Rev.* **1954**, *54*, 195–223; b) D. W. Roberts, D. L. Williams, *Tetrahedron* **1987**, *43*, 1027–1062; c) P. Metz, *J. Prakt. Chem.* **1998**, *340*, 1–10; d) S. Mondal, *Chem. Rev.* **2012**, *112*, 5339–5355; e) C. Gaunersdorfer, M. Waser, *Monatshefte für Chemie - Chemical Monthly* **2017**, 1–14.
- [147] Q. Qin, S. Yu, *Org. Lett.* **2015**, *17*, 1894–1897.
- [148] a) R. M. Joyce, W. E. Hanford, J. Harmon, *J. Am. Chem. Soc.* **1948**, *70*, 2529–2532; b) R. Huff, F. Mutterer, C. D. Weis, *Helv. Chim. Acta* **1977**, *60*, 907–921; c) K. Saotome, H. Komoto, T. Yamazaki, *Bull. Chem. Soc. Jpn.* **1966**, *39*, 480–484.
- [149] Y. Sawama, T. Imanishi, R. Nakatani, Y. Fujiwara, Y. Monguchi, H. Sajiki, *Tetrahedron* **2014**, *70*, 4540–4546.
- [150] a) R. Teraoka, Y. Matsushima, I. Sugimoto, K. Inoue, S.-y. Morita, S. Kitagawa, *Chem. Pharm. Bull.* **2009**, *57*, 1343–1347; b) E. M. Antunes, A. F. Afolayan, M. T. Chiwakata, J. Fakee, M. G. Knott, C. E. Whibley, D. T. Hendricks, J. J. Bolton, D. R. Beukes, *Phytochemistry* **2011**, *72*, 769–772.
- [151] A. J. Clark, G. M. Battle, A. Bridge, *Tetrahedron Lett.* **2001**, *42*, 1999–2001.
- [152] D. Menigaux, P. Belmont, E. Brachet, *Eur. J. Org. Chem.* **2017**, *2017*, 2008–2055.
- [153] H. Subramanian, Y. Landais, M. P. Sibi, in *Comprehensive Organic Synthesis II (Second Edition)*, (Ed: P. T1-4.12 Radical Addition Reactions A2-Knochel), Elsevier, Amsterdam **2014**, pp. 699–741.
- [154] M. A. Cismesia, T. P. Yoon, *Chem. Sci.* **2015**, *6*, 5426–5434.

- [155] a) T. Tsuritani, H. Shinokubo, K. Oshima, *J. Org. Chem.* **2003**, *68*, 3246–3250; b) C. Martínez, K. Muñiz, *Adv. Synth. Catal.* **2014**, *356*, 205–211; c) G. Heuger, R. Göttlich, *Beilstein Journal of Organic Chemistry* **2015**, *11*, 1226–1234; d) L. Song, S. Luo, J.-P. Cheng, *Organic Chemistry Frontiers* **2016**, *3*, 447–452; e) X. Liu, K. Tong, A. H. Zhang, R. X. Tan, S. Yu, *Organic Chemistry Frontiers* **2017**, *4*, 1354–1357.
- [156] Q. Qin, D. Ren, S. Yu, *Org. Biomol. Chem.* **2015**, *13*, 10295–10298.
- [157] a) A. S. Kalgutkar, R. Jones, A. Sawant, in *Metabolism, Pharmacokinetics and Toxicity of Functional Groups: Impact of Chemical Building Blocks on ADMET*, The Royal Society of Chemistry **2010**, pp. 210–274; b) Y. Zhang, C. Jin, W. Zhong, H. Xie, J. Zhang, *Sulfonamide derivatives and pharmaceutical applications thereof*, WO2015158313 (A1), **2015**; c) A. U. Meyer, A. L. Berger, B. König, *Chem. Commun.* **2016**, *52*, 10918–10921.
- [158] X.-Y. Liu, P. Gao, Y.-W. Shen, Y.-M. Liang, *Adv. Synth. Catal.* **2011**, *353*, 3157–3160.
- [159] C. Hansch, A. Leo, R. W. Taft, *Chem. Rev.* **1991**, *91*, 165–195.
- [160] P. G. M. Wuts, T. W. Greene, *Greene's protective groups in organic synthesis*. 4th ed., Wiley-Interscience, Hoboken, N.J. **2007**.
- [161] L. J. Allen, P. J. Cabrera, M. Lee, M. S. Sanford, *J. Am. Chem. Soc.* **2014**, *136*, 5607–5610.
- [162] D. D. M. Wayner, D. J. McPhee, D. Griller, *J. Am. Chem. Soc.* **1988**, *110*, 132–137.
- [163] Y. Fu, L. Liu, H.-Z. Yu, Y.-M. Wang, Q.-X. Guo, *J. Am. Chem. Soc.* **2005**, *127*, 7227–7234.
- [164] S. Z. Zard, *Org. Lett.* **2017**, *19*, 1257–1269.
- [165] a) S. Hünig, P. Kreitmeier, G. Märkl, J. Sauer, *Arbeitsmethoden in der Organischen Chemie: (mit Einführungspraktikum)*. 2., überarbeitete Auflage, Lehmanns Media, Berlin **2008**; b) W. L. F. Armarego, C. L. L. Chai, *Purification of laboratory chemicals*. 6th ed., Elsevier, Oxford **2009**.
- [166] D. Rackl, V. Kais, P. Kreitmeier, O. Reiser, *Beilstein J. Org. Chem.* **2014**, *10*, 2157–2165.
- [167] V. V. Pavlishchuk, A. W. Addison, *Inorg. Chim. Acta* **2000**, *298*, 97–102.
- [168] G. H. Coleman, G. E. Honeywell, *Org. Synth.* **1936**, *16*, 54.
- [169] O. Pavlyuk, H. Teller, M. C. McMills, *Tetrahedron Lett.* **2009**, *50*, 2716–2718.
- [170] A. J. Arduengo III, R. Krafczyk, R. Schmutzler, H. A. Craig, J. R. Goerlich, W. J. Marshall, M. Unverzagt, *Tetrahedron* **1999**, *55*, 14523–14534.
- [171] A. S. Jones, J. F. Paliga, M. D. Greenhalgh, J. M. Quibell, A. Steven, S. P. Thomas, *Org. Lett.* **2014**, *16*, 5964–5967.
- [172] Z.-M. Lin, C. Zheng, J.-J. Xiao, R.-F. Chen, P. Zhao, J. Song, Z.-F. An, H. Tian, W. Huang, *New J. Chem.* **2012**, *36*, 1512–1518.

- [173] R. B. Chhor, B. Nosse, S. Sörgel, C. Böhm, M. Seitz, O. Reiser, *Chem. Eur. J.* **2003**, *9*, 260–270.
- [174] L. Pils, *Enantioselective cyclopropanation of heterocycles and the use of high-pressure techniques for the conformational analysis of peptide foldamers*; Dissertation, Universität Regensburg, **2015**.
- [175] H. C. Guo, R. H. Zheng, H. J. Jiang, *Org. Prep. Proced. Int.* **2012**, 392–396.
- [176] H. Yorimitsu, H. Shinokubo, S. Matsubara, K. Oshima, K. Omoto, H. Fujimoto, *J. Org. Chem.* **2001**, *66*, 7776–7785.
- [177] L. Neuville, A. Bigot, M. E. Tran Huu Dau, J. Zhu, *J. Org. Chem.* **1999**, *64*, 7638–7642.
- [178] Z. Liu, J. Xu, W. Ruan, C. Fu, H.-J. Zhang, T.-B. Wen, *Dalton Trans* **2013**, *42*, 11976–11980.
- [179] Y. Oe, Y. Uozumi, *Adv. Synth. Catal.* **2008**, *350*, 1771–1775.
- [180] M. Hesse, H. Meier, B. Zeeh (Eds.), *Spektroskopische Methoden in der organischen Chemie*, Georg Thieme Verlag, Stuttgart, New York **2005**.
- [181] U. Megerle, R. Lechner, B. König, E. Riedle, *Photochem. Photobiol. Sci.* **2010**, *9*, 1400–1406.

Acknowledgement

Zuallererst möchte ich mich bei Herrn Prof. Dr. Oliver Reiser für die Überlassung des interessanten Themas, die beständige Unterstützung während der gesamten Arbeit und die hilfreichen und anregenden Diskussionen bedanken.

Für die finanzielle Unterstützung während meiner Promotion im Rahmen des GRK 1626 Chemische Photokatalyse danke ich der DFG.

Dankeschön an Dr. Peter Kreitmeier für seine fachkundige Hilfe bei technischen und chemischen Problemen sowie für die vielen fachlichen und vor allem nicht fachlichen Diskussionen. Ebenso danke ich Klaus Döring, Roxane Harteis, Helena Konkel und Brigitte Eichenseher für die synthetische Unterstützung und die tollen Gespräche. Dank gebührt unseren Sekretärinnen Antje Weigert und Michaela Schüle für die Hilfe durch den Bürokratiedschungel.

Vielen Dank an die Mitarbeiter der zentralen Analytik der Universität Regensburg für die Expertise sowie für die Hilfe bei der Aufnahme von NMR Spektren, der Durchführung von Massenspektroskopie und Elementaranalyse wie auch beim Vermessen und Lösen von X-ray Strukturen.

Dankeschön an Regina Hoheisel für ihre nette Unterstützung bei der Cyclovoltammetrie sowie für das schnelle und gewissenhafte Vermessen aller CVs meiner Verbindungen.

Für die Unterstützung und Expertise in spektroskopischen Angelegenheiten an der Universität Regensburg bedanke ich mich besonders bei Fabian Brandl, Uwe Faltermeier und Dr. Jose Luis Pérez Lustres. Dank an Dr. Rafał Czerwieniec für seine Geduld, mir die photophysikalische Welt von Kupferkomplexen näherzubringen sowie für die wertvollen Diskussionen. Alexander Schinabeck danke ich insbesondere für die viele Zeit, die er für verschiedenste photophysikalische Messungen meiner Komplexe opferte – danke vor allem für die angenehme Atmosphäre und die schönen Gespräche dabei. Für die Beratung in physikalischen Angelegenheiten aller Art bedanke ich mich bei Matthias Block (LMU).

Danke an meine Forschungspraktikanten Thomas Föll, Lukas Wirth und Andreas Graml für die synthetische Unterstützung sowie die gute Atmosphäre, zu der auch ihr alle beigetragen habt.

Für das Korrekturlesen dieser Arbeit bedanke ich mich herzlich bei meinem langjährigen Trainingskameraden David Akers, sowie bei meinen Kollegen Eugen Lutscher und Simon Budde. Danke euch allen für die viele wertvolle Zeit, die ihr dafür geopfert habt!

Bedanken möchte ich mich bei allen, die zum Gelingen dieser Arbeit beigetragen haben, egal ob in fachlicher, technisch-synthetischer oder freundschaftlicher Hinsicht. Vielen Dank an alle aktuellen und ehemaligen Mitarbeiter am Reiser-Lehrstuhl für eure Hilfe, die ausgezeichnete und freundliche kollegiale Atmosphäre sowie die verschiedenen Aktivitäten auch abseits der Arbeit.

Meinen Laborkollegen Vinh Ngoc Huynh, Dr. Thomas Rawner, Eugen Lutscher, Thomas Weinbender und Natalija Moor danke ich herzlich für die super Zusammenarbeit und die hilfreichen Diskussionen und Anregungen. Vor allem danke ich euch für die tolle freundschaftliche Atmosphäre und die vielen lustigen Gespräche und Aktionen!

Selbstverständlich danke ich meinen Kommilitonen, Leidensgenossen und Freunden Fabian B., Markus B., Daniel D., Tom E., Uwe F., Martin (Jimmy) H., Michael K., Verena L., Verena M. und Hans S. für die vielen fachlichen Diskussionen und die großartige Zeit. Danke aber vor allem für die wunderschönen Aktivitäten. Dank gilt natürlich auch all meinen treuen Freunden außerhalb der Universität, durch die ich in meiner Freizeit immer wieder wertvolle Energie tanken konnte.

Großer Dank gilt meiner gesamten Familie. Insbesondere möchte ich meinen Eltern danken, nicht nur für die stetige finanzielle Unterstützung, sondern vor allem für ihr Vertrauen in mich und ihren Rückhalt, auf den ich mich immer verlassen kann.

Zu guter Letzt danke ich von ganzem Herzen meiner lieben Christina, die von allen am meisten Verständnis für meine zeitintensive Leidenschaft gegenüber der Chemie aufbringen musste, mit mir durch Dick und Dünn ging und immer hinter mir stand und steht. Danke dir!

Declaration

Herewith I declare that this present thesis is a presentation of my original work prepared single-handed. Wherever contributions from others are involved, all of them are marked clearly, with reference to the literature, license and acknowledgement of collaborative research.

Regensburg, 08.12.2017

Christian Lankes